

School of Chemical Engineering

**Ash formation mechanisms during combustion/co-firing of biomass and
coal**

Kalpiti Vrajeshkumar Shah

**This thesis is presented for the Degree of
Doctor of Philosophy
of
Curtin University of Technology**

October 2010

Declaration:

To the best of my knowledge and belief this thesis contains no material previously published by any other person except where due acknowledgement has been made.

The thesis contains no material which has accepted for the award of any other degree or diploma in any university.

Signature:

Date:

Abstract

In case of PF firing, solid fuels such as coal and biomass undergo various chemical and physical transformations (devolatilization, char oxidation, fragmentation and gas to particle conversion followed by nucleation, coagulation and condensation etc.) just in milliseconds after fuel enters to the furnace. These transformations depend on several operating parameters (temperature, pressure, heating rate etc.) along with several chemical and physical properties (ash, moisture content, density, porosity, mineral matter composition and their association in the fuel matrix, particle size, shape and density etc.). The resultant ash formed during combustion after such parallel transformations in relation with several physical and chemical transformations along with the operating parameters will have different particle sizes and mineralogical composition compare to the original fuel. The scope of this research work is to perform the experimental and modelling work to investigate the ash formation process in terms of particle sizes and their mineralogical composition after combustion. A vast experimental study was planned in the lab scale combustion simulator at ECN with six biomass and two coals (Bark, wood chips, waste wood, saw dust, olive residue, straw, UK and a Polish etc.) under typical PF-firing conditions. Ash release, conversion, size reduction and size distribution alongside with the change in inorganic chemical compositions, are derived at different char burn out levels in the reactor at 20, 90, 210 and 1300 milliseconds of residence times. Several of the past observations made in the literature review are reconfirmed with performed set of experiments. A qualitative predictive tool is also suggested to envisage the extent of first line physical transformations. Based on the extensive data pool at hand, a simple but reliable ($R^2 > 0.95$) set of linear correlations have been proposed to predict the elemental release of potassium, sodium, chlorine and sulfur. It is also concluded that such linear expressions can be particularly effective for the prediction of elemental release from the fuels of similar characteristics, such as woody biomass. Mathematical model is developed to predict the particle size after combustion by simplifying Dunn-rankin's particle population balance model analytically and kinetically. Ash formation modelling has also been attempted. The developed understanding and models can be further used for the investigations of several ash related problems during combustion and co-firing such as slagging, fouling, corrosion and erosion etc.

Brief Biography of the Author

Kalpiti Shah received the Bachelor of Engineering in Chemical Engineering with academic distinctions from the Shri Sad Vidyamandal Institute of Technology, South Gujarat University, India in 2001. After finishing his graduation, for a period of around six years, he worked with several medium to large scale multinational companies in their technical service and/or project department mainly dealing with the issues related to power and utility. He has distinction of clearing “National level certification exam for Energy Auditor” in the first attempt with distinction marks in the youngest age group in all over India in the year 2005. Prior joining with Department of Chemical Engineering Curtin University of Technology in 2007 for his PhD, he was offered a position in Energy department of world’s largest refinery - Reliance Industries Ltd. for their Gujarat based plant in India. He has conducted more than 35 thermal/electrical energy and process audits in small-medium-large scale industries. Due to his excellent career in the Energy sector, he was offered a PhD program at Curtin University of Technology in association with Energy Research Centre of the Netherlands in the area of coal and biomass combustion and/ co-firing. He is the recipient of Curtin International Research Tuition Scholarship from August 2007 to August 2010.

Journal Publications

Part of the research work carried out in Chapter 3, 4 and 5 are already published in several journals. Literature review paper will also be attempted by next year for publication after reviewing more relevant papers in this field.

1. K V. Shah, R. Vuthaluru & H.B. Vuthaluru. CFD based investigations into optimization of coal pulverizer performance: Effect of classifier vane settings. *Fuel Processing Technology*, 90 (9) (2009) 1135-1141.
2. Kalpit V. Shah, Mariusz K. Cieplik, Christine I. Bertrand, Willem L. van de Kamp and Hari B. Vuthaluru; Correlating the effects of ash elements and their association in the fuel matrix with the ash release during pulverized fuel combustion, *Fuel Processing Technology*, 91 (2010) 531–545.
3. Rob Korbee, Kalpit V. Shah, Mariusz K. Cieplik, Christine I. Bertrand, Hari B. Vuthaluru and Willem L. van de Kamp; First line ash transformations of

- coal and biomass fuels during PF combustion, *Energy Fuels*, 24 (2) (2010) 897–909.
4. Kalpit V. Shah, Mariusz K. Cieplik, Christine I. Bertrand, Willem L. van de Kamp and Hari B. Vuthaluru; A kinetic-empirical model for particle size distribution evolution during pulverised fuel combustion, *Fuel* 89 (9) (2010) 2438-2447.
 5. Kalpit V. Shah, Mariusz K. Cieplik, Christine I. Bertrand and Hari B. Vuthaluru, A Review on ash formation during pulverized fuel combustion: State of art and future research needs, *Bioenergy and Bioresources* (Will be Submitted in *Biomass and Bioenergy*).

Every reasonable effort has been made to acknowledge the owners of the copyright material. I would be pleased to hear from any copyright owner who has been omitted or incorrectly acknowledged.

Acknowledgements

This thesis work was carried out as a part of research collaboration between Curtin University of Technology and Energy research centre of the Netherlands (ECN). First of all, I wish to express my highest gratitude to my supervisor A/Prof H. B. Vuthaluru who showed complete faith and trust on my technical skills and provided me an opportunity and enough guidance to conduct research in the challenging field of Renewable energy. I also wish to acknowledge sincere thanks to Dr. Jaap Kiel (ECN) who and A/Prof H. B. Vuthaluru jointly planned scholarship for me for a period of three years. I am highly grateful to Dr. Christine Bertrand for becoming a tough mentor and friendly industrial supervisor. Her clear understanding about the requirement of the objectives allowed me to work quickly and in time onto my goals during my PhD. I wish to deeply acknowledge Dr. Cieplik Mariusz for all his support starting from conducting lab-scale trials to writing a journal papers during my working at ECN. I gained invaluable enthusiasm and thorough knowledge about the subject while discussing various ingredients of my research with him. A deep acknowledgement also goes to Prof. Ming Ang from Curtin University of Technology, for both the financial support and also his genuine care for the well being of his students. I feel truly privileged to have been given the opportunity to carry out my research work at ECN as I have gained extensive technical knowledge and skills that goes well beyond the scope of this thesis. I am also thankful to HR department of ECN, especially Desiree Selbach and Irma Hollander for arranging immigration for the Netherlands and sweet accommodation for nearly one and half year. I wish to thank many special friends, Dr, Sathiah Pratap and Dr. Laltu Chandra from Netherlands for being a good listener to me. I have discussed my research with them several times and got some useful tips about mathematical modeling.

I am also thankful to my mother, in-laws and siblings for their encouraging words and mental support. Lastly, I want to dedicate this work to my soul mate for her throughout support during my PhD and also for rest of life. It was not possible to finish my research in time if she didn't allow me to work from home in the nights and during weekend. She provided me all the strength needed to focus on my research with a cup of tea at anytime.

Thesis Contents

Abstract.....	I
Brief Biography of Author.....	II
Acknowledgment	IV
List of Figures.....	XI
List of Tables.....	XVI
Nomenclature.....	XVIII

Chapter 1

Introduction and Objectives	1
1.1 Introduction.....	1
1.2 Objectives	2
1.3 Outline of thesis	4
References.....	7

Chapter 2

Literature Review	9
2.1 Introduction.....	9
2.2 Parameters responsible for mineral transformations during PF combustion.....	11
2.2.1 Fuel mineral matter composition and their association	11

2.2.2	Mineralogy	13
2.2.3	Particle shape, size and density.....	14
2.2.4	Fuel characteristics after milling.....	16
2.2.5	Char structure.....	17
2.2.6	Other fuel characteristics	21
2.2.7	Relation with operating parameters	21
2.3	Prediction of ash formation during PF combustion	24
2.3.1	Analytical methods	24
2.3.2	Mathematical modelling	27
2.3.2.1	Coarse ash formation	28
2.3.2.1.1	Break up model	29
2.3.2.1.2	Fragmentation model based on thermally induced stress	29
2.3.2.1.3	Shrinking core model.....	30
2.3.2.1.4	Percolation model	31
2.3.2.1.5	Particle population balance model	32
2.3.2.2	Ash release / Aerosol formation	33
2.4	Summary.....	35
2.5	Conclusions and future research needs	37
2.6	Objectives (based on the literature review)	38
	References.....	40

Chapter 3

First line ash transformations during PF combustion	50
3.1 Introduction.....	50
3.2 Experimental.....	53
3.2.1 Fuel Preparation and analyses.....	53
3.2.2 Laboratory Set-up	53
3.2.3 Sampling and analyses.....	56
3.3 Results.....	60
3.3.1 Conversion	60
3.3.2 Ash Release.....	61
3.3.3 Size distribution	63
3.3.4 Relative Size Reduction.....	63
3.3.5 Elemental Distribution with PSD.....	64
3.4 Summary	71
3.5 Qualitative prediction.....	72
3.6 Conclusions.....	73
References.....	75

Chapter 4

Ash release of minerals during PF combustion.....	77
--	-----------

4.1 Introduction.....	77
4.1.1 Inorganic elemental gas phase release – a review	81
4.1.1.1 Release of S.....	81
4.1.1.2 Release of Cl.....	81
4.1.1.3 Release of Ca and Mg.....	82
4.1.1.4 Release of K and Na	82
4.2 Experimental.....	84
4.3 Results and Discussion	84
4.3.1 Release from tested coals and biomass fuels	85
4.3.2 Element-specific Release of the Inorganic Matter.....	88
4.4 Summary.....	99
4.5 Conclusions.....	100
References.....	102

Chapter 5

Modeling of particle size evolution after PF combustion.....	105
5.1 Introduction.....	106
5.1.1 Background.....	107
5.2 Mathematical modeling	108
5.2.1 Overall mass balance equation.....	108
5.2.2 Population balance equation	109

5.2.3 Assumptions and Simplifications	111
5.2.4 Empirical parameters	112
5.2.5 Mode of Fragmentation.....	115
5.2.6 Conversion and Particle size reduction due to Burning and Fragmentation	115
5.2.7 Mineral matter distribution	117
5.3 Analytical solution	118
5.4 Experimental	121
5.4.1 Burning rate constant	121
5.4.2 Fragmentation rate constant.....	121
5.5 Validation against different coal and biomass combustion	122
5.6 Validation against co-firing (Polish coal and Straw).....	130
5.6 Conclusions.....	131
References.....	133

Chapter 6

Ash formation modeling	136
6.1 Introduction.....	137
6.2 Model plan	139
6.2.1 Assumptions.....	141
6.2.2 Release of mineral elements from the char particle.....	142
6.2.3 Particle size evolution after combustion	143

6.2.4	Redistribution of the mineral elements in the char particle	144
6.3	Experimental	144
6.4	Validation.....	146
6.4.1	Overall release of the mineral elements.....	146
6.4.2	Particle size distribution after combustion.....	148
6.4.3	Mineralogical transformations in the different particle sizes after combustion.....	149
6.5	Conclusions.....	154
6.6	Future Recommendations	154
	Reference	156

Chapter 7

	Practical implications, Conclusions and Future recommendations	158
7.1	Practical implications.....	159
7.2	Conclusions.....	161
7.3	Future recommendations.....	162
	Appendix A.....	164
	Appendix B.....	166
	Appendix C.....	167
	Appendix D.....	175
	Appendix E.....	180
	Appendix F.....	181

List of Figures

Figure 1. 1: Outline of Thesis	5
Figure 2. 1: Physical transformations involved for ash formation during coal/biomass combustion [2].....	10
Figure 2. 2: Variation in the extent of the fragmentation of a coal against compressive strength. [20].....	15
Figure 2. 3: BSE images with Comparison of PSD (by Volume) of char and Coal [28]	16
Figure 2. 4: Classifier Effect: Size distributions for excluded minerals, organic particles with included mineral, and organic-only for typical coal [18].....	17
Figure 2. 5: SEM. images of char samples generated at various burnout levels at a gas temperature of 1300 C in a drop tube furnace under atmospheric condition.....	18
Figure 2. 6: Negative prints of three successive frames from high speed film (approximately 4000 frames per second) [16]	19
Figure 2. 7: The porosity and swelling ratio as a function of heating rate [30].....	21
Figure 2. 8: Fly ash Particles formed at 900°C (left-top), 1100°C (right-top), 1300°C (left-bottom) and 1500°C (right-bottom) [43].....	23
Figure 2. 9: Particle Size distribution of ash generated at different pressures [44]..	23
Figure 3. 1: Schematics of the Lab-scale Combustion Simulator (LCS) used to study the formation of ash (incl. aerosols) from biomass and coal.....	55
Figure 3. 2: Example of cascade impactor sample (one stage) with an indication of the part of the sample which was analyzed using a scanning electron microscope.....	56

Figure 3. 3: Secondary electron images for different fuels for different residence time and cascade impactor stages	57
Figure 3. 4: Mass balance per element for cascade impactor measurements	58
Figure 3. 5: Mass-based fuel conversion as a function of residence time	61
Figure 3. 6: Amount and distribution of inorganic elements released after 1300 ms residence time. (Percentages represent the ratio of the sum of inorganic elements released to the sum of inorganic elements in the fuel.).....	62
Figure 3. 7: Particle size distribution with weight percentage of size fractions (such as coarse, fine and aerosols particles with sizes >10 μm , >1 μm and <1 μm respectively) and devolatilization (Vap) at different char burnout level.....	66
Figure 3. 8: Particle size distribution with weight percentage of size fractions (< = 15 μm) at different residence	67
Figure 3.9: Particle size distribution with weight percentage of size fractions (< = 15 μm) at different residence times	68
Figure 3. 10: Relative size reduction at different residence times.....	69
Figure 3. 11: Mineral matter distribution in different size fractions at different char burnout level	70
Figure 4. 1: Equilibrium species concentrations for the major potassium-containing, gas-phase species present under typical biomass combustion conditions; Source: Baxter et al. [22].....	83
Figure 4. 2: Amount and distribution of inorganic elements released after 1300 ms residence time. (percentages represent the ratio of the sum of inorganic elements released to the sum of inorganic elements in the fuel).....	85
Figure 4. 3: Sulfur release during combustion of coal and biomass fuels (BM1: Bark, BM2: Wood Chips, BM3: Waste wood, BM4: Saw Dust, BM5: Olive Residue, BM6: Straw, C1: Polish Coal, C2: UK Coal)	89

Figure 4. 4: Effect of elemental mineral matter composition on chlorine release during combustion of coal and biomass fuels (BM1: Bark, BM2: Wood Chips, BM3: Waste wood, BM4: Saw Dust, BM5: Olive Residue, BM6: Straw, C1: Polish Coal, C2: UK Coal)..... 89

Figure 4. 5: Effect of elemental mineral matter composition on chlorine release during combustion of woody biomass fuels (BM1: Bark, BM2: Wood Chips, BM3: Waste wood, BM4: Saw Dust)..... 90

Figure 4. 6: Calcium and Magnesium release during combustion of coal and biomass fuels (BM1: Bark, BM2: Wood Chips, BM3: Waste wood, BM4: Saw Dust, BM5: Olive Residue, BM6: Straw, C1: Polish Coal, C2: UK Coal) 91

Figure 4. 7: Effect of elemental mineral matter composition on potassium release during combustion of coal and biomass fuels (BM1: Bark, BM2: Wood Chips, BM3: Waste wood, BM4: Saw Dust, BM5: Olive Residue, BM6: Straw, C1: Polish Coal, C2: UK Coal)..... 93

Figure 4. 8: Effect of elemental mineral matter composition on potassium release during combustion of woody biomass fuels (BM1: Bark, BM2: Wood Chips, BM3: Waste wood, BM4: Saw Dust)..... 94

Figure 4. 9: Effect of elemental mineral matter composition on sodium release during combustion of coal and biomass fuels (BM1: Bark, BM2: Wood Chips, BM3: Waste wood, BM4: Saw Dust, BM5: Olive Residue, BM6: Straw, C1: Polish Coal, C2: UK Coal)..... 97

Figure 4. 10: Effect of elemental mineral matter composition on sodium release during combustion of woody biomass fuels (BM1: Bark, BM2: Wood Chips, BM3: Waste wood, BM4: Saw Dust)..... 98

Figure 5. 1: Modeling chart of PSD evolution during pf combustion.....109

Figure 5. 2: Particle surface regression computed with the one dimensional coal combustor program 1-DICOG [4] 117

Figure 5. 3: Classifier effect on size distributions for minerals for typical coal [27]118

Figure 5. 4: Algorithm chart for the calculation of particle sizes along with particle numbers for the given time step t..... 120

Figure 5. 5: Power-law particle size distribution of polish coal at different char burnout level using current described model 122

Figure 5. 6: Dunn-Rankin model power-law particle size distribution at different residence time [4]..... 123

Figure 5. 7: Polish coal different residence times: Comparison of model with experimental data (Cumulative mass fractions (w/w %))..... 124

Figure 5. 8: UK coal at different residence times: Comparison of model with experimental data (Cumulative mass fractions (w/w %))..... 125

Figure 5. 9: Wood chips at different residence times: Comparison of model with experimental data (Cumulative mass fractions (w/w %))..... 126

Figure 5. 10: Olive residue at different residence times: Comparison of model with experimental data (Cumulative mass fractions (w/w %))..... 127

Figure 5. 11: Straw at different residence times: Comparison of model with experimental data (Cumulative mass fractions (w/w %))..... 128

Figure 5. 12: Standard average deviation (%) of the model and experimental results for different fuels 129

Figure 5. 13: Polish coal and Straw during combustion at 1300 ms: Comparison of model with experimental data (Cumulative mass fractions (w/w %))..... 131

Figure 6. 1: Conceptual plan of the overall ash formation modelling.....140

Figure 6. 2: Modeled vs. experimental overall elemental mineral release - Polish coal 147

Figure 6. 3: Modeled vs. experimental overall elemental mineral release – Olive residue.....	148
Figure 6. 4: Modeled vs. experimental particle size evolution - Polish coal.....	149
Figure 6. 5: Modeled vs. experimental particle size evolution - Olive residue	149
Figure 6. 6: Mineral elemental distribution in different ash particles formed after combustion for Polish coal.....	152
Figure 6. 7: Mineral elemental distribution in different ash particles formed after combustion for Olive residue.....	153
Figure B. 1: Particle size distribution of raw coals and biomass fuels.....	166

List of Tables

Table 2. 1: Proximate and Ultimate analysis of Biomass [29]	17
Table 2. 2: Summary of the three-fold char structure classification system by Bailey and Benfell [30]	20
Table 3. 1: Ranking of test fuels according to their ash and volatile matter content..	53
Table 3. 2: Qualitative prediction of the devolatilization, char conversion and fragmentation	73
Table 5. 1: Analytical solutions for the different modes of fragmentation along with burning.....	119
Table 6. 1: Overall elemental releases of minerals.....	145
Table 6. 2: Particle size distribution along with their cumulative mass fractions and mineralogical composition.....	146
Table A. 1: Proximate and ultimate analyses.....	164
Table C. 1: Mass fraction of different particle sizes at different residence time.....	167
Table C. 2: Elemental mineral composition and mass fraction for different ash particle sizes at different residence time for Wood chips	168
Table C. 3: Elemental mineral composition and mass fraction for different ash particle sizes at different residence time for Waste wood	169
Table C. 4: Elemental mineral composition and mass fraction for different ash particle sizes at different residence time for Olive residue	170
Table C. 5: Elemental mineral composition and mass fraction for different ash particle sizes at different residence time for Straw	171
Table C. 6: Elemental mineral composition and mass fraction for different ash particle sizes at different residence time for Polish coal.....	172

Table C. 7: Elemental mineral composition and mass fraction for different ash particle sizes at different residence time for UK coal.....	173
Table C. 8: Elemental release at different residence times.....	174
Table D. 1: Fragmentation rate constants.....	175
Table D. 2: Particle size evolution at 20 ms (model and LCS-experimental results).....	176
Table D. 3: Particle size evolution at 90 ms (model and LCS-experimental results).....	177
Table D. 4: Particle size evolution at 210 ms (model and LCS-experimental results).....	178
Table D. 5: Particle size evolution at 1300 ms (model and LCS-experimental results).....	179
Table E. 1: CCSEM analysis of Polish coal.....	180

Nomenclature

c_i	Mass fraction of the mineral element obtained in the different cascade impactor stages (wt%)
M_i	Total mass of the mineral element obtained in the different cascade impactor stages (Kg)
c_0	Mass fraction of the mineral element in the feed (wt%)
M_0	Total mass of the mineral element in the feed (Kg)
G	Gas plus aerosol mass added to the gas stream (Kg)
L	Losses of the Lab-scale Combustion Simulator (LCS) (Kg)
$\dot{\eta}_s$	Recovery in the cascade impactor out of the total feed in the Lab-scale Combustion Simulator (LCS) (wt%)
$\dot{\eta}_r$	Release out of the total feed in the Lab-scale Combustion Simulator (LCS) (wt%)
M'_0	Initial mass number of the each size bin having $m_{1(0)}$ and $m_{2(0)}$ weighted particles with $N_{1(0)}$ and $N_{2(0)}$ particle numbers respectively (Kg)
G'	Total char conversion for each size bin due to devolatilization and char oxidation (wt%)
$m_{1(0)}$ and $m_{2(0)}$	The mass of the particles of size class 1 and 2 respectively for the raw fuel at time step $t=0$ (Kg)
$N_{1(0)}$ and $N_{2(0)}$	The particle numbers of the size class 1 and 2 respectively for the raw fuel at time step $t=0$
$m_{1(t)}$ and $m_{2(t)}$	The mass of the particles of size class 1 and 2 respectively after certain char burnout and fragmentation at time step t (Kg)
$N_{1(t)}$ and $N_{2(t)}$	The particle numbers of size class 1 and 2 respectively after certain char burnout and fragmentation at time step t
b_{ij}	Progeny matrix (the number of fragments that enter higher size bin i per particle that fragments in lower size bin j)
γ	Ratio between the larger and smaller particle sizes of each size bin
Q	Particle burning rate (Kg/m ² Sec)
D_p	Particle diameter (m)

ρ_{pc}	Apparent density of the particle having mass m_c and diameter D_p (Kg/m ³)
dm_c/dt	Mass loss rate (Kg/Sec)
x	Particle Diameter (m)
C_i or A	Burning rate constant
S_i or B	Fragmentation rate constant

Chapter 1

Introduction and Objectives

1.1 Introduction

Several technologies are used to generate electricity worldwide. Compare to the other technologies such as hydro power station, wind mill, solar and nuclear power station have limited resource availability; thermal power station is the most suitable technology in terms of resource availability, capacity, cost and uninterrupted quality power [1, 2]. Solid hydrocarbon fuels such as coal and biomass are the potential natural resources for the generation of electricity using thermal power stations worldwide due to easy availability, transportation and cheap cost etc. It is also known that co-firing of coal with appropriate biomass can reduce the emissions of GHGs (green house gases) and other pollutants [3]. For example, reactions of sulfur from coal with alkali chlorides from biomass during co-firing significantly reduce the SO_x emissions and also lower the corrosive behaviour of the deposited ash [4]. Despite of several advantages, one of the major problems with the use of coal and biomass is the ash related issues such as slagging, fouling, corrosion, erosion and environmental and health hazards etc. [2, 5, 6]. The ash related problems during solid fuel combustion or co-firing can be minimized if we are able to measure or predict them at the design stage or well before their values reach beyond their critical limits in the existing running set up.

Extensive research has been carried out for more than three decades to address the ash related issues with the use of the coal [2]. Biomass is considered as new generation fuel and several issues still exist regarding how biomass material will behave in boilers in terms of combustion and ash related issues [7]. Coals and biomass contain various inorganic matters along with organic structure. The organic matter gets burnt during combustion leaving inorganic residue termed ash. Ash formation during combustion is a complex mineral evolution process due to several

physical and chemical transformations occurring just in milliseconds after fuel enters to the furnace. Several methods/ models/ submodels/ tools are developed to predict or measure the slagging, fouling, corrosion, erosion and environmental and health hazards etc [8, 9,10]. The predictive tools for the slagging, fouling, corrosion, erosion and aerosol formation often need input in terms of particle size distribution of ash, their respective mass fractions and mineralogical composition at different time steps in the furnace [10]. The particle size distribution of the ash, their respective mass fractions and mineralogical composition are usually obtained using expensive and time consuming lab/pilot/plant scale trails. Several models are also developed in this area to avoid such expensive and time consuming trails.

The present research is about predicting the extent of ash formation mechanisms occur during PF combustion or co-firing of different coal and biomass. The developed understanding on the ash formation mechanisms from the present research work will be quite useful for the prediction of several ash related problems.

1.2 Objectives

Solid fuels such as coal and biomass undergo various chemical and physical transformations (devolatilization, char oxidation, fragmentation and gas to particle conversion followed by nucleation, coagulation and condensation etc.) just in milliseconds after fuel enters to the furnace. These transformations depend on several operating parameters (temperature, pressure, heating rate etc.) along with chemical and physical properties of the fuel (ash, moisture content, density, porosity, mineral matter composition and their association in the fuel matrix, particle size, shape and density etc.). The resultant ash formed after such parallel transformations in relation with several physical and chemical transformations along with the operating parameters will have different particle size and mineralogical composition compared to the original fuel.

Physical and chemical properties will significantly vary for different coals and biomass fuels due to their age, rank, handling etc. [11]. Moreover, mineral distribution after milling and classifying will also be dissimilar in different particle sizes of the similar fuel [12]. The operating parameters can also be different for different combustion technologies Atmospheric Fluidized Bed Combustors (AFBC),

Pressurized Fluidized Bed Combustors (PFBC), Pulverised Fuel Combustor and Grate Combustor etc). Therefore, extent and criticality of the several chemical and physical transformations will be different for the different fuels especially with different firing technologies [13].

This PhD project is an extension work of Doshi's PhD work [14] at Curtin university of Technology in collaboration with Energy research centre of the Netherlands. Doshi [14] modeled the ash release during PF combustion by using chemical fractionation and FACTSage (thermo-chemical equilibrium calculations) and validated for different coal and biomass. Doshi [14] also modeled the aerosol formation by simple calculations on gas-to-particle conversion for alkali chlorides and alkali sulfate.

In an extended effort, the main objective of the present research work is to study and model the several ash transformation mechanisms responsible for coarse ash formation during combustion and/or co-firing of several coals and biomass.

A research strategy has been devised as outlined below (in Candidacy report):

1. Characterize and quantify the ash formed in terms of particle size and mineralogy.
2. Quantify the release of mineral element under given operating conditions
3. Model the various ash formation processes for the development of CAT (Co-firing advisory tool) at Energy research centre of the Netherlands (ECN)
4. Define methods/sub models, either empirical or mathematical, so as to arrive at:
 - a. The composition of the gaseous phase as well as the concentration of inorganic elements released;
 - b. The composition and particle size distribution of fly-ash
5. Use ash deposition post processor at ECN to model the ash deposition
6. Applications of CAT to new processes such as Ultra Super Critical vapor characteristics, Oxy fuel combustion

The detailed ash formation map (particle size distribution along with their respective mass fractions and mineralogical compositions etc.) after combustion is really helpful for predicting various ash related problems in the solid fuel firing. Therefore, rather than directly working on the several ash related problems (slagging, fouling, corrosion, erosion, environmental and health hazards etc.), the present work focuses on deriving the ash formation mechanisms during the combustion process in terms of particle size distribution, mass fractions and mineralogical composition.

A detailed literature review is carried out on the ash formation during solid fuel firing and based on that the objectives are further refined in the chapter 2. The proposed project is aimed at making major contributions to the development of Co-firing Advisory Tool (CAT) at ECN by focusing on specific aspects of CAT that require further in-depth R&D.

1.3 Outline of thesis

The outline of the thesis is presented as a block diagram in Figure 1.1.

The thesis commences with Chapter Two which is a literature review on the current status of the investigations about the ash formation process during pulverized fuel combustion. This chapter mainly provides a review about the effect of the operating parameters and the fuel characteristics on ash formation. Analytical methods available and used so far in this field are also reviewed. This chapter also highlights the modeling efforts made to date in this field. Finally, the chapter concludes with the specific objectives based on the literature review which is targeted further in this PhD work.

Chapter 3 describes the enormous experimental study carried out on the Lab scale combustion simulator (LCS) under typical pulverized fuel firing conditions (i.e. high heating rate (10^5 K/s) and high temperature (1450 °C-1600 °C)) with six different coals and biomass to investigate the first line physical transformations such as char oxidation, devolatilization and fragmentation. A qualitative predictive tool has been suggested to predict the extent of these first line physical transformations.

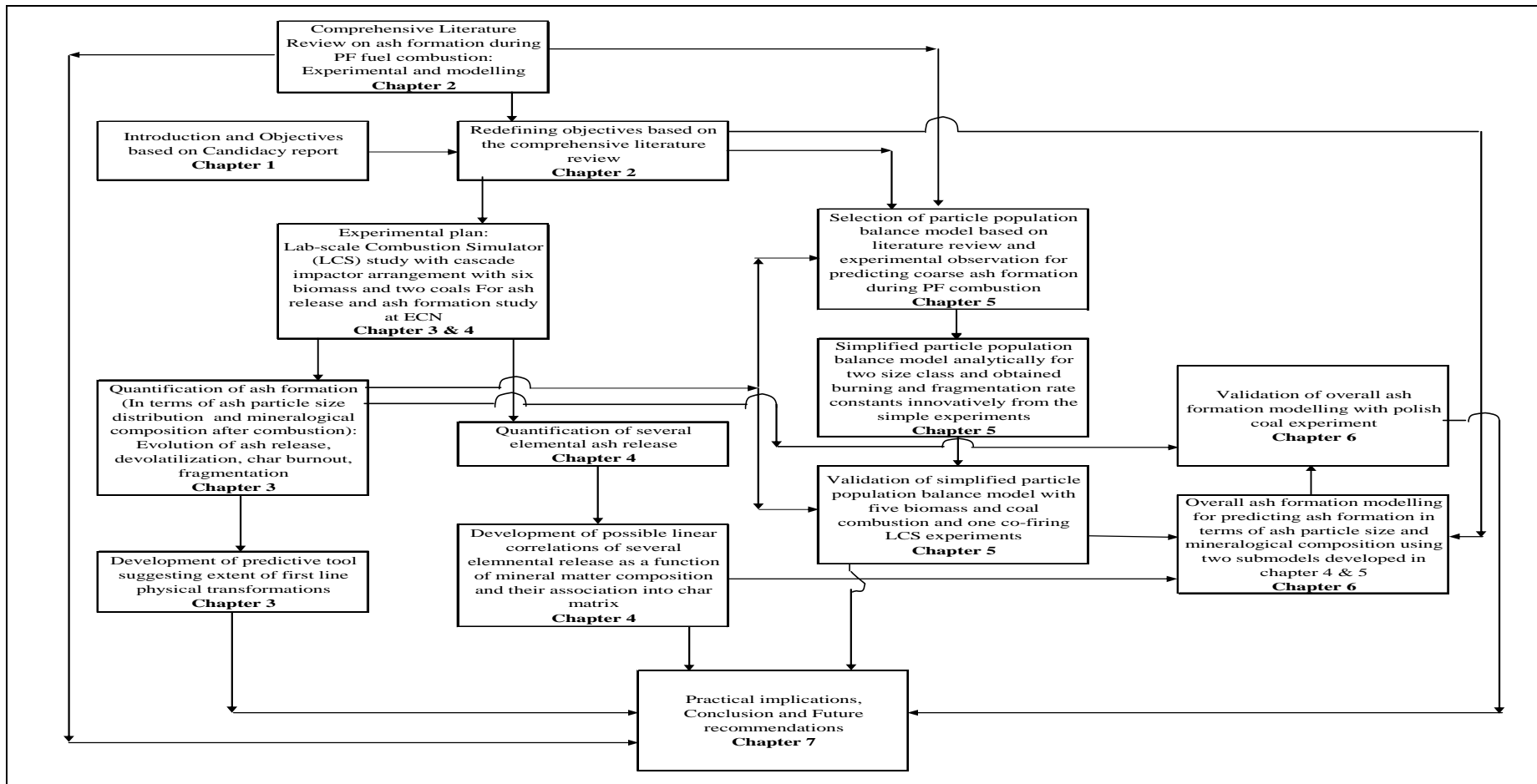


Figure 1. 1: Outline of Thesis

Chapter 4 explains the detailed experimental study on the devolatilization of several volatile minerals under typical PF-firing operating conditions. The release of potassium, sodium, calcium, magnesium, chlorine and sulfur has been investigated for the total eight different coals and biomass and simple but novel linear correlations (empirical indices) with ($>0.95 R^2$ value) have been attempted for the same as a function of mineral matter elemental composition and their association to the fuel matrix. It is also concluded that such indices work well for the group of fuel having similar physical and chemical characteristics.

In Chapter 5, a mathematical model is developed to predict the particle size evolution during combustion. The particle population balance model developed by Dunn-Rankin and Mitchell has been selected from the literature review and experimental observations made in chapter 2 and chapter 3 respectively. This model is simplified analytically for two size classes. Moreover, the burning and fragmentation rate constants derived from the experiments are incorporated into the model. The model is validated with five different coal and biomass combustion experiments conducted on Lab-Scale combustion simulator (LCS) at ECN. The model gives good agreement with experimental results with 10-15% standard average deviation. Model validation with LCS co-firing experiments is also done for Polish coal (37%) and Straw (63%) combination. The model works well with maximum of 15-20% standard average deviation for the experimental results. However, the model is at initial stage of development and needs to be improved further in many areas.

The empirical indices developed for ash release and the simplified particle population model described in chapter 5 works well separately. The ash formation modeling is also attempted in Chapter 6 by integrating both of the above sub models with a relatively simple approach. The model predicts the devolatilization, particle size distribution, their respective mass fractions and mineralogical composition after combustion. It has been validated with Polish coal and Olive residue experiments. The model needs to be further improved in many areas. The set of assumptions applied so far should also be re-addressed to improve the model outputs.

The final chapter (Chapter 7) ends with practical implications and conclusions drawn from the present work followed by recommendations for the future work to refine the modeling tool.

References

1. P. Breeze, Book on Power generation Technologies, ISBN-13: 978-0-7506-6313-7, Elsevier, (2005).
2. L. Baxter, Biomass-coal co-combustion: opportunity for affordable renewable energy, *Fuel* 84 (10) (2005) 1295-1302.
3. S. van Loo, Handbook of biomass combustion and co-firing, Twente University press, Enschede (2002).
4. J. Robinson, H. Junker, L. Baxter, Pilot scale investigations of the influence of Coal-Biomass co-firing on ash deposition, *Energy and Fuels* 16 (2002) 343-355.
5. J. Fernandez, O.L. Wendt, M. L. Wittenb, Health effects engineering of coal and biomass combustion particulates: influence of zinc, sulfur and process changes on potential lung injury from inhaled ash, *Fuel* 84 (2005) 1320-1327.
6. H. Westberg, M. Bystrom, B. Leckner, Distribution of potassium, chlorine and sulfur between solid and vapor phases during combustion of wood and coal. *Energy and Fuels* 17 (2003) 18-28.
7. R.P. Gupta, C. Beacher, A. Bhargava, T. F. Wall, The fate of Inorganic matter in biomass during combustion, 19th Annual Pittsburgh coal science conference (2002).
8. Z. Maa, F. Imana, P. Lua, R. Searsa, L. Kongb, A.S. Rokanuzzamanb, D. P. McCollorb and S. A. Bensonb, A comprehensive slagging and fouling prediction tool for coal-fired boilers and its validation/application, *Fuel Processing Technology* 88 (2007) 1035-1043.
9. N. Syred, K. Kurniawan, T. Griffiths, T. Gralton, R. Ray, Development of fragmentation models for solid fuel combustion and gasification as subroutines for inclusion in CFD codes, *Fuel* 86 (2007) 2221–2231.
10. K. A. Christensen, H. Livbjerg, A Plug Flow Model for Chemical Reactions and Aerosol Nucleation and Growth in an Alkali-Containing Flue Gas *Aerosol Science and Technology* 33 (2000) 470–489.

11. L. Terttalisia, Ash formation in circulating fluidized bed combustion of coal and solid biomass, PhD thesis, Helsinki University of Technology, Finland, (1999).
12. F. Wigley, J. Williamson, W. H. Gibb, The distribution of mineral matter in pulverized coal particles in relation to burnout behavior, Fuel 76 (13) (1997) 1283-1288.
13. European Biomass Industry Association official website <http://www.eubia.org/333.0.html>
14. V. Doshi, H. B. Vuthaluru R. Korbee, J.H.A. Kiel, Development of a modeling approach to predict ash formation during co-firing of coal and biomass, Fuel Processing Technology 90 (9) (2009) 1148-1156.

Chapter 2

Literature Review

This chapter provides a review on typical fuel characteristics and operating parameters responsible for ash transformations during pulverized fuel combustion based on critically reported investigations and modeling efforts to date. The present work briefly describes the different basic analytical methods used by researchers so far to measure various parameters responsible for ash formation. It also recognizes the modeling efforts made to date covering simple calculations up to advance numerical simulations. Finally, it concludes with the summary of information on ash formation along with future research needs in this field. The objectives are finally set based on the critical literature review.

2.1 Introduction

Pulverized coal and a variety of biomass fuels are used as a feed in the power station boilers, where a large amount of thermal energy is generated because of the exothermic reaction taking place during the combustion of fed hydrocarbon which is later converted to electrical energy by several other means. The mineral matter present in quite significant proportions alongside with the hydrocarbons usually fragments, devolatilize (evaporates) and subsequently partly condenses during combustion. This inorganic, mineral residue after combustion, commonly called ash, travels towards the smokestacks carried by the flue gas, may lead to various operational problems such as slagging, fouling, corrosion and erosion of heat exchanging, internal boiler and flu gas duct surfaces etc.

Extensive studies on ash formation during combustion have been conducted World-wide. As a result, theories on ash formation mechanisms have been formulated and described in detail by several researchers [1,2,3,4,5]. It is evident from several experimental investigations that solid fuel particles undergo various physical transformations during combustion, as shown in Figure 2.1. The important physical

transformations are fragmentation and/or coalescence and vaporization. It is postulated that the fragmentation/coalescence of the ash/char particles along with chemical oxidation and physical devolatilization, will lead to coarse ash formation. The vaporized minerals chemically react with other gas-borne matter, and may condense homogeneously or heterogeneously to form submicron aerosols and fine ash particles. The physical and chemical transformations during thermal conversion of solid fuel are time-dependent and very difficult to understand as a continuous process.

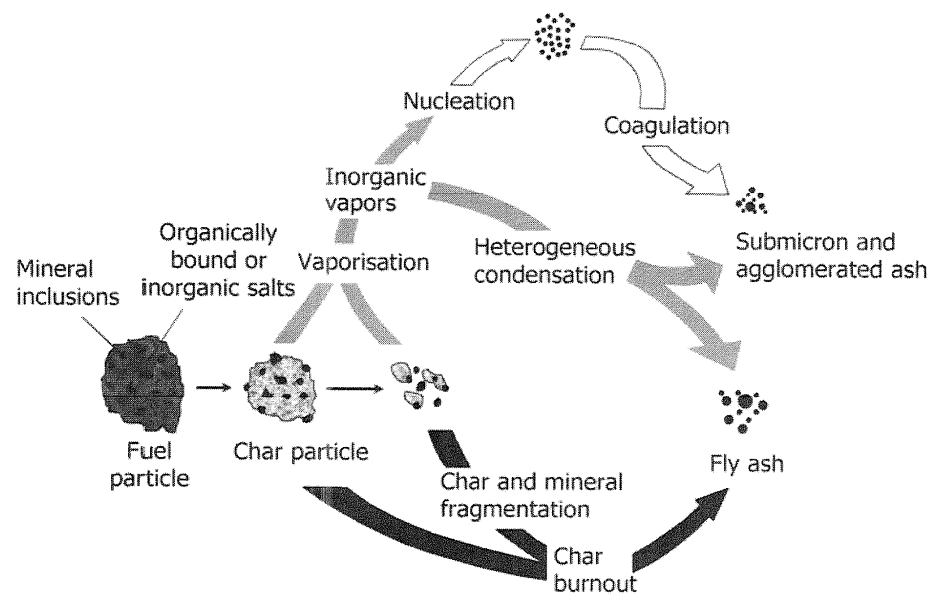


Figure 2. 1: Physical transformations involved for ash formation during coal/biomass combustion [2]

These physical and chemical transformations of minerals depend on several fuel characteristics i.e. fuel, fixed carbon, volatile matter, total ash content and mineral matter elemental composition, mineralogy (either included or excluded especially for coal), char reactivity, char morphology, density, particle size etc. The fuel characteristics will be different for different fuels according to their age, formation history and handling. This chapter highlights the effects of all the above fuel characteristics on ash transformations during combustion.

The mineral transformations can also be significantly influenced by several operating conditions i.e. mode of combustion, temperature, pressure, heating rate, residence time, reaction kinetics of various mineral gaseous, slag and solid species etc.

Currently, a broad range of technologies is available for the combustion and co-firing of coal and biomass. These include: Atmospheric Fluidized Bed (AFBC), Pressurized Fluidized Bed (PFBC), Pulverized Fuel (PF) and Grate Fired (GF) combustors. All the technologies have their own advantages and limitations [6]. The route of mineral transformations will be similar in nearly all the mentioned options, but the extent and criticality will be different for each technology due to differences in operating conditions. The present chapter reviews mainly the efforts made to identify the effect of the mentioned operating parameters on ash transformations during pulverized fuel (PF) combustion.

Experiments ranging from lab-scale-combustion simulators to pilot- and plant-scale furnaces under laminar- through turbulent flow conditions, are usually designed and analyzed to understand the ash formation processes during combustion. To date, several methods/ sub models/ models have been employed to study and identify the effect of different fuel characteristics and operating parameters on ash formation. The present work also briefly reviews some of the basic analytical methods used to measure various parameters responsible for ash formation. It also highlights the modeling efforts undertaken to date, ranging from the simple calculations to advanced numerical simulations for predicting the ash transformations during PF combustion. As there appears to be a lack of a comprehensive literature review to date covering all of this basic information related to ash transformations, such synthesized information may give an overview on the updates in the concerned field. Furthermore it also gives some insight on the future research needs in this area.

2.2 Parameters responsible for mineral transformations during PF combustion

2.2.1 Fuel mineral matter composition and their association

Coal and Biomass (or their blend) can be subjected to different ash formation mechanisms during pulverized fuel (PF) combustion, as the fuel mineral matter composition and their association varies greatly in different fuels. The mineral matter in the fuel may be present in the form of free ions, salts, organically bound or as excluded minerals. The lignite and woody biomass contain a major fraction of

volatile compounds (and less excluded minerals) compared to Bituminous or anthracite coals. Alkalis in low rank coals and woody biomass, remain primarily in included minerals as free ions, salts and organically associated inorganic elements and start vaporizing at lower temperatures. Even before reaching the char burnout, these vaporized species will chemically react and will condense, nucleate and coagulate on each other or onto the furnace surfaces, to produce submicron ash. Other elements such as calcium and magnesium partly devolatilize, fragment or coalesce [3,7]. Thy [8] found that if alkali metals occur as network-modifying and charge balancing cations in highly depolymerized melts, such as typical for wood ash, they are easily evaporated during prolonged heating and subsequently deposit onto the heat exchanger surfaces. However, if the melt is highly polymerized such as in the case for rice straw, where alkali metals occur as network modifying cations, they are strongly retained in the polymerized network. During diffusion-limited char combustion, the interior of the particle becomes hot and fuel rich. The non volatile oxides (e.g. Al_2O_3 , SiO_2 , MgO , CaO , Fe_2O_3) can be reduced to more volatile suboxides or even down to elements, and partly vaporized. These reduced species re-oxidize while passing through the boundary layer surrounding the char particle, becomes instantaneously highly supersaturated which make them nucleate homogeneously [9].

Ash melting behavior is affected by the elemental composition of ash (alkali metals, phosphorous, chlorine, silicon and calcium species), as well as the chemical concentration of the compounds which can alter reaction kinetics of the fuel combustion. Commonly analyzed ash-forming elements are silicon (Si), aluminum (Al), iron (Fe), calcium (Ca), magnesium (Mg), manganese, (Mn), sodium (Na), potassium (K), phosphorus (P), sulfur (S) and chlorine (Cl).

Baxter [10] studied three different ranks of coal (high-volatile bituminous, sub-bituminous, and lignite) and observed that for high-volatile bituminous coals more than 100 fly ash particles were formed from a single 80 μm (initial diameter) char particle, whereas only 10 fly ash particles are produced from single 20 μm (initial diameter) char particle. However, regardless of its initial size, fragmentation of lignite particles was far less extensive, with less than five fragments from a single char particle.

The volatile inorganic matter content is one of the most important parameter in coal and biomass as far as submicron particulate formation is concerned. Buhre et al. [11] observed that formation of submicron aerosol ash particles during coal combustion is mainly due to condensation of evaporated species and not due to the fragmentation.

2.2.2 Mineralogy

Mineralogy of coal and biomass can also play a critical role in various physical and chemical transformations. Physically, the inorganics can be present as included and excluded minerals in the fuel especially for coal. Excluded minerals present in biomass are mainly a result of the contamination with soil during the harvest or handling while presence in coal is due to mining or handling. It is quite obvious that the amount of excluded minerals in most of the biomass fuels will be significantly lower than the in coals, of which deposits are inherently in close contact with rocks and soil. Included minerals in the biomass are the inorganics required for plant growth; and as such they are still present in coals even after millennia of peatification and coalification [12], however their physical and chemical form may be altered by the said geological processes.

Included minerals have a higher tendency to remain in the char during combustion. Due to exothermic reactions occurring in the char during combustion, the included mineral matter can reach very high temperatures (above the temperature of the surrounding flue gas). As included minerals are situated close to each other, reactions between them can easily take place. Included minerals may contain more volatile inorganic matter than excluded minerals. The volatile minerals from the included and excluded minerals will be vaporized in the early stage of combustion. The vaporized minerals will condense later on to produce sub-micron ash. During char burnout, the included minerals may either appear as molten particle on a reducing char surface or as a lattice network in char particle. As char burnout proceeds, the minerals may coalesce within a single particle or fragment into several smaller entities. The extent of fragmentation or coalescence depends on several operating parameters and fuel characteristics. This subject has been studied in detail by many research groups, combining both experimental as well as modeling work. Wilemski et al. [13] and Kang [14] tried to validate experimental results with no and a full coalescence limit.

Morone in her PhD thesis [15] reported that a partial coalescence is likely to occur in real life systems. Helble et al. [16] observed very small number of fragments being created during devolatilization. Wilemski et al. [17] later on validated his shrinking core model with partial coalescence limit. Wigley et al. [18] stated that coal particles containing included mineral matter will have a greater specific heat capacity than particles consisting of organic material alone, hence included particles would be expected to heat up and combust more slowly. Included minerals may fuse and coat the surface of burning char particles, reducing the rate of char combustion. On the other hand, the included mineral matter may catalyze char combustion. The difference in thermal expansion between included minerals and their organic matrix may cause localized thermal stress, thus, leading to an increased char fragmentation. Agglomeration may occur when particles collide or when they meet on a deposit surface on a boiler wall or tube. Mitchell [19] observed attrition, breakage and percolative-type fragmentation of included minerals during the devolatilization stage. Excluded minerals (especially in the case of coal) on the other hand will reach lower temperatures than included minerals, and they will not be influenced by locally reducing environment. The transformations occurring in excluded minerals and the behavior with respect to the ash deposition may therefore be significantly different from included minerals. Excluded minerals can either be carried through the combustion system with their original structure intact or they can melt and fragment. Decombe et al. [20], Yan et al. [21] and many others concluded that excluded minerals always fragment randomly, due to thermal stress. Brink et al. and Yan et al. [22,23] observed that calcite and pyrite as excluded minerals fragment at high temperature and high heating rate conditions while siderite and ankerite grains did not fragment at the same conditions.

2.2.3 Particle shape, size and density

Experimental and theoretical investigations indicate that particle shape, size and density influence particle dynamics, including drying, heating rate and oxidation reaction rate [24]. It is generally observed that spherical particles devolatilize quickly compared to other shape particles. Badzioch et al. [25] found that particle size had no significant effect on the weight loss because the heating rate of the particle was controlled mainly by the heating rate of the carrier gas, so that the large particles

heated only at slightly lower rates than the fine particles. Mathews et al. [26] observed that mineral matter and macerals composition of the char will be different for different particle sizes, which can affect the devolatilization rate. Syred et al. [27] and Decombe et al. [20] observed that large particles form more fragments than small particles, likely due to larger internal temperature gradient. Wigley et al. [18] confirmed that a decrease in char particle size may lead to more complete combustion. Decombe et al. [20] suggested the relationship of fragmentation extent with compressive strength as shown in Figure 2.2. However, compressive strength of the coal particle is inversely proportional to the particle size.

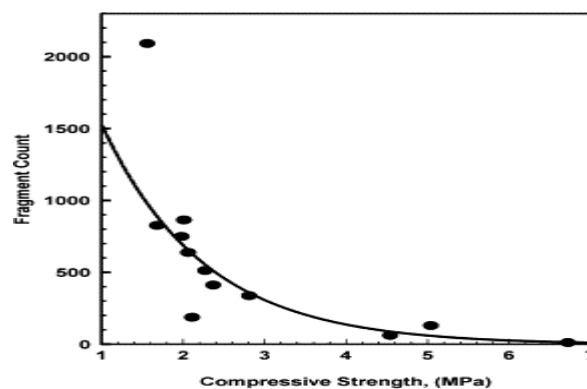


Figure 2. 2: Variation in the extent of the fragmentation of a coal against compressive strength. [20]

The ash transport behavior is affected to a large extent by the size of the particle after combustion. Large ash particles tend to impact onto boiler heat transfer surfaces by inertia, whereas fine ash particles tend to reach wall surfaces by thermophoresis or Brownian motion. For example, a 60 micrometer ash particle was estimated to reach the deposit surface almost three times faster compared to 30 micrometer particle primarily due to inertial effect. [21].

Liu et al. [28] studied Chinese bituminous coal with three density fractions. The fragmentation was severe with light density fractions as shown in Figure 2.3. The median size of each coal fraction was almost the same. The reasons for the above were particle size, mineralogy and swelling ratio. The light fraction and the medium fraction of the coal contained mostly included minerals, and the heavy fraction contained largely excluded minerals.

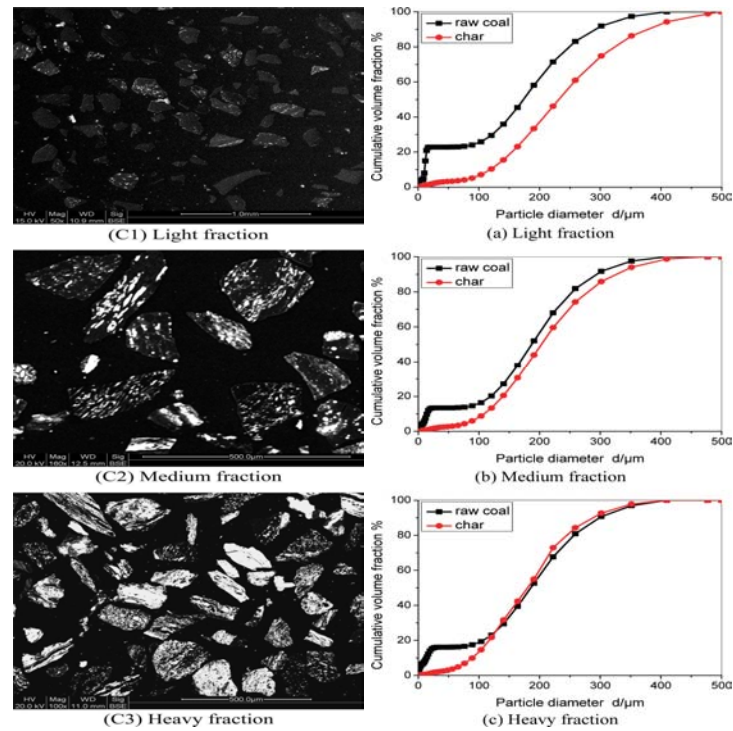


Figure 2. 3: BSE images with Comparison of PSD (by Volume) of char and Coal [28]

2.2.4 Fuel characteristics after milling

Milling of raw coals or biomass fuels, i.e. fineness of the material after grinding as well as the applied mill technology, has a profound effect on ash formation. It has been observed by several researchers that mineralogy, ash percentage, volatile matter, density and char reactivity will be different for different particle size ranges (PSD). Bridgeman et al. [29] studied two energy crops (switchgrass and reed canary grass) in terms of their physical and chemical properties in different size fractions after grinding with ball mills at lab scale. The results summarized in Table 2.1 indicate that smaller particles of the two grasses have a significantly higher concentration of inorganic matter as well as the moisture content than larger particles. In contrast the larger-sized fractions had higher carbon content and lower nitrogen content, with a resulting higher calorific value. The volatile content was also higher in the larger sized fraction.

However, Wigley et al. [18] stated that the presence of included mineral matter could alter the size distribution of pulverized coal particles leaving the mill classifier and entering the boiler. The mineral inclusions will increase the average density of a coal

particle. As classifiers separate particles on a combined size and density basis, denser coal particles would be expected to be slightly finer.

Table 2. 1: Proximate and Ultimate analysis of Biomass [29]

Ultimate, proximate and CV analyses of different size fractions of reed canary grass and switchgrass (Institution 1), where RCG = reed canary grass, and SW = switchgrass					
%		RCG < 90	RCG > 90	SW < 90	SW > 90
		μm	μm	μm	μm
Moisture		6.45	5.71	8.64	7.93
Ash		6.0	3.62	6.88	3.12
Volatiles		72.62	74.89	70.58	72.57
Fixed carbon		14.92	15.78	13.9	16.37
C		43.56	44.9	42.33	44.32
H		6.1	6.14	5.98	5.99
N		0.47	<0.04	0.23	0.03
O		37.65	39.07	37.58	38.24
CV (kJ/kg)	Measured	17,100	17,700	16,600	17,100
	OLS	17,200	17,700	16,700	17,500
	PLS	17,300	17,800	16,800	17,500

The observations on particle size distribution do indicate that included minerals have slightly finer size distributions than organic-rich particles, and the very largest particles are almost purely organic, as shown in Figure 2.4.

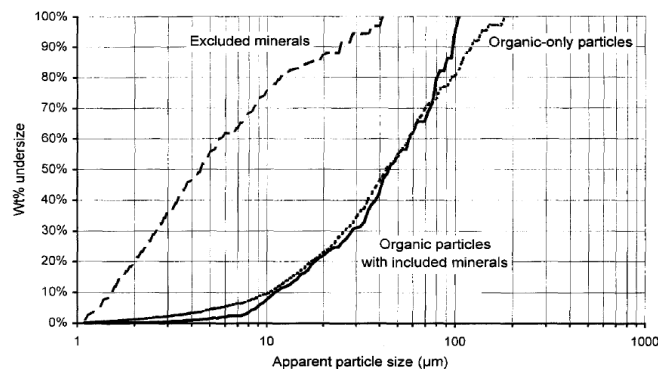


Figure 2. 4: Classifier Effect: Size distributions for excluded minerals, organic particles with included mineral, and organic-only for typical coal [18]

2.2.5 Char structure

The change in the internal structure of a char particle is one of the most important issues during coal devolatilization and is closely associated with the coal particle swelling phenomenon, during the plastic stage. The extent to which the pore structure changes is dependent on the fuel type and is strongly affected by the

conditions under which the fuel is devolatilized [30]. Hurt et al. [31] concluded that CO₂ gasification reactions took place primarily on the surfaces of larger pores during kinetic-diffusion controlled regime. The fragmentation will be increased as char burnout shifts from a diffusion-controlled to a chemically-controlled regime [32] as shown in Figure 2.5. It was observed by many researchers that during the initial heat up and devolatilization in a kinetic-diffusion controlled regime, char particles do not change much in shape and size. As shown in Figure 2.6, Helble et al. [16] observed with a high speed camera (approximately 4000 frames per second) that at 1250 K and at high oxygen partial pressure (>0.80 atm) initially fragmentation occurs at the perimeter of the bituminous coal char particles. Mitchell [19] also mentioned attrition-type of behavior during the initial heat up and devolatilization of char particles. He also noted that large amount of aerosols were formed by the attrition of large particles from the peripheral diffusion in regime II which describes the particle burning rate during the char oxidation at high temperatures in which the characteristic rates for pore diffusion and chemical reaction are comparable, making both effects important in determining overall mass loss rates.

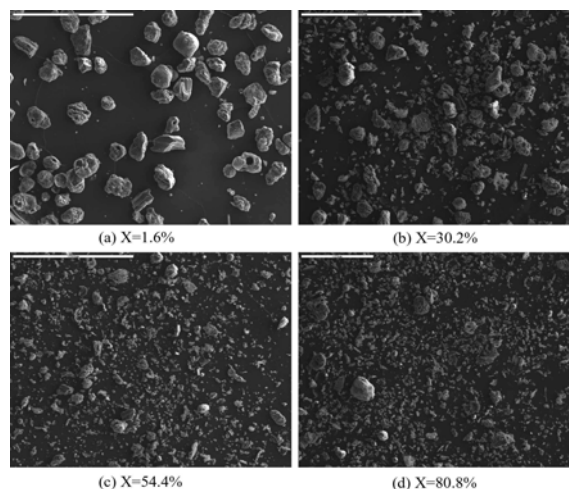


Figure 2. 5: SEM. images of char samples generated at various burnout levels at a gas temperature of 1300 C in a drop tube furnace under atmospheric condition. The scale bar is 500 μ m. [32]

Menendez et al. [33] ranked the most important char characteristics with gradual increase in combustion temperature as follows: (1) The total surface which may be accessible to the reacting gases; (2) Porosity of the char particle; and (3) Char particle size. These parameters are crucial in modeling of PF combustions and gasification. Mitchell observed a significantly higher degree of fragmentation, with

less porous chars during the heat-up and devolatilization stages, suggesting that the more open the porous char structure, the lesser will be the extent of fragmentation during heat-up and devolatilization, induced by either thermal stresses or stresses due to build-up of pressure of volatiles in the pore work.

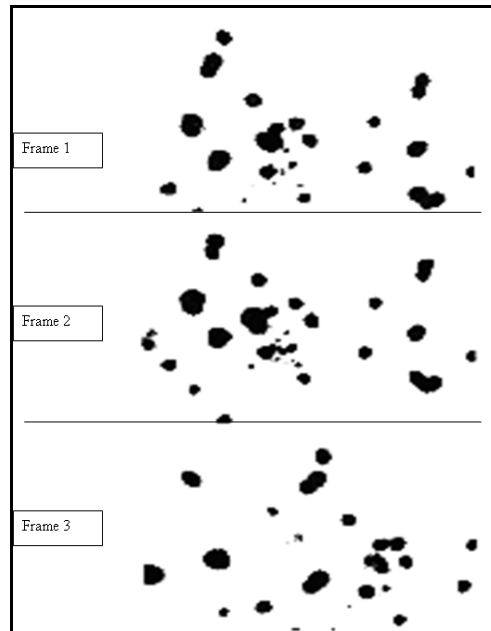





Figure 2. 6: Negative prints of three successive frames from high speed film (approximately 4000 frames per second) [16]

Highly porous char particles can attain the chemically-controlled regime earlier than dense chars, due to a higher extent of both the devolatilization and fragmentation. The fragmentation has also been found to have a significant impact on the chemistry of the final ash particles. Kaiho et al. [34] and Ezra et al [35] examined the role of pore structure in the fragmentation of highly-porous char particles and claimed that the reason for local fragmentation under non-uniform oxidation is the increase in the local macro-porosity. Kang et al. [36] with his experiments concluded that the fragmentation of a macro-porous char can influence the final ash size distribution.

Yua et al. [30] summarized extensive efforts made in the past decades to classify morphologically complicated char structures. Char structures have been classified on the bases of char morphological parameters including macro-porosity, the wall thickness, particle shape etc. [30, 37]. A three-group classification system (Table 2.2) suggested by Benfell and Bailey has been adopted by number of researchers [23, 30].

Table 2. 2: Summary of the three-fold char structure classification system by Bailey and Benfell [30]

Char groups	Group I	Group II	Group III
			
Char subtypes	Cenosphere tenuisphere, tenuinetwork	Crassisphere, crassinetwork, mesosphere, mixed porous (mixed dense)	Inertoid, solid, fusinoid (mixed dense)
Char particle shape	Spheroidal	Spheroidal to irregular	Subspheroidal, rectangular or irregular
Porosity	> 80%	> 50%	~50%
Pore shape	Spheroidal	Variable	Spheroidal to elongate and angular
Wall thickness	< 5 μm	Variable	> 5 μm
Dominant maceral components	Vitrinite	Vitrinite and inertinite	Inertinite
Swelling ratio	> 1.3	< 1.0	< 0.9

The macerals composition of coal plays a dominant role in the morphology of the char during devolatilization. Vitrinite-containing bituminous coal particles commonly produce cenospheric chars while the inertinite produces a char with low porosity.

For softening coals, the formation of different types of char structures is closely associated with their thermoplastic behavior such as fluidity and swelling during heating [30]. The porosity of the chars from non-plastic coal increases steadily with increasing temperature. Gale et al. [38] found that the overall porosity and swelling ratio of char increases with increasing heating rates up to 10^3 K s^{-1} , with a further increase in the heating rate above $2 \times 10^4 \text{ K s}^{-1}$ resulting in a decreased porosity and swelling, as shown in Figure 2.7. This is due to the rapid release of volatile matter than the relaxation time for expanding the char particle. The temperature gradient in a particle at a very fast heating rate may also affect the process.

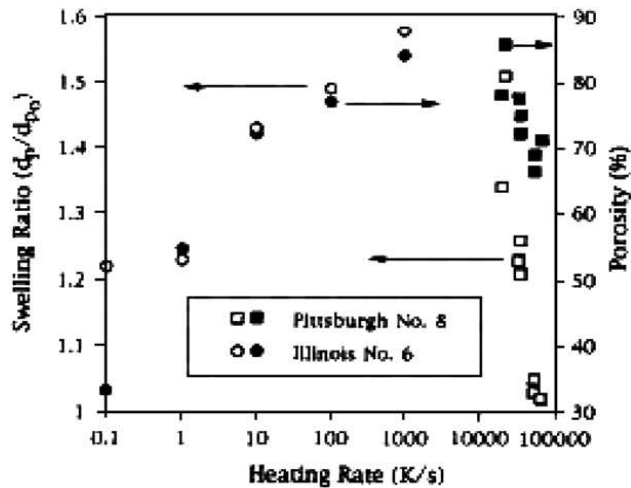


Figure 2. 7: The porosity and swelling ratio as a function of heating rate [30].

2.2.6 Other fuel characteristics

The ignition temperature of the fuel particle has an indirect relation with ash formation as it is an important parameter for defining the early start of the combustion process. A number of investigations [39] has been devoted to this issue and it was found that the ignition temperature decreases with an increase in particle size, oxygen partial pressure and volatile matter content. And larger particle size and higher volatile content can lead to various ash related problems.

Char reactivity is defined as the mass loss per unit external surface area. The average char reactivity was found to decrease with an increase in burn out levels but was ranging greatly even within the same particle size [39]. Koranyi et al. [40] found within a set of three British bituminous coals that a qualitatively good correlation exists between the char reactivity and its micro-porosity. Ash, moisture and fixed carbon percentages can also be interlinked with other fuel characteristics such as ignition temperature, char reactivity, char morphology, char mineralogy, char structure and particle size.

2.2.7 Relation with operating parameters

During the char oxidation at high temperatures, particle burning rates initially lie in the so called zone II burning regime, in which the characteristic rates for pore diffusion and chemical reaction are comparable, making both effects important in determining overall mass loss rates. As burning progresses, particles become smaller

and pores become enlarged, decreasing mass transport limitations. Thus, later in the burn-off, a transition is expected from the “zone II” burning regime to the zone I regime, in which chemical reaction rates are dominant in controlling overall mass loss rates [41]. Zone I, can be summarized as a chemically controlled regime and Zone II as a kinetic-diffusion controlled regime. In all the regimes, density and particle size are the most important parameters which change with mass loss rate simultaneously [19, 30, 41]. The effect of operating parameters will be different in the two regimes.

Heating rate has a significant effect on ash formation. The effect of heating rate will be different for included and excluded minerals, porous vs. non-porous structures and small vs. large-sized particles. Excluded minerals have more specific heat capacity and will therefore heat up slowly compared to included mineral matter or purely organic particles. Highly porous char that undergoes much more extensive devolatilization during heating will burn out at an earlier stage compared to less porous (solid) char particles; even though they burn at a similar “per carbon site” rate [42]. Large particles, although experiencing a higher temperature gradient making them susceptible to fragmentation, will heat up later than the small entities.

Temperature and pressure can significantly affect the extent of ash formation, as well as its characteristics. For instance, Erickson et al. [43] found in his experiments with synthetic coal in a drop tube furnace at temperatures of 900, 1100, 1300, 1500°C, and at constant heating rate conditions, that at high temperature fly ash formation was dominated by fragmentation, as shown in Figure 2.8.

Wu et al. [44] performed combustion experiments employing a bituminous coal with a size fraction of 63-90 micron, under oxidizing atmosphere (air) in a drop tube furnace (DTF) and a pressurized drop tube furnace (PDTF) at a gas temperature of 1300°C with same heating rate conditions and pressures of 0.1, 0.5, 1.0, and 1.5 MPa. As shown in Figure 2.9, ash generated at high pressure was found to be much finer than ash generated at low pressure due to the differences in the pressure gradient.

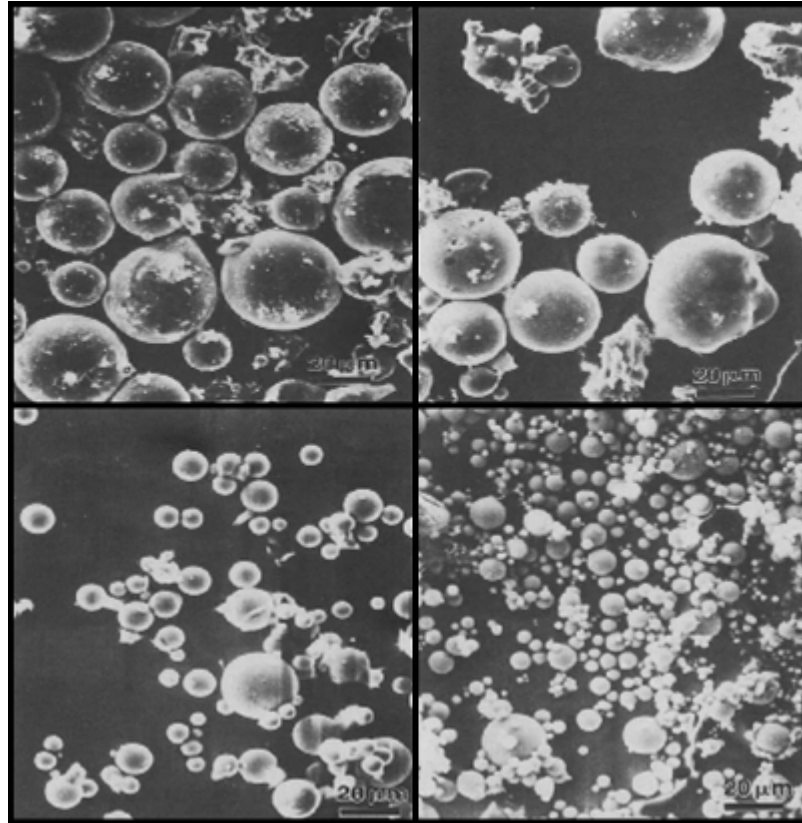


Figure 2. 8: Fly ash Particles formed at 900°C (left-top), 1100°C (right-top), 1300°C (left-bottom) and 1500°C (right-bottom) [43]

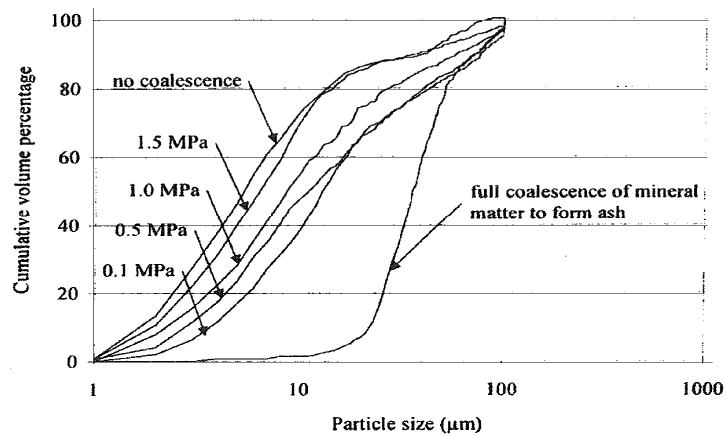


Figure 2. 9: Particle Size distribution of ash generated at different pressures [44]

Usually, PF combustion occurs at atmospheric pressure and high temperature with high heating rates (in excess of 10^5 K/s). Though operating parameters such as temperature, pressure, heating rate will be in a relatively narrow, specified range for PF combustion, the effect of operating conditions will be varying significantly for different fuels. The measures of the fuel characteristics such as char reactivity, ash,

moisture, volatile matter and fixed carbon percentages, as well as its density and porosity will also be different even within the same fuel with varying particle size. Therefore, each particle size range in single fuel will behave differently under PF combustion conditions. Kinetic reaction rates of the mineral chemical conversions are also highly dependent on several operating parameters (temperature, pressure, residence time etc.) and fuel characteristics (ash contents, mineralogy, particle size etc).

2.3 Prediction of ash formation during PF combustion

Extensive research has been carried out to identify the inorganic behavior during coal, biomass combustion and co-firing and many uncertainties have been clarified. Experiments ranging from lab-scale-combustion simulators to pilot- and plant-scale furnaces under laminar through turbulent flow conditions have been run and analyzed. Many methods/model/sub models starting from simple and traditional ash analysis to advance numerical modeling have been attempted based on the achieved understanding so far.

2.3.1 Analytical methods

Proximate and ultimate analyses of the fuel are considered as the most basic and necessary analyses that need to be carried out to understand the combustion characteristics of the fuel and deciding on optimum operating conditions in an installation of a particular design [45] . A typical proximate analysis includes the moisture, ash, volatile matter, and fixed carbon contents. It also gives an idea about the calorific value of the fuel. The ultimate analysis indicates the various elemental chemical constituents such as carbon, hydrogen, oxygen, sulfur, etc. It is useful in determining the quantity of air required for combustion and the volume and composition of the resulting combustion gases. However these analyses combined are only giving clues for optimal operating conditions and are incapable of measuring the mineralogical composition of the fuel [45].

The elemental analysis of a fuel/ash can be performed by means of several traditional methods such as atomic absorption spectroscopy (AAS), graphite furnace atomic

absorption spectroscopy (GFAAS), inductively coupled plasma atomic emission spectrometry (ICP-AES), inductively coupled plasma/ mass spectrometry (ICP/MS), X-ray fluorescence spectrometry (XRF), glow discharge mass spectrometry (GDMS) and spark source mass spectrometry (SSMS) [46]. Molecular beam mass spectrometry (MBMS) [47] and high pressure mass spectrometry (HPMS) [48] are also found to be used at lab-, pilot- or plant scales to measure the alkali gaseous phase release. Korbee et al. [49] and Frandsen et al. [50] used ICP-AES and SEM-EDX for finding the elemental characteristics for a range of coals and biomasses.

However, the traditional elemental analysis is of little use in getting insights into ash formation characteristics. To know about the mineral matter association in the fuel, pH-static leaching and chemical fractionation are often used. Doshi et al. [51] used these methods to analyze the mineral association in the fuel matrix, classifying the elements present as free ions, salts, organically bound and excluded minerals. This was done by measuring the solubility of inorganics in water, ammonium acetate and HCl. The free ions, salts and organically bound minerals easily devolatilize and are responsible mainly for aerosol ash formation, primarily through condensation processes during combustion. Excluded minerals remain in the solid form and play the primary role in coarse ash formation. However, the pH-static leaching and chemical fractionation methods were found to overestimate the release measured dynamically in lab-scale facilities. This is mainly due to the assumption that the entire 'reactive' fraction (the fraction of the inorganic elements leachable in water or ammonium acetate) is released into the gas phase during combustion. In a real combustion situation, the 'reactive' fraction may interact with the 'less reactive' fraction (leachable in HCl or not leachable at all), thereby decreasing the fraction of the inorganic elements being released to the gas phase [50].

Thermogravimetric analysis (TGA/ STA) is often used to find out the reaction kinetics of the fuel organics alongside with their included and excluded minerals. TGA measures the weight change in the materials as a function of time and temperature [52]. The measurements provide basic information about the thermal stability of the fuel and its composition. TGA is nowadays one of the most commonly applied thermal techniques used to characterize both char oxidation and devolatilization rates. It is often also used for predicting the total residence time

required for a fuel under given operating conditions. Lu et al. [52] studied the combustion kinetics for various coals and biomass using the TGA method. Vuthaluru et al. [53] used thermogravimetric analysis to study the pyrolytic behavior of coal and biomass blends. Hurt et al [54] did his kinetics study using TGA to investigate the fuel transformations during advanced coal combustion and gasification. Filho et al. [55] studied the kinetics of Brazilian coal while Zhaosheng et al. [56] and Miranda et al. [57] studied rice, wheat straw and olive residue using thermogravimetric analysis.

Traditional ash analyses and chemical methods are time-consuming and often of limited scope. Furthermore, such methods are incapable of providing physical characteristics like the size and shape of coal mineral particles and mineral distribution on a particle basis, which clearly play important roles in understanding the ash formation during combustion to the full extent [58]. For this purpose, computer controlled scanning electron microscopy (CCSEM) has been extensively used. This technique is relatively expensive, and still not very common and mostly used for research. Terma et al. [58] studied the ash transformations of coal during PF combustion by extensive use of CCSEM. Chen et al. [59] investigated the mineral matter composition of fine particulate matter of coal using CCSEM, while Wang et al. [60] used CCSEM to investigate the interactions of the inherent minerals. Yu et al. [61] studied six highly heterogeneous Chinese coals while Bruner et al. [62] studied bark, waste wood and wood chips using the CCSEM technique. The use of CCSEM has increased remarkably in the last two decades. It can be used to find out the mineral matter distribution along with organic matter in different size fractions of the raw fuel as well as ashes from various stages of the combustion process. Many unknown facts and uncertainties are made clear using CCSEM techniques, adding to a better understanding of the combustion process. CCSEM has been also used to identify and characterize ash particles in deposits, in order to gain insights into deposition and fouling characteristics of coals under conditions of various combustion regimes. In recent efforts, QEMSCAN has been used to determine mineral-mineral associations, particle size, mineral compositions, and particle texture in coal and ash samples. The above mentioned procedure is similar as CCSEM analysis, but characterized by an even higher degree of automation [63]. Vuthaluru et al. [64,65] have analyzed the ash chemistry and mineralogy of an Indonesian coal at

various stages of combustion. Many other coals have been analyzed using QEMSCAN. However, analysis of different biomass using the same is very limited to date.

Chemical transformations can be predicted using thermo-chemical equilibrium calculations based on Gibbs-free energy minimization principle. This method assumes that the chemical equilibrium exists at each time fraction but ignores any intermediate products. As an input, this method requires the elemental mineral matter composition in gas-slag-solid phases. It describes the composition of stable gas-solid species at different temperature conditions. The input elemental composition is provided using traditional ash analyses, possibly extended with the chemical fractionation method. Such an approach was used by Doshi et al. [51] who applied FACTsage (Thermo-chemical equilibrium software) to predict compositions of gas and solid species for different coal and biomass fuels.

Several empirical indices for several aspects of coal combustion and ash formation have been proposed based on the experiments performed at lab, pilot and plant scale in the function of mineral matter composition. These empirical indices quantify primarily various ash-related issues such as slagging, fouling, corrosion, erosion and aerosol formation etc. rather than lead to an in-depth knowledge of ash formation mechanisms. The well-known empirical indices are ash fusion temperature, base-acid ratio, slagging factor, T250°C temperature, iron/calcium ratio, iron plus calcium, slagging index, silica percentage etc. [66]. Large discrepancies were observed in the use of the majority of these indices on a wider range of coals, let alone for coals and biomass co-firing. The empirical indices were found to be a rather poor tool for the prediction of ash formation or deposition behavior [67]. Nonetheless for an isolated set of fuels and under constant firing conditions, where variations in mineral matter are small, mechanisms of ash formation and depositions are consistent and operating and design variables remain constant, a well developed set of indices may actually predict the ash behavior very well.

2.3.2 Mathematical modelling

Several mathematical/analytical (sub) models have been developed to predict the stepwise combustion process. As discussed in Section 2.2, inorganics may undergo a number of physical and chemical transformations during combustion and these transformations depend on multiple operating parameters and fuel characteristics. Therefore, it is difficult to develop an integrated mathematical model for all the mechanisms, as with more of variables complexity of the models increase [68]. To make the simulations simpler, the different mechanisms, such as char oxidation, devolatilization, fragmentation, chemical reactions along with gaseous phase nucleation, coagulation, homogeneous and heterogeneous condensation etc. are studied separately, supported by different analytical methods as discussed above, often resulting in the development of several “rival” sub models describing the same system. Also the effects of various operating parameters such as the heating rate, temperature, pressure, and the residence time with different particle sizes, mineralogy and mineral matter composition ranges, as well as each of the chemical and physical transformations are often represented by separate subroutines to avoid simulation complexity. For a more realistic simulation interlinking of the above described sub models is also attempted.

A common approach for the ash formation modeling during PF combustion comprises a dual size ash mode [69, 70]. 1. Coarse ash and 2. Aerosol. Coarse ash formed during combustion usually participates in slagging, fouling, corrosion and erosion while aerosols contribute to environmental and health hazards, although they can also play a role in fouling at intermediate temperatures. The two important mathematical/numerical models for the prediction of the overall ash formation process are the aerosol ash formation models and the coarse particle size distribution evolution model, which are described in more details in the following section.

2.3.2.1 Coarse ash formation

The critical physical transformations responsible for coarse ash formation considered in most of the studies reported in the literature are fragmentation and/or coalescence. From the experimental and the industrial observations, it was found that fragmentation/coalescence during combustion is a very complex phenomena, particularly when covering a broad range of fuels at different operating conditions. Flagen et al. [71], Kang et al. [72], Decombe et al. [20], Wilemski et al. [17],

Mitchell [19] and Yan et al. [23] all modeled fragmentation/coalescence. The different models developed to date include particle break up and/or the coalescence of molten grains [17, 71], macroporosity due to the thermal stress [20], the percolative fragmentation, based on macroporosity, in which oxidation progressively erodes the solid network until the solid phase becomes spatially discontinuous [21, 23, 32, 72, 73, 74], collision-induced attrition [75, 76] and pressure-induced fracture and macroporosity due to attrition, breakage and percolation during devolatilization [19]. This section summarizes the gradual development of the individual models from simple theory based calculations to advanced numerical modeling.

2.3.2.1.1 Break up model

Laboratory work and studies of full scale coal-fired boilers in the early 1980's encouraged Flagen et al. [71] to model the residual ash formation during coal combustion. The simple breakup model described by Flagen et al. [71] assumed that char particles containing mineral matter, fragment during combustion. Major assumptions in the model include: (1) all coal particles contain same percentage and amount of mineral matter, independently of size, (2) all coal particles break into exactly the same number of char particles during combustion. The breakup number identified in this model is influenced by the breakup of char during burnout, from shedding at burning char surface and from the fragmentation of discrete included and excluded minerals. Despite several assumptions, the basic breakup model has proven to be a useful engineering and interpretative tool. Building further on Falgen's model, Damle et al. [77] added the vaporization-condensation model for submicron particle formation and evaluated the performance of the model with actual experiments.

2.3.2.1.2 Fragmentation model based on thermally induced stress

This mechanism implies that the fragmentation due to thermal stress is the dominant driving force for particle breakage, as there are always internal temperature gradients during particle heating up, especially with large particles. These internal temperature gradients cause significant thermal stress, leading to the production of more tiny fragments than those generated from small parent particles. Decombe et al. [20] developed a theoretical model for initial fragmentation based on thermally-induced

stresses. A transient analysis of these stresses allowed the fragmentation point to be determined. The results suggest a mode of fragmentation where many small particles are produced from the outer region and a few large particles from the inner one. As small particles experience a smaller temperature gradient resulting in much lower stress, fragmentation can be delayed to the char burnout phase [24]. Decombe et al. [20] found the relationship of the fragmentation extent with compressive strength. Furthermore, he observed that the extent of the fragmentation was found to increase with the particle size. To the best of the authors' knowledge, no further model was developed based on compressive strength.

2.3.2.1.3 Shrinking core model

Wiesmiki et al. [13, 17] developed a shrinking core model based on the observations that ash particles are produced during combustion by transformations and interactions of the mineral inclusions within the coal particle. The growth behavior of ash particles on the char surface is described in the model by considering redistribution and coalescence processes (ash formation mode). Several redistribution sub models have been used in the shrinking core model. Cahron et al. [78] applied Monte Carlo methods to simulate the random distribution of minerals among a set of coal particles. Berta et al. [79] developed an analytical model based on Poisson statistics for determining the size and chemical composition distributions for the minerals based on CCSEM data. Later on the same group developed the Random coalescence model to predict the PSD with elemental composition. However, all these models inaccurately predict that no small inorganic particles are present as excluded minerals. Wilemski et al. [13] used a composite method that combines Poisson statistics for distributing the smallest minerals among the smallest coal particles with a Monte Carlo method for handling all of the larger minerals and coal particles. Ash distributions were predicted with a full and no coalescence ash formation modes [13]. In the no coalescence mode, each mineral inclusion is assumed to produce one ash particle while in the full coalescence mode, the minerals in each coal particle are assumed to coalesce fully, producing one ash particle per coal particle. Based on Kang's thesis [14], the char fragmentation mode was also studied for cenospherical chars. In this case, ash particles are formed by the coalescence of inclusions that have high probabilities of encountering each other, as

the cenospherical char shell burns away. In the said model, the char fragmentation mode has independent variables such as porosity, swell volume of char particle, and cenosphere shell thickness. These parameters are entered in the model with the use of CCSEM analysis of the coal. Yan et al. [23] investigated the implications of the shrinking core model on ash deposition and thermal behavior. Liu et al. [32] used the shrinking core model to mechanistically predict ash particles size distributions and chemical compositions of the included and excluded minerals, throughout coal combustion. The upgraded mechanistic model of shrinking core method is based on partial coalescence (Morone [15]) of included minerals with three different groups of chars (Benfell et al. [37]). The excluded mineral fragmentation in this model is calculated with the Poisson statistical distribution method [23].

2.3.2.1.4 Percolation model

Based on a series of experiments by various researchers during the 1970-1980's, it was found that char oxidation is percolative in nature and char macroporosity is the single most important factor governing char breakup and the resulting residual ash size. Mohanty et al. [80] was the first to suggest the application of percolation theory to fluid-solid reaction systems, accompanied by pore volume changes. Kerstein et al. [81] applied this theory to char oxidation system, and developed a model to explain the fragmentation of chars in the chemically controlled reaction regime. Reyes et al. [82] applied the same theory to the Bethe lattice char model. Kerstein et al. [83] performed the simulation of char oxidation and fragmentation using the percolation model on lattice. To target the effect of char fragmentation on ash formation, Kang et al. [84] developed the first stochastic model based on the percolation theory on lattice for the external diffusion controlled regime. Porosity, mineral matter grain size distribution in the coal particle, reaction rate, and ash surface coalescence are the independent variables in the model. Salatino et al. [75, 76] stated that the fragmentation process may extend to the entire particle structure (uniform percolation- occurs only in chemical-kinetic-controlled regime, porosity develops uniformly within the particle, simultaneously throughout the particle, until conditions for loss of particle connectedness are reached) or may be restricted to its periphery (peripheral percolation- under diffusion controlled regime, where porosity increases non-uniformly and the fragmentation threshold is reached at particle periphery earlier

than within the particle). However, they proposed that peripheral percolation is to be considered for carbon oxidation studies as both chemical kinetic and intraparticle diffusive resistance are considered in this approach. Salatino et al. [75, 76] developed discrete, uniform percolation and peripheral percolation model. Most of the percolation-based models were discrete models with one of the main disadvantages of the discrete model being the associated high computational power. Continuous models, however, take less computational power but provide only qualitative results. Salatino et al. [76] developed the percolative fragmentation model combining discrete and continuous methods where continuity equations are pseudo-stationary, as far as the oxygen concentration is concerned. Yan et al. [23] studied the above percolation model in the diffusion-controlled regime. It was further extended and used to predict structural changes such as particle swelling due to coal devolatilization [85, 86, 87].

2.3.2.1.5 Particle population balance model

Most models that include time-dependent relationships for the growth of numbers of particles are based on the work of Dunn-Rankin et al. [88, 89]. Mitchell [19, 41], Decombe et al. [20] and many others found that during the initial conversion stages like heating up and devolatilization, the char particle will be under peripheral kinetic-diffusion controlled regime and later on after significant char burnout, it will be diverted to chemical-kinetic-controlled regime. Mitchell [19] observed three types of fragmentation behavior during combustion at different stages in his experiments with synthetic chars at different heating rate affecting the attrition, breakage and percolation. During attrition fragmentation, numerous small particles are produced from the surface while parent particle diminishes in size slightly. During breakage fragmentation, only a few large fragments are produced, not much smaller than the parent particle. Percolation fragmentation refers to the transition from a connected solid network to a completely fragmented state. It was observed during the experiments that the degree of fragmentation with less porosity was much higher during the heat-up and devolatilization stages, which suggest that the more open the porous structure, the lesser will be the extent of fragmentation during heat-up and devolatilization induced by either thermal stresses or stresses due to build-up of pressure of volatiles in the pores. Experimental studies showed that both char particle

diameter and apparent density change as burning progresses. Based on his experimental observations, Mitchell [41] adopted the particle population balance model of Dunn-Rankin et al. [88, 89] to predict particle size distribution (PSD) as a function of time during coal combustion. The particle population model was developed based on a power law expression used to correlate mass, density and diameter changes with burning rate. The burning rate constant in the model is based on an Arrhenius parameter that was obtained for each fuel experimentally. As this approach failed to account for functional variations, later on the intrinsic kinetic-based particle population model was developed that employ power-law-controlled mode of burning, in which particle size and apparent density variations are dependent on the particular physical and chemical characteristics of char [41]. Syred et al. [90] solved the particle population balance model analytically for fragmentation and tried to incorporate it into CFD modeling. However, fragmentation alone is not a complete way of presenting combustion, as particle should be burnt in a finite time period. Recently, Shah et al. [91] in their simple approach, have extended Syred's work by solving the particle population balance model analytically for two size class with inclusion of a burning term. The simplified model has then been validated with Polish coal experiments. However, the model is at initial stage of development and needs further improvement in the future.

The above described coarse ash formation models have only occasionally been developed and deployed for biomass fuels or co-firing modeling. Furthermore they predict ash size distributions qualitatively, except a few, which give also quantitative results. Likewise only a few models [15, 23] predict chemical compositions along with the qualitative or quantitative size distributions.

2.3.2.2 Ash release / Aerosol formation

The second major ash formation mechanism is the generation of submicron aerosols through vaporization and a number of gas-to-particle conversion mechanisms. When the ash size distribution is plotted in terms of number density or particles numbers, the submicron generally peak at around 0.1 micrometer. Although these particles account only for a small mass fraction, they can present a large fraction of surface area and become the preferred site for the condensation of more volatile oxides and toxic metal components deeper in the boiler. To avoid complexity in the simulations,

vaporization and condensation mechanisms are treated separately with dedicated models.

The vaporization is often predicted by a combination of several analyses and sub models. Proximate and ultimate analyses alongside with chemical fractionation techniques are used to decide the volatile matter in the fuel. Additionally, several empirical correlations are used to predict the vaporization mechanism accurately. Recently, CCSEM techniques have also been used to quantify the volatile matter in the fuel. TGA (Thermogravimetric analysis) has also been used to model the char devolatilization rate. Finally the vaporization is then often predicted using thermochemical equilibrium modeling (FACTSage).

Buhere et al. [11] and several others observed that aerosols are mainly formed due to condensation of released gaseous species rather than fragmentation. There are two competing routes for the condensing vapor. Firstly, the vapor may condense directly onto the internal surface of the furnace forming slag. Alternatively, the vapors may undergo gas-to-particle conversion to form aerosols by either homogeneous nucleation or heterogeneous condensation on existing particles entrained in the flue gas [51]. The droplets and aerosols begin to form larger particles through coagulation and agglomeration until finally accumulating as ash particles. The condensation of the aerosols onto the coarse ash fraction developed by fragmentation or coalescence is also possible. Several methods/models ranging from simple calculation to numerical modeling have been developed to predict the gas-to-particle conversion processes.

Doshi et al. [51] have reported simple calculations based on the aerosol formation of the alkali chlorides and sulfates to model the aerosol ash formation. In the numerical methods, finite element techniques have also been applied with some degree of success [92], and the method of moments can be applied if the equations for evolution of the moments of the size distribution can be obtained in a closed form [93]. However, Gelbard et al. [94] found that for problems involving simultaneous nucleation, growth, and coagulation, the methods most widely used are based on a sectional representation of the size distribution. In sectional methods, the size distribution is divided into a number of sections or size classes within which all particles are assumed to have the same properties. Jokiniemi et al. [95] used plug

flow model developed by Im et al. [96] for aerosol dynamics by simulating alkali species during coal combustion process. However, the use of fixed size sections for problems involving aerosol growth, may lead to numerical diffusion that in turn results in the error of sharp changes in size distributions. Gelbard [97] introduced the moving sectional method for gas-to-particle conversion. Jacobson et al. [98] and Wu et al. [99] modified aspects of coagulation and condensational growth. Later on Christensen et al. [100] numerically simulated the Plug flow model with nucleation, growth, coagulation and gas phase reactions using moving sectional method. Zeuthe [101] in his PhD thesis, validated the one dimensional model of Christensen for aerosol formation from biomass fuels such as straw and household waste with a detailed view at particle composition and particle size distribution. The main particle formation mechanisms included in the aerosol formation plug flow model are nucleation, condensation, coagulation and agglomerations, together with the precipitation mechanisms (diffusion, thermophoresis, inertial impaction and gravitational settling) on to the particle or on the furnace wall. The gas phase is usually modeled with thermodynamic equilibrium model (FACTSage) or with advanced fuel characteristics.

The mentioned simulation models, focused primarily on coal combustion and if biomass combustion was considered, straw was the fuel of choice. Furthermore, if particle formation mechanisms were treated in detail, either alkali metal compounds or heavy metal compounds were considered for particle formation from the gas phase.

2.4 Summary

1. It can be inferred from the literature review that ash formation during PF combustion depends on several fuel characteristics and operating parameters.
2. PF combustion is performed normally at atmospheric pressure, at a high temperature with high heating rates. Though operating parameters such as temperature, pressure, heating rate will be in a relatively narrow, specified range for PF combustion, the effect of operating conditions will be varying significantly for different fuels. The measures of the fuel characteristics such as char reactivity, ash, moisture, volatile matter and fixed carbon percentages, as

well as its density and porosity will also be in same range for the same fuel with varying particle size. Therefore, each particle size range in a single fuel will behave differently under PF combustion conditions. Kinetic reaction rates of the mineral chemical conversions are also highly dependent on several operating parameters (temperature, pressure, residence time etc.) and fuel characteristics (ash contents, mineralogy, particle size etc).

3. Several analytical methods/tools/models are available and used so far to quantify ash formation process. Proximate and ultimate analysis of the fuels are the basic and essential primary test which decides several design parameters and gives an idea about the mineral percentage present in the fuel. To know the mineral matter composition in the fuel or residual ash, several traditional ash analysis techniques such as atomic absorption spectrophotometer (AA), graphite furnace atomic absorption (GFAA), inductively coupled plasma optical emission spectrometry (ICP / ICP-OES), inductively coupled plasma/mass spectrometry (ICP/MS), X-ray fluorescence spectrometry (XRF), glow discharge mass spectrometry (GDMS) and spark source mass spectrometry (SSMS) are used. However, the traditional ash analysis methods are time consuming and of limited scope sometimes as they are inadequate of providing the mineral matter distribution with varying particle sizes in the fuel or residual ash. Therefore, these techniques are complimented by more efficient and advanced CCSEM analysis. The use of CCSEM has increased considerably in the last two decades. QEMSCAN has also been used in place of CCSEM to determine mineral-mineral associations, particle size, mineral compositions, and particle texture in the coal and ash samples with higher degree of automation in recent efforts. To decide the mineral matter association in the fuel mineral matrix, pH dependent leaching and/or chemical fractionation methods are often employed. STA/TGA is performed to decide the overall reaction kinetics which includes residence time, char oxidation and devolatilization rate etc. Thermochemical equilibrium models are used to find out the stable gaseous and solid species at given operating conditions.
4. The mathematical modeling efforts made to predict ash formation are also quite significant. The modeling of ash formation is mainly divided into two parts such as coarse ash formation due to the fragmentation/coalescence and aerosol ash formation due to vaporization followed by condensation. Models

mentioned in this chapter, focused mostly on coal combustion and if biomass combustion was considered, straw was the most commonly modeled fuel. Furthermore, if particle formation mechanisms were treated in detail, either alkali metal compounds or heavy metal compounds were considered for particle formation from the gas phase.

2.5 Conclusions and future research needs

1. Ash formation during PF combustion is a very complex phenomenon, depending on a broad range of variables, either associated with the fuel or the conversion technology.
2. Different fuels will have different physical and chemical properties and therefore will behave differently during combustion. Moreover, within the same fuel, different particle size will have different physical and chemical properties after milling and classifying based on size and density. The investigations on lab/pilot/plant scale with narrow/single size range particles under well-controlled conditions and a greater number and more diverse fuels are very limited in the literature and therefore much needed in future research to predict the ash formation process more precisely.
3. Analytical methods are well advanced to determine the particle sizes and their mineralogy at different residence times. Nevertheless, the particle size reduction rate is difficult to measure or calculate accurately even with the methods available in the literature. This is primarily due to the various size altering processes (such as burning and fragmentation) occurring simultaneously during combustion. The size reduction rate is often assumed in the models or derived inaccurately from the experiments. Innovatively, the use of Particle image velocimetry (PIV) is appreciated for the same in future.
4. The determination of the extent of slagging and fouling phenomena are usually tackled on the industrial scale by quantitative methods such as thermal conductivity and slag thickness measurements, ash deposition probes etc., which are good indicators for local phenomena but are not efficient in bringing the overall chart along with more importantly the reasons and details of the underlying deposition mechanisms. These aspects will therefore need more scientific attention in the future.

5. Aerosol formation creates serious environmental and health hazards while coarse ash creates problems such as erosion and also participates in slagging, fouling, corrosion etc. At the research level, they are often quantified by expensive and time consuming lab-pilot-plant scale trials. The use and development of ash formation modeling to date is very limited in predicting various ash related problems. The experimental and measurement techniques are more accurate but often time consuming and expensive. Therefore, the development and extensive use of ash formation modeling is highly recommended in the future.
6. Ash formation models are mainly of two types: coarse ash and aerosol formation. They are mostly used separately and for different purposes such as flow, slagging, fouling, corrosion erosion, environmental and health hazards modeling, and to date seldom brought together and interlinked to simulate the overall combustion and ash formation process. The integration of these ash transformations is essential to predict overall ash formation hence, the integration of both of these models is highly appreciated in future to detail the over all ash formation process in detail.
7. The models typically developed for coals are yet to be validated for biomass and co-firing conditions.

2.6 Objectives (based on the literature review)

1. Ash formation during PF combustion/co-firing is a very complex phenomenon which depends upon a number of variables. Therefore, to limit the problem, the present investigations will be made for typical PF firing combustion conditions. The investigations onto biomass co-firing will be made on the basis of time and budget available.
2. Some of the interesting observations found from the literature review based on the effect of fuel characteristics and operating parameters onto ash formations during PF combustion will be reconfirmed using specific lab scale experiments.
 - a. For that ash release and cascade impactor experiments will be planned for different pulverized coal and biomass combustion/co-firing conditions.

- b. Char conversion, devolatilization and fragmentation will be quantified for all the fuels.
 - c. Ash release should be separately studied to find out the effect of mineral matter composition and their association in the char matrix.
- 3. Experiments with narrow size range particles are very expensive and time consuming. Therefore, they will be planned based on the time and budget available.
- 4. Ash release is modeled using the chemical fractionation method and thermochemical equilibrium calculations by Doshi [51]. In an extended effort in this PhD project, simple correlations will be attempted to predict the ash release of several minerals during combustion/co-firing of several coals and biomass.
- 5. Aerosol formation modeling is done by Doshi [51]. Therefore, the main research task in this PhD project will be to develop the coarse ash formation model. The coarse ash formation model will be developed and validated with a number of coals and biomass combustion/co-firing conditions.
- 6. Overall ash formation modeling will also be attempted which gives particle size distribution along with mineral composition after combustion.
- 7. The developed model will be incorporated in the CAT (Co-firing advisory tool) at ECN.
- 8. Further, it will be used in an ash deposition post processor developed at ECN as an input to predict ash deposition.
- 9. Applications of CAT to new processes such as Ultra Super Critical vapor characteristics, Oxy fuel combustion (OXY- or MILD) will also be evaluated.

All objectives are addressed apart from 3,8 and 9 which are recommended to be addressed in the future. Moreover, the present study does not include specific co-firing experiments.

References

1. W. R. Livingston, Biomass ash characteristics and behavior in combustion, gasification and pyrolysis systems, Report No : 34/07/005, Project/Sub-Project :78541/SD001, Doosan Babcock Energy Limited (2007).
2. A. F. Sarofim, J. J. Helbe, In The impact of Ash Deposition on Coal Fired Plants: Proceedings of the Engineering Foundation Conference, (1993) Solihull, England, Williamson, J., Wigley, F. (Eds.), Taylor & Francis, London (1994).
3. L. L. Baxter, Ash deposition during biomass and coal combustion: a mechanistic approach, *Biomass Bioenergy* 4 (2) (1993) 85–102.
4. A. F. Sarofim, J. B. Howard, A. S. Padia, The Physical Transformation of the Mineral matter in Pulverized Coal under Simulated Combustion Conditions, *Combustion Science and Technology* 16 (1977) 187-204.
5. S. C. Van Lith, Release of Inorganics Elements during Wood-firing on grate, PhD Thesis, CHEC Research Centre, Technical University of Denmark (2005).
6. European Biomass Industry Association official website <http://www.eubia.org/333.0.html>
7. H. Schurmann, P. B. Monkhouse, S. Unterberger, K. R. G. Hein, In situ parametric study of alkali release in pulverized coal combustion, *Proceedings of the combustion Institute* 31 (2007) 1913-1920.
8. P. Thy, C. E. Leshner, B. M. Jenkins, Experimental determination of high-temperature elemental losses from biomass slag, *Fuel* 79 (2000) 693-700.
9. J. C. Kramlich, B. Chenvert, J. Park, Suppression of Fine ash formation in pulverized coal flames, DOE grant no. DE-FG22--92PC92548, Quarterly Technical progress report no.10, For U.S Department of Energy (1995).
10. L. L. Baxter, Char fragmentation and fly ash formation during pulverized-coal combustion, *Combustion and Flame* 90 (1992) 174–184.
11. B. J. P. Buhre, J. T. Hinkley, R. P. Gupta, T. F. Wall, P. F. Nelson, Submicron ash formation from coal combustion, *Fuel* 84 (2005) 1206-1214.

12. L. Terttalisia, Ash formation in circulating fluidized bed combustion of coal and solid biomass, PhD thesis, Helsinki University of Technology, Finland (1999).
13. G. Wilemski, S. Srinivaschar, A. Sarofim, Modeling of mineral matter redistribution and ash formation in pulverized coal combustion, ASME, New York (1992) 545.
14. S. G. Kang, Fundamental studies of mineral matter transformations during Pulverized coal Combustion, PhD Thesis (1991).
15. L. S. Morone, An experimental and modeling study of residual fly ash formation in combustion of a bituminous coal, PhD Thesis, Massachusetts Institute of Technology (1989).
16. J. J. Helble, A. F. Sarofim, Influence of Char Fragmentation on Ash particle size distributions, Combustion and flame 76 (1989) 183-196.
17. G. Wilemski, S. Srinivasachar, Prediction of Ash formation in Pulverized coal combustion with mineral distribution and Char fragmentation Models, Proceeding of the Engineering Foundation Conference, England (1993) 151-164.
18. F. Wigley, J. Williamson, W. H. Gibb, The distribution of mineral matter in pulverized coal particles in relation to burnout behavior, Fuel 76 (13) (1997) 1283-1288.
19. R. E. Mitchell, Char fragmentation and its effect on unburned carbon during pulverized coal combustion, Contract no.:DE-FG22-92PC92528, For U.S Department of Energy (1997).
20. P. Dacombe, M. Pourkashanian, A. Williams, L. Yap, Combustion-induced fragmentation behavior of isolated coal particles, Fuel 78 (1999) 1847-1857.
21. L. Yan, R. Gupta, T. Wall, The implication of mineral coalescence behavior on ash formation and deposition during pulverized coal combustion, Fuel 80 (2001) 1333-1340.
22. H. M. ten Brink, S. Eenkhoorn, M. Weeda, The behavior of coal mineral carbonates in a simulated coal flame, Fuel Processing Technology 47 (1996) 233-243.
23. L. Yan, R. Gupta, T. Wall, Fragmentation behavior of Pyrite and Calcite during high-temperature processing and mathematical simulation, Energy and fuel 15 (2001) 389-394.

24. L. Baxter, H. Lu, E. Ip, J. Scott, P. Foster, M. Vickers, Effect of Particle shape and size on devolatilization of biomass particle, *Fuel* (2008); article in press, doi:10.1016/j.fuel.2008.10.023.
25. S. Badzioch, P. G. W. Hawksley, Kinetics of thermal decomposition of pulverized coal particles. *Industrial Engineering and Chemistry Process Design and Development* 9 (1970) 521–530.
26. J. P. Mathews, P. G. Hatcher, A. W. Scaroni, Particle size dependence of coal volatile matter: is there a nonmaceral- related effect?, *Fuel* 76 (1997) 359–362.
27. S.Y. No, N. Syred, Thermal stress and pressure effects on coal particle fragmentation and burning behavior in a cyclone combustor, *Journal of the Institute of Energy* 63 (1990) 151–159.
28. X. Liu, M. Xu, H. Yao, D. Yu, D. Lv, K. Zhou, The Formation and Emission of Particulate Matter during the Combustion of Density Separated Coal Fractions, *Energy & Fuels* 22 (2008) 3844-3851.
29. T.G. Bridgeman, L.I. Darvell, J.M. Jones, P.T. Williams, R. Fahmi, A.V. Bridgwater, T. Barraclough, I. Shield, N. Yates, S.C. Thain, I.S. Donnison, Influence of particle size on the analytical and chemical properties of two energy crops, *Fuel* 86 (2007) 60–72.
30. J. Yua, J. A. Lucasb, T. F. Wall, Formation of the structure of chars during devolatilization of pulverized coal and its thermoproperties: A review, *Progress in Energy and Combustion Science* 33 (2007)135–170.
31. R. H. Hurt, A. F. Sarofim, J. P. Longwell, The role of microporous surface area in the gasification of chars from a subbituminous coal. *Fuel* 70 (1991)1079–1082.
32. G. Liu, H. Wu, R.P. Gupta, J.A. Lucas, A.G. Tate, T.F. Wall, Modeling the fragmentation of non-uniform porous char particles during pulverized coal combustion, *Fuel* 79 (2000) 627–633.
33. R. Menendez, J. M. Vleeskens, H. Marsh, The use of scanning electron microscopy for classification of coal chars during combustion, *Fuel* 72 (1993) 611–617.
34. M. Kaiho, Y. Toda, Change in thermoplastic properties of coal under pressure of various gases, *Fuel* 58 (1979) 397–398.

35. Z. Ezra, I. I. Kantorovich, Mutual effects of porosity and reactivity in char oxidation, *Progress in Energy and Combustion Science* 27 (2001) 667-697.
36. S. G. Kang, A. F. Sarofim, J. M. Beer, Effect of Char Structure on Residual Ash Formation during Pulverized Coal Combustion, 24th Symposium (International) on combustion, The Combustion Institute (1992) 1153-1159.
37. K. E. Benfell, J. G. Bailey, Comparison of combustion and high pressure pyrolysis chars from Australian black coals, Eighth Australian Coal Science Conference (1998) 157-162.
38. T. K. Gale, C. H. Bartholomew, T. H. Fletcher, Decreases in the swelling and porosity of bituminous coals during devolatilization at high heating rates, *Combustion and Flame* 100 (1995) 94–100.
39. R.P. Gupta, Coal research in Newcastle—past, present and future, *Fuel* 84 (2005) 1176–1188.
40. A. D. Koranyi, The relationship between specific reactivity and the pore structure of coal chars during gasification. *Carbon* 27 (1989) 55-61.
41. R. Mitchell, An intrinsic kinetics-based, particle population balance model for char oxidation during pulverized coal combustion, *Proceedings of the Combustion Institute* 28 (2000) 2261–2270.
42. T. F. Wall, G. S. Liu, H. W. Wu, D. G. Roberts, K. E. Benfell, S. Gupta, J. A. Lucas, D. J. Harris, The effect of pressure on coal reactions during pulverized coal combustion and gasification, *Progress in Energy and Combustion Science* 28 (2002) 405–433.
43. T. A. Erickson, D. K. Ludlow, S. A. Benson, Fly ash development from sodium, sulphur and silica during coal combustion, *Fuel* 71 (1992) 15-18.
44. H. Wu, G. Bryant, T. Wall, The Effect of Pressure on Ash Formation during Pulverized Coal Combustion, *Energy & Fuels* 14 (2000) 745-750.
45. J. G. Speight, *Handbook of Coal Analysis (chemical Analysis: A Series of Monographs on Analytical Chemistry and Its Applications)*, ISBN 0-471-52273-2 (cloth), Wiley-Interscience (2005).
46. Dr. M. L. Jacobs, Instrumentation for elemental analysis of coal ash products, Denver Division, Wyoming Analytical Laboratories, Inc., Golden, Colorado (2000). <http://www.mcrcc.osmre.gov/PDF/Forums/CCB3/2-2.pdf>.

47. D. C. Dayton, D. Belle-Oudry, A. Nordin, Effect of coal minerals on chlorine and alkali metals released during biomass/coal cofiring, *Energy & fuels* 13 (1999) 1203-1211.
48. K. J. Wolf, Studies of Alkali Sorption Kinetics for Pressurized Fluidized Bed Combustion by High Pressure Mass Spectrometry (2002). www.osti.gov/bridge/servlets/purl/836714.pdf
49. R. Korbee, J. Lensselink, M. Cieplik, Energy Research Centre of the Netherlands, Final report of task 1.3 – Release of ash forming matter in pulverized fuel systems, SES6-CT-2003-502679, (2006).
50. F. J. Frandsen, S. C. van Lith, R. Korbee, P. Yrjas, R. Backman, I. Obernberger, T. Brunner, M. Jöller, Quantification of the release of inorganic elements from biofuels, *Fuel Processing Technology* 88 (2007)1118-1128.
51. V. Doshi, H. B. Vuthaluru R. Korbee, J.H.A. Kiel, Development of a modeling approach to predict ash formation during co-firing of coal and biomass, *Fuel Processing Technology* 90 (9)(2009) 1148-1156.
52. H. Lu, C. Jia, L. Zhang, G. Su, The Study on Combustion Characteristics and Kinetics of Coal and Biomass, *Challenges of Power Engineering and Environment*, Springer, Berlin, Heidelberg(doi: 10.1007/978-3-540-76694-0) (2007).
53. H. B. Vuthaluru, Investigations into the pyrolytic behavior of coal/biomass blends using thermogravimetric analysis, *Bioresource Technology* 92 (2004) 187-195.
54. R. H. Hurt, J. C. Calo, T. Fletcher, A. Sayre, *Fundamental Investigations of Fuel Transformations in Advanced Coal Combustion and Gasification Processes* (2003).
55. C. G. da S. Filho, F. E. Milioli, A thermogravimetric analysis of the combustion of a Brazilian mineral coal, *Química Nova* 31 (2008).
56. Y. Zhaosheng, M. Xiaoqiana, L. Aoa, Thermogravimetric analysis of rice and wheat straw catalytic combustion in air- and oxygen-enriched atmospheres, *Energy Conversion and Management* 50 (2009)561-566.
57. T. Miranda, A. Esteban, S. Rojas, I. Montero, A. Ruiz, Combustion Analysis of Different Olive Residues, *International Journal of Molecular Sciences* 9 (2008) 512-525.

58. T. Terama, T. Yamashita, T. Ando, Behavior of Inorganic Materials during Pulverized Coal Combustion, Impact of Mineral Impurities in Solid Fuel Combustion, Springer US (1999).
59. Y. Chen, N. Shah, F. E. Huggins, G. P. Huffman, W. P. Linak, C. A. Miller, Investigation of primary fine particulate matter from coal combustion by computer-controlled scanning electron microscopy, Fuel processing technology 85 (2004) 743-761.
60. Q. Wang, L. Zhang, A. Sato, Y. Ninomiya, T. Yamashita, Interactions among Inherent Minerals during Coal Combustion and Their Impacts on the Emission of PM10. 1. Emission of Micrometer-Sized Particles, Energy Fuels 21 (2) (2007) 756–765.
61. D. Yu, M. Xu, L. Zhang, H. Yao, Q. Wang, Y. Ninomiya, Computer-Controlled Scanning Electron Microscopy (CCSEM) - Investigation on the Heterogeneous Nature of Mineral Matter in Six Typical Chinese Coals, Energy and Fuels 21 (2) (2007) 468–476.
62. T. Brunner, I. Obernberger, M. Jöller, A. Arich, P. Polt, Behavior of ash forming compounds in biomass furnaces – Measurement and analysis of aerosols formed during fixed bed biomass combustion, Aerosols from Biomass Combustion (International Seminar), International Energy Agency (IEA) and the Swiss Federal Office of Energy, BioenergyTask 32: Biomass Combustion and Cofiring (2001) 75-80.
63. Y. Liu, R. P. Gupta, A. Sharma, T. F. Wall, A. Butcher, G. Miller, P. Gottlieb, D. French, 'Mineral matter-organic matter association characterisation by QEMSCAN and applications in coal utilization, Fuel 84 (2005) 1259-1267.
64. H. B. Vuthaluru, D. French, Ash chemistry and mineralogy of an Indonesian coal during combustion: Part 1 Drop-tube observations, Fuel Processing Technology 89 (6) (2008) 595-607.
65. H. B. Vuthaluru, D. French, Ash chemistry and mineralogy of an Indonesian coal during combustion: Part II — Pilot scale observations, Fuel Processing Technology 89(6) (2008) 608-621.
66. F. C. Lockwood, P. G. Costen, M. M. Siddiqi, P. J. Harrison, Mineral ash Transformations, Technical report SW7 2BX JOF3-CT95-0024, The Imperial College of Science, Technology and Medicine; Mechanical

- Engineering Department; London. <ftp://ftp.euro-cleancoal.net/pub/pdf/JOF3-CT95-0024-pdf-files/JOF3-CT95-0024-02%20Lockwood-ICSTM.pdf>
67. J. Barrosoa, J. Ballester, A. Pinaa, Study of coal ash deposition in an entrained flow reactor: Assessment of traditional and alternative slagging indices, *Fuel processing technology* 88 (2007) 865-876.
 68. S. A. Benson, T. A. Erickson, R. R. Jensen, J. D. Laumb, Transformations Model for Predicting Size and Composition of Ash During Coal Combustion, *Fuel Chemistry Division Preprints* 47 (2) (2002) 796.
 69. H. Wu, T. Wall, G. Liu, G. Bryant, Ash Liberation from Included Minerals during Combustion of Pulverized Coal: The Relationship with Char Structure and Burnout, *Energy Fuels* 13 (6) (1999) 1197–1202.
 70. I. Oberberger, Aerosols in fixed-bed biomass combustion, *Bio-aerosols*, Budapest,16-17
ftp://ftp.cordis.europa.eu/pub/sustdev/docs/energy/bioenergy_c04.pdf;
(2003).
 71. R. C. Flagen, S. K. Friedlander, Recent developments in Aerosol Science (D.T. Shaw. Ed.) (1978).
 72. S. G. Kang, A. R. Kerstein, J. J. Helble, A. F. Sarofim, Simulation of Residual Ash Formation During Pulverized Coal Combustion: Bimodal Ash Particle Size Distribution, *Aerosol Science and Technology* 13 (1990) 401-412.
 73. B. F. Edwards, A. K. Ghosal, Model of Ash size distribution from coal char oxidation, Department of Physics, West Virginia University Morgantown, WV 26506.
 74. F. Wigley, J. Williamson, Modeling Fly ash generation for pulverized coal combustion, *Energy Combustion and Science* 24 (1998) 337-343.
 75. P. Salatino, F. Miccio, L. Massimilla, Combustion and Percolative fragmentation of carbons, *Combustion and Flame* 95 (1993) 342–350.
 76. P. Salatino, F. Miccio and L. Massimilla, Monte Carlo simulation of combustion induced percolative fragmentation of carbons, Twenty-fourth Symposium (International) on combustion, The combustion Institute (1992) 1145-1151.
 77. S. Demle, D.S. Ensor, M.B. Ranade, Coal combustion aerosol formation mechanisms: A Review; *Aerosol Science and Technology* 1 (1982) 119-133.

78. O. Charon, A. F. Sarofim, J. M. Beer, Distribution of mineral matter in pulverized coal, *Progress in Energy and Combustion Science* 16 (1990) 319-326.
79. L. E. Barta, M. A. Toqan, J. M. Beer, A. F. Sarofim, Prediction of Fly Ash size and Chemical Composition Distributions : The Random Coalescence Model, *Twenty-Fourth Symposium (International) on Combustion*, The Combustion Institute (1992) 1135-1144.
80. K. K. Mohanty, J. M. Ottino, H. T. Davis, Reaction & transport in disordered composite media: Introduction of percolation concepts. *Chemical Engineering Science* 37 (1982) 905-924.
81. A. R. Kerstein, S. Niksa, Fragmentation during carbon conversion: predictions and measurements, In *Proceedings of Twentieth Symposium (International) on Combustion*, The Combustion Institute (1984) 941-949.
82. S. Reyes, K. F. Jensen, Percolation concepts in modeling of gas-solid reactions—I, Application to char gasification in the kinetic regime, *Chemical Engineering Science* 41 (2) (1986) 333-343.
83. A. R. Kerstein, B. F. Edwards, Percolation model for simulation of char oxidation and fragmentation time-histories, *Chemical Engineering Science* 42 (7) (1987) 1629-1634.
84. S. G. Kang, J. J. Helble, A. F. Sarofim, J. M. Beer, Time-Resolved Evolution of Fly Ash during Pulverized Coal Combustion, In *Proceedings Twenty Second Symposium (International) on Combustion*, The Combustion Institute, Pittsburgh (1988) 231-238.
85. R. Kurose, H. Makino, N. Hashimoto, A. Suzuki, Application of percolation model to particulate matter formation in pressurized coal combustion, *Powder Technology* 172 (1) (2007) 50-56.
86. R. Kurose, H. Matsuda, H. Makino, A. Suzuki, Characteristics of particulate matter generated in pressurized coal combustion for high-efficiency power generation system, *Advanced Powder Technology* 14 (6) (2003) 673-694.
87. A. Suzuki, T. Yamamoto, H. Aoki, T. Miura, Percolation model for simulation of coal combustion process, *Proceedings of the Combustion Institute* 29 (1) (2002) 459-466.

88. D. Dunn-Rankin, A. R. Kerstein, Numerical simulation of particle size distribution evolution during pulverized coal combustion, *Combustion and Flame* 69 (1987) 193–209.
89. D. Dunn-Rankin, Kinetic model for simulating the evolution of particle size distributions during char combustion, *Combustion Science Technology* 58 (1988) 297–314.
90. N. Syred, K. Kurniawan, T. Griffiths, T. Gralton, R. Ray, Development of fragmentation models for solid fuel combustion and gasification as subroutines for inclusion in CFD codes, *Fuel* 86 (2007) 2221–2231.
91. K. V. Shah, M. K. Cieplik, C. I. Bertrand, W. L. van de Kamp, H. B. Vuthaluru, A kinetic-empirical model for particle size distribution evolution during pulverized fuel combustion. *Fuel* – Article in press, Available online from 29th December 2009.
92. F. Gelbard, J. H. Seinfeld, Numerical Solution of the Dynamic Equation for Particulate Systems, *Journal of Computational. Physics* 28 (1978) 357–375.
93. R. McGraw, Description of Aerosol Dynamics by the Quadratum Method of Moment, *Aerosol Science. Technology* 27 (2) (1997) 255–265.
94. F. Gelbard, Y. Tambour, J. H. Seinfeld, Sectional Representation for Simulating Aerosol Dynamics, *Journal of Colloid Interface Science* 76 (2) (1980) 541– 556.
95. J. K. Jokiniemi, M. Lazaridis, K. E. J. Lehtinen, E. I. Kauppinen, Numerical Simulation of Vapor-Aerosol Dynamics in Combustion Processes, *Journal of Aerosol Science* 25 (3) (1994) 429–446.
96. K. H. Im, R. K. Ahluwalia, C. F. Chuang, RAFT: A Computer Model for Formation and Transport of Fission Product Aerosols in LWR Primary Systems, *Aerosol Science Technology* 4 (1985) 125–140.
97. F. Gelbard, Modeling Multicomponent Aerosol Particle Growth by Vapor Condensation, *Aerosol Science. Technology* 12 (1990) 399–412.
98. M. Z. Jacobson, R. P. Turco, Simulating Condensational Growth, Evaporation, and Coagulation of Aerosols Using a Combined Moving and Stationary Grid, *Aerosol Science Technology* 22 (1995) 73–92.
99. C. Y. Wu, P. Biswas, Study of Numerical Diffusion in a Discrete-Sectional Model and Its Application to Aerosol Dynamics Simulation, *Aerosol Science. Technology* 29 (1998) 359–378.

100. K. A. Christensen, H. Livbjerg, A Plug Flow Model for Chemical Reactions and Aerosol Nucleation and Growth in an Alkali-Containing Flue Gas *Aerosol Science and Technology* 33 (2000) 470–489.
101. J. H. Zeuthe, The formation of aerosol particles during combustion of biomass and waste, PhD thesis, The Aerosol Laboratory, Department of Chemical Engineering, Technical University of Denmark, Lyngby (2007).

Chapter 3

First line ash transformations during PF combustion

As decided from the literature review, the present research work will be limited to PF combustion only. In this chapter an attempt is made to shed light on the first line ash transformations such as char oxidation, devolatilization and fragmentation for six different coal and biomass fuels, by carrying out a thorough experimental study in the Lab-scale Combustion Simulator (LCS) of the Energy Research Centre of the Netherlands (ECN) under typical PF-firing conditions at high initial heating rates (10^5 K/s) and high temperature (1450-1600 °C). Ash release, conversion, size reduction and size distribution alongside with the change in inorganic chemical compositions, are derived at different char burn out levels in the reactor at 20, 90, 210 and 1300 milliseconds of residence times. Several of the past observations made in the literature review are reconfirmed with performed set of experiments. A qualitative predictive tool is also suggested to envisage the extent of first line physical transformations.

3.1 Introduction

One of the major obstacles to the economical use of coal and biomass is managing the behavior of its ash. During combustion, minerals in the fuel undergo various chemical and physical transformations [1, 2] as discussed in the literature review (chapter 2) which under certain conditions may lead to the occurrence of various problems such as slagging, fouling and corrosion [3]. The physical and chemical transformations during the thermal conversion of the solid fuels are time-dependent and very difficult to understand as a continuous process [2]. They largely depend on several fuel characteristics. The linkage between the operating conditions (i.e. type of combustion, temperature, pressure, heating rate, residence time, chemical equilibrium of the gaseous species and reaction rate of different gaseous and slag phases minerals etc.) with fuel characteristics (fuel mineral matter composition, ash

percentage in fuel, fixed carbon, volatile matter, mineralogy - either included or excluded especially for coal, char reactivity, char morphology, density, particle size etc.) are also essential to study for understanding the ash transformations. Detailed review of the parameters of crucial importance can be found in the Chapter 2.

During the char oxidation at high temperatures, initially char particle lie in the so called kinetic -diffusion controlled regime, in which the rates for pore diffusion and chemical reaction are comparable while later in the burnout, a transition is expected from the kinetic-diffusion controlled burning regime to the kinetic controlled regime only. In the latter stages, chemical reaction rates are dominant in controlling overall mass loss rates [3]. However, from the past experiments it was concluded that all major types of pulverized fuels will be in the kinetic-diffusion controlled regime even with extended residence time during the typical PF combustion conditions where mass loss rates due to chemical reaction and pore diffusion are comparable [4,5].

Char burnout, devolatilization and fragmentation are the most important first line physical transformations which occur in the radiant zone [2]. Char burnout of the fuel, depends on the reactivity of the char. The more reactive the char, the quicker and the more complete will be the fuel chemical conversion. It is well known, that the overall char reactivity is affected by the presence of minerals [6,7]. At the high temperature levels of the furnace, char oxidation rates are highly dependent of the intrinsic char reactivity, which is in turn linked with the char's ash content [8]. Volatilization processes depend also to a large extent on the mineral matter composition and its association with the carbon matrix. The mineral matter can be present as free ions, salts, organic bound or as hard minerals in the fuel. Alkalis in the younger fuel, such as low rank coal and woody biomass remain mostly in included mineral as free ions, salts and organically associated inorganic and start vaporizing at lower temperatures [9,10]. Chlorine, sulfur and partly calcium and magnesium along with alkalis primarily present as organically bonded or dispersed phases, are expected to devolatilize at moderate to high temperatures. Silicon, aluminum and iron on the other hands are considered as stable or conservative elements, which remain in the solid ash matrix in the melt form.

The devolatilization of the above volatile minerals is due to several chemical transformations occurring between the solid, slag and gaseous mineral phases [11,12]. Alkali chlorides and sulfates are the main possible products of the chemical transformations at even moderate temperatures. Nonetheless, it is evidently found that alkali metal oxides inclusions in silicate network in the char matrix, make them significantly less volatile [13]. The volatilization of alkali minerals increases with the higher chlorine concentrations, because of the high saturation vapor pressure of alkali chlorides at combustion temperatures [13].

An increase in the fragmentation can be observed at high chemical conversion and devolatilization levels of the fuel. Larger particles fragment more compared to smaller size particles [14,15]. Mitchell [16] observed attrition, breakage and percolation-type fragmentation behavior during coal combustion at different regimes in his experiments with synthetic chars. During the initial stage of combustion, burning and little attritive fragmentation are found to occur, with shedding of smaller particles from the surface which extends to breakage mode after certain conversion where a particle breaks into two or three similar sized particles. Later in the combustion process fragmentation is found to be of percolative nature [3] where particles disintegrate into an array of larger and smaller particles.

The physical and chemical transformations during thermal conversion of the solid fuels can be termed as complex time- dependent process. For prediction of the actual overall ash formation process, it is essential to understand the integration of the most important first line physical and chemical transformations such as char burnout, volatilization and fragmentation. In the present study, several coals and biomass fuels have been tested in the Lab-scale Combustion Simulator (LCS) at the Energy Research Centre of the Netherlands (ECN) under typical PF firing conditions. Ash release, conversion, size reduction and size distribution alongside with changes in inorganic chemical compositions are derived at different char burn out levels in the advanced drop tube furnace-like reactor at 20, 90, 210 and 1300 milliseconds of residence times. Char burnout, devolatilization and fragmentations are quantified for all burn out levels.

3.2 Experimental

3.2.1 Fuel Preparation and analyses

The study includes wood chips, waste wood, olive residue, straw alongside with a UK and a Polish coal. The proximate and ultimate analysis of these fuels along with the mineral matter elemental composition can be found in the Appendix A while a ranking of the studied fuels according to their ash and volatile matter contents is presented in Table 3.1.

Table 3. 1: Ranking of test fuels according to their ash and volatile matter content

High Ash	High Volatile matter	❖ Olive Residue ❖ Straw
	Low Volatile matter	❖ Polish coal ❖ UK Coal
Low Ash	High Volatile matter	❖ Waste wood ❖ Wood Chips

The fuels were milled and sieved on a Retsch SM 100 cutter mill, equipped with a 1 mm sieve/knife. The final particle size distribution of the fuels was analyzed by light scatter technique (Malvern Mastersizer) and can be found in Appendix B.

3.2.2 Laboratory Set-up

Coal and biomass were combusted in the LCS. An overall schematic of this tests rig is given in Figure 3. 1. The LCS is an advanced drop tube furnace, that can be applied to study the behavior of a single or blended solid fuels under typical pulverized fuel fired furnace conditions. It consists of a drop tube reactor with an integrated, premixed and multi-stage flat flame gas burner. The staged gas burner accommodates high initial heating rates and temperatures and also provides the possibility to simulate air staging as in Low-NO_x burners along with the presence of specific combustion products such as, e.g., SO₂. The flat flame gas burner consists of

two concentric sub-burners viz. a primary, inner burner and a secondary, outer burner. A tertiary nitrogen flow is applied to create suitable mixing profiles and for thermal protection of the reactor tube. Fuel particles are fed through the inner burner and are rapidly heated ($> 10^5$ K/s) to the high temperature level of, e.g., a coal flame (1450-1600 °C), at which the devolatilisation takes place. The particles, together with the volatile-laden flue gases, travel down with the gas towards the entrance of an all alumina reactor tube for combustion. Due to the aerodynamically optimized design of the system, a majority of the flue gases is purged, while only a minor part, which however contains almost all char particles, is actually led into the reactor tube. The said tubular reactor is externally heated by two 3.4 kW furnaces equipped with Kanthal Super 1800 elements with a maximum element temperature of 1700 °C. The temperature of each furnace is independently controlled by a Eurotherm controller and two S-type thermocouples.

The fuel particles are fed by means of a commercial Pallas RMG 1000 ram/brush feeder in which the fuel is pressed out of a cylinder against a rapidly rotating brush into a dispersion chamber and transported into the reactor pneumatically. Typically, low particle feed rates are used in order to control the gaseous environment of each particle by means of the imposed gas burner conditions. For this study, a fixed 3g/h feed rate was applied throughout. For low-NO_x operation, this implies that heating and devolatilization of the fuel particles takes place in an oxygen-deficient zone (indicated as zone I in Figure 3.1) provided by the primary, inner burner, whereas subsequent char combustion takes place in a zone with excess oxygen (indicated as zone II in Figure 3. 1).

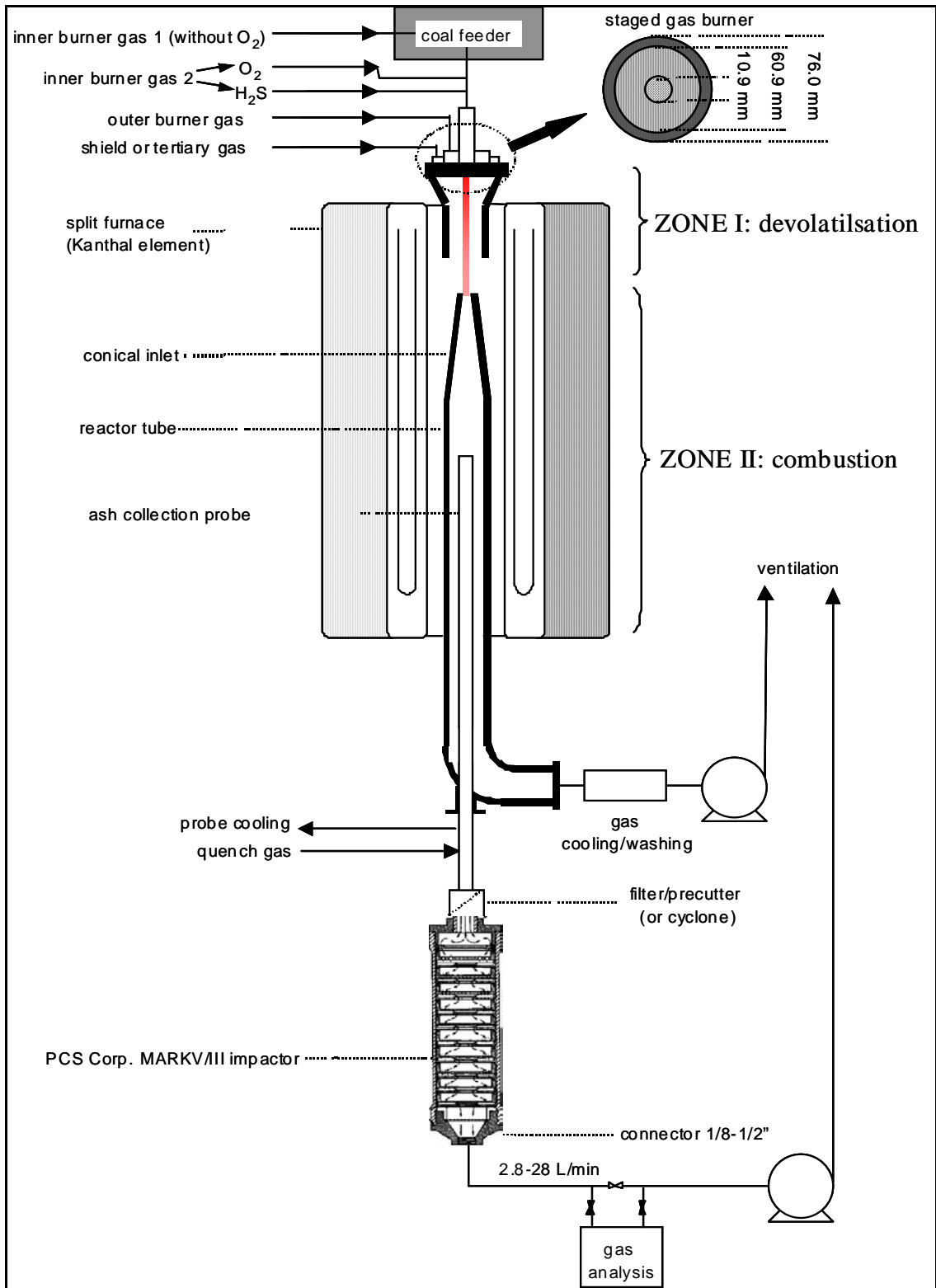


Figure 3. 1: Schematics of the Lab-scale Combustion Simulator (LCS) used to study the formation of ash (incl. aerosols) from biomass and coal

3.2.3 Sampling and analyses

An oil-cooled, quenched gas/particle probe was used for sampling char and ash at four locations along the reactor vertical axis. The particle residence time is taken to be that of a particle with an aerodynamic diameter of 50 μm . Residence time calculations based on the gas velocity, assuming laminar flow and taking into account the reactor geometry, axial gas temperature profile and the particle terminal velocity, showed little ($\pm 10\%$) influence of the particle size when below 100 μm . A University of Washington/PILAT Mark V cascade impactor was used to obtain eleven fractions in the size range $>50 \mu\text{m}$ down to 0.3 μm approximately. Aerodynamic particle diameters are estimated using calibration curves of the cascade impactor, taking into account sampling flow and temperature.

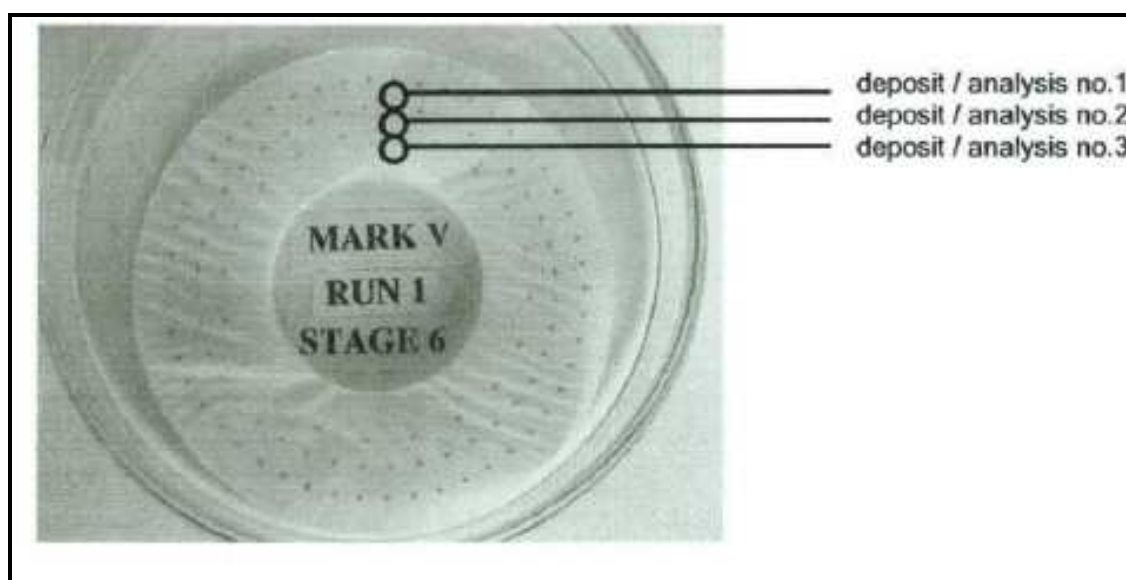


Figure 3. 2: Example of cascade impactor sample (one stage) with an indication of the part of the sample which was analyzed using a scanning electron microscope

Nuclepore® polycarbonate substrates were used for their smooth surface to allow subsequent microscopic analysis. A JEOL FEG-SEM with a coupled EDX system was used to analyze each stage of the impactor. An EDX measurement was performed by scanning the whole of a deposit of particles formed underneath an orifice in the corresponding impactor jet stage (see Figure 3. 2).

In this way a ZAF-corrected analysis of 1-3 deposits per stage was obtained, including the following elements: Si, Al, Fe, Ca, Mg, Na, K, Ti, P, S, Cl, Mn and O.

The elements Zn and Pb were measured using a higher acceleration voltage (15 or 20 kV). In all cases the various analyses on a single stage were found to be very similar, indicating a homogenous loading of the stage. Results are expressed on an oxygen-free basis. Secondary and backscattered electron images (exemplified in Figure 3.3) were stored for all cascade impactor stages from all residence times for visual evaluation. From these, the modal particle sizes were derived from visually inspecting SEM frames containing several hundred particles. Subsequently the distribution of the coarse, fine and aerosols are done based on the modal particle sizes obtained for different cascade impactor stages. Coarse - $>10\ \mu\text{m}$, Fine - $>1\ \mu\text{m}$; $< 10\ \mu\text{m}$, and aerosols - $< 1\ \mu\text{m}$.

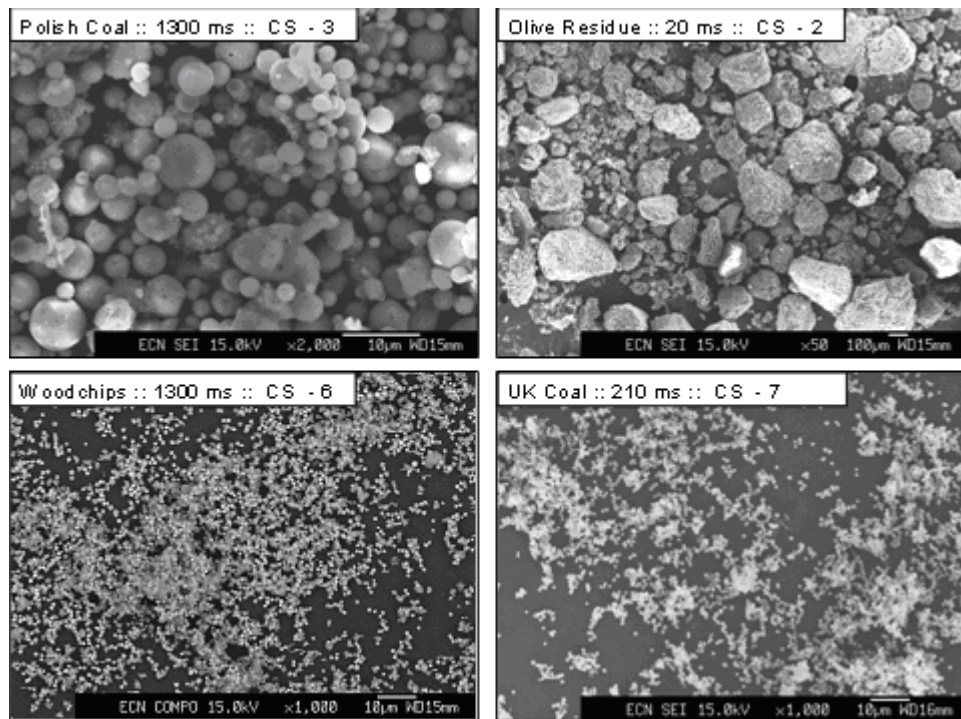


Figure 3. 3: Secondary electron images for different fuels for different residence time and cascade impactor stages

Inorganic matter released from fuel particles during pyrolysis or char combustion can be identified in different ways. In this study, the release of inorganic matter is determined as the difference between the amount of inorganic matter in the fuel and the amount of inorganic matter left over in the solid residue after (partial) combustion.

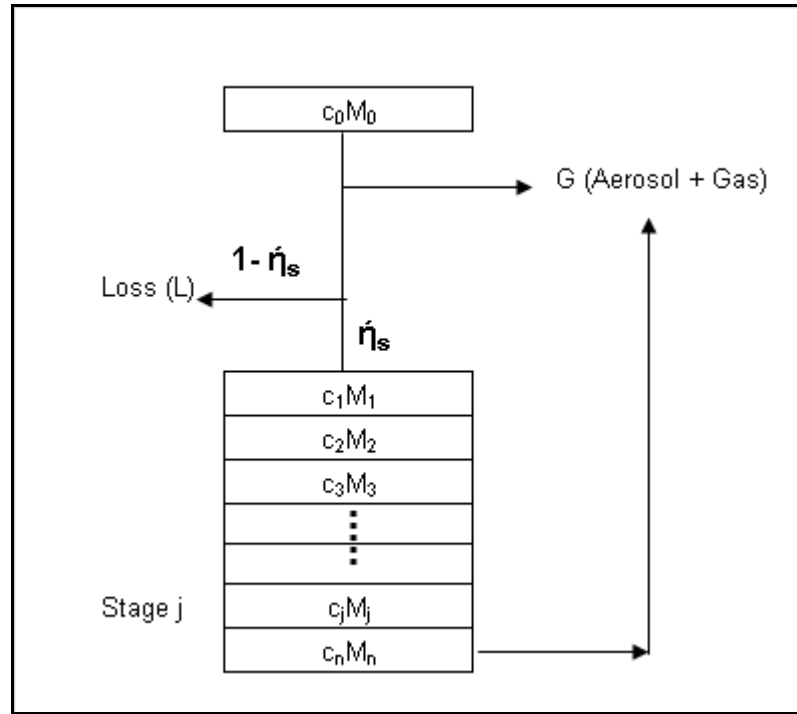


Figure 3. 4: Mass balance per element for cascade impactor measurements

Particulate matter with a particle size smaller than 1 μm (aerosol) is mathematically added to the released part as shown in Figure 3. 4

Overall mass balance equation for the single mineral element will be

$$\sum_{i=1}^j c_i M_i + G + L = c_0 M_0$$

(1)

Where c_i = mass fraction of the mineral element obtained in the different cascade impactor stages

M_i = total mass of the mineral element obtained in the different cascade impactor stages

c_0 = mass fraction of the mineral element in the feed

M_0 = total mass of the mineral element in the feed

Release

The release is calculated according to the formula shown in equation (2) :

$$\eta_r \equiv \frac{G}{c_0 M_0} = \frac{c_0 M_0 - \sum_{i=1}^j c_i M_i - L}{c_0 M_0} \quad \text{and} \quad \frac{L}{\sum_{i=1}^j c_i M_i} = \frac{1 - \eta_s}{\eta_s} \quad (2)$$

So

$$\eta_r = 1 - \frac{1}{\eta_s} \sum_{i=1}^j \frac{c_i M_i}{c_0 M_0} \quad (3)$$

The recovery (η_s) (not to be confused with the sampling efficiency) is calculated by assuming the release (G) of the stable elements (such as Si, Al and Fe) as zero. The choice of these conservative “marker” elements is done by considering the specific chemistry of fuel: i.e. for wood it may be Ca while for both the coals, Al and Si. On the other hand Ca is not a good marker for bark, where it is available in the form of oxalate and is almost integrally mobilized into the gas phase in the form of superfine CaO aerosol. The η_s can be calculated from equation (3) as below.

$$\frac{\sum_{i=1}^j c_i M_i}{c_0 M_0} \equiv \eta_s \quad (4)$$

If multiple stable elements are considered:

$$\left\{ \left[\frac{\sum_{i=1}^j c_i M_i}{c_0 M_0} \right]_{\text{element 1}} + \left[\frac{\sum_{i=1}^j c_i M_i}{c_0 M_0} \right]_{\text{element 2}} + \left[\frac{\sum_{i=1}^j c_i M_i}{c_0 M_0} \right]_{\text{element 3}} + \dots \right\} \frac{1}{\text{no. elements}} \equiv \eta_s \quad (5)$$

All the details of the above calculations can be found in [17].

3.3 Results

The results are graphically presented in Figures 3.5-3.10, which are tackling various aspects of the fuel particle size evolution in due course of the combustion process. The detailed experimental results are tabulated in Appendix C. The char chemical conversion and devolatilization rates are quantified using the ash tracer method, thus allowing for understanding the effect of varying ash content in the different fuels. Mass-based distributions across particle sizes and size reduction factors are calculated to identify the extent of the fragmentation in the different fuels with varying chemical and physical properties. Size-resolved mineral distributions are calculated to see the effect of mineral matter and its association onto the char matrix reactivity.

3.3.1 Conversion

The association of the mineral matter with the carbon matrix and the characteristics of the carbonaceous matter itself, define to a high degree the subsequent physical properties of the formed char, such as the available surface area for char oxidation during combustion. The relative surface area available will be less for the fuel having high ash content due to the lower abundance of active carbon sites. Thus a fuel with high ash content can be expected to form relatively less reactive char compared to a fuel with low ash content. The lower the ash content, the higher will be the relative char reactivity and the quicker will be its conversion. The higher the volatile matter, the higher will be the devolatilization and therefore the higher will be the overall fuel conversion. Thus, it can be concluded that ash and volatile matter contents are the two most important factors for the relative char reactivity. The third important

parameter is the type of the carbonaceous matter. Figure 3. 5 presents the (ash-tracer based) fuel conversion as a function of residence time.

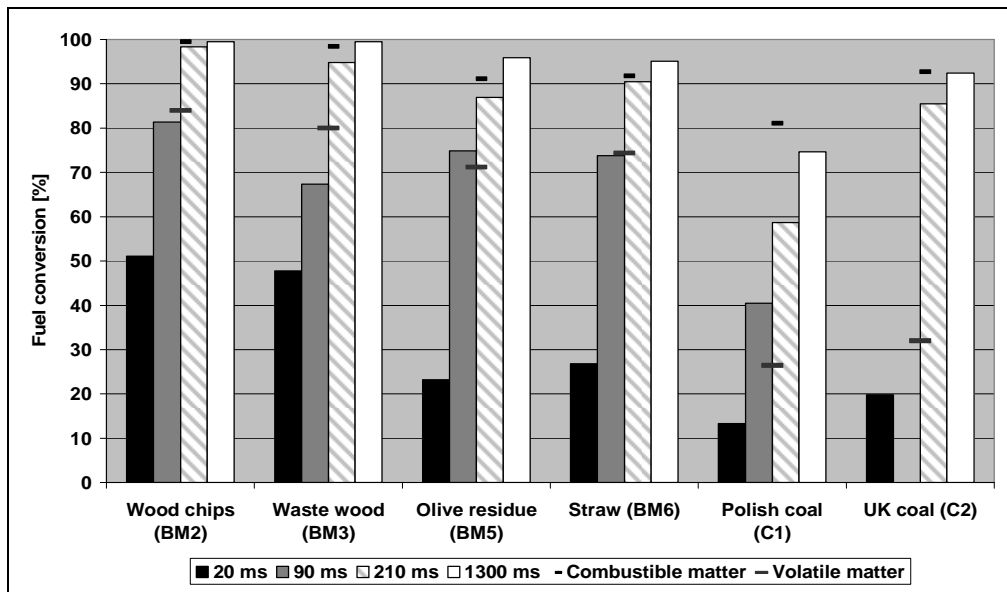


Figure 3. 5: Mass-based fuel conversion as a function of residence time

The volatile matter (from the proximate analysis) and the combustible matter content (taken as 100 % of the dry ash base) are included for reference. All studied biomasses are found to be much more chemically reactive than coals due to the comparatively lower ash and the high volatile matter contents. Both the Polish and the UK coals are much richer in ash and significantly less volatile, hence their conversion is lower and delayed considerably as compared to the biomasses. For example, the wood chips and the waste wood are reaching higher overall degrees of conversion already in the flame (20 ms). The devolatilization of inorganic matter is also a time-dependent process and not merely an instantaneous phenomenon, as can be seen in the graphs presented in Figure 3. 11.

3.3.2 Ash Release

Most of the inorganic matter is released in the first ~200 ms, however the release in the last burnout stage (1300 ms) with extended residence time is still countable.

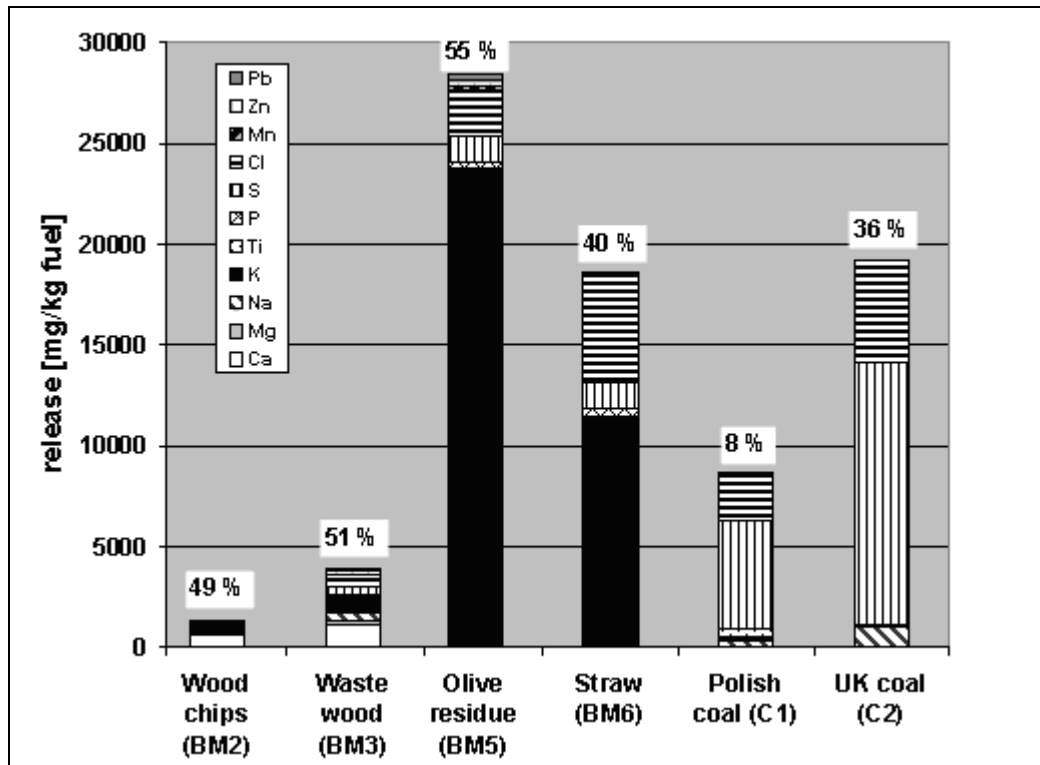


Figure 3. 6: Amount and distribution of inorganic elements released after 1300 ms residence time. (Percentages represent the ratio of the sum of inorganic elements released to the sum of inorganic elements in the fuel.)

Figure 3. 6 presents an overview of the amount of the different elements released after 1300 ms of residence time in the combustion chamber.

The data are expressed as the amount of element X released in milligrams per kilogram of dry fuel, so they can be easily applied in combustion process calculations. The percentage plotted over each stacked bar represents the mass ratio of the sum of inorganic elements released to the sum of inorganic elements in the fuel.

Large differences are observed between fuels. The release in mg/kg is influenced by the fuel's ash content and the reactivity of the ash constituents [17]. The relatively small ash release from the wood type fuels reflects their low ash content, while the high ash release from olive residue and straw is caused by the higher ash content but especially by the high ash volatility. The release from both coals is dominated by the elements sulfur and chlorine. If the sulfur content of the coal is high, then the release will be high too.

3.3.3 Size distribution

This section describes the mass-based particle size distributions (PSD) (in % w/w) during char burnout stage for different coal and biomass fuels. The mass-normalized PSDs of all fuels presented in Figure 3.7 and Figure 3.8 have been calculated by converting the volume fractions, obtained by Malvern Mastersizer analyses (Appendix 2), assuming a single bulk average density and a spherical particle shape. In contrast, the mass fractions of the ashes at different residence times have been obtained from direct gravimetric analyses of the cascade impactor samples. This is done to help identify the type as well as the extent of the fragmentation and size reduction at different char burnout levels. The presented particle size distribution is based on weight share of the three size fractions (namely the coarse, the fines and aerosols particles with the corresponding sizes $>10\ \mu\text{m}$, $>1\ \mu\text{m}$ and $<1\ \mu\text{m}$ respectively) and vap (devolatilization) at each stage for all fuels as shown in Figure 3.7.

Significant increase in the aerosol concentration during the initial char burnout (20 and 90 ms) is possibly a sign of burning with attritive fragmentation (Figure 3.8 and Figure 3.9). Furthermore, fine ash particle concentration (Figure 3.7) is decreasing in the first 20 ms for all fuels and this proves that lower size particles oxidize and devolatilize quickly compared to larger particles. The faster conversion of the smaller char particles is clearly observed for all the fuels except Polish coal where ash content is the highest. It is evident from the experiments that after a certain conversion, larger particles fragment in breakage or percolation mode more than the smaller particles for all fuels and therefore their concentration decrease more rapidly in the later time steps. Biomass was found to be fragmenting more than coal. Percolative fragmentation during the final char burnout stage is clearly manifesting itself in the considerable increase in fine, fly ash and aerosol concentrations.

3.3.4 Relative Size Reduction

Particle size reduction factors calculated for all cascade impactor stages at different residence times are shown in Figure 3.10. Modal particle sizes for each cascade impactor stages have been read visually using SEM images for all different residence times. Relative size reduction is calculated by considering the size reduction of the

final char burnout (1300 ms residence time) as 100 %. Although, it is a very rough method to calculate particle size reduction, it gives an idea how particle size will reduce at different residence times. The resulting sizes for the upper cascade impactor stages ($> 30 \mu\text{m}$) are due to burnout and fragmentation while for the lower cascade impactor stages ($< 30 \mu\text{m}$) it is assumed as only due to burnout, as smaller particles will not fragment much.

From Figure 3.10, it can be clearly seen that particle size reduction is very complex and no specific trend can be derived for particle size reduction with the different biomass and coals. For all fuels, irrespectively of their different char conversions due to different chemical and physical properties, the average size reduction between two successive initial residence times of 20 ms and 90 ms (so within 70 ms) is observed to be between 20-30%. The smallest size reduction of 10 % is observed during the longest residence time “slot” ($1300-210 = 1090$ ms), between the last two successive residence time 210 ms and 1300 ms. This proves that particles reduce their sizes most in the devolatilisation phase (kinetic – diffusion controlled regime) where particle size reduces due to burnout and breakage mode of fragmentation while they reduce less at extended residence time (kinetic controlled regime) where very little or no burnout along with percolative mode of fragmentation is expected.

Initially in the combustion process, fine ash particles reduce in size more rapidly compared to coarse particles, as volatilization and rapid char oxidation occur fast in the smaller particles due to less surface area and high oxygen concentration around the surface. It can be seen in the all studied fuels except the UK coal where no such trends are observed.

3.3.5 Elemental Distribution with PSD

The elemental distribution has been derived for each char burnout stage, which is presented in Figure 3.11. Elemental release and size-resolved distribution after char burnout, devolatilization and fragmentation are calculated for all residence times. It is observed that sulfur and chlorine starts vaporizing earlier at 20 ms in the flame itself where the release of alkali and other mineral elements are negligible. Alkali minerals appear to be vaporizing in the second time steps at around 90 ms. In silica and aluminum rich fuels such as straw and the two coals, the overall release of alkali

minerals is limited which proves that alkaline metals in intimate contact with silicious network make them less volatile. The release of calcium and magnesium is observed to be significant in calcium and magnesium rich woody fuels. Alkali rich fuel such as olive residue is found to be most volatile compared to all other fuels.

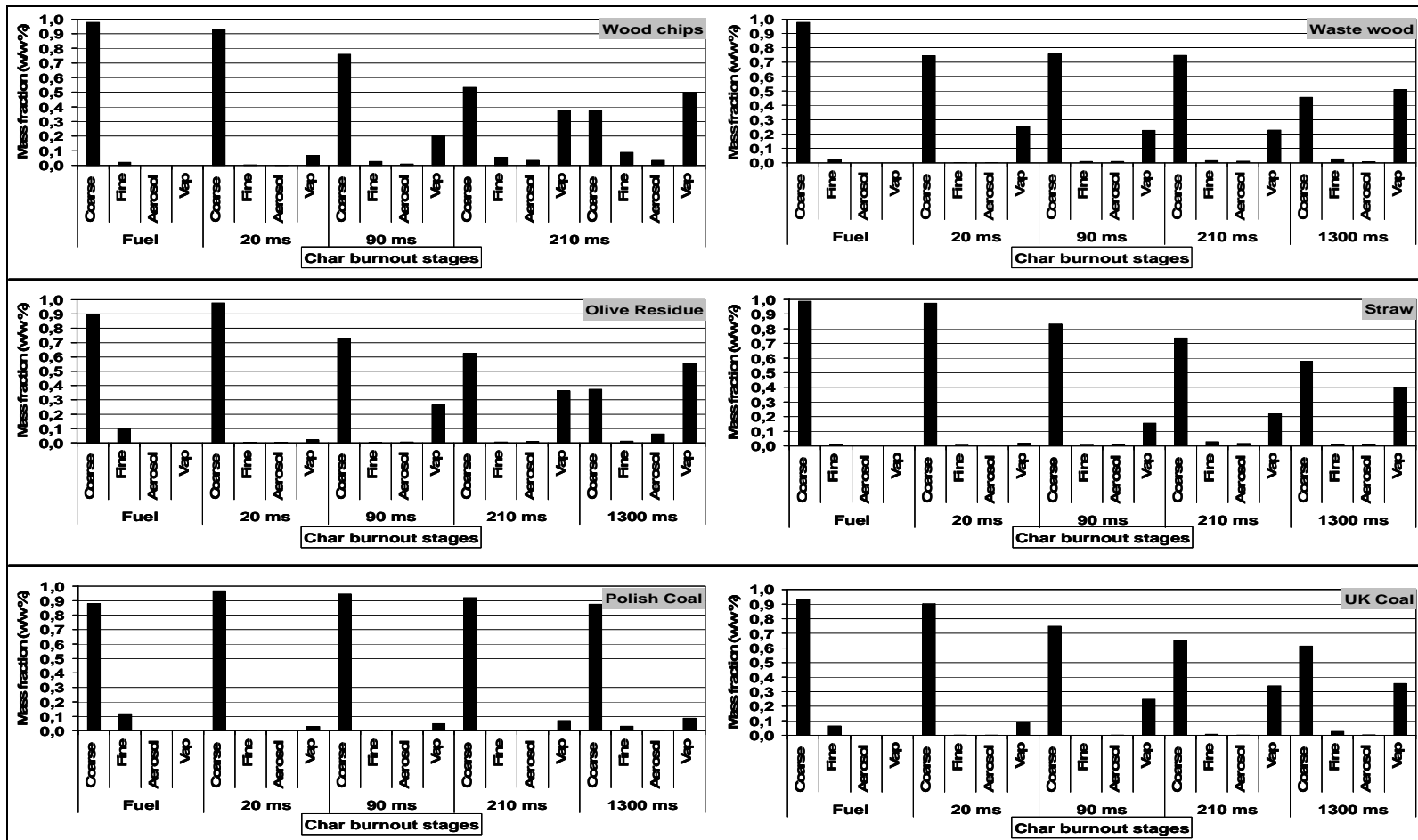


Figure 3. 7: Particle size distribution with weight percentage of size fractions (such as coarse, fine and aerosols particles with sizes $>10 \mu\text{m}$, $>1 \mu\text{m}$ and $<1\mu\text{m}$ respectively) and devolatilization (Vap) at different char burnout level

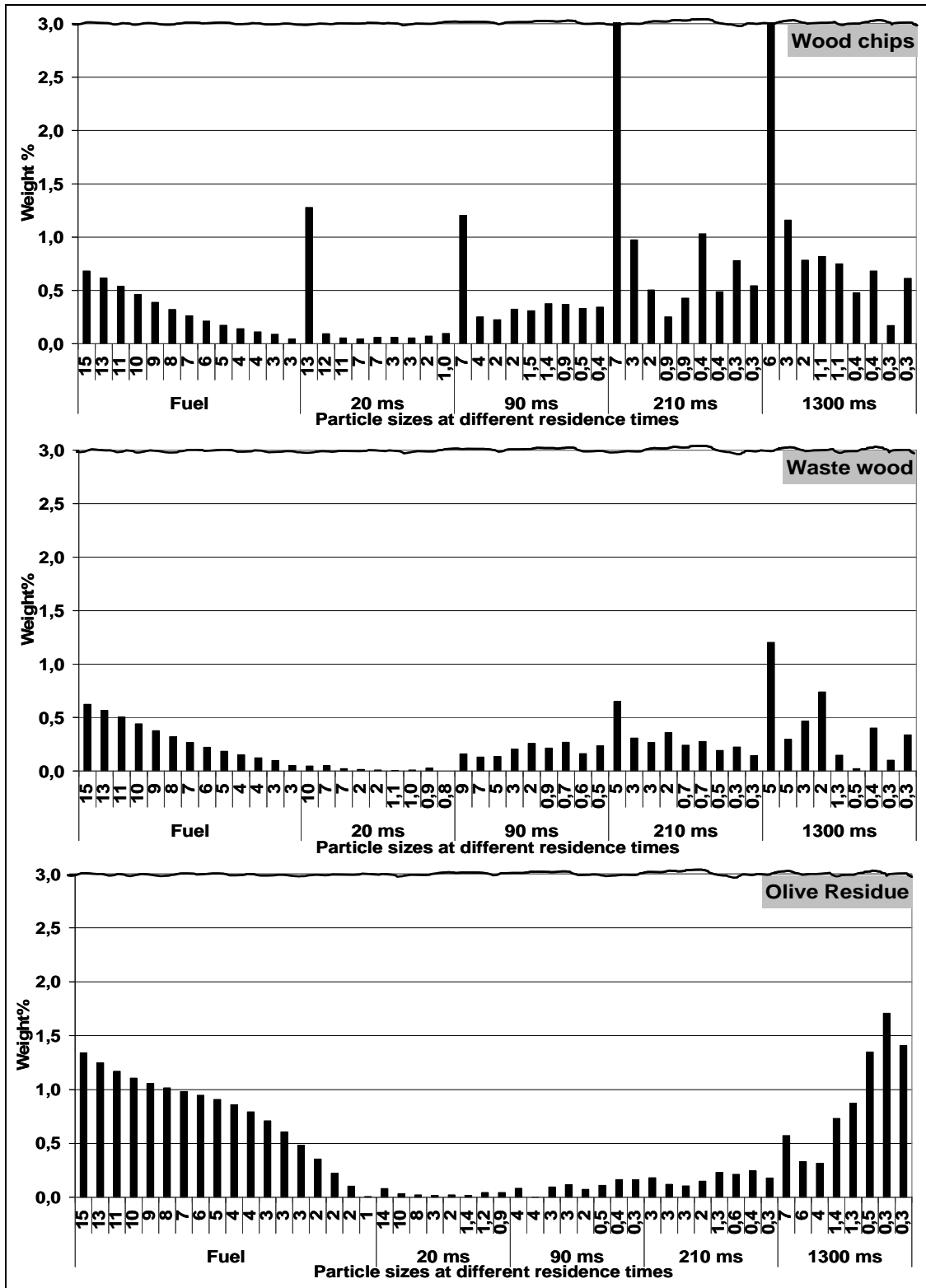


Figure 3. 8: Particle size distribution with weight percentage of size fractions ($\leq 15 \mu\text{m}$) at different residence

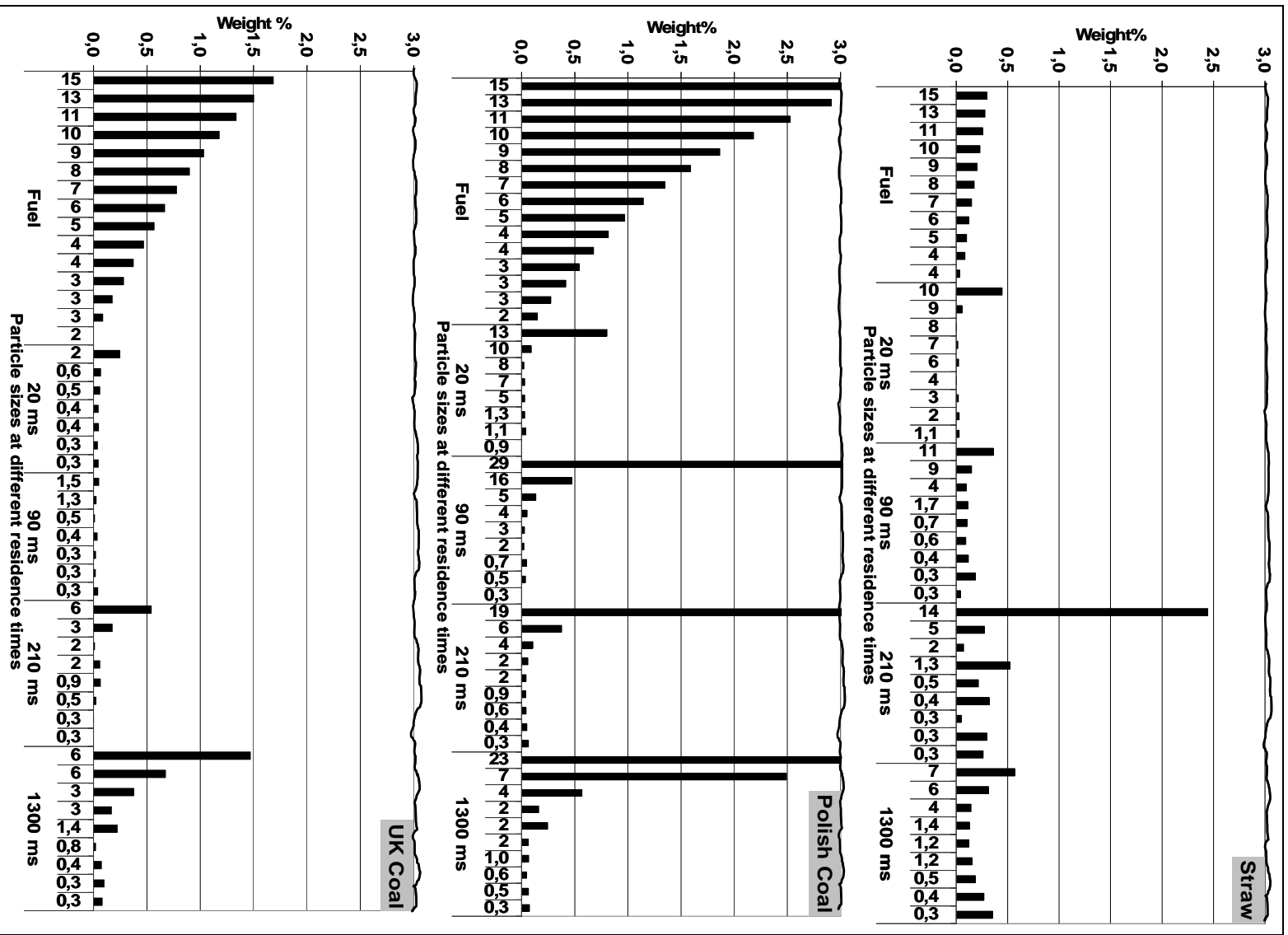


Figure 3.9: Particle size distribution with weight percentage of size fractions ($\leq 15 \mu\text{m}$) at different residence times

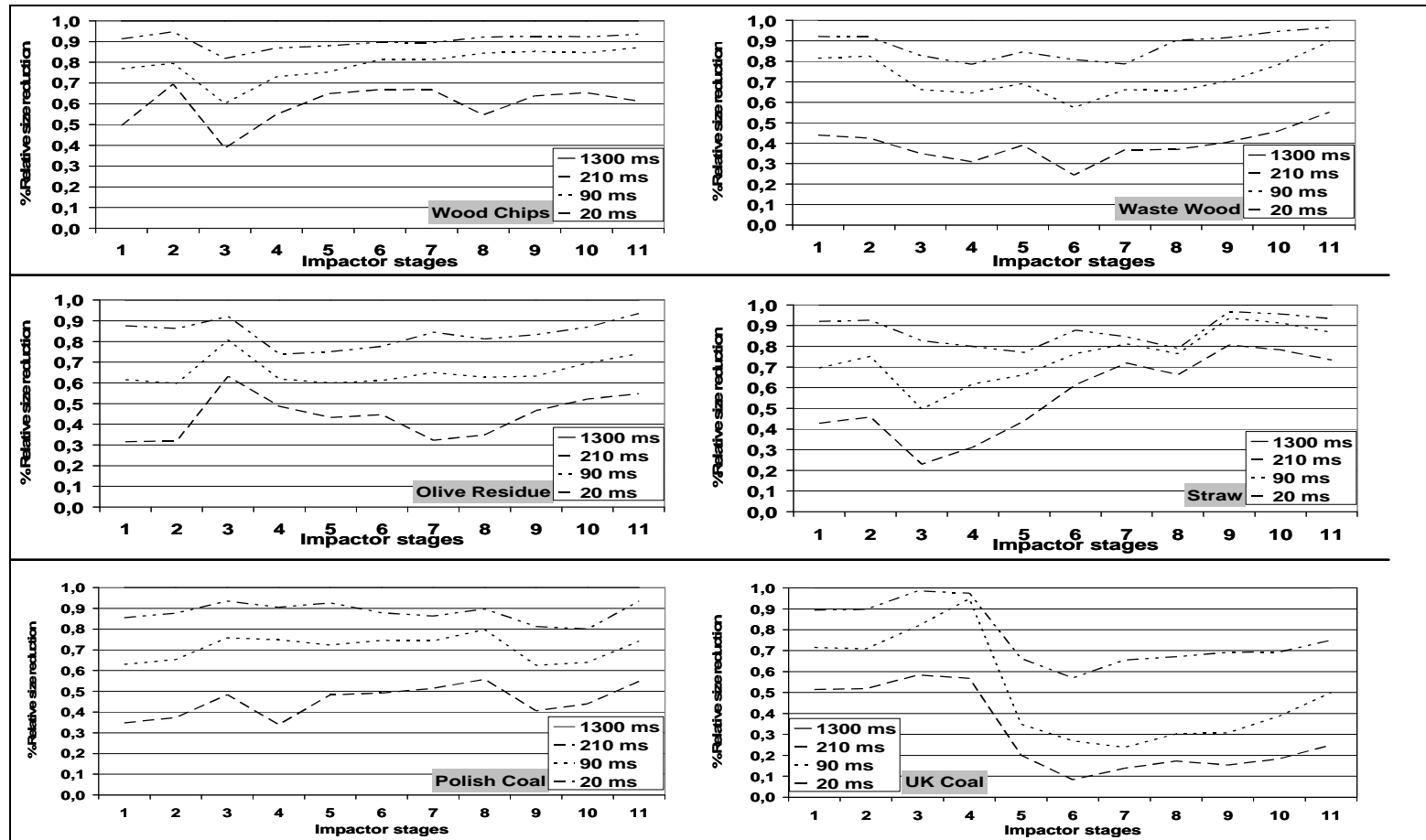


Figure 3. 10: Relative size reduction at different residence times

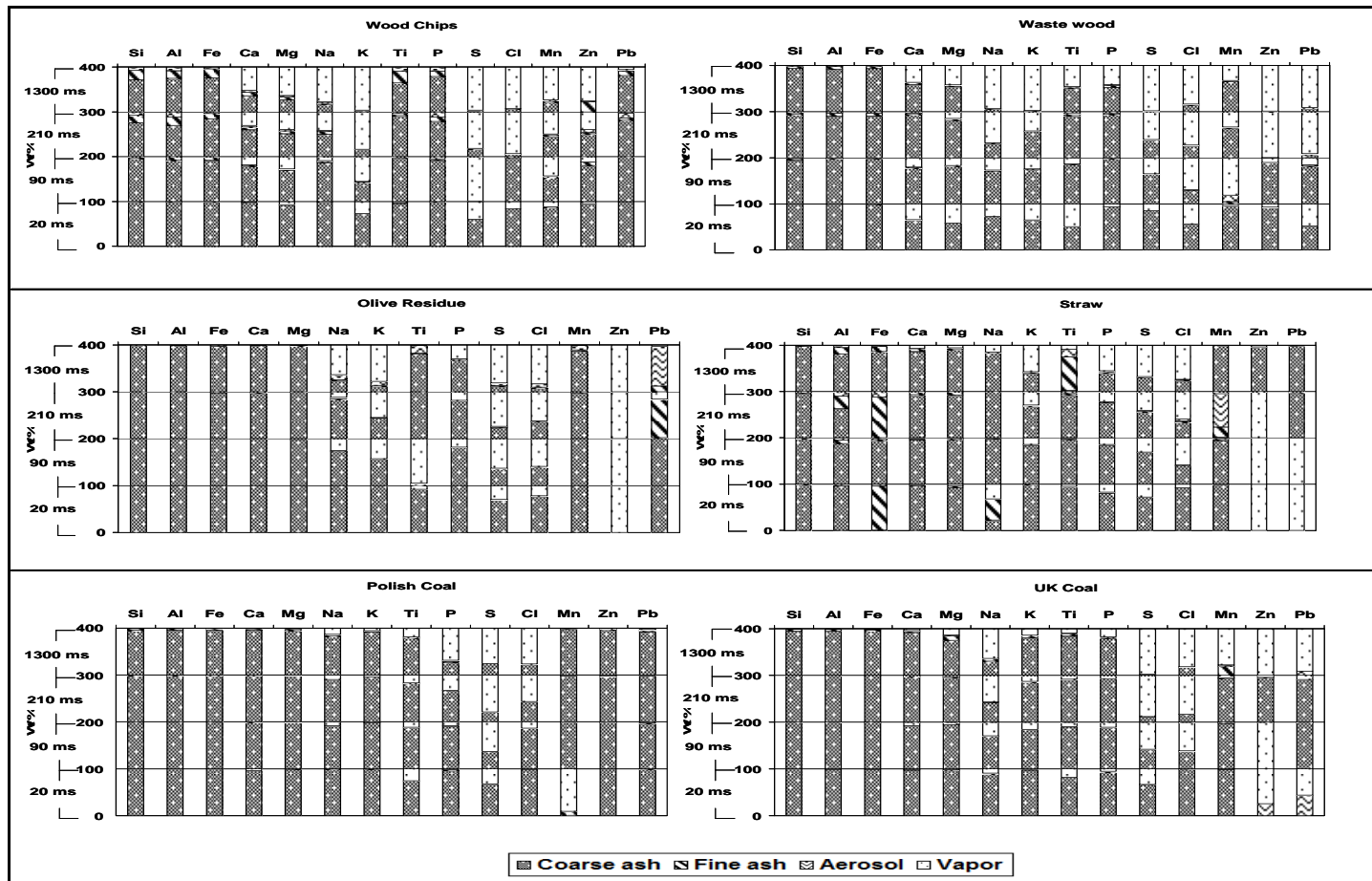


Figure 3. 11: Mineral matter distribution in different size fractions at different char burnout level

3.4 Summary

Polish Coal has the highest ash content compared to all other fuels studied, amounting to ca. 19 % w/w d.b., while its volatile matter content is the lowest constituting approximately 26 % w/w d/b. It can be described as producing the least reactive char of the test fuels range. The other physical line transformations such as devolatilization and fragmentation are also observed to occur to a lesser degree. As this coal is rich in reactive silicious components, alkali release is also found to be the lowest compared with the other experimental fuels.

UK Coal has an ash content around 7 % w/w d.b., while the volatiles account for ca. 32 % w/w/ d.b. Compared with the biomass fuels, this coal too can be termed as relatively unreactive, yet it is significantly more reactive than the Polish coal. Therefore, char burnout, devolatilization and fragmentation can be described as moderate. The UK Coal is less rich in silica compared to the Polish coal, moreover, it has high content of sulfur and chlorine (23 and 13% w/w d.b., respectively). Alkali release is quite significant from this compared to Polish coal.

Wood chips have a very low ash content if not negligible ($\ll 1$ % w/w). It is a highly volatile fuel having VM contents of around 84 % w/w d.b. This also translates into relatively highly reactive char compared even to other biomass fuels. The total char conversion is very fast and almost 50 % conversion is achieved upon 20 ms residence time. A high extent of devolatilization and fragmentation is also observed. The wood chips ash composition is dominated by calcium and magnesium. The release of Ca, Mg, Na, K, S and Cl is observed to be significant. However, since the ash content is very low in wood chips, very little carbonaceous matter in the char will be associated with minerals and devolatilization will be quite low in terms of mg/ kg of dry fuel. Due to the said low mineral element content and the corresponding low ash release, at high char conversion levels the char particle is likely to attain very high temperature. Therefore, significant fragmentation is observed, initially with attrition mode of fragmentation - by shedding of small particles from the surface due to the increase in thermal stress at the surface of the particles - and later on significant percolative fragmentation inside the particles due to the increase in overall thermal stress.

Waste wood is similar to the earlier described wood chips, as this too is characterized by a low ash contents (2 % w/w d.b.). Likewise, it has also a high volatile matter (80%) content. In general, all the aspects of this fuel conversion are very similar to those of the clean wood chips. Hence it too can be termed as a highly reactive fuel. The extent of the char conversion, devolatilization as well as the fragmentation is comparable to that of the wood chips.

Olive Residue is an alkali-rich fuel, having ash percentages around 9 % w/w d.b. - quite high compared to woody biomasses. Yet, it also has high volatile matter (71 % w/w d.b.) content, similar to that of the woody biomass and equally it forms a medium to highly reactive char. The char particles however contain less active carbon sites due to the high ash content. Therefore initially at 20 ms, char conversion is lower in this fuel. Nonetheless due to the high alkalis and volatile matter contents, after a relatively short residence time (90 ms), presumably when char achieves a certain minimum temperature, further conversion, devolatilization and fragmentation are observed to proceed very fast. At the onset of the combustion process less initial fragmentation is observed due to less conversion and devolatilization as compared with wood. Nonetheless excessive percolative fragmentation is observed due to the quick conversion and high devolatilization during later stages. The ash release is dominated by alkalis, alongside with chlorine and sulfur. It is also one of the reasons for increase in aerosol particles formation.

Straw has almost the same ash content (around 8 % w/w d.b.) as the olive residue. The volatile matter is also high (74 % w/w d.b.). This fuel can also be termed as producing moderate to highly reactive char, similar as the olive residue. However unlike the olive residue, in this case volatilization of alkalis is less pronounced even once char achieves minimum temperature after certain conversion. This is most likely due to relatively high levels of silica present in the fuel; compared to olive residue. Fragmentation is also less extensive, due to the lower extent of devolatilization. The ash release is predominated by potassium, chlorine and sulfur.

3.5 Qualitative prediction

As shown in Table 3.2; the conversion, devolatilization and the fragmentation can be predicted qualitatively by taking into account the fuels ash, as well as the volatile

matter contents. In general terms, higher ash contents reduce the relative char reactivity. Higher volatiles in the fuel result in a higher devolatilization and thus a higher overall conversion already early on in the combustion process. The higher overall conversion can result in a higher fragmentation. The higher carbonaceous matter and lower ash content increases the char particle temperature to a great extent during combustion which leads to high fragmentation due to the increased thermal gradient. Silica and alumina are both responsible for lowering the devolatilization of alkalis. Sulfur on the other hand volatilizes quickly and fully.

Table 3. 2: Qualitative prediction of the devolatilization, char conversion and fragmentation

FUEL	Ash Content	Volatile matter content	Si & Al content	Sulfur content	Devolatilization	Conversion	Fragmentation
Wood chips	Low	High	Low	Low	Less (but quicker)	High	High
Waste wood	Low	High	Low	Low	Less (but quicker)	High	High
Olive Residue	High	High	Low	Low	High (but slower)	High	High
Straw	High	High	High	Low	Medium	Medium	High
Polish coal	High	Low	High	Low	Less	Less	Less
UK Coal	High	Low	Medium	High	Medium	Medium	High

3.6 Conclusions

Based on the lab-scale tests with different coals and biomass fuels, first line ash transformations were investigated. The following conclusions can be drawn from the said work:

1. Ash transformations and char combustion will be in the kinetic-diffusion controlled regime, even with extended residence time with typical pulverized fuel firing conditions.
2. Char chemical conversion is found to be dependent on ash content and volatile matter at typical pulverized fuel firing conditions. Fuels having high ash content with fewer active carbon sites for smooth char oxidation are converted more slowly. Within the test fuel range examples of such fuels are the UK coal, the Polish coal and to a lesser extent the olive residue and the straw. The UK and Polish coals are further characterized by high ash- and low volatile matter

contents. Therefore, overall chemical conversion is lower for both of these fossil fuels. On the contrary, the olive residue and straw have relatively high contents of volatile matter. Therefore, the initially low conversion is quickly accelerated when the fuels reach a certain critical temperature. The high volatiles result in a high overall conversion. Also, smaller sized particles convert more quickly than larger sized particles.

3. Devolatilization of the fuels also depends on the mineral elemental matter and its association with the carbon matrix. Fuels having high volatile matter contents are found to be highly devolatilizing. Chlorine and sulfur starts devolatilizing early in the combustion. Alkalis release will be limited under the presence of silica and alumina in the fuel. The other non-volatile oxides such as calcium and magnesium are also found to be devolatilizing in some of the fuels where their content is high. The devolatilization of individual minerals will be studied separately in the next Chapter 4.
4. Fragmentation is found to be dependent on fuel chemical conversion and devolatilization. The quicker and higher the fuel chemical conversion and devolatilization, the more pronounced will be the fragmentation. Woody biomass is a good example of this mechanism. Three kinds of fragmentations are observed: attrition, breakage and percolative fragmentation. During the initial heat up and devolatilization, biomass and coal were found to be fragmenting attritively. Excessive percolative fragmentation was observed only after a critical conversion (approximately 60-70%) of the char. Larger sized particles fragment more compared to smaller sized particles.
5. Although the present study does not include the effect of particle size, shape, density and mineralogy (included/excluded minerals) at constant high operating conditions, the qualitative predictions based on the fuels mineral elemental matter composition, as well as the volatile matter contents appear to approach the experimental results very closely and can be used as an efficient predictive tool for the new fuels.

References

1. S. C. Van Lith, Release of Inorganic during wood firing on grate, PhD Thesis, CHEC Research Centre, Technical University of Denmark, (2005).
2. A. F. Sarofim, J. J. Helbe, In The impact of Ash Deposition on Coal Fired Plants: Proceedings of the Engineering Foundation Conference, June 20-25, (1993), Solihull, England: Williamson, J.; Wigley, F. (Eds.); Taylor & Francis; London, (1994).
3. R. Mitchell, An intrinsic kinetics-based, particle population balance model for char oxidation during pulverized coal combustion, Proceedings of the Combustion Institute 28 (2000) 2261–2270.
4. P. Campbell, R. Mitchell, A. Liqiang, Characterization of coal and biomass char reactivity to oxygen. Proceedings of the Combustion Institute 29 (2002) 519-526.
5. R. H. Hurt, K. D. Davis, Percolative Fragmentation and Spontaneous Agglomeration, Combustion and Flame 116 (1999) 662–670.
6. S. Charpenay, A. Serio, R. Solomon, The Prediction of Coal Char Reactivity Under Combustion Conditions, Twenty-fourth symposium (international) on combustion, The Combustion Institute (1992) 1189.
7. G. Hargrave, M. Pourkashanian, A. Williams, The combustion and gasification of coke and coal chars, Twenty-first symposium (international) on combustion, The Combustion Institute (1987) 1008.
8. M. L. Chan, J. M. Jonesa, M. Pourkashaniana, A. Williams, The oxidative reactivity of coal chars in relation to their structure, Fuel 78 (1999) 1539–1552.
9. L. Baxter, Ash deposition during biomass and coal combustion: a mechanistic approach, Biomass Bioenergy 4 (1993) 85–102.
10. H. Schurmann, P. Monkhouse, S. Unterberger, K. Hein, In situ parametric study of alkali release in pulverized coal combustion, Proceedings of the combustion Institute 31 (2007) 1913-1920.
11. H. Westberg, M. Bystrom, B. Leckner, Distribution of potassium, chlorine and sulphur between solid and vapor phases during combustion of wood and coal. Energy and Fuels 17 (2003) 18-28.

12. S. Jimenez, J. Ballester, Effect of co-firing on the properties of submicron aerosols from biomass combustion, *Proceedings of the Combustion Institute* 30 (2005) 2965-2972.
13. P. Thy, C. E. Leshner, B. M. Jenkins, Experimental determination of high-temperature elemental losses from biomass slag, *Fuel* 79 (2000) 693-700.
14. N. Syred, K. Kurniawan, T. Griffiths, T. Gralton, R. Ray, Development of fragmentation models for solid fuel combustion and gasification as subroutines for inclusion in CFD codes, *Fuel* 86 (2007) 2221–2231.
15. P. Dacombe, M. Pourkashanian, A. Williams, L. Yap, Combustion-induced fragmentation behavior of isolated coal particles, *Fuel* 78 (1999) 847–1857.
16. R. Mitchell, Char fragmentation and its effect on unburned carbon during pulverized coal combustion. Contract no.: DE-FG22-92PC92528, For U.S Department of Energy (1997).
17. R. Korbee, J. Lensselink, M. Cieplik, Energy Research Centre of the Netherlands; Final report of task 1.3 – Release of ash forming matter in pulverized fuel systems; SES6-CT-2003-502679, (2006).

Chapter 4

Ash release of minerals during PF combustion

It was one of the conclusions from the Chapter 2 that the chemistry of mineral matter composition and their association in the fuel matrix play an important role in devolatilization. In this chapter, ash release of individual mineral element is investigated as a function of elemental mineral matter composition and their association in the fuel matrix under the same PF operating conditions as applied in Chapter 2. In the previous chapter char oxidation, devolatilization and fragmentation were quantified for six different coals and biomass (Wood chips, Waste wood, Olive residue, Straw, Polish coal and UK coal). In the present chapter, ash release for individual mineral element is studied for a total of eight coals and biomass by adding two more biomass fuels (Bark and Saw dust) to the previous list.

Ash release was modeled using chemical fractionation method and thermo chemical equilibrium calculations at ECN. In an extended effort in the present work, simple correlations (empirical indices) have been attempted to predict the ash release of several mineral element as a function of elemental mineral matter composition and their association in the char matrix. The empirical indices developed in this chapter can work as an effective tool to predict the ash release and have also been used in Chapter 6 for modeling the overall ash formation.

4.1 Introduction

Power generation from biomass fuels and coals poses several technical and economic challenges. In chemical terms, coal and biomass fuels are complex composite materials which contain inorganic species along with organic matter. In the fuel matrix, these inorganics are present as free ions, salts and organically-bound as well as in the form of fine crystalline materials such as quartz, carbonates, oxalates and sulfides etc. Upon combustion, volatile minerals release from the fuel matrix in the form of gaseous and condensed ash [1]. The gas phase inorganic elements may

undergo numerous physical transformations such as nucleation, coagulation and homo/heterogeneous condensation in few milliseconds just after fuel enters the combustion furnace. Ultimately these gas-to-particle transformations lead to the formation of homogeneous aerosol particles and / or heterogeneous fine ash particles. The gas phase release / condensed particles lead to problems such as slagging, fouling, corrosion, erosion and harmful emissions of gases and particulate matter.

Chemical equilibrium and reaction kinetics at the given temperature are known to be responsible for the release of gas phase inorganic species. Baxter et al. [2], in their lab scale PF combustion experiments with six different coals examined them at more rapid heating rates (5×10^5 K/s), more devolatilization of the alkali and alkaline earth metals are expected. Oleschko et al. [3] studied the gas phase release of sodium, potassium, sulfur and chlorine at 800 °C and 1200 °C and reported that different reaction kinetics at both temperature regimes influence the release of alkalis. In general terms the gaseous release of the inorganic elements can be linked with the two phases of material conversion, namely devolatilization and char combustion. During devolatilization, at relatively low temperatures, loosely bound free ions, salts and organically associated alkali minerals will be released. During the char combustion phase, generally at high temperatures, strongly bonded alkalis and alkaline earth metals will also be released [3]. Other important factors for the release of inorganics into the gas phase during combustion include particle size, shape and density. Experimental and theoretical investigations indicate that the particle shape, size and density influence particle dynamics, including drying, heating rate and reaction rate [4]. It is generally observed that spherical particles devolatilize quickly compared to particles of other shapes. Badzioch et al. [5] found that particle size had no significant effect on the weight loss because the heating rate of the particle was controlled mainly by the heating rate of the carrier gas, so that the large particles heated only at slightly lower rates than the fine particles. However, Eyk et al. [6] and Ninomiya et al. [7] studied the release of sodium as a function of the particle diameter and its temperature, for a single burning particle system and observed that during the devolatilization phase, sodium concentrations were found to be reciprocally dependent on the particle diameter, at the same residence times. During the char burnout Na levels were found to decay exponentially with increasing particle temperature. It is also found that the higher the porosity and lesser the

density of the fuel, higher will be the volatilization [6,7]. Mathews et al. [8] observed that mineral matter and macerals composition of the char will be different at different sizes which can affect the devolatilization rates.

A wide range of coal and biomass fuels have been extensively studied to understand their chemical and physical properties [9,10,11]. As a result it has been concluded that the inorganic matter in biomass, is mostly associated in the fuel matrix as free ions, salts and organically bound inorganics, while elder fuels, e.g. peat, lignites and hard coals, contain more excluded minerals. The mode of occurrence of the minerals is specific for each type of the fuel, and allows for ranking them according to their age, origin or pre-treatment/handling. For instance, coals can be divided based on their age and degree of metamorphism into high, medium and low rank coal. The older the coal and higher the degree of metamorphism, the higher the rank and the lower will be the content of the loosely bound inorganics. In the case of biomass fuels, however, such an age-based ranking can not be proposed and it is much better to consider its origin. Such classification would then include for example woody biomass, energy crop, animal or agriculture waste etc. Also this classification could be associated with some general characteristics and so wood and energy crops can be considered to be the purest fuels with low ash content. The agricultural residues and animal wastes or byproducts can be characterized as the more contaminated fuels. In addition within this latter group, the mineral content and its association can be varying due to the nature of the process they stem from, i.e. animal fat will contain significantly less mineral matter than meat and bone meal etc. The higher the free ions, salts and organically bound inorganics, higher will be the ash release.

Coals and biomass fuels contain various mineral elements composed mainly of sodium, potassium, calcium, magnesium, chlorine, sulfur, silica, aluminum and iron, along with trace elements such as zinc, lead, titanium, phosphorous, manganese etc. These trace elements are not discussed further within this work.

Sodium, potassium and partly calcium, magnesium are known to be present as free salts or cations bonded to the carboxylic groups in the biomass (organically bound). Sulfur can be a part of the organic coal structure, but also present as crystalline pyrite (iron sulfide). Chlorine can be found as bound to the organic matter in the fuel or as dissolved chlorides in the inherent moisture [9]. Free ions, salts and organically

bound inorganics are easily devolatilized into the gas phase and react with other gaseous species to form chlorides, hydroxides and oxides. Thus, it can be concluded that the mode of occurrence of the minerals affect their release to the gas phase [12]. It is understood from the literature review that the release of volatile inorganics also depends on the composition of the more conservative inorganic elements in the fuel [13]. Results of the co-firing experiments by Wei et al. [14] and by Cieplik et al. [15] suggest that the inorganic elements present in the fuel such as Si, Al, Ca, Mg, may greatly affect the gas phase release of Cl, K, and Na. It has been found that higher aluminosilicate contents in the fuel makes alkalis significantly less volatile during combustion. Also calcium and magnesium have shown affinity towards aluminum and silica during high temperature PF combustion and may therefore interfere with the alkali capture by aluminosilicates. Additionally the presence of sulfur and chlorine, both released nearly to completion into the gas phase upon combustion, may aid the volatilization of alkalis. A more detailed review of elemental gaseous phase release is described in the following Section 4.1.1.

From the literature review, it is understood that gaseous phase release of inorganic elements during pf combustion is a complex phenomenon depending upon several parameters such as heating rate, temperature, residence time, particle size, shape, density and mineral matter composition along with their association in the carbon matrix. Parameters such as heating rate, temperature, pressure, particle size, shape, density and the residence time (kinetics) can be well described using relatively straightforward numerical or analytical methods. Several simple correlations also exist in this regard. Also, the stable gaseous and solid species composition can be calculated using FACT-Sage or several other thermochemical equilibrium software packages, but these models are giving good results only for thermodynamically stable systems, or for elements with rapid conversion kinetics and are limited to fuel range analysed by chemical fractionation methods [12]. However, there is no simple correlation which exists or has been attempted to identify the effect of elemental mineral matter composition and their association in the char matrix on ash release.

In the present study, given the complex ash release phenomenon involving a number of variables, an experimental attempt is made with limited investigations only on the role of the elemental mineral matter composition and their association in the fuel

matrix onto the gaseous release at typical high temperature PF combustion conditions. The tested fuels are of different groups such as woody biomass and forestry residues, energy crop, agricultural/food waste and high rank coals. The study is carried out in the Lab-scale Combustion Simulator (LCS). The typical pf combustion operating conditions are atmospheric pressure, 1500°C flame/furnace temperatures and heating rates of 10^5 K/s. Gas phase release of alkalis, sulfur, chlorine, calcium and magnesium are quantified and translated into novel linear correlations (empirical indices) aimed at predicting elemental release during PF combustion.

4.1.1 Inorganic elemental gas phase release – a review

4.1.1.1 Release of S

Most of the sulfur in coals and biomass is released into the gas phase in the form of SO_2 . However, if present at sufficient levels as compared with chlorine, sulfur dioxide is prone to react with alkali chlorides to form alkali sulfates. Wall [16] also mentioned that sulfur may react with calcium and magnesium to form sulfates below 1450 °C. Furthermore, Schurmann et al. [13] verified that sulfur and aluminosilicates compete for alkalis and the dominance of one or the other depends on temperature as well as the actual flue gas composition. The increased combustion temperature favors alkali aluminosilicates over sulfate formation, even though both processes are thermodynamically less favorable at higher temperatures. Nonetheless, sufficiently high sulfur contents can support the formation of alkali sulfates even at high temperature [3], in spite of the presence of the aluminosilicates.

4.1.1.2 Release of Cl

Chlorine present in the fuel will be released almost completely to the gas phase as HCl already at low temperatures. With the increase in the temperature, more alkalis released into the flue gas will convert chlorine into alkali chlorides. Also, chlorine has been observed to have pronounced influence on the alkalis release. Thompson et al. [17] predicted that under both coal combustion and gasification conditions, the effect of sulfur on the distribution of potassium and sodium between the gas phase and the slag is minimal, but that the role of chlorine in alkali volatilization is very

pronounced, with the potassium and sodium levels in the gas phase linearly dependent on the chlorine levels. In his experiments also Baxter et al. [2] found that the amount of alkali vaporized during biomass combustion is determined more by the amount of chlorine available to form stable vapors than by the amount of alkali in the fuel.

4.1.1.3 Release of Ca and Mg

Calcium and magnesium cations in most lignites, sub-bituminous coals and woody biomasses are molecularly dispersed and bound to the carboxylic groups [18]. This organically bound calcium can be easily liberated as CaO(g) during pf combustion at high temperatures. Calcium can be found in two principle solid phases during combustion, namely a Ca-aluminosilicate slag or glass and Na-Ca-sulfate. Very few studies [18,19] are reported in the literature addressing the effects of Ca and Mg on the behavior of chlorine and alkali metals. Yet it was found that, aluminosilicates are more likely to react with Ca and Mg, rather than with alkalis. Therefore it may be expected that higher levels of calcium in the fuel will cause more alkalis to remain as gaseous alkali chlorides or sulfates even at high temperatures.

4.1.1.4 Release of K and Na

Alkalis, especially potassium, play an essential role in plant metabolism and are present in organic structures as simple, easily accessible inorganic compounds [20,21]. Alkalis are known to be an important plant nutrient and are required in osmotic processes inside the plant cells. In biomass, they remain organically bound, as free ions, salts, hydroxides or in the aluminosilicate structures (such as microcrystalline quartz-like backbone in straw). Upon coalification and peatification of different biomasses the organically bound alkalis will become less giving way to more mineral-bonded mode of occurrence.

Numerous studies [4,12,13,22] suggest that most of the alkalis present as free ions, salts and organically bound in the fuel will be released to the gas phase during combustion. Hence, under typical PF combustion conditions, the alkaline metals will be mostly released in the form of free ions, hydroxides and salts while in slag or solid residual ash phase, it will occur predominantly as alkali-aluminosilicates.

In the absence of sufficient reactive aluminosilicates, while taking into account relevant levels of sulfur and chlorine the release and the resulting partitioning/speciation of potassium can be very well predicted by thermodynamic calculations (backed up by extensive gas-phase measurements [22]), as illustrated in Figure 4. 1.

As can be seen in the Figure 4.1, at lower temperatures, potassium sulfate vapor condenses to form liquid or solid potassium sulfate while at higher temperatures, it decomposes. The dominant gas-phase, potassium-bearing species at flame temperatures $>1400^{\circ}\text{C}$, are potassium hydroxide, followed by potassium chloride. In the absence of sufficient chlorine for reaction, only the hydroxide is present.

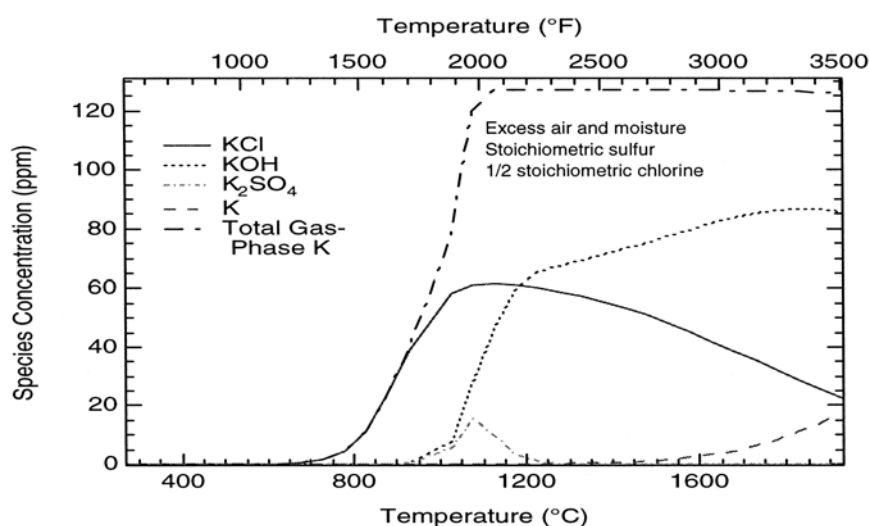


Figure 4. 1: Equilibrium species concentrations for the major potassium-containing, gas-phase species present under typical biomass combustion conditions; Source: Baxter et al. [22]

Sodium also behaves in a similar way to potassium. Osborn [19] observed that sodium associated with carboxylic acid groups has been shown to decompose early in the devolatilization stage. At temperatures in excess of 1500°C , most of the sodium is released into the gas phase primarily as chloride and hydroxide [3]. But, similarly to the earlier-discussed potassium, Gallagher et al. [23] concluded under laboratory-scale pulverized combustion conditions that the fraction of sodium in the vapor is reduced by the presence of silicates under high temperature combustion regimes. Also Wall [16] observed that high proportion of the water soluble sodium vaporizes (i.e. chlorides and as salts of carboxyl groups), but then reactions between

sodium containing gases with silicate fly ashes at high temperature reduces the concentration of these gases. It has also been verified that sodium chloride decomposes in the flue gas to form HCl and sodium carbonate at high temperatures. In the earlier-mentioned study, Wall [16] suggested the relative order of stability of sodium compounds in a non-reducing atmosphere for the range of 1300-200 K as: $\text{NaCl}_{(c,g)} > \text{Na}_2\text{SiO}_5_{(c)} > \text{NaOH}_{(g)} > \text{Na}_{(g)}$. Also Sarofim et al. [24] reported high alkali release dependence on the extent and size of silicon containing minerals in the coal.

4.2 Experimental

From the literature review, it is found that the ash release transformations are very much complex and difficult to study with the more number of variables. Therefore, to limit this problem, it was decided to investigate only the effect of elemental mineral matter composition and their association in the fuel matrix onto the ash release. It is well known that different coals and biomass will have different elemental mineral matter composition and association in the fuel matrix according to their type, age, rank and handling etc. Therefore, an extensive experimental ash release study with eight different coals and biomass was planned at Energy Research Centre of the Netherlands, especially to investigate the effect of elemental mineral matter composition and their association in the fuel matrix on the release of several volatile elements such as potassium, sodium, chlorine, sulfur, calcium and magnesium etc.

The elemental ash release for the nearly complete combustion (1300 ms) for Woodchips, Waste wood, Olive residue, Straw, Polish coal and UK coal have been obtained from the experiments carried out in Chapter 3 while new experiments for the ash release at complete combustion (1300 ms) were planned for two more biomass fuels i.e. Bark and Sawdust etc. with the same methodology explained in Chapter 3. The mineral elemental ash release for these six biomass and coals are tabulated in Appendix C.3.

4.3 Results and Discussion

The selected test matrix for coals and biomass fuels is characterized by a broad range of mineralogy entailing also varying association of the inorganics in the fuel matrix. The mineral elemental release for all the fuels is quantified by experiments and then described by means of simple linear correlations (with $> 0.95 R^2$ value) as a function of elemental mineral matter composition and their association in the char matrix.

4.3.1 Release from tested coals and biomass fuels

Firstly, the experimentally found release of each of the tested fuels is graphically presented in Figure 4.2.

The present study discusses only the release of potassium, sodium, chlorine, sulfur, calcium and magnesium which contributes to the major share of the total elements with respect to their presence and association in the fuel matrix.

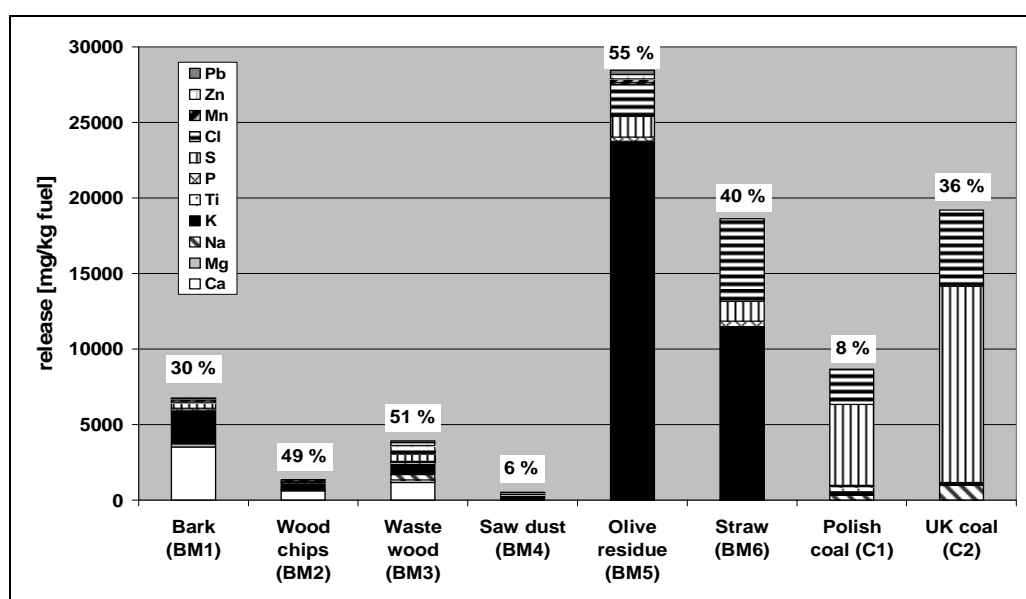


Figure 4. 2: Amount and distribution of inorganic elements released after 1300 ms residence time. (percentages represent the ratio of the sum of inorganic elements released to the sum of inorganic elements in the fuel)

Bark (BM1)

Bark is a product of extraneous surface of woody biomass. This falls into the forestry residues category within the woody biomass group. It is characterized by a moderate ash level. These inorganic constituents are highly volatile and hence the overall ash release in this fuel is also high (30%). The alkali release is nearly complete as this

fuel is likely to contain water soluble alkalis (free ions, salts and organically bound). Moreover, it has low silica and high calcium content, both contributing to an even higher alkali release. Sulfur and chlorine, both at levels significantly lower than the alkalis are also released nearly completely. The more conservative calcium and magnesium are also volatilized partly, and it has been verified that much of these elements is present in the form of crystalline oxalates which decompose at the increased temperature, releasing finely dispersed calcium and magnesium oxides.

Wood chips (BM2)

It is a pure form of woody biomass which has low ash content and high volatiles. Although, ash is composed to a large extent of calcium, with a minor proportion of silicon and potassium it has a high overall ash release (49%). The release of alkali, sulfur and chlorine is almost complete and accompanied by a partial release of calcium and magnesium.

Waste wood (BM3)

It is a waste/byproduct from forestry refinery. Like pure wood, this has also little ash and high volatile matter content. The overall ash release is also high in this fuel (51%), similar to the wood chips. However, the release of sodium from this fuel is observed to be little less than expected. The potassium, chlorine and sulfur are released completely with partial release of calcium and magnesium.

Sawdust (BM4)

Same as wood chips and the waste wood, this is also a pure form of woody biomass, a byproduct from the wood mills. Compared to the other fuels of the same woody biomass category, it has higher ash content, and contains more aluminosilicates (clays). It could be argued that this additional mineral matter is soil entrained during handling of this waste material, which is often stored on prisms simply outside the mills. Therefore, although the water soluble alkali is high, its release is observed to be lower in this fuel (6%). Sulfur and chlorine are almost completely released. Calcium and magnesium, which are also present at lower levels than in wood chips, are released to a lesser extent .

Olive residue (BM5)

This material is a residue from olive oil extraction and falls therefore into the category of agricultural/food production residues. Overall it contains significantly more ash, which is also very volatile. Therefore, overall ash release is highest (55%). This can be traced back by its very high potassium content, with little silica, aluminum, calcium and magnesium. The release of potassium, sodium, chlorine and sulfur is as good as complete. Calcium and magnesium release is comparatively low, on the other hand.

Straw (BM6)

Like the olive residue, this too belongs to the category of agricultural/ food production residues. It is a byproduct of basic food crops such as rice, wheat etc, the straw used during this study was a residue of hard wheat. It has a relatively high ash content and the elemental mineral matter is also highly volatile. Therefore, overall ash release is high in this fuel (40%), particularly caused by high chlorine and alkali emissions. The release of alkali is nonetheless reduced by the presence of high levels of silica. A nearly complete release for sulfur and chlorine is observed. Calcium and magnesium release is comparatively less.

Polish Coal (C1)

It is a high rank coal. Within this test fuel range, it has the highest ash content with the lowest volatile matter. It has also the lowest share of water soluble minerals. In consequence, the overall release is observed to be the lowest of all the tested fuels (8%). Due to high silica and aluminum, alkali release is observed to be minor, while the release of sulfur and chlorine is complete. Calcium and magnesium release is the lowest.

UK Coal (C2)

It is also a high rank coal. It has a moderate to high ash content and has a lower volatile content in comparison with biomasses, yet more so than the Polish coal. It

has also little water soluble minerals. Although the observed overall release is high (36%), it is primarily caused by the relatively high sulfur contents, followed by chlorine. Surprisingly, the individual release of chlorine is observed to be less than expected, which could be due to its inclusion in the conservative aluminosilicate minerals. Calcium and magnesium release is also lowest in this case.

4.3.2 Element-specific Release of the Inorganic Matter

The raw release data have been plotted against different indices identified in the literature review to evaluate the effect of elemental mineral matter compositions i.e. chlorine, aluminum, silicon and sulfur, onto the release of single mineral element. The elemental release is described as linear correlations in several sub figures starting from (a) to (j). Sub-figure (a) shows the elemental mineral release compared to the elemental mineral matter present in the fuel while sub-figures (b) to (j) presents different linear expressions with R^2 value. The correlations with $>0.95 R^2$ value can be considered suitable for prediction of different elemental release with the same group of tested fuels for given PF operating conditions.

S

An almost quantitative release of sulfur is observed for all the studied fuels. This is probably due to the fact that majority of this element is present as organically-bonded sulfur and will be rapidly oxidized to release as SO_2 from the surface of the burning fuel particle. The rest of the inherent sulfur will likely react with alkalis, first to form a low-melting alkali sulfate-rich slag which will then decompose during char combustion phase at high temperature, releasing SO_2 . Alkalis during this reaction will be incorporated into siliceous or alumino-silicate structures. Also sulfur present in already mineralized (excluded) forms in the fuel will be released to a great extent, either by the oxidation of sulfides or by volatilization of sulfates. Overall a close match of $>0.99 R^2$ value is obtained for S released against the fuel levels, as shown in Figure 4.3.

Cl

From Figure 4.4 (a), Chlorine is found to be released completely from woody biomass such as Bark (BM1), Wood chips (BM2) and Waste wood (BM3).

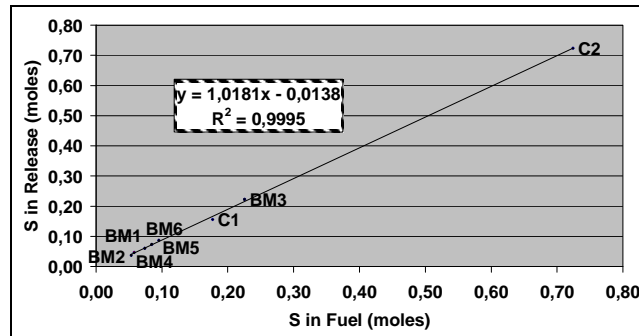


Figure 4. 3: Sulfur release during combustion of coal and biomass fuels (BM1: Bark, BM2: Wood Chips, BM3: Waste wood, BM4: Saw Dust, BM5: Olive Residue, BM6: Straw, C1: Polish Coal, C2: UK Coal)

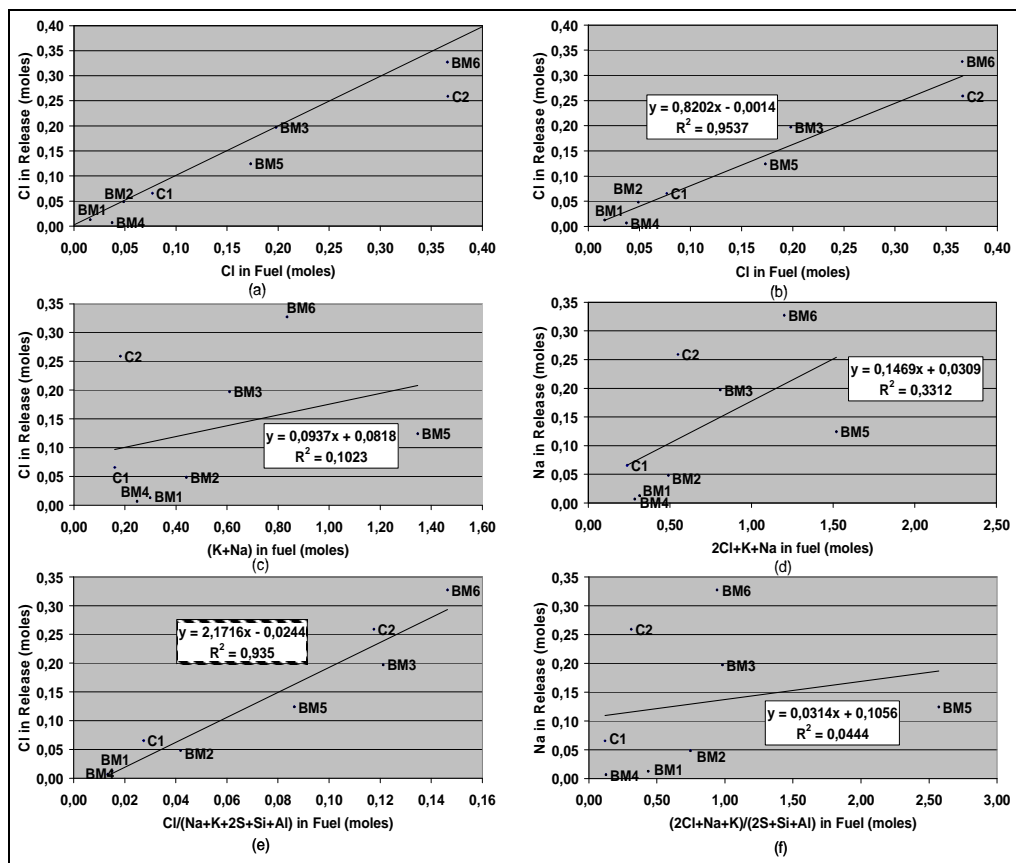


Figure 4. 4: Effect of elemental mineral matter composition on chlorine release during combustion of coal and biomass fuels (BM1: Bark, BM2: Wood Chips, BM3: Waste wood, BM4: Saw Dust, BM5: Olive Residue, BM6: Straw, C1: Polish Coal, C2: UK Coal)

The other fuels such as Saw Dust (BM4), Olive residue (BM5), Straw (BM6) and Polish coals (C1) also demonstrate nearly complete but still noticeably lower release. Interestingly, the UK coal (C2) has the lowest chlorine fraction release, though its content is the highest in this fuel compared with the other studied materials.

As shown in Figure 4.4 (b), chlorine release correlates well with the Cl fuel levels ($>0.98 R^2$ value). The closest match ($>0.96 R^2$ value) for a elemental mineral matter-dependent regression is obtained when plotting the release against the ratio of $Cl/(Na+K+Si+Al+2S)$ as shown in Figure 4.4 (e). This is an indication of the interconnection of the primary release mechanisms for chlorine and alkalis.

Furthermore, all four woody biomasses behave very comparably, with closer match ($>0.99 R^2$) as shown in Figure 4.5 (e).

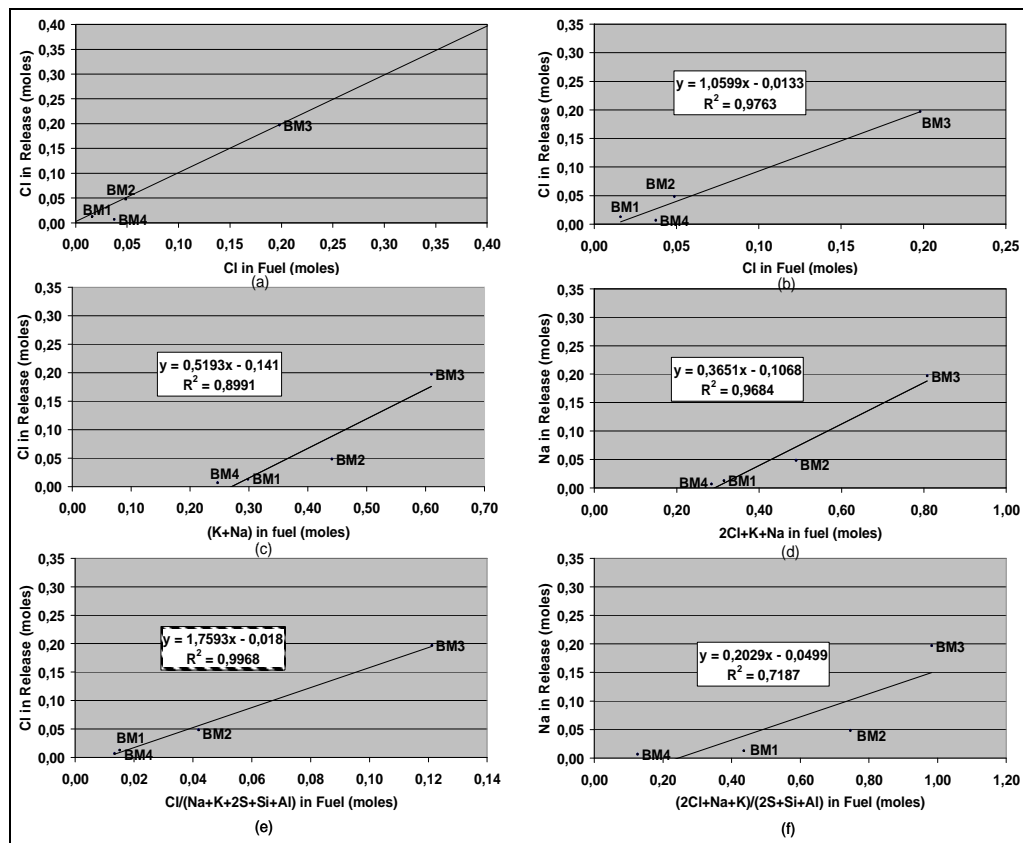


Figure 4. 5: Effect of elemental mineral matter composition on chlorine release during combustion of woody biomass fuels (BM1: Bark, BM2: Wood Chips, BM3: Waste wood, BM4: Saw Dust)

Ca and Mg

Only a partial release of calcium and magnesium has been observed throughout the test fuel range, as depicted in Figure 4.6. The woody biomasses such as the Bark (BM1), Wood chips (BM2) and the Waste wood (BM3) contain very high share of calcium in the ash and its release into the gas phase is significant (marked separately). Fuels richer in silicon such as the Saw dust (BM4), Olive residue (BM5) and Straw (BM6) along with the high rank Polish and UK Coals (C1 & C2), release much less calcium.

Such behavior of calcium can be traced back to the mode of occurrence, which strongly depends on the age of the fuel, and therefore its classification/rank. In biomass (younger and pure fuels), calcium is predominantly dispersed in the macerals and is bound to carboxyl groups, whereas in coal (elder fuels), it is present as the discrete mineral, calcite.

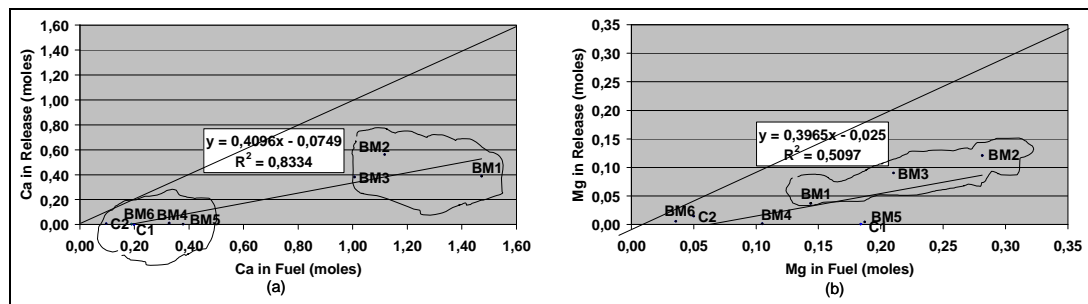


Figure 4. 6: Calcium and Magnesium release during combustion of coal and biomass fuels (BM1: Bark, BM2: Wood Chips, BM3: Waste wood, BM4: Saw Dust, BM5: Olive Residue, BM6: Straw, C1: Polish Coal, C2: UK Coal)

This difference in the form of occurrence plays an important role in the behavior of calcium during combustion, as the dispersed esterified calcium will be likely to form superfine CaO aerosol, while (micro/microcrystalline) calcite will at best decompose to CaO, likely forming much larger particles. Furthermore in the presence of aluminosilicates the release of calcium, also in its dispersed form, will greatly diminish as this element will react similarly to the common alkalis.

Release of magnesium is similar to the release of calcium and no sturdy correlation of the elemental mineral matter composition is observed. The release of magnesium is also higher for woody biomass including the Bark (BM1), Wood chips (BM2) and the Waste wood (BM3).

K

Gaseous phase release of potassium has been studied separately for all the fuels. Figure 4.7 (a) shows that the potassium present in the fuel is released to a high degree into the gas phase from all the fuels, but not quite in a linear correlation with its concentration in the fuel.

It can be clearly seen from the Figure 4.7 (a) that the almost complete release of potassium is observed for clean woody biomass fuels, i.e. the bark (BM1), the wood chips (BM2) and the waste wood (BM3) in which the water soluble minerals are the highest, while silica and aluminum are the lowest. A much lower potassium fraction release is recorded in the case of the saw dust (BM4), as well as the Polish coal (C1) and the UK coal (C2).

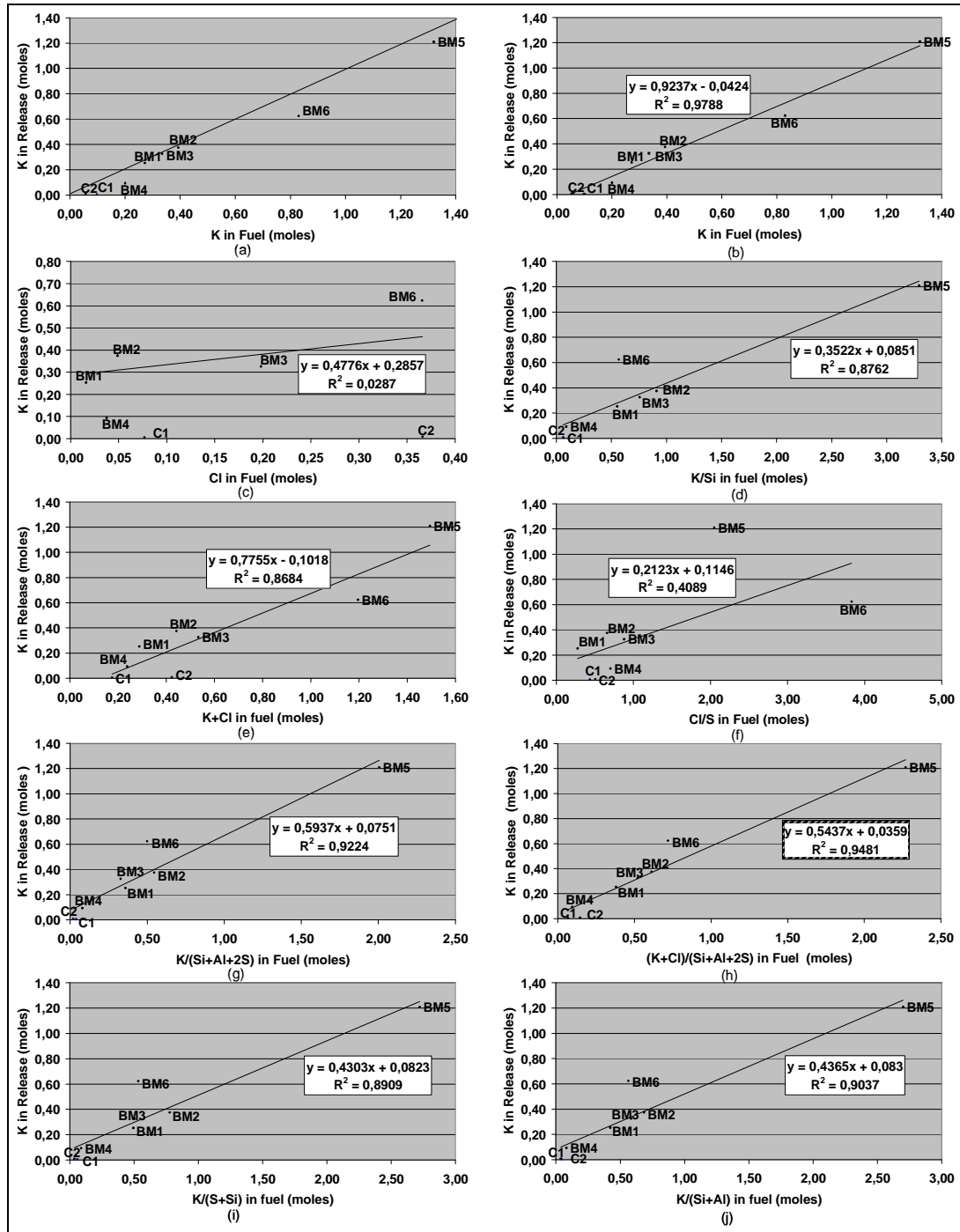


Figure 4. 7: Effect of elemental mineral matter composition on potassium release during combustion of coal and biomass fuels (BM1: Bark, BM2: Wood Chips, BM3: Waste wood, BM4: Saw Dust, BM5: Olive Residue, BM6: Straw, C1: Polish Coal, C2: UK Coal)

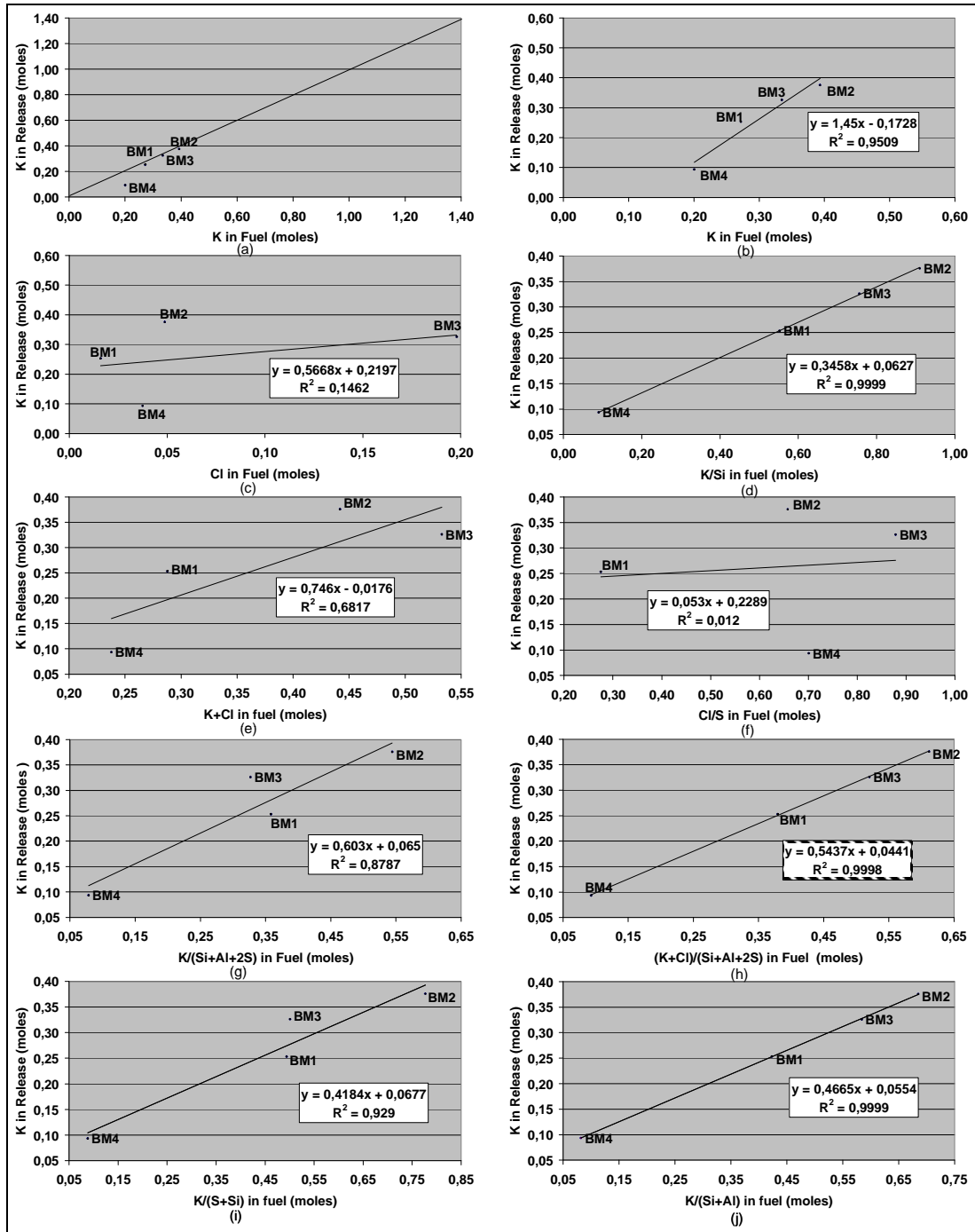


Figure 4. 8: Effect of elemental mineral matter composition on potassium release during combustion of woody biomass fuels (BM1: Bark, BM2: Wood Chips, BM3: Waste wood, BM4: Saw Dust)

The reason for this is likely the higher levels of silica and aluminum. Moreover, both the coals contain significantly less water soluble minerals and volatile matter alongside with a high share of excluded minerals. At least some of the potassium contained in the two fossil fuels can be bound with the excluded minerals, which during the combustion process will not reach as high a temperature as burning char

particles and therefore release less potassium. The incomplete, though considerable in comparison with other studied fuels, release of potassium from the Olive residue (BM5) is likely due to the high share of organically bound potassium (insoluble in water) which still remains for a part in the unburnt carbon.. The main reason for the observed lower potassium release from the Straw (BM6) is the much higher silica content with lower calcium and magnesium. Also this fuel contains significantly less water soluble potassium than clean wood biomass.

As shown in Figure 4.7(b) potassium release shows a good linear correlation with potassium levels in the fuel for pure woody biomass fuels, with high levels of water soluble potassium, However, for coals as well as straw this correlation is very poor. The closest match ($0.95 R^2$ value) is obtained as shown in Figure 4.7(h) when plotting the release against the ratio of $(K+Cl)/(Si+Al+2S)$ in the fuel. Translated into the release behavior this correlation implies that the higher potassium and chlorine levels in the fuels, the higher will be the potassium volatilization. But the release will be limited by the silica, aluminum and sulfur present in the fuel. The correlations prove that there will be less direct effect of calcium and magnesium on the potassium release.

Despite the fairly good overall correlation obtained for all the tested fuels, it is clearly noticeable that the coals as well as straw correlate significantly worse than woody biomass. This is likely due to the earlier discussed different speciation of potassium in the said fuels as compared with woody biomass. Therefore a similar set of correlations has been developed for the four woody biomass fuel, which is plotted in Figure 4.8 (h). As a result of this, a better correlation ($>0.99 R^2$) is obtained indeed for this group of woody biomass fuels, which underscores the fact that fuels of similar rank/class behave very similarly, despite fairly broad fuel ash composition (eg. wood chips and bark).

Na

The complexation and modes of occurrence of sodium in the biomass and coal is similar as that of potassium, as both elements reveal almost the same chemical and physical properties. One would then expect a fairly comparable release behavior.

Surprisingly however, the sodium release was found to be substantially lower compared to potassium as shown in Figure 4.9 (a). The release of sodium is nearly complete from Bark (BM1) and Wood chips (BM2). The release from Waste wood (BM3) is found to be less than expected. Saw dust (BM4) releases less sodium, which can be justified by its higher silicon content. The low to moderate release in the case of Olive residue (BM5) may be due to a higher share of organically-bonded sodium in the fuel compared to woody biomass. In the case of the Straw (BM6) however, the complete release of sodium against a lower release of potassium appears somewhat contradictory, but it can be likely justified by the high chlorine content which is of great importance for the volatilization of potassium. The release from both the coals (C1 and C2) is observed to be much less, mainly due to high silica and alumina content.

Sodium release appears to give a fairly good correlation with the sodium fuel levels. However, the release of Na is shown to interact with the release of potassium, as can be seen from the best correlation shown in Figure 4.9 (j) where the best regression ($>0.98 R^2$ value) is obtained for plotting the release against the ratio $Na/(K+Si+Al)$ in the fuel. An even better correlation ($>0.99 R^2$ value) is obtained for the four woody biomasses, as shown in Figure 4.10 (j).

It should be stressed however, that the data on sodium release presented and analyzed in this work should be considered less reliable, as levels of Na in all the studied fuels were fairly low.

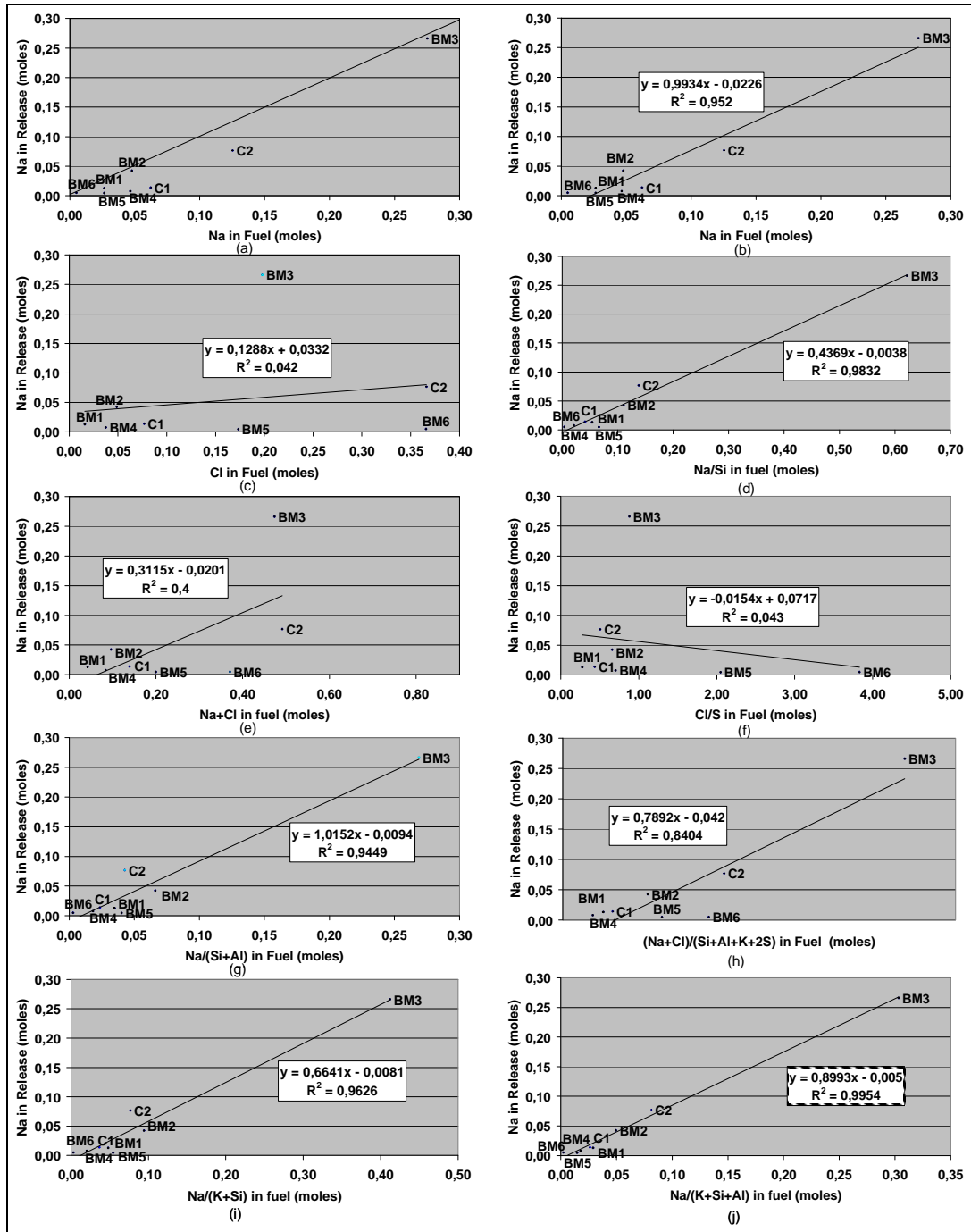


Figure 4. 9: Effect of elemental mineral matter composition on sodium release during combustion of coal and biomass fuels (BM1: Bark, BM2: Wood Chips, BM3: Waste wood, BM4: Saw Dust, BM5: Olive Residue, BM6: Straw, C1: Polish Coal, C2: UK Coal)

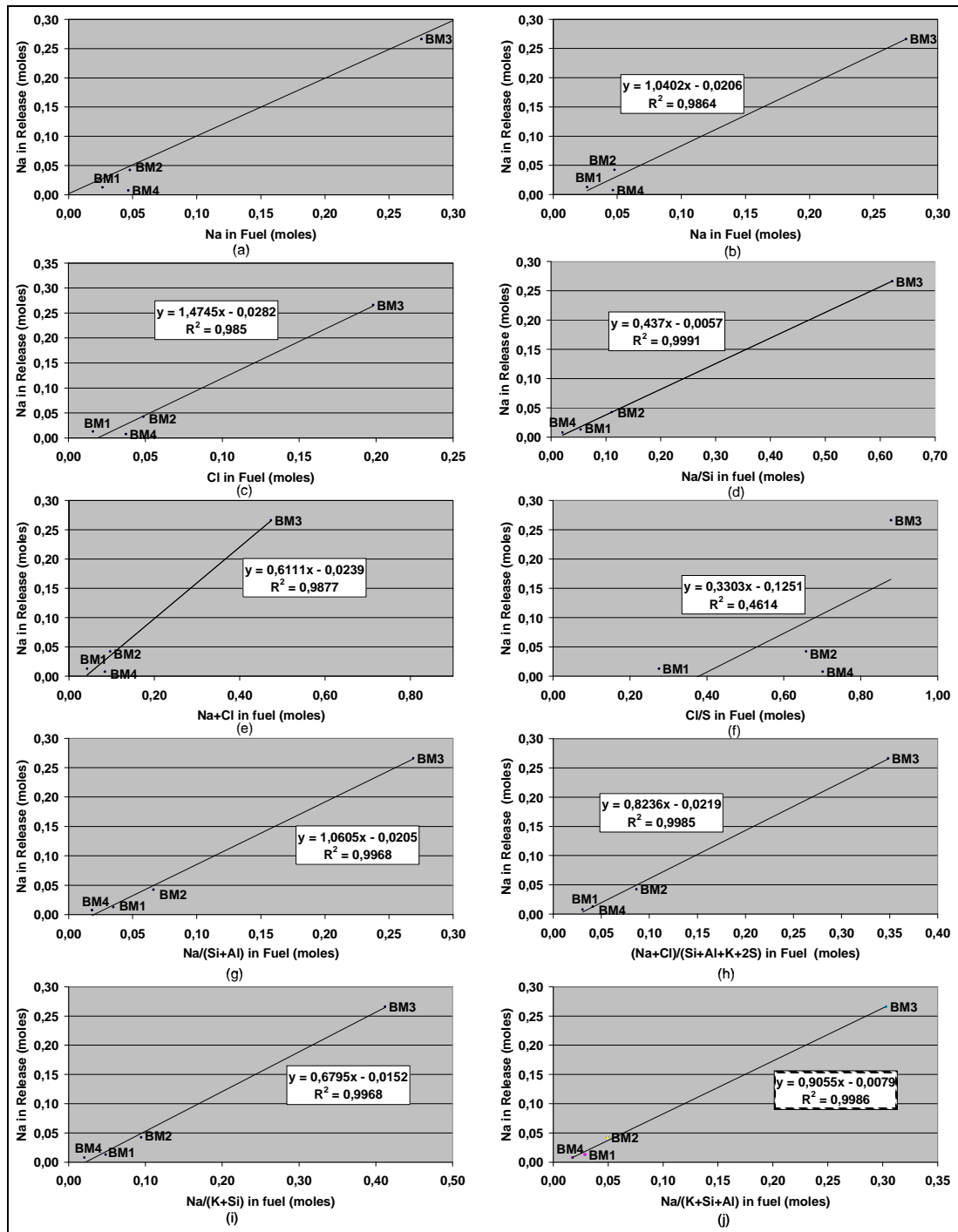


Figure 4. 10: Effect of elemental mineral matter composition on sodium release during combustion of woody biomass fuels (BM1: Bark, BM2: Wood Chips, BM3: Waste wood, BM4: Saw Dust)

4.4 Summary

The elemental release behavior has been studied under typical PF combustion conditions, employing high temperatures and high heating rates. It is concluded that fuel elemental mineral matter and its association in the fuel matrix influences the release of ash-forming elements to a large extent.

1. Several observations from the literature review have been reconfirmed in this study are as follows:
 - a. Biomass and low rank coals will contain more water soluble (free ions, salts and organically bound) minerals than higher rank coals which will have more insoluble elements. This difference in mode of occurrence of the mineral element in the fuel matrix has a direct effect on their release.
 - b. The presence of silica and aluminum in the fuel limits the release of alkaline metals. This underscores the effect of mineralogical composition on the elemental release.
 - c. The release of sulfur and chlorine will be nearly complete at high temperature and high heating rate PF combustion conditions for all the fuels.
 - d. Calcium and magnesium will only release in the younger fuel when their content in the fuel ash is high and not counterbalanced by aluminum and silicon.
 - e. The total ash content, volatile matter and excluded minerals can also affect the elemental release. The higher the ash content and volatile content the higher the observed release.
 - f. The processing and handling of pure, waste and byproducts of coal and biomass can alter the elemental mineral matter composition and their association, which can change the gaseous release of the mineral elements.
 - g. The concentration and ratios of the elements can alter the reaction kinetics and chemical equilibrium, both affecting the release.
2. Effect of ash %, volatile matter %, mineralogy (included/excluded), particle shape, size and density are also substantial. Mineralogy, particle shape, size and

density should also be studied in further detail in order to quantify the overall elemental release.

3. It is observed that the mineral elements of the same group/ rank of biomass and coal have similar association in the fuel matrix and behave similarly during combustion. Significantly better correlations for the elemental release can be derived for fuel type separately. Also, non-linear correlations should also be attempted.

4.5 Conclusions

Experimental investigations reported in the present work have clearly demonstrated the effects of the elemental composition and their association on the gas-phase release of ash constituents. Firstly, the differences in the mode of occurrence of volatile minerals in the fuel matrix were found to have direct effect on their release pattern into the gas phase. Secondly, the presence of other, conservative elements, such as Si and Al, are also observed to influence the vaporization of Na, K, Cl and S. Ash release is also affected by the ash and volatile matter contents.

From the current study, it is evident that different fuels of the same type will exhibit fairly similar chemical and physical properties. Woody biomass (BM1, BM2, BM3 and BM4), fuels with a higher proportion of water soluble (free ions, salts and organically bound), are characterized by a very comparable release of alkalis, chlorine and sulfur. However, the presence of silicon and aluminum can reduce release of alkalis, as clearly noticeable in the case of the saw dust (BM4). The olive residue BM5, the straw (BM6) and the studied coals (C1 and C2), fuels belonging to different groups/ranks but are all generally characterized by a lower proportion of water soluble inorganics and behave different to woody biomass.

These correlations are simplistic but innovative and are non-existent in the literature to the best of authors' knowledge with such a massive experimental study. The release of sodium, potassium, chlorine and sulphur can be calculated with simple linear correlations presented in this chapter having $>0.95 R^2$ value. These simple linear equations (with $>0.95 R^2$ value) can be considered as a valuable tool for predicting ash release as a function of elemental mineral matter composition and their association in the fuel matrix for the typical constant PF firing conditions.

The correlations developed for woody biomass in the present work can be applied to any other fuels of the same biomass group under the tested standard operating conditions. Significantly better correlations of the elemental and overall ash release with respect to elemental mineral matter composition can be achieved separately for each different fuel groups. However, in the case of coals, ash contents and amount of ash vary significantly, more than for woody biomass. There might be doubts that such correlations exist for coals. More research is necessary for separate group of coals.

The correlations derived from this work and the proposed methodology based on the limited number of fuels possibly provides a platform for arriving at a robust predictive tool, if a greater number of fuels and their groups could be included in future studies.

References

1. R. Manzoori and P. K. Agarwal, The fate of organically bound inorganic elements and sodium chloride during fluidized bed combustion of high sodium, high sulfur low rank coals, *Fuel* 71 (1992) 513-522.
2. L.L. Baxter, R. E. Mitchell, T. H. Fletcher, Release of Inorganic Material During Coal Devolatilization, *Combustion and flame* 108 (1997) 494-502.
3. H. Oleschko, A. Schimrosczyk, H. Lippert, M. Muller, Influence of coal composition on the release of Na-, K-, Cl-, and S-species during the combustion of brown coal, *Fuel* 86 (2007) 2275–2282.
4. L. Hong, I. Elvin, S. Justin, F. Paul, V. Mark and L. Baxter; Effect of Particle shape and size on devolatilization of biomass particle, *Fuel* (2008), Article in press, doi:10.1016/j.fuel.2008.10.023.
5. S. Badzioch, P.G.W. Hawksley, Kinetics of thermal decomposition of pulverized coal particles, *Industrial and Engineering Chemistry Process Design and Development* 9 (1970) 521–30.
6. P.J. van Eyk, P.J. Ashman, Z.T. Alwahabi, G.J. Nathan, Simultaneous measurements of the release of atomic sodium, particle diameter and particle temperature for a single burning coal particle, *Proceedings of the combustion institute* 32 (2009) 2099–2106.
7. Y. Ninomiya, L. Zhang, A. Sato, Z. Dong, Influence of coal particle size on particulate matter emission and its chemical species produced during coal combustion, *Fuel Processing Technology* 85 (2004) 1065– 1088.
8. J.P. Mathews, P.G. Hatcher, A.W. Scaroni, Particle size dependence of coal volatile matter: is there a nonmaceral- related effect, *Fuel* 76 (1997) 359–62.
9. S.C. van Lith, Release of Inorganic Elements during Wood-Firing on a Grate, Ph.D. Thesis, Technical University of Denmark, Lyngby, Denmark, ISBN 87-91435-29-3, (2005).
10. S.C. van Lith, V. Alonso-Ramírez, P.A. Jensen, F.J. Frandsen, P. Glarborg, Release to the gas phase of inorganic elements during wood combustion. Part 1: development and evaluation of quantification methods, *Energy and Fuels* 20 (2006) 964–978.

11. L. J. Wibberley and T. F. Wall, Alkali-ash reactions and deposit formation in pulverized-coal-fired boilers: the thermodynamic aspects involving silica, sodium, sulfur and chlorine, *Fuel* 61 (1982) 87-92.
12. F. J. Frandsen, S. C. van Lith, R. Korbee, P. Yrjas, R. Backman, I. Obernberger, T. Brunner, M. Jöller, Quantification of the release of inorganic elements from biofuels, *Fuel Processing Technology* 88 (2007) 1118–1128.
13. H. Schurmann, P.B. Monkhouse, S. Unterberger, K.R.G. Hein, In situ parametric study of alkali release in pulverized coal combustion: Effects of operating conditions and gas composition, *Proceedings of the Combustion Institute* 31 (2007) 1913–1920.
14. X. Wei, C. Lopez, T. V. Puttkamer, U. Schnell, S. Unterberger, and K.R.G. Hein, Assessment of Chlorine-Alkali-Mineral Interactions during Co-Combustion of Coal and Straw, *Energy & Fuels* 16 (2002) 1095-1108.
15. M.K. Cieplik, R. Korbee and J.H.A. Kiel, Investigations of Particulate Emissions in Coal-fired Power Plants Under Biomass Co-Firing, in the proceedings of the Air Quality V conference, Arlington (VA), USA (2005).
16. T.F. Wall, Mineral matter transformations and ash deposition in pulverized coal combustion, Twenty-Fourth Symposium (International) on Combustion/The Combustion Institute (1992) 1119-1126.
17. D. Thompson, B.B. Argent, The mobilisation of sodium and potassium during coal combustion and gasification; *Fuel* 78 (1999) 1679–1689.
18. A.D. Shah, G. P. Huffman, F E. Huggins, N Shah, J J Helble, T W Peterson, A F. Sarofim, Reactions of calcium and sodium during combustion of lignite, International ash utilization symposium, Center for applied energy research (1999) 69.
19. G. A. Osborn, Review of sulfur and chlorine retention in coal-fired boiler deposits; *Fuel* 71 (1992) 131-142.
20. E. Raask, The mode of occurrence and concentration of trace elements in coal, *Progress of Energy and Combustion Science* 11 (1985) 97-118.
21. Y. Zheng, P.A. Jensen, A.D Jensen, B. Sander, Helle J.B, Ash transformation during co-firing coal and straw, *Fuel* 86 (2007) 1008–1020.
22. L.L. Baxter, T.R. Miles, T.R. Miles Jr., B.M. Jenkins, T. Milne, D. Dayton, R.W. Bryers, L.L. Oden, The behavior of inorganic material in biomass-fired

power boilers: field and laboratory experiences, *Fuel Processing Technology* 54 (1998) 47–78.

23. N.B. Gallagher, T.W. Peterson, J.O.L. Wendt, Sodium partitioning in a pulverized coal combustion environment, *Twenty-Sixth Symposium (International) on Combustion/The Combustion Institute* (1996) 3197–3204.
24. M. Neville and A. F. Sarofim, The fate of sodium during pulverized coal combustion, *Fuel* 64 (1985) 384-390.

Chapter 5

Modeling of particle size evolution after PF combustion

Particle size is an essential parameter in pulverized fuel (PF) combustion as many of the problems or further areas of development in these systems are strongly influenced by the fuel and ash size distribution after combustion. The evolution of the PSD after combustion represents the convolution of several competing physical and chemical transformations, operating over the entire size distribution. It has also been distinguished in the literature that PSD after combustion comprises of two modes of ash sizes namely aerosol and coarse.

The aerosol formation was studied at ECN by simple calculations on gas-to-particle conversion for alkali chlorides and alkali sulfate. Therefore, the present work encompasses the modeling of coarse ash formation. Various models such as break-up, thermal stress, shrinking core, percolation and particle population model as reviewed in Chapter 2 have been developed by incorporating numerous ash transformation mechanisms to predict the coarse particle size evolution during the pulverized fuel combustion. The present work describes an adaptation of the numerical kinetic-based particle population balance for predicting particle size evolution during PF combustion developed by Dunn-Rankin and Mitchell. The model is further simplified analytically. Several empirical parameters are derived from the experiments and incorporated into the model. The resulting simplified PSD evolution model shows good agreement with several combustion and co-firing experimental results of different coal and biomass, with maximum 15-20 % absolute standard deviation.

5.1 Introduction

Over the past decades significant progress has been made in understanding and quantifying the processes governing ash formation during pulverized fuel combustion [1]. From the experimental investigations explained in Chapter 3, it is concluded that particles fragment along with the pore diffusion during char oxidation. Processes such as char oxidation, devolatilization and fragmentation are considered as the first line physical transformations responsible for coarse ash formation in the radiation zone of the boiler. Other physical transformations such as nucleation, coagulation and condensation of devolatilized inorganic gaseous species are responsible mainly for submicron aerosol formation. Experimental and theoretical investigations indicate that particle shape, size and density influence particle dynamics, including drying, heating and conversion rates. Therefore, their effect on first line physical transformations in the radiation zone, will be quite significant [1,2]. These transformations compete with each other in the radiant zone of the PF furnace [3]. From the experiments it is observed that devolatilization (of both organics and inorganics) is significant, even at the char combustion phase. Fragmentation of the char particle depends on char burnout and thermal stress. Fragmentation starts from 10 % burnout and occurs throughout in both diffusion (char burnout) and chemically kinetic controlled regimes [4]. Overall, the evolution of particle sizes in a combustion system is a combination of all such various competing physical transformations.

Particle size after combustion is a very important parameter in pulverized coal combustion systems as processes such as pollutant formation, corrosion, erosion, slagging and fouling are strongly influenced by the fly ash size distribution after combustion [4]. Furthermore, ash particle size after combustion has been found to affect the ash transport behavior to a great extent. Large ash particles tend to impact onto boiler heat transfer surfaces by inertia, whereas fine ash particles tend to reach wall surfaces by thermophoresis or Brownian motion. For instance, a 60 micrometer ash particle was estimated to reach the deposit surface with higher probability compared to 30 micrometer particle primarily due to inertial effect. [1].

Evolution of particle sizes after combustion has been described by numerous researchers and details of their findings can be found elsewhere [5]. Various mechanisms have been studied in depth to understand the overall ash formation process [6,7]. Explanation of why and how char oxidation, devolatilization and fragmentation are likely to occur, have been illustrated [1]. Separate mathematical models for prediction of char oxidation, devolatilization and fragmentation have been developed. The integration of the mechanisms alongside with the mineral matter distribution, particle size, shape and density has been incorporated in the models with linear, nonlinear, deterministic or probabilistic relationships. The models developed [5] are break-up [8], thermal stress [9], shrinking core [10,11,12], percolation [13,14,15,16] and particle population [20,21,22,23] models etc..

The present work describes an adaptation of a kinetic population balance model, which predicts PSD evolution of particles after PF combustion in the radiation zone mainly working with three ash transformations i.e. char oxidation, devolatilization and fragmentation. The model is a set of first order linear ordinary differential equations and therefore particle-particle interaction in the space is neglected. Also, other physical transformations such as nucleation, coagulation, homogeneous and heterogeneous condensation with gaseous phase chemical reactions are also not included in this model. The fragmentation and burning rate constants are derived from lab-scale experiments and incorporated into the present model. These experiments have been performed in a Lab-scale Combustion Simulator (LCS), under very well-defined and controlled conditions. Furthermore, the model is simplified analytically. In order to do so, instead of predicting the full particle size distributions at every time step, fragmentation into two distinct particle diameters within each particle size class/bins are solved analytically. Particle shape and density changes are also neglected in the present model.

5.1.1 Background

Kinetic models (or population balances) are applied in the analysis of many size degradation and size enhancements processes. Wolf [17] gives exact solutions of first order kinetic equations describing the degradation of chain molecules by random scission. In their formulation, a fragmentation event gives rise to a pair of daughter

fragments while all fragment pairs are assumed equally probable. The solutions give the molecular weight distribution as a function of time. The kinetic simulations of Wolf [17] assume that single fragmentation event produces only two daughter fragments. However, other kinetic simulations presume that a single fragmentation event produces a family of fragments. Austin [18] reported similar solutions of size-continuous form of kinetic equations with specific breakage functions and fragmentation families for grinding processes. Waldie [19] employs the population balance method with familial fragmentation to simulate competing processes of particle growth, attrition and fragmentation during palletization in a rotating drum. Dunn-Rankin [3, 4] introduced a kinetic model using a particle population balance approach to simulate PSD evolution during the oxidation and fragmentation of char. This model however, does not include the density changes occurring due to particle swelling. Subsequently Mitchell [20] modified the particle-population balance model by incorporating these density changes. Their extended model was then used to evaluate PSD as a result of fragmentation occurring during both coal devolatilization as well as the char oxidation. Recently, Syred [5] simplified the present model analytically for two size classes for fragmentation only. The present model is an extended version of Syred's work with the inclusion of burning together with fragmentation.

5.2 Mathematical modeling

5.2.1 Overall mass balance equation

The present simplified model predicts the cumulative mass fraction using a PSD derived from the particle number calculations at different distinct time steps. The initial particle size distribution represents different size bins as shown in Figure 5.1.

The γ (also shown in Figure 5.1) is a very important parameter, defining the upper and the lower cut-offs of each interval and can be expressed as a ratio of larger and smaller size particle for each size bin. The overall mass balance for each size bin has been considered as follows:

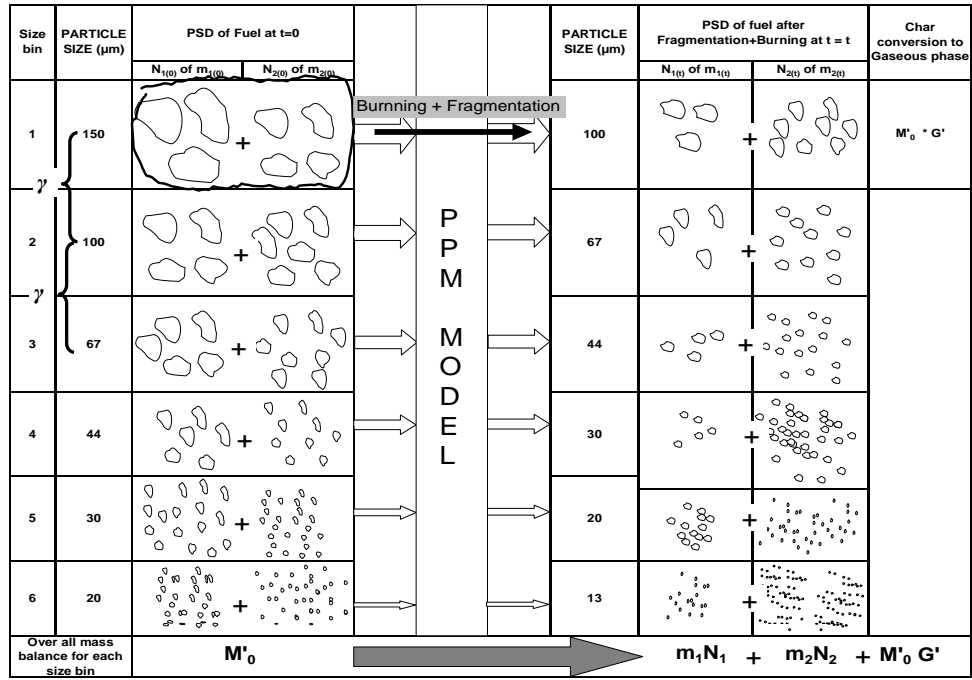


Figure 5. 1: Modeling chart of PSD evolution during pf combustion

$$M'_0 (1-G') = m_{1(t)} N_{1(t)} + m_{2(t)} N_{2(t)} \quad (1)$$

The M'_0 is the initial mass number of the each size bin having $m_{1(0)}$ and $m_{2(0)}$ weighted particles with $N_{1(0)}$ and $N_{2(0)}$ particle numbers, respectively. Equation 1 implies that the residual mass after conversion G' is divided into two size classes. The ‘ G' ’ is the total char conversion of the particular size bin into the gas-phase due to devolatilization and char oxidation. Burning (chemical conversion) and fragmentation are the main cause for the two resultant size classes.

The particle numbers $N_{1(t)}$ and $N_{2(t)}$ after burning and fragmentation have been calculated by solving the population balance equation of Mitchell [20] analytically for two size classes.

5.2.2 Population balance equation

The structure of the particle population balance model by Mitchell [21] is presented as a set of differential equations having the following form (Equation (2)):

$$\frac{dN_{i,k}}{dt} = \underbrace{-S_{i,k}N_{i,k} + \sum_{j=1}^i \sum_{\lambda=1}^K (b_{ij,k\lambda}S_{j,\lambda}N_{j,\lambda})}_{\text{Fragmentation}} - \underbrace{C_{i,k}N_{i,k} + C_{i-1,k}N_{i-1,k}}_{\text{Size}} - \underbrace{D_{i,k}N_{i,k} + D_{i,k-1}N_{i,k-1}}_{\text{Density}} \quad (2)$$

The indices i and k refer to size-class and density class. The first two terms on the right-hand side of the Equation (1) represent the rates at which particles leave and enter a particular class (i, k), as a result of fragmentation. The third and the fourth terms represent the rates at which particles leave and enter the class, as a result of changes in size due to burning. The last two terms represent the rates, at which particles leave and enter the class, as a result of changes in density due to burning. Thus, $N_{i,k}$ is the number of particles in size-class i and density-class k . $S_{i,k}$ is the fragmentation rate constant and $C_{i,k}$ and $D_{i,k}$ are the burning rate constants. The $b_{i,j}$ are elements of the fragmentation progeny matrix, which specify the number of fragments that enter higher size bin i per particle that fragments in lower size bin j . Particles fragmenting in bin j can produce fragments only in bin i where $i \geq j$, therefore, $b_{ij} = 0$ for $i < j$. The progeny elements were determined for each type of fragmentation considered. Three kinds of fragmentation described are considered i.e., attrition, breakage and fragmentation. The fragmentation modes used in the present model are described below [5].

Attrition is incorporated in the model by assuming 0.01 % volume of largest particles to fragment attritively to lowest size bins.

Progeny matrix for break-up fragmentation can be expressed as (Equation (3)):

$$b_{ij} = \begin{cases} 0 & i \leq j \\ \gamma^3 & i = j+1 \\ 0 & i > j+1 \end{cases}$$

(3)

Progeny matrix ($b_{i,j}$) for percolative fragmentation can be defined as (Equation (4)):

$$b_{ij} = \begin{cases} \gamma^3 (i-j) / (n-j+1) & i \geq j \\ 0 & \text{Otherwise} \end{cases} \quad (4)$$

The present work uses the population balance approach developed by Mitchell [21] to simulate the evolution of the particle size distribution during char combustion. The simulation includes both the burning and the fragmentation. The burning includes both char oxidation and devolatilization. Therefore, this model predicts the PSD evolution during the combustion by taking into account all three important first line physical transformations: i.e. char oxidation, devolatilization and fragmentation and their revaluations with size changes. The model is a set of isolated first order linear ordinary differential equations; therefore particle-particle interaction in the space is neglected. Other physical transformations for gaseous phase such as nucleation, coagulation, homogeneous and heterogeneous condensation with chemical reactions are also not included in this model. Although the present model is considering only ash transformation mechanisms occurring in the radiation zone and considerable simplifications have been made in the numerical approach by selecting ODE structure instead of PDE, it is still analytically too complex to incorporate Mitchell's model into simple visual basic or even Excel-based engineering models and CFD routines. For this reason, this model is further simplified and solved analytically as below. Several parameters obtained from the ash formation experiments conducted at ECN are used in the simplified model.

5.2.3 Assumptions and Simplifications

In the present kinetic model, it is assumed that the particle combustion rate depends on the instantaneous particle diameter. Changes in the particle density, due to the steady diameter char oxidation or to cenospheres formation are neglected. Consequently, Mitchell's [21] model is simplified as shown in Equation (5), overall

resembling much the original model of Dunn-Rankin [3, 4], but with the progeny matrix from Mitchell's model [5, 21] described in equations (3) and (4).

$$\frac{dN_i}{dt} = -S_i N_i + \sum_{j=1}^i b_{ij} S_j N_j - C_i N_i + C_{i-1} N_{i-1} \quad (5)$$

The described simplifications are considered while solving the model equation analytically for two size class for each size bin. Instead of using a PSD classification for the combustion, the particle size bins before and after combustion are classified only in two sizes, having a higher (m_1) and a lower (m_2) particles masses. Therefore, every combustion time step in each size bin would create new child particles classified in higher and lower mass sizes. The values of (m_1) and (m_2) are time-dependent; however, their change is limited within the ratio between the higher and the lower particle mass (γ^3) in each size bin, assumed to be constant during the process. This simplification is the same as proposed by Syred [5], who simplified and solved the model equation analytically for pure fragmentation. However, pure fragmentation is an incomplete representation of char oxidation, since these particles must burnout in a finite time. Therefore, instead of only the fragmentation, the present adaptation of the model is extended onto burning. The analytical solutions of the above equation (5) for burning and fragmentation are derived in Section 5.3. In contrast to Dunn-Rankin's, Syred's and Mitchell's model, fragmentation rate and burning rate constants are derived empirically from dedicated experiments. Throughout, the particle shape is considered to be spherical, in order to avoid complexity and no shape factor is included in the developed model.

5.2.4 Empirical parameters

Apart from the progeny matrix, the burning and fragmentation rate constants are the two unknown values in the model equation. Fragmentation and burning are the two parallel ash transformations which are responsible for PSD evolution after combustion. Both rate constants are derived from experiments and incorporated into

the model. The detail of the derivation of the constants from the experiments is explained in Section 5.4.

Burning rate Constant

The overall spherical particle burning rate [23] is defined as the mass loss rate per unit of external surface area and can be expressed as described below:

$$Q = \frac{1}{\pi D_p^2} \frac{dm_c}{dt} = \frac{\rho_{pc}}{2} \frac{dD_p}{dt} + \frac{D_p}{6} \frac{d\rho_{pc}}{dt} \quad (6)$$

Where m_c and ρ_{pc} are the mass and apparent density respectively of the particle diameter D_p . The first term on the RHS of the equation (6) can be defined as the apparent external burning rate due to size changes with time and second term as the apparent internal burning rate due to density changes with time. As mentioned in the simplification section above, this model assumes shrinking core burning, hence density changes are neglected in the present model, thus zeroing the second term. The equation (6) is then reduced to:

$$Q = \frac{1}{\pi D_p^2} \frac{dm_c}{dt} = \frac{\rho_{pc}}{2} \frac{dD_p}{dt} \quad (7)$$

So, from the above equation particle size changes due to burning can be derived. For this, the burning rate constant C_i is calculated [23] as below:

$$A = C_i = \frac{\left(\frac{dD_p}{dt} \right) x_{i+1}}{(x_i - x_{i+1})} \quad (8)$$

The burning rate is a time dependent function, which describes how rapidly particles leave a given size class due to the overall burning. To treat this rate as a constant for a particular time step, its value is calculated using experimental data for that selected time step.

The burning rate constant will be a single value derived from experimental data for each size class for the defined time step (as $C_1 = C_2$) and can be termed as A for further calculations.

Fragmentation rate constant

The physical significance of a fragmentation event is made evident by solving, without burning, the basic kinetic equation only for larger particles.

$$\frac{dN}{dt} = -S N$$

$$B = \int_0^t S dt = \ln [N_{(0)} / N_{(t)}]$$

(9)

Where $N_{(0)}$ is the initial number of largest particles ($> 30\mu\text{m}$), and $N_{(t)}$ is the particle number at time step t. Thus, S is directly related to the fraction of the largest particles that ultimately fragment during the simulation. In the described study, though S is a function of time, it is obtained from the experiments for different residence times and incorporated into the model. Therefore, it can be taken as a distinct value/constant for that selected time step.

The fragmentation rate constant will have a single value for all size classes ($> 30\mu\text{m}$) for a particular time step for each size bin and can be termed as B for further calculations.

As, S_i and C_i will be a value for a particular time step, an analytical solution of equation 2 for that corresponding time step is possible and is derived in Section 5.3.

5.2.5 Mode of Fragmentation

In several studies [22, 23], it was observed that the char combustion will be in a kinetic -diffusion controlled regime (where mass loss rates due to pore diffusion and chemical reactions are comparable), even with extended residence time under typical PF firing conditions. Three kinds of fragmentation are considered in this model: attrition, breakage and percolation. Initially, a particle will be forming small particles from its outer surface, which is essentially simply the phenomenon of attrition. As soon as the particle starts devolatilizing and oxidizing, thermal stress within the particle increases, due to rapid vaporization and the increased temperature. This in turn causes the particle to break into relatively large particles, which process is called breakage. After a certain conversion, due to very high thermal stress, particle fragment percolatively into smaller and larger size particles excessively. It is observed that significant percolative fragmentation does not occur until substantial chemical conversion (60-70 %) of the fuel [24, 25]. To quantitatively incorporate the possibility of attrition, breakage and delayed excessive percolative fragmentation, the progeny matrix discussed previously (Section 5.2.2) is used and analytical solution for these different modes of fragmentation alongside with burning have been given in Section 5.3.

5.2.6 Conversion and Particle size reduction due to Burning and Fragmentation

Particle size reduction during combustion depends on the fuel chemical conversion and fragmentation. The size reduction will be high for smaller sized particles compared to larger ones. This appears to be confirmed by the one dimensional coal combustor program (1-DICOG) developed by Smith and Smoot [26] and described in Dunn-Rankin's modeling work [4] for typical operating conditions of 1700 K and 5 % vol. O₂ as shown in Figure 5.2. The 1-DICOG software [4,26] uses equilibrium chemistry in the gas phase, and requires conservation of energy, momentum, and mass for separate particles. This model assumes that the particles swell linearly with

the extent of devolatilization. It will change the particle density significantly in the devolatilization phase only. The average particle diameter increase is often in the order of 10 percent for highly bituminous coal. After complete devolatilization, the particle will burn with an almost constant density in the shrinking core mode. The results verified by the model developed by Smith and Smoot [26] for this typical conditions show that the particle surface regression rate during char oxidation is nearly independent of time, and relatively insensitive to the initial particle diameter. In the present approach, results are not generated with the help of 1-DICOG program but instead of that the graph presented in Dunn-Rankin's [4] work as shown in Figure 5.2 is used to decide the particle size reduction for each size bin.

The total char conversion for a given time step is derived from the LCS experiments, as described further. The char conversion for each size bin is assumed in such a way that total char conversion derived from experiments matches with the sum of the assumed char conversion for all size bins. The burning rate constant is calculated using equations 7 and 8 for the assumed char conversion for each size bin for a given time step t . The fragmentation rate constant is also derived experimentally (see section 5.4). The particle sizes together with particle numbers for given time steps, have been calculated for each of the size bins using burning and fragmentation rate constants with the help of the present simplified model. The particle size reduction rate has been calculated as the ratio of the final particle size to the initial particle size for each size bin for the given time step t .

The calculated particle size reduction rate for each size bin should match with the size reduction rate derived using 1-DICOG coal combustor program, as shown in Figure 5.2. If not, then a new value of the char conversion for each size bin is assumed in such a way, that the calculated size reduction rate also matches with the size reduction rate derived from the graph of 1-DICOG coal combustor program [4]. It should be stressed here, that this approach is crude and it needs to be further verified with specific single particle experiments to identify particle size reductions based on char conversion and fragmentation.

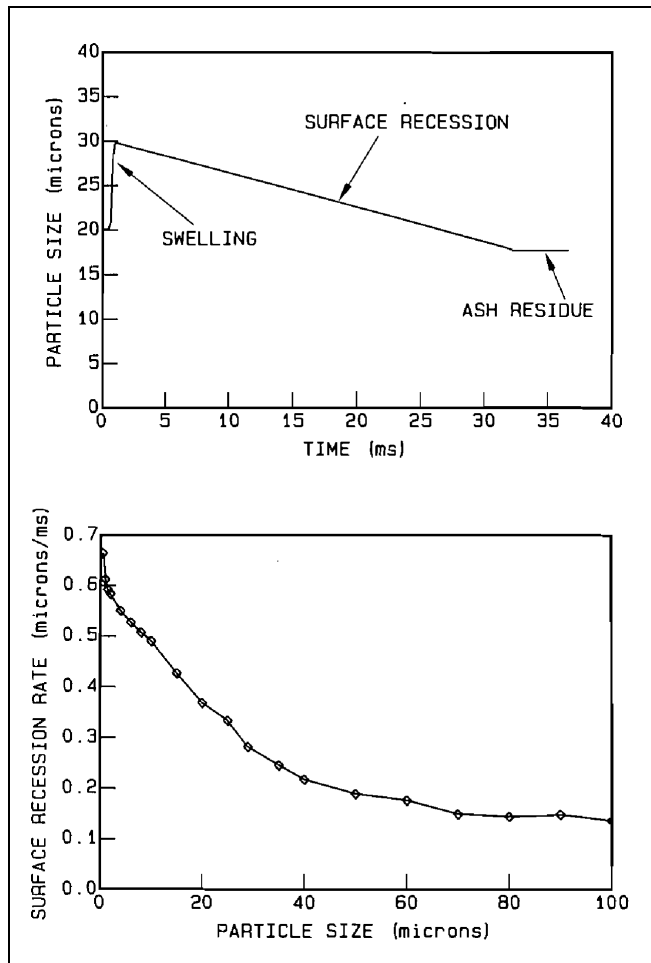


Figure 5. 2: Particle surface regression computed with the one dimensional coal combustor program 1-DICOG [4]

5.2.7 Mineral matter distribution

Each size bin is marked with ash and combustible matter contents in a way that the sum of the ash contents assumed in all size bins matches with the total ash content of the fuel. The organic and the inorganic matter distribution from higher to lower size bins is made according to Figure 5.3.

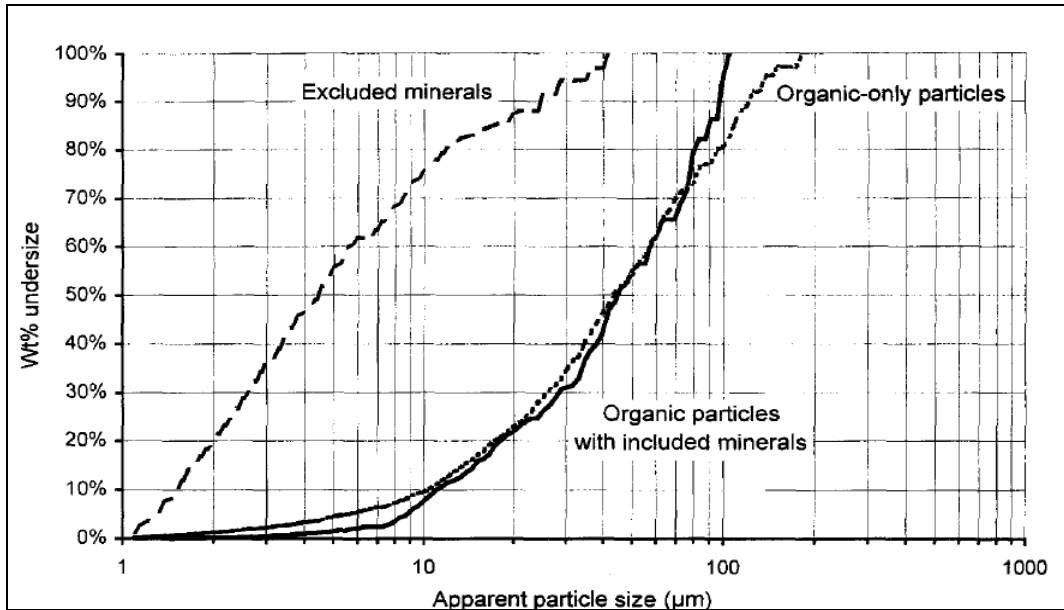


Figure 5. 3: Classifier effect on size distributions for minerals for typical coal [27]

It is observed that the inorganics in the char particles increase the density of the overall char particle [27]. Therefore, after milling and classifying based on the density and the diameter, the fuel will have a different organic and inorganic matter distribution for different sizes [27]. In the present approach, it is assumed that higher size char particles will have a higher organic content, while smaller sized particles will contain more mineral matter. The total char conversion of each size bin is also assumed by taking into account its mineral matter content. However, this model does not account for excluded minerals.

5.3 Analytical solution

As described above, in the particle population balance model equation 5, the C_i and S_i are respectively the time dependent burning and fragmentation rate constants. The analytical solution of equation 5 has been derived for each particular time step by treating them as constants for the selected time step. The values of the fragmentation and burning rate constants for different time steps are derived from the LCS experiments, described further in detail. For simplicity, when obtaining an analytical solution, the fragmentation and burning rate constants are termed as A and B respectively.

As a result of the simplifications discussed in the mathematical modelling Section 5.2, the model equation 5 is solved analytically for two sizes namely the higher (m_1) and the lower (m_2) mass particles in each size class. The particle number for the larger (N_1) and the smaller (N_2) entities in each size class are derived in Table 5.1. Burning, fragmentation and the combination of both processes are considered as three separate cases. The analytical solutions for the different cases are used for all size bins according to the chemical conversion achieved at the selected time step. For shorter time steps (conversion <5%), only attrition is considered together with burning. For conversions up to 65 %, breakage mode of fragmentation together with burning is considered, while above 65 % percolation mode is considered as well.

Table 5. 1: Analytical solutions for the different modes of fragmentation along with burning

Mode	Analytical solution for two size class	
Burning	$N_{1(t)} = N_{1(0)} \text{Exp} (-A t)$	$N_{2(t)} = \text{Exp}(-A t) [N_{2(0)} + A N_{1(0)}]$
Burning + Breakage	$N_{1(t)} = N_{1(0)} \text{Exp} (-(B+A)t)$	$N_{2(t)} = \text{Exp}(-(B+A)t) [N_{2(0)} + N_{1(0)} (\gamma^3 B + A)]$
Burning + Percolation	$N_{1(t)} = N_{1(0)} \text{Exp} (-(0.5 B + A)t)$	$N_{2(t)} = \text{Exp}(-A t) [N_{2(0)} - \frac{(0.5 \gamma^3 B + A) N_{1(0)} \cdot (\text{Exp}(-0.5 B t) - 1)}{(0.5 B)}]$

A modeling chart of the PSD evolution during pulverized fuel combustion is given in Figure 5.1. The marked size bin contains the two size particles having masses $m_{1(0)}$ and $m_{2(0)}$ at the initial ($t = 0$) time step. These particles are having $N_{1(0)}$ and $N_{2(0)}$ particle numbers according to their weight fractions in the fuel. Particle shape is assumed to be spherical throughout all the calculations. This marked size class will be solved by the current described mathematical model for $t = t$ time step for burning and fragmentation which will produce two resultant size class having masses $m_{1(t)}$ and $m_{2(t)}$ with particle numbers $N_{1(t)}$ and $N_{2(t)}$. The same way different particle size bins, representing different sizes in the initial particle size distribution, will be solved through the currently described model. The $m_{1(t)}$, $m_{2(t)}$, $N_{1(t)}$ and $N_{2(t)}$ for each size bin at a given time step t is derived from the algorithm chart as shown in Figure 5.4.

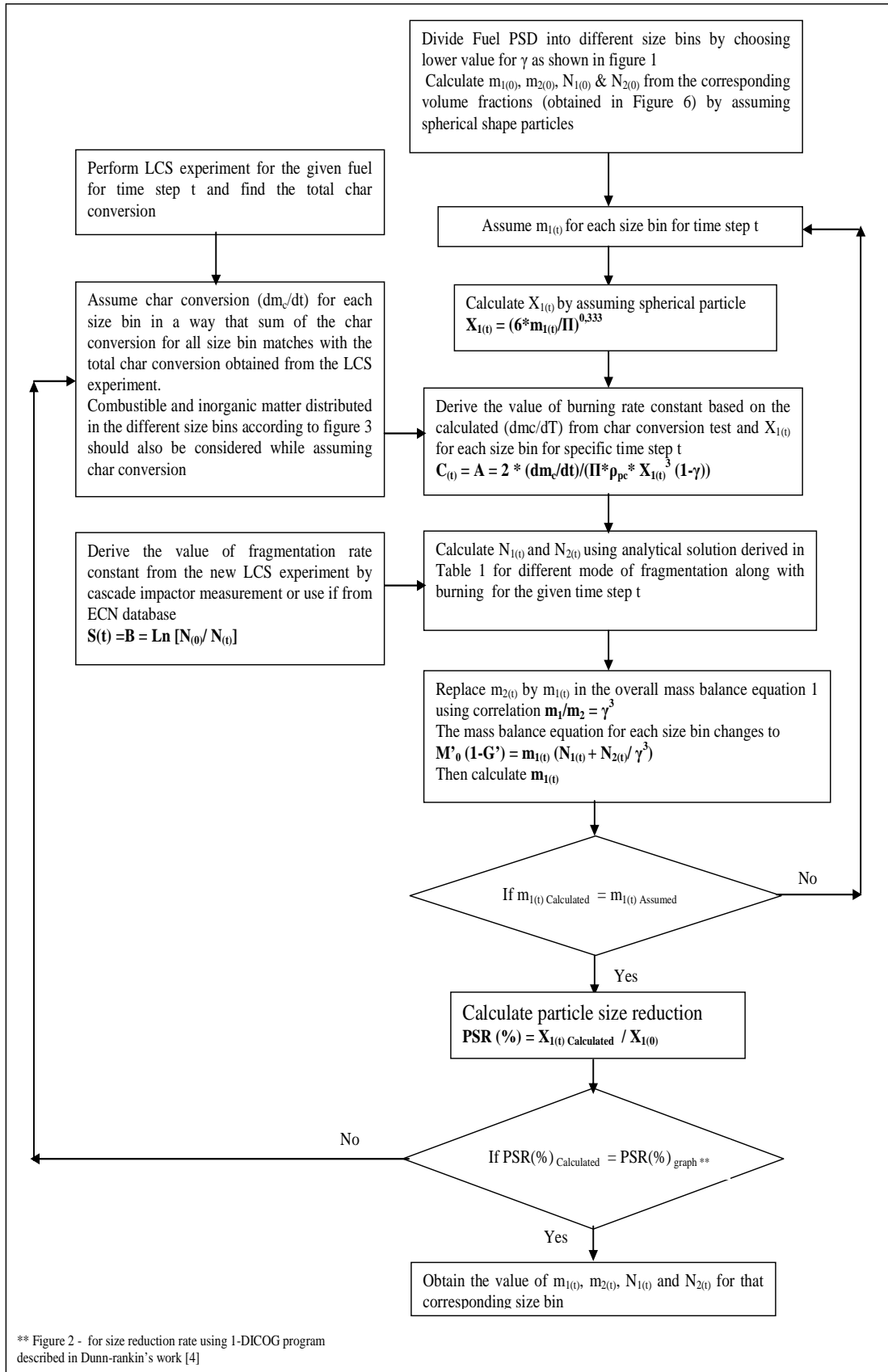


Figure 5. 4: Algorithm chart for the calculation of particle sizes along with particle numbers for the given time step t

5.4 Experimental

The experiments described in Chapter 3 are used for validation here. The burning rate constant and fragmentation rate constants are calculated as follows:

5.4.1 Burning rate constant

An oil-cooled probe was used for sampling char and ash at four heights along the reactor vertical axis in the system, representing particle residence times of 20 ms, 90 ms, 210 ms and 1300 ms.

Total char conversion was calculated using the ash tracer method and can be found in Chapter 3 (Figure 3.5). The value of char conversion ($[dm_c/dt]$ or $[m_{c(0)} - m_{c(t)}]$) for each size bin is assumed in such a way that the total char conversion obtained from the experiment matches with the sum of the char conversion assumed for all size bins. Moreover, char conversion for each size bin is also assumed by keeping in mind that the calculated particle size reduction rate using the present simplified model matches with the size reduction rate suggested by Dunn-Rankin's coal combustor program (1-DICOG). The burning rate constant has been calculated from equation 7 and 8 for different time steps using assumed char conversion for different size bins.

5.4.2 Fragmentation rate constant

A Pilat/University of Washington MarkV cascade impactor was used to obtain eleven mass fractions in the given size range for all different residence times of 20 ms, 90 ms, 210 ms and 1300 ms. Aerodynamic particle diameters are read out from the calibration tables of the instrument, while true particle diameters are verified from SEM inspection. The corresponding particle number for different given time steps for all higher particle sizes ($> 30\mu\text{m}$) was then calculated from the mass fractions by assuming spherical shape particles. The fragmentation rate constant has been calculated with the particle numbers using equation 10 for different time steps.

Cumulative mass fractions with particle diameters for different char burnout were also measured for comparison with model results.

5.5 Validation against different coal and biomass combustion

Dunn-Rankin's and Mitchell's population balance models have been simplified by solving the system of the first order linear ODE analytically for two size classes. In contrast to Dunn-Rankin's, Mitchell's and Syred's efforts; fragmentation rate constant, burning rate constant, particle size reduction and chemical conversion for the Polish coal derived from the experiments have been incorporated into the present simplified kinetic model. The model and experimental data are tabulated in Appendix D. Figure 5.5 shows the simulated PSD evolution, beginning with a roughly power-law initial size distribution. After burning and fragmentation at increased residence time, the power law is shifting for small particles. However, the self-preserving power law has different exponents from the initial PSD power law. The model qualitatively behaves nearly in a same way as the Dunn-Rankin's simulation [3, 4], as visualized in Figure 5.5 and Figure 5.6.

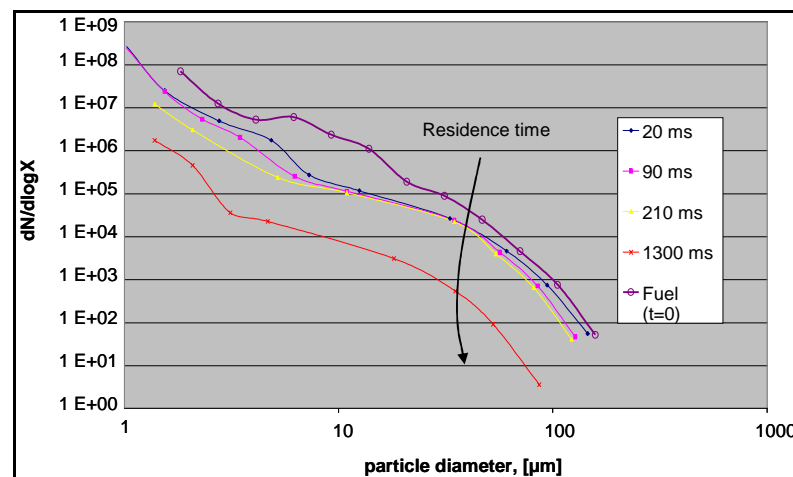


Figure 5. 5: Power-law particle size distribution of polish coal at different char burnout level using current described model

This confirms that the concentration of larger particles decreases due to burning and fragmentation during combustion, which modifies the particle size distribution. These large particles initially contribute fragments to the smaller particle sizes, counter balancing the quick burnout of the smaller particles. The balance between

burning and fragmentation produces nearly constant decrease in particle concentration throughout all particle sizes.

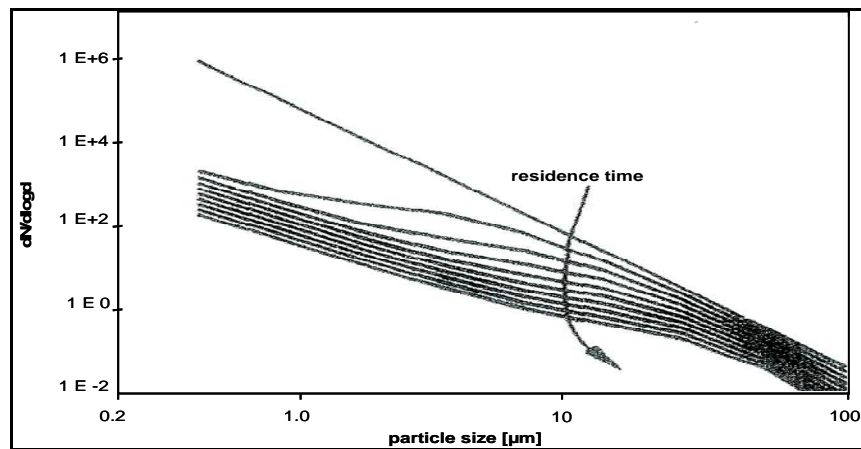


Figure 5. 6: Dunn-Rankin model power-law particle size distribution at different residence time [4]

The cumulative mass fractions obtained for the different char burnout levels from experiments with five different coal and biomass (Polish coal, UK coal, Wood chips, Olive residue, Straw) are compared with the model predictions, given in Figure 5.7-5.11. It can be seen from Figure 5.12 that the model results are in good agreement with the experiments apart from small absolute standard deviation of around maximum 15-20% for all the time steps for all the fuels.

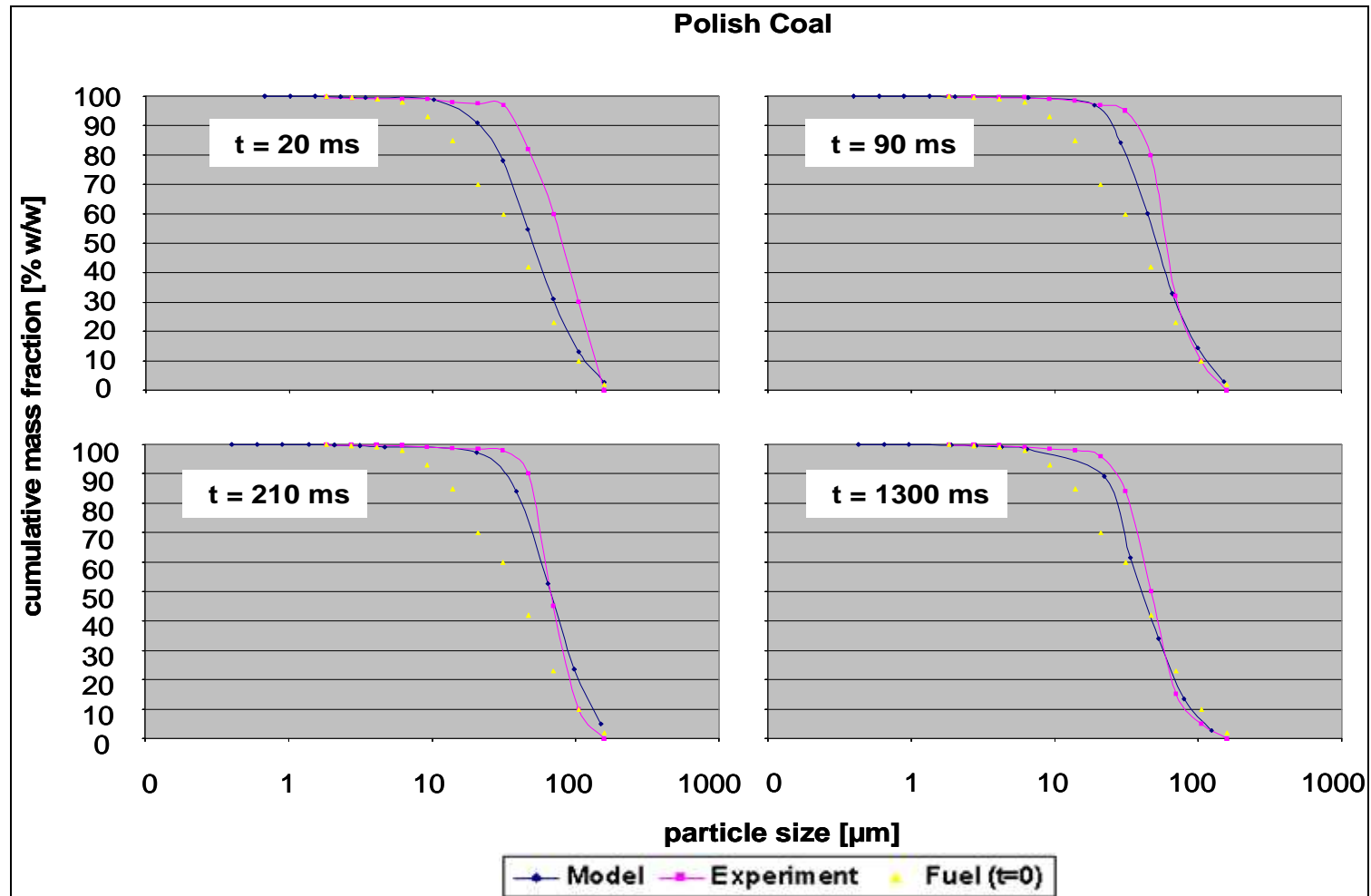


Figure 5. 7: Polish coal different residence times: Comparison of model with experimental data (Cumulative mass fractions (w/w %))

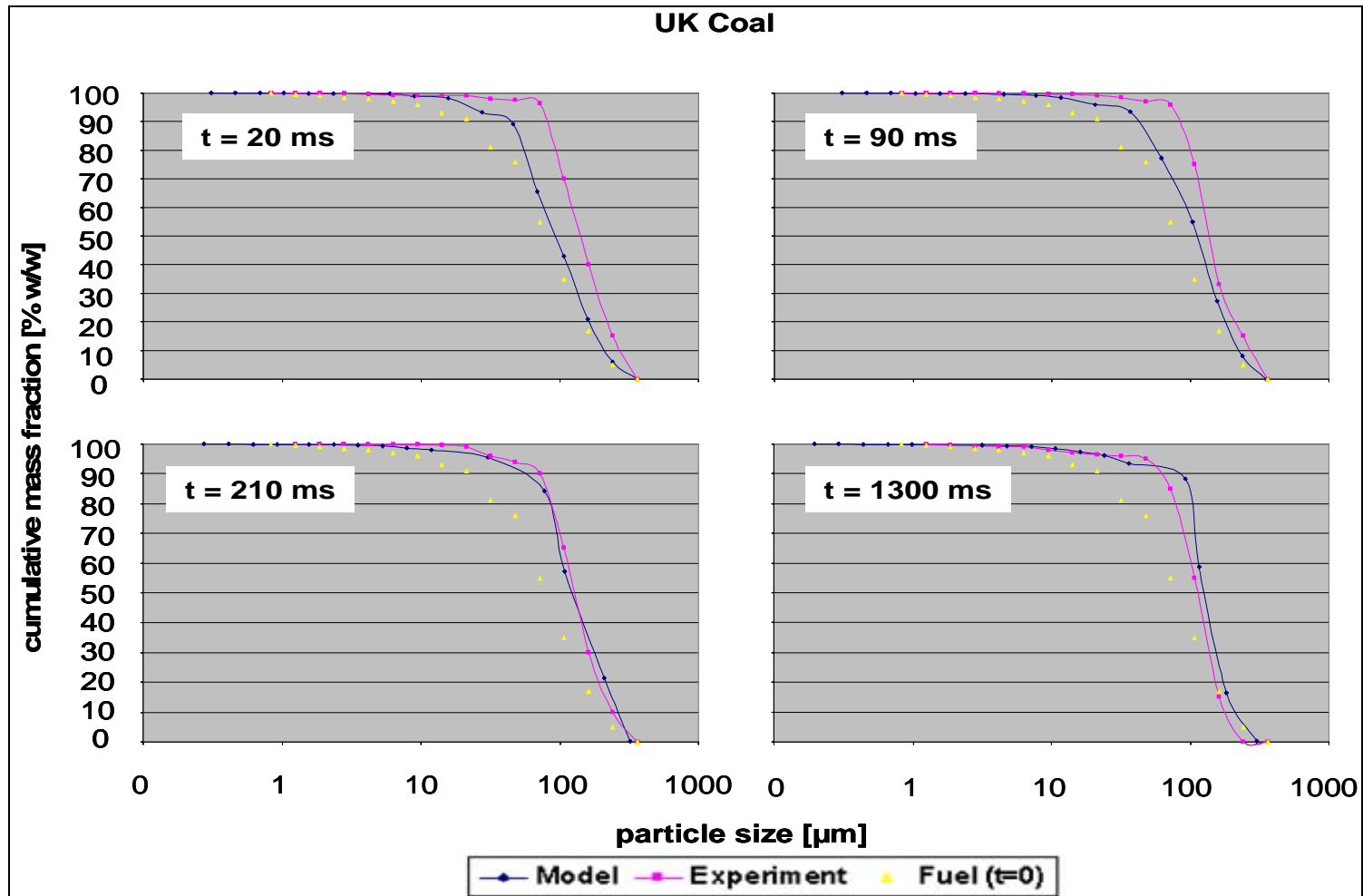


Figure 5. 8: UK coal at different residence times: Comparison of model with experimental data (Cumulative mass fractions (w/w %))

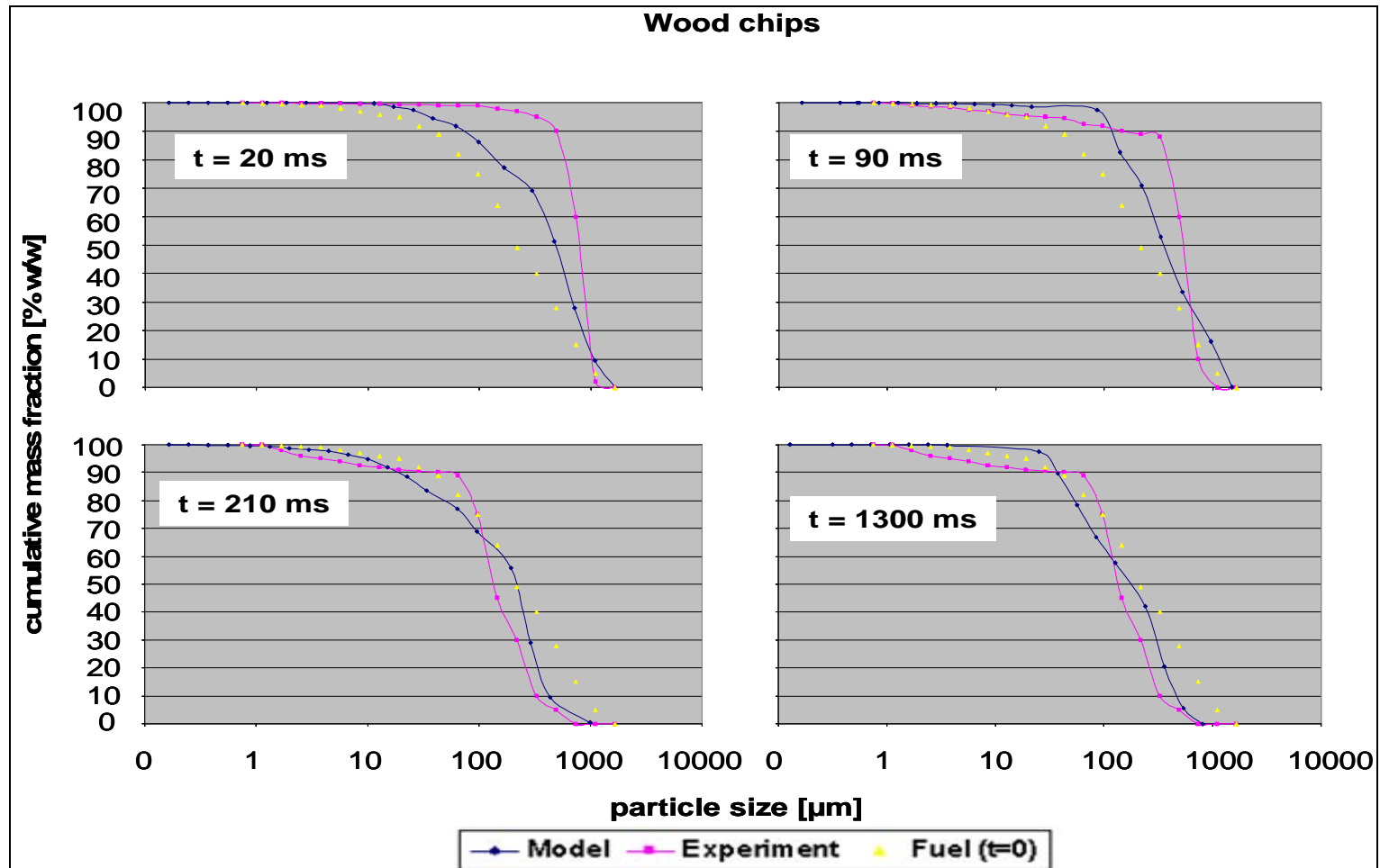


Figure 5. 9: Wood chips at different residence times: Comparison of model with experimental data (Cumulative mass fractions (w/w %))

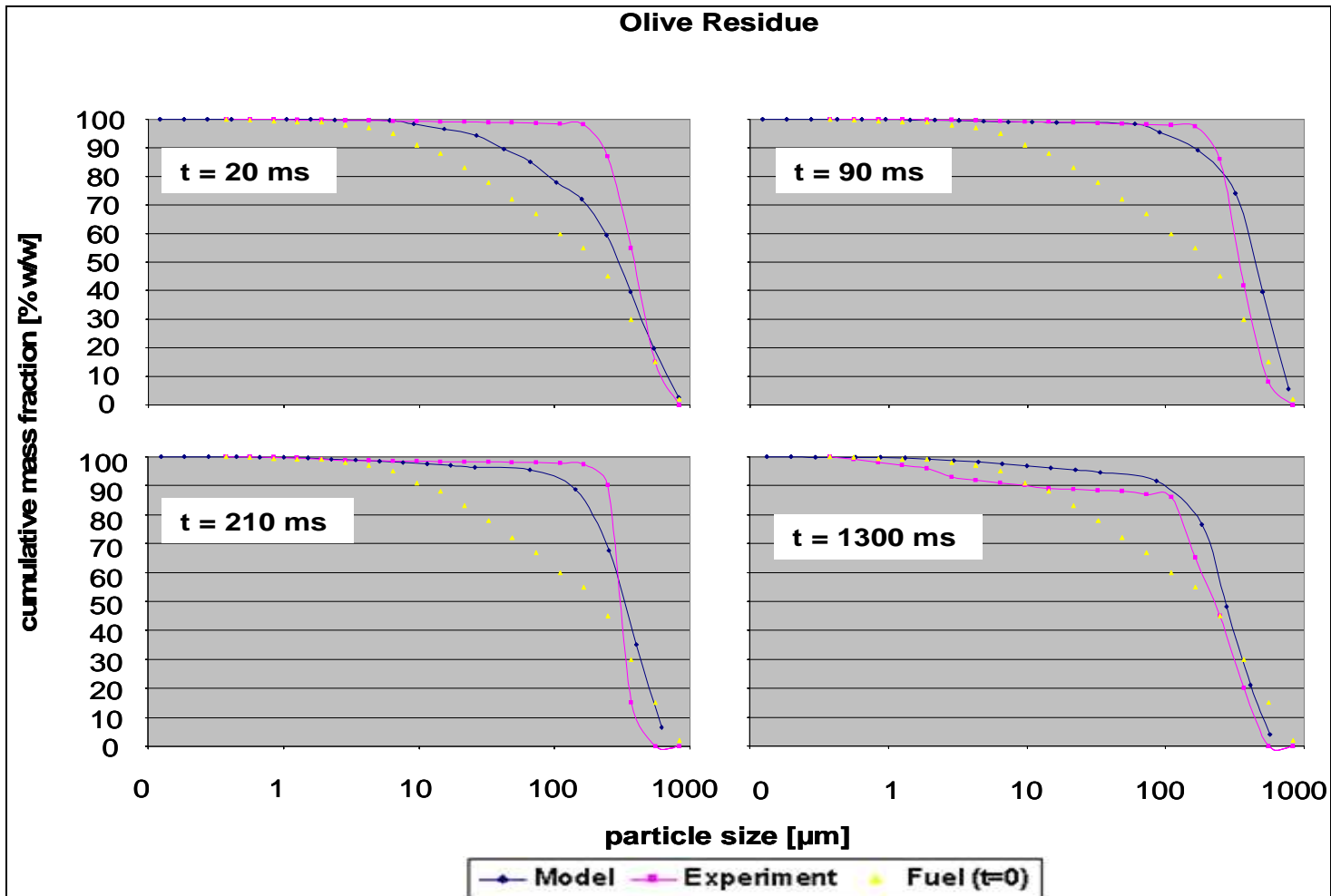


Figure 5. 10: Olive residue at different residence times: Comparison of model with experimental data (Cumulative mass fractions (w/w %))

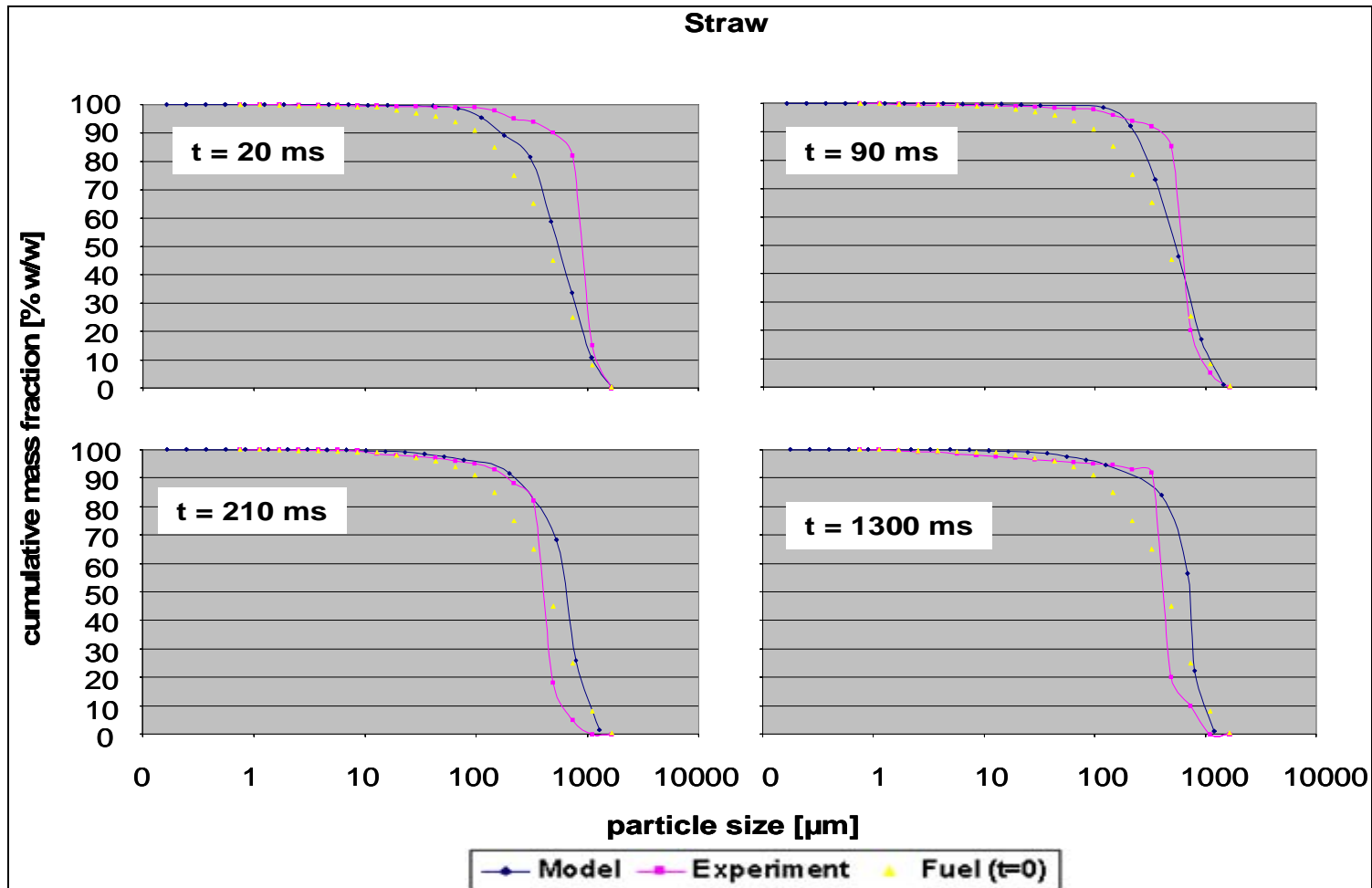


Figure 5. 11: Straw at different residence times: Comparison of model with experimental data (Cumulative mass fractions (w/w %))

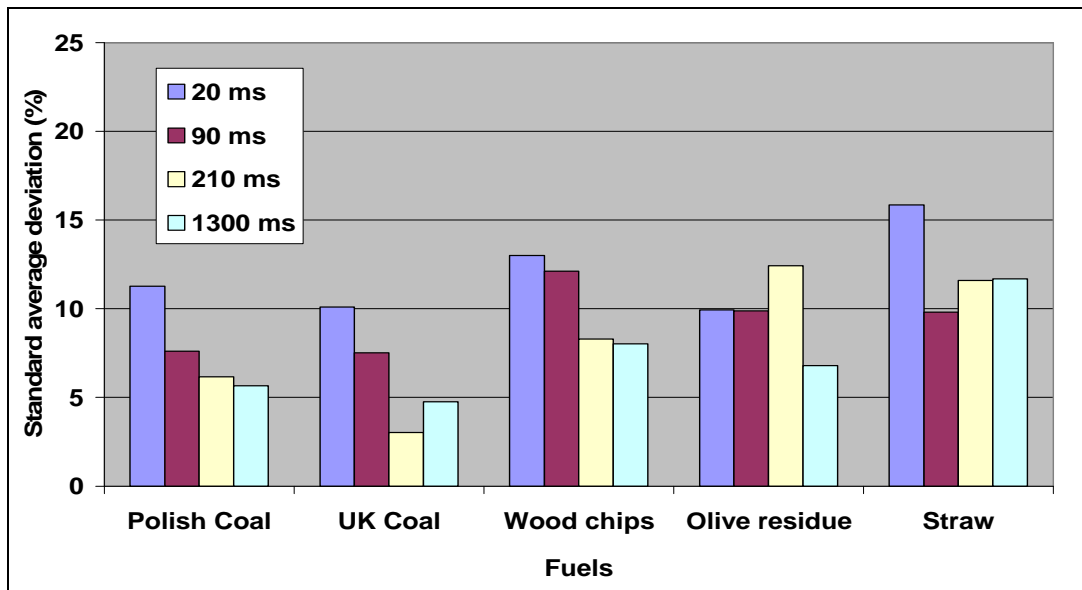


Figure 5. 12: Standard average deviation (%) of the model and experimental results for different fuels

This variation may be due to several of the following reasons:

1. To avoid complexity, only external burning is considered and, therefore effects of density changes are neglected in the present simulation.
2. Particle shapes are assumed to be spherical one and no shape factor is introduced in the modeling, which may affect the particle number calculations.
3. Sizing of the cascade impactors samples for experiment is done visually on the basis of the SEM images. However, this proves difficult in the case of smaller particles, primarily due to clustering by salts.
4. Conversion analyses for each separate cascade impactor stage have not been performed and instead of that only a single bulk conversion test was performed for each char burnout level. The conversion per size bin is therefore assumed. The fragmentation rate constant is also crudely derived for all the particle sizes ($>30 \mu\text{m}$). In the future, single particle experiments will be performed to evaluate single particle conversion and fragmentation rate constants more accurately.
5. It has been observed that two coals have less deviation compare to other biomass fuels. Such deviation may be due to the reason that two coals are having less devolatilization, char burnout and fragmentation events than biomass fuels.

5.6 Validation against co-firing (Polish coal and Straw)

All of the above detailed cascade impactor measurements along with release and conversion analysis were done for different coals and biomass under the BIOASH project at ECN. Co-firing tests were not planned under the BIOASH project for creating such a large, complex data base. However, only few filter samples for blends were available at ECN which were taken during ash deposition tests for investigating elemental mineral matter composition of the ash. One such filter sample for blends (Polish coal (63%) and Straw (37%)) was selected for the model validation. The filter sample was collected for the longest residence time (1300 ms) in the furnace. Fragmentation and burning rate constants for Polish coal and Straw are taken from the individual experiments described as above. The char conversion of the blend was found (4.2 wt% carbon in ash) using the ash tracer method. The char conversion for different size bins of Polish coal and Straw have been assumed from their individual experiments in a way that total char conversion assumed matches with the value obtained for the ash sample using ash tracer method. The filter sample was analyzed by Malvern Mastersizer (with pure Ethanol solution) for final ash particle size distribution. The derived ash particle size distribution was then compared with model results as shown in Figure 5.13. The model results were deviating more than 20% against filter sample analysis mainly for the higher sizes.

The large deviation may be due to several reasons including model simplification, experimental errors and limitations as mentioned in Section 5.5. However, one of the main reasons for such a large deviation could be experimental. Higher size particles might have impacted high on the deposition probe and not collected properly on the filters. Moreover, the other reason could be the analyses technique. The filter ash derived from the experiment was analyzed by Malvern Mastersizer (light scatter technique) with pure Ethanol solution which still would have dissolved salts from the outermost surface of the char particles. Considering the large deviation, specific experiments with cascade impactor measurements need to be considered in the future for the true validation of the model for co-firing. However, the model assumptions could also be considered as one of the reasons for the deviation.

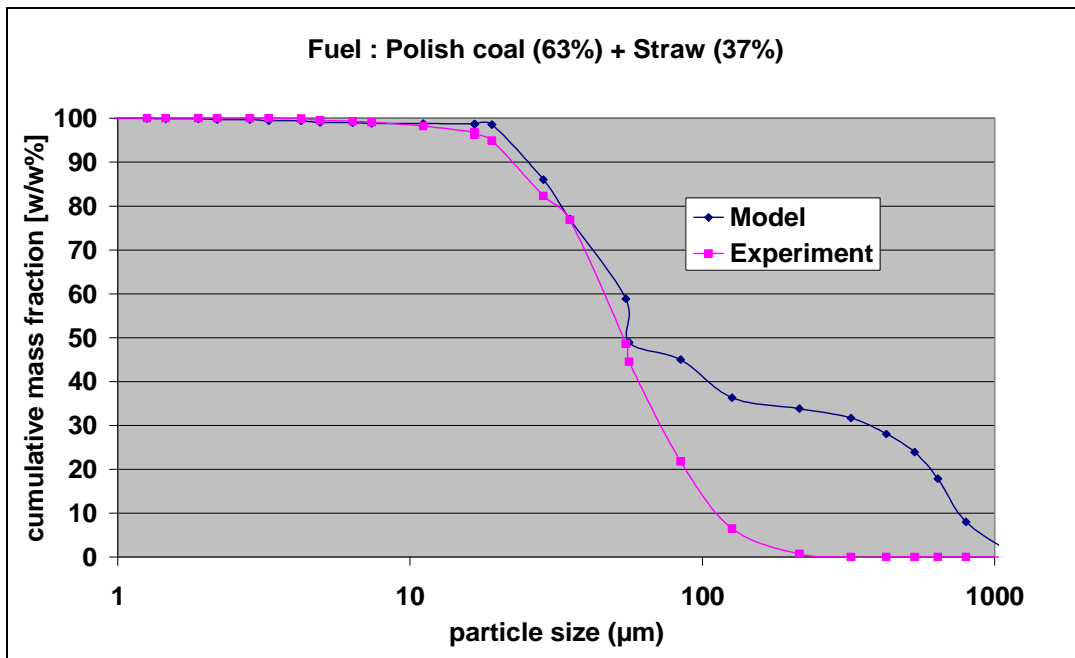


Figure 5. 13: Polish coal and Straw during combustion at 1300 ms: Comparison of model with experimental data (Cumulative mass fractions (w/w %))

5.6 Conclusions

The population balance model has been simplified kinetically and analytically. The fragmentation rate constant and the burning rate constant derived from the experiments have been incorporated into the present model. The model shows a good agreement with experimental results, with a maximum of 15-20 % absolute standard deviation, yet the model is still considered to be in an initial stage of development. So far, according to the author’s knowledge very few validations [28,29] of the particle population balance model for PSD evolution under typical PF combustion conditions have been reported with specific experiments. The experiments conducted at ECN confirm the ability of the PPM model to predict PSD evolution during PF combustion under high temperature conditions.

Conversion kinetics which form a backbone input for the discussed model vary widely for different fuels with widespread chemical and physical characteristics. Therefore, burning rate constants and fragmentation rate constants will be derived for different types of fuels under different combustion conditions (T, λ), which will be incorporated into the ECN model as a set of ideal fuels. The selection for the constants for a new trial fuel at any scale measures will be based on their close match of the chemical and physical properties with the ideal fuel and the type of scale. In the current model, the constants are derived for five

different coal and biomass under lab scale experiments. In the future, the following activities are aimed to improve the quality of the results:

1. Single or narrow sized particle tests will be performed to estimate the fragmentation rate constant more precisely for different fuels and size ranges.
2. Particle size reduction and chemical conversion assumptions will be studied further with more accurate trials and analyses.
3. Instead of two sizes per bin, more sizes with lesser γ value will be attempted in future.
4. A shape factor will also be introduced especially for biomass fuels.
5. The present model will be integrated or interlinked with other numerical models or CFD to evaluate overall ash formation process.
6. Specific Co-firing experiments will also be conducted for model validation.

References

1. J. Yua, J.A. Lucasb, T.F. Wall, Formation of the structure of chars during devolatilization of pulverized coal and its thermoproperties: A review, *Progress in Energy and Combustion Science* 33 (2007) 135–170.
2. L. Baxter, H. Lu, E. Ip, J. Scott, P. Foster, M. Vickers, Effect of Particle shape and size on devolatilization of biomass particle, *Fuel* (2008), Pre published on the web on (2008).
3. D. Dunn-Rankin, A.R. Kerstein, Numerical simulation of particle size distribution evolution during pulverized coal combustion, *Combustion and Flame* 69 (1987) 193–209.
4. D. Dunn-Rankin, Kinetic model for simulating the evolution of particle size distributions during char combustion, *Combustion and Science Technology* 58 (1988) 297–314.
5. N. Syred, K. Kurniawan, T. Griffiths, T. Gralton R. Ray, Development of fragmentation models for solid fuel combustion and gasification as subroutines for inclusion in CFD codes, *Fuel* 86 (2007) 2221–2231.
6. S. Benson, E. Steadman, C. Zygarlicke, T. Erickson, Ash formation, deposition, corrosion and erosion in conventional boilers, *Applications of advanced technology to ash related problems in boilers* (1996) 265-281.
7. A. Sarofim, J. Helbe, The impact of ash deposition on coal fired plants, *Proceedings of the Engineering foundation conference, England* (1993).
8. R. Flagen, and S. Friedlander, *Recent developments in Aerosol Science* (1978).
9. P. Dacombe, M. Pourkashanian, A. Williams and L. Yap, Combustion-induced fragmentation behavior of isolated coal particles, *Fuel* 78 (1999)1847–1857.
10. G. Wilemski, S. Srinivaschar, S. Sarofim, Modeling of mineral matter redistribution and ash formation in pulverized coal combustion, *ASME, New York*(1992) 545.
11. G. Wilemski and S. Srinivasachar, Prediction of Ash formation in Pulverised Coal Combustion with Mineral Distribution and Char Fregmentation Models, *Proceeding of the Engineering Foundation Conference, England, (1993)* 151-164.
12. L. Yan, R. Gupta and T. Wall, The implication of mineral coalescence behavior on ash formation and deposition during pulverized coal combustion, *Fuel* 80 (2001) 1333-1340.

13. A. R. Kerstein, and B. F. Edwards, *Chemical Engineering. Science.* 42 (1987) 1629- 1634.
14. S. Kang, J. Helble, A. Sarofim and J. Beer, *Twenty Second Symposium (International) on Combustion, Proceedings of the Combustion Institute* (1988) 231-238.
15. P. Salatino, F. Miccio and L. Massimilla, *Combustion and Percolative fragmentation of carbons, Combustion and Flame* 95 (1993) 342–350.
16. P. Salatino, F. Miccio and L. Massimilla, Monte Carlo simulation of combustion induced percolative fragmentation of carbons, *Twenty-fourth Symposium (International) on combustion, Proceedings of the combustion Institute* (1992) 1145-1151.
17. M. Ballauff. and B.A. Wolf, *Degradation of chain molecules. 1. Exact solution of the kinetic equations, Macromolecules* 14 (1981) 654.
18. L. G Austin, R. Kimpel and P.T Luckie, *Process engineering of size reduction: Ball milling, Society of Mining Engineers New York* (1984).
19. B. Waldie and D. Wilkimson, *Modeling of product size distribution from formation process. Powertech, Particle technology, Symposium series 69, The Institution of Chemical Engineers.* (1983).
20. R. Mitchell, *An intrinsic kinetics-based, particle population balance model for char oxidation during pulverized coal combustion, Proceedings of the Combustion Institute* 28 (2000) 2261–2270.
21. R. Mitchell, *Char fragmentation and its effect on unburned carbon during pulverized coal combustion, Contract no.:DE-FG22-92PC92528; For U.S Department of Energy* (1997).
22. P. Campbell, R. Mitchell, M. Liqiang, *Characterization of coal char and biomass char relativities to oxygen, Proceedings of the Combustion Institute* 29 (2002) 519–526.
23. M. Liqiang, R. Mitchell, *Modeling char oxidation behavior under Zone II burning conditions at elevated pressures, Combustion and Flame* 156 (2009) 37–50.
24. K. Mathews, P. Street, *Combustion histories of various coal water fuels. Proceedings of the sixth international coal slurry combustion and technology, Orlando, FL* (1984) 25-27.

25. A. Kerstein, S. Niksa., Fragmentation during carbon conversion: Predictions and measurements, Twentieth Symposium (International) on combustion, The Combustion Institute, Pittsburgh (1984) 941.
26. P. Smith, L. Smoot, One dimensional model for pulverized coal combustion and gasification, Combustion Science and Technology 23 (1980) 17.
27. F. Wigley, J. Williamson, H. Will, B. Gibb, The distribution of mineral matter in pulverized coal particles in relation to burnout behavior, Fuel 76 (1997) 1283-1288.
28. R. Mitchell and A. Akanetuk, The Impact of Fragmentation on Char Conversion during Pulverized Coal Combustion, Twenty-Sixth Symposium (International) on Combustion, The Combustion Institute (1996) 3137-3144.
29. J. Santiago , B. Javier, Study of the evolution of particle size distributions and its effects on the oxidation of pulverized coal, Combustion and Flame 151 (2007) 482-494.

Chapter 6

Ash formation modeling

There are various method/models available to measure or predict ash related problems such as slagging, fouling, erosion, corrosion, aerosol formation etc. in power utilities. These methods are often not powerful enough to properly predict the extent of these problems especially with biomass fuels, varying greatly in inorganic composition, both from coals as well as from one another. Particle size and mineralogy of ash after combustion are often indispensable as a valuable input in these methods/models to further investigate the ash related problems. Particle size evolution alongside with mineralogical transformations in the course of combustion are complex phenomena depending on numerous operating parameters and several physical and chemical properties of the fuels, as discussed in Chapter 2. These two important parameters are often obtained using several expensive and time consuming lab-, pilot- and plant-scale trials. Numerous models have also been developed to predict the particle size and mineralogy of the ash after combustion and their application for efficient design has increased remarkably in recent years. In the present PhD project, a simplified particle population model has been developed and validated with five different coal and biomass fuels. This work, described in Chapter 5, allows for the prediction of evolution of the particle size population, alongside with the respective mass fractions after combustion. Several useful empirical indices are also suggested in Chapter 4 as a function of elemental mineral matter composition and their association in the char matrix to predict the overall elemental release. These two submodels work well separately. In this chapter however, as an extended effort, these two models have been integrated, with some assumptions in place, to predict the overall ash release and ash formation in terms of PSD, the respective mass fractions and the corresponding elemental mineral compositions. It is concluded that with this simple yet novel approach that the final particle size distribution along with their respective mass fractions and mineralogical compositions after combustion can be predicted with a reasonable quality for a number of fuels. Nonetheless it is recognized that the model needs to be significantly improved further in many areas.

6.1 Introduction

Solid fuels such as coal and biomass consist of several inorganics alongside with the organic matrix. These organics are burnt off during combustion leaving inorganics termed as ash [1], which often leads to operational problems, including fouling of the boiler surfaces.

Ash deposition problems such as slagging and fouling have been investigated in the industry for several decades using boiler diagnostic methods [2], including on-line thermal conductivity, heat flux and remote slag thickness measurement systems, as well as local diagnostics deploying for example a mobile ash deposition probe [3,4]. These methods however are merely used to quantify ash-related problems and do not provide in depth insights on the ash formation mechanisms with different fuels in terms of particle size distribution along with mineral redistribution after combustion. For this purpose, several empirical indices have been used in the past [5]. These measurement techniques and empirical indices may be a good tool for improving the availability of the boiler but can not be considered as a complete guide for all the ash related problems [6,7].

Corrosion, erosion and aerosols (creating environmental and health hazards) can also be measured online with different techniques. Methods for corrosion measurement or monitoring fall into three main groups: metal loss types, electrochemical types, and visual or microscopic inspection [8]. The result of downtime inspection is of limited value for pro-active corrosion management because it provides only historical data [9], but it can certainly be very useful in new efficient design of the furnace. The simplest metal loss type is the weight-loss coupon, which is the most commonly used technique in corrosion research. A sample of the material of interest, of known weight, is exposed to the process for a known period. When it is removed, carefully cleaned and weighed, the change in weight is used to calculate the metal loss that may then be expressed as an annualized rate of loss (mils or millimeters per year). The coupon requires a relatively long exposure time to the combustion process to yield accurate results. The constraints imposed by the time of exposure naturally limit the number of data points that can be obtained from a location, and ultimately do not detect process changes quickly. Electrochemical techniques measure the corrosivity of an environment independent of actual material loss. In recent efforts, metal loss type sensors can be combined with electrical resistance measurement to provide an on-

line monitoring capability [9]. All these methods are widely used at low temperature regions. However, these technologies are not efficient for fireside measurement at relatively higher temperature [9]. Erosion can be calculated using several empirical indices. A thin layer activation technique is also used to measure erosion rate online [10].

A commonly used technique for measuring particulate mass concentrations (aerosols) involves filtration [11]. This can be done both by deploying traditional membrane-type flat filters or more advanced cascade impactors, which suffer much less from artifacts. In any case filters (or in the case of the cascade impactor deposition substrates) are weighed under controlled temperature and relative humidity conditions before and after sampling, and mass concentrations are determined from the increase in filter/substrate mass and the volume of air sampled.

These measurements are however laborious and expensive, therefore numerous models have been developed to deal with different ash related problems. These models are used as an effective tool for the efficient design of the furnace with different fuels. To achieve a good prediction quality, in all these models, the mineral redistribution alongside with the evolution of fuel and ash particle sizes throughout the combustion is often needed as an important input. This is usually obtained from relatively expensive and time-consuming lab-, pilot- or plant-scale trials and present global trends encourage the use of models to avoid such trials.

The ash formation after combustion is a very complex process, consisting of several parallel physical and chemical transformations such as devolatilization, char burnout, fragmentation and condensation of the devolatilized minerals etc. In his experiments, Mitchell [12] observed that attritive, breakage and percolative-type of fragmentation is observed throughout the devolatilization and char burnout processes. It is also observed that large particles will have a high probability to fragment while small particles will shrink. The fragmentation events will be random and the mineral distribution in the newly formed particles after fragmentation will not be the same as in the parent particles. It is also observed that devolatilization (mineral release) is dependent on particle size, shape and density [13]. Taking into account the critical experimental observations made, as outlined above, the process appears to be very difficult to model with a simple approach. The ash formation modelling which predicts PSD with their respective mass fractions and mineral

composition is rarely attempted. When tried, it is done only by using a percolation model which is a probabilistic approach [14].

The present work uses a simple but novel approach to predict the overall ash formation upon combustion. The ash formation calculations in this work include particle size evolution alongside with the mineral redistribution after combustion. It comprises two submodels, calculating mineral release and particle size evolution after combustion, as described in Chapter 4 and Chapter 5 respectively. These two models work well separately and predict the overall elemental release and particle size evolution after combustion. As an extended effort, these two models have been integrated with a simple approach by making a few assumptions to start with. The list of assumptions and the conceptual plan are explained in detail in the following section of this chapter. The present attempt shows that PSD evolution after combustion and overall elemental release can be well predicted using this model. However, there is considerable deviation from experimental results in the terms of mineral compositions of the different ash size bins for both studied model fuels, namely the Polish coal and the Olive residue. The model needs to be improved further in many areas and the initial assumptions made should also be refined for the model to work better.

6.2 Model plan

The conceptual plan for calculating overall ash formation is presented in Figure 6.1. The model needs particle size and mineral elemental distribution of the raw fuel as an input. The particle sizes have been divided into number of size bins according to given PSD, as explained in Chapter 5. The release of elements such as sodium, potassium, chlorine, sulphur, calcium and magnesium in each size bin has been calculated using empirical indices, developed in Chapter 4.

6.2.1 Assumptions

Since the integral ash formation model comprises the two submodels, the assumptions made for these two will be applicable to this integrated model too. Moreover, to start with the present model the following additional assumptions have been made:

1. In Chapter 4, the experiments were performed for eight fuels having particle sizes in the range $>500 \mu\text{m}$ to $<1 \mu\text{m}$. The empirical indices from Chapter 4 have been developed for predicting overall elemental release for the given fuel having wide particle size distribution. In the present integrated ash formation model, these indices are applied to each size bin assuming that ash release is independent of particle size, shape and density.
2. It is assumed that devolatilization will be limited to a single char particle and therefore particle to particle devolatilization (chemical) interactions are neglected.
3. The physical condensation of released mineral elements will be preferably taking place onto the smaller sized particles, due to their large surface-to-volume ratio. Chemical condensation/capture of volatile alkalis will be more efficient in the case of clay-rich particles. However, none of the condensation mechanisms are considered in the present model.
4. The indices are only developed for sodium, potassium, sulfur, chlorine, calcium and magnesium. Therefore, it is assumed that the rest of the elements in the fuel are not going to be released even at negligible levels.
5. It is also assumed that fragmentation will occur only after complete devolatilization. According to the simplified PPM model developed in Chapter 5, each size will be fragmented into two corresponding size classes only. Instead of a random fragmentation event, it is assumed that fragmented particles from each size bin will have the same mineralogical composition after devolatilization.
6. The particle formed after the certain char burnout and fragmentation which in size matches with the original fuel particle will not behave in the same way in the combustion environment as the particle will attain different temperature, heating rate and elemental mineral composition. The present model does not include such differentiation.

6.2.2 Release of mineral elements from the char particle

It is concluded in Chapter 4 that although ash release is a complex process depending on several parameters, the effect of mineral matter composition alongside with their association in the carbon matrix will be the most significant. To model this, empirical indices for the release of calcium, magnesium, sulphur, sodium, potassium and chlorine have been developed for typical PF firing conditions (atmospheric pressure, temperatures of 1450-1650°C and a heating rate of 10^5 K/s) with the use of eight different coal and biomass samples having a size range of around $>500 \mu\text{m}$ to $<1 \mu\text{m}$ in the function of the mineral matter composition and its association in the fuel matrix.

Based on the assumptions described in section 6.2.1, the said indices ($>0.95 R^2$) have been applied to each size bin to determine the release from that particular size bin.

The indices applied to calculate the different element release are as listed below:

For Potassium:

$$K_{(R)} = 0.5437 (K + Cl / Si + Al + 2S)_{(F)} + 0.0359 \quad (1)$$

For Sodium:

$$Na_{(R)} = 0.8993 (Na / K + Si + Al)_{(F)} - 0.005 \quad (2)$$

For Sulfur:

$$S_{(R)} = 1.0181 S_{(F)} - 0.0138 \quad (3)$$

For Chlorine:

$$Cl_{(R)} = 2.1716 (Cl / Na + K + 2S + Si + Al)_{(F)} - 0.0244$$

(4)

For Calcium:

$$\text{Ca}_{(R)} = 0.4096 \text{Ca}_{(F)} - 0.0749$$

(5)

For Magnesium:

$$\text{Mg}_{(R)} = 0.3965 \text{Mg}_{(F)} - 0.025$$

(6)

Note: The elemental mineral matter in the above equations (1)-(6) are in mole % basis. R= release and F= Fuel. For more details, please refer to Chapter 4.

6.2.3 Particle size evolution after combustion

Particle size evolution after PF combustion is a combination of various competing physical transformations such as char oxidation, devolatilization and fragmentation.

The present simplified integral model calculates the particle size evolution during PF combustion at different given time steps. The initial particle size distribution of the fuel represents different size bins. The overall mass balance for each size bin has been considered as outlined in Equation (7):

$$M'_0 (1-G') = m_{1(t)} N_{1(t)} + m_{2(t)} N_{2(t)}$$

(7)

The M'_0 is the initial mass number of each size bin having $m_{1(0)}$ and $m_{2(0)}$ weighted particles with $N_{1(0)}$ and $N_{2(0)}$ particle numbers, respectively. Equation 7 implies that the residual mass after conversion G' is divided into two size classes. The ' G ' is the total char conversion of the particular size bin into the gas-phase due to devolatilization and char oxidation. Burning (chemical conversion) and fragmentation are the main cause for the two resultant size classes.

The particle number densities $N_{1(t)}$ and $N_{2(t)}$ after burning and fragmentation have been calculated by solving population balance equation 2 analytically for two size classes.

$$\frac{dN_i}{dt} = -S_i N_i + \sum_{j=1}^i b_{ij} S_j N_j - C_i N_i + C_{i-1} N_{i-1} \quad (8)$$

S_i and C_i given in Equation 8 are the fragmentation and burning rate constants derived from experiments. The details of the derivation of rate constants and analytical solution have been given in Chapter 5.

The particle sizes and their corresponding mass fractions at given time step t have been obtained from the methodology explained in Chapter 5.

6.2.4 Redistribution of the mineral elements in the char particle

The release of the mineral elements from each size bin is calculated using Equations 1-6. After the complete devolatilization (mineral elemental release) and char oxidation, each size bin has been fragmented into two corresponding size bins. The elemental composition is assumed to be the same in the newly formed two size bins. The released elements have been subtracted from each size bin. The residual elements in each size bin are normalized after subtraction of the release amount.

In summary, the particle sizes after burning and fragmentation has been calculated using a simplified particle population balance model developed in Chapter 5. The release of the mineral elements and their redistribution into each particle size bin is calculated using simple linear correlations (empirical indices) developed in Chapter 4. The particle size and elemental mineral matter composition after combustion derived using this simple approach has been validated in section 6.4 with Polish coal and olive residue experiments conducted in the Lab-scale Combustion Simulator (LCS) at ECN.

6.3 Experimental

The experiments with Polish coal and Olive residue conducted in the Lab scale combustion simulator at ECN are detailed in Chapter 3. The experiments conducted at LCS (for nearly complete combustion 1300 ms residence time) are used for validating ash formation

modeling. The proximate and ultimate analyses for the Polish coal and Olive residue are given in Appendix A. The fragmentation and burning rate constants derived for Polish coal and Olive residue are detailed in Chapter 5 and Appendix D.1.

The CCSEM analysis applied as an input in the present model for the Polish coal in terms of particle size along with elemental mineral matter composition is given in Appendix E, while in case of Olive residue the PSD is applied, as given in Appendix B and it is assumed that all the mineral elements are homogeneously distributed throughout all size bins.

6.3.1 Experimental results

The overall mineral elemental release, particle size distribution along with their cumulative mass fractions and mineralogical composition for Polish coal and Olive residue for 1300 ms residence time derived from the LCS experiments are given in table 6.1 and 6.2, respectively.

Table 6. 1: Overall elemental releases of minerals

Fuel	Total R (kg)	Minerals (wt %)											
		Al	Si	P	S	Na	Mg	Cl	K	Ti	Fe	Ca	Mn
Polish coal	8.69	0	0	1	61	4	0	27	3	3	0	0	0
Olive residue	55.33	0	0	1	5	1	0	8	85	0	0	0	0

The overall release for Polish coal is very little compared to the Olive residue. Furthermore, sulphur and chlorine are mainly responsible for the elemental mineral release in Polish coal while in the Olive residue potassium is the most significant released element. The more detailed considerations on the nature of the observed release are given in Chapter 3.

It can be inferred from the experimental release that the mineral elemental redistribution in the different size bins in the Polish coal after combustion is nearly homogeneous while in the case of the Olive residue the concentration of volatiles such as potassium, chlorine and sulphur is higher for lower sized particles. One of the reasons is that the Polish coal is less volatile than Olive residue. As the overall release is very limited from the Polish coal, the concentration of the mineral elements will not be significantly changing throughout the particle sizes. In contrast, as a result of a much higher inorganic volatility, the studied Olive residue has a higher concentration of volatiles in the lower size class. .

Table 6. 2: Particle size distribution along with their cumulative mass fractions and mineralogical composition

PD (μm)	CM (Wt%)	Mineral Composition (Wt%)										
		Al	Si	P	S	Na	Mg	Cl	K	Ti	Fe	Ca
Polish Coal												
52	40	24	32	0	3	3	5	1	4	0	16	12
23	56	25	35	0	1	2	5	1	5	2	14	9
7	2	28	41	0	0	3	5	0	4	0	10	8
4	0	26	35	0	0	2	6	1	4	1	14	12
2	0	26	36	0	1	3	7	1	2	2	15	8
2	0	27	35	1	0	2	7	0	3	2	16	8
2	0	28	39	0	1	3	6	1	3	1	11	7
1	0	20	26	2	4	4	5	1	5	2	19	13
1	0	14	25	2	3	2	4	2	4	1	25	17
1	0	21	26	0	4	5	6	1	7	1	20	9
0	0	14	23	2	4	2	3	2	4	2	29	15
Olive residue												
156	61	4	17	5	1	1	9	1	22	0	5	35
129	21	3	16	4	1	1	7	1	26	0	6	33
32	2	4	17	6	0	0	9	1	12	0	3	47
7	1	2	8	4	2	0	5	4	48	0	2	23
6	1	0	1	1	4	0	0	8	82	0	0	4
4	1	0	0	1	3	1	0	6	87	0	0	1
1	2	0	1	4	0	3	1	5	85	1	1	0
1	2	0	0	1	4	1	0	7	86	0	1	1
1	3	0	0	1	4	1	0	8	84	0	1	1
0	4	0	0	1	4	1	0	7	85	0	1	0
0	3	0	0	1	4	0	0	6	87	0	0	2

6.4 Validation

The present model predicts particle size distribution after combustion alongside with the corresponding mass fractions and mineralogical compositions. The model is validated against the Polish coal experiments.

6.4.1 Overall release of the mineral elements

The experimental and model results are compared for Polish coal and Olive residue in Figures 6.2 and 6.3 respectively.

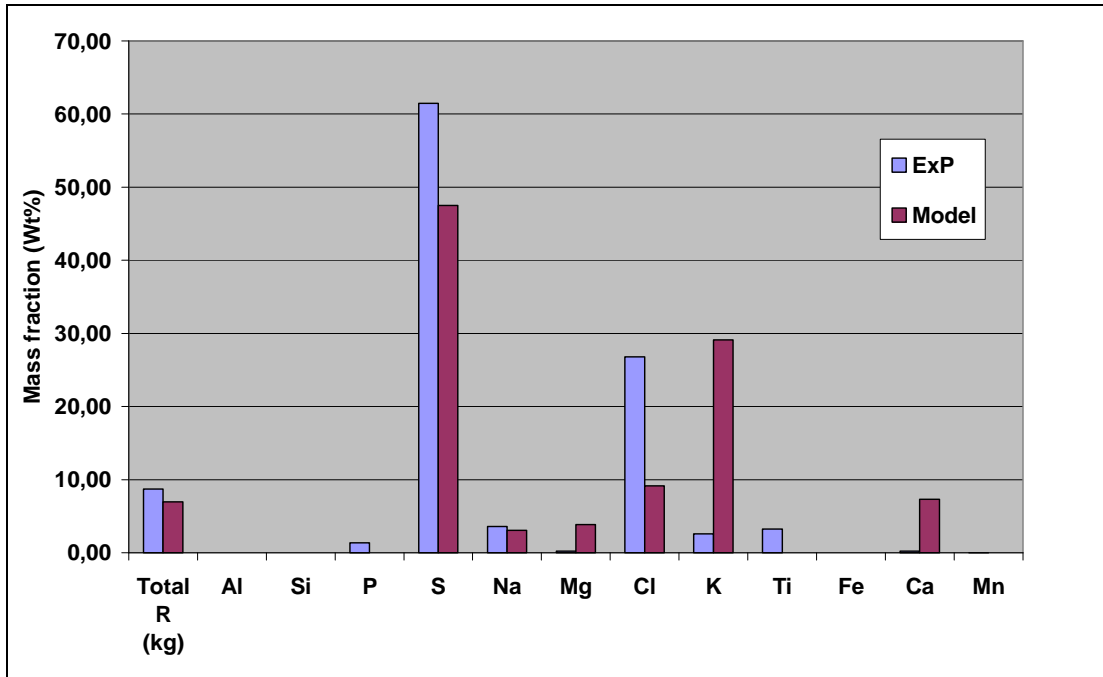


Figure 6. 2: Modeled vs. experimental overall elemental mineral release - Polish coal

As can be seen in the above Figures, the deviation in the predicted elemental release vs. the observed experimental value in the case of Polish coal is significant, when compared with Olive residue. This can be explained by the fact that the applied release indices have been developed with both coal as well as biomass fuels (six biomass and two coal experiments). Since the indices span a rather broad range of inorganics volatility, they may not work efficiently for coals, characterised by a very low volatility compared with biomasses. Therefore, as already suggested in Chapter 4 indices should be better developed for different groups of fuels. Nonetheless, in the case of coal large differences in release are particularly found for potassium and chlorine, which both are present only at trace levels compare with the main ash forming elements Si and Al. Therefore in absolute terms the models still predicts the composition of the ash fairly reliably.

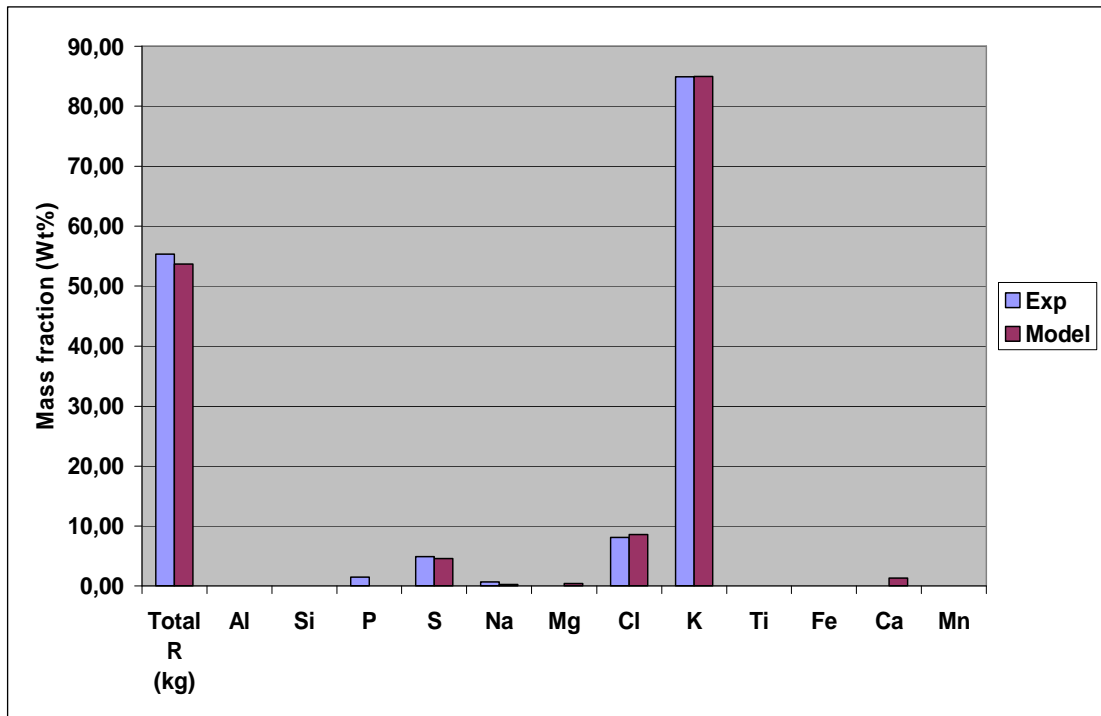


Figure 6. 3: Modeled vs. experimental overall elemental mineral release – Olive residue

6.4.2 Particle size distribution after combustion

The particle size distribution and their respective cumulative mass fractions after combustion are predicted using the simplified PPM model. The comparison between the model and experimental PSD's for the two fuels are given in Figures 6.4 and 6.5. As can be seen in the Figures, the maximum standard average deviation of the model results from the experiments is around 12%, which is more than satisfactory for the modelling purposes. Detailed discussion on the implications of this issue has already been given in Chapter 5.

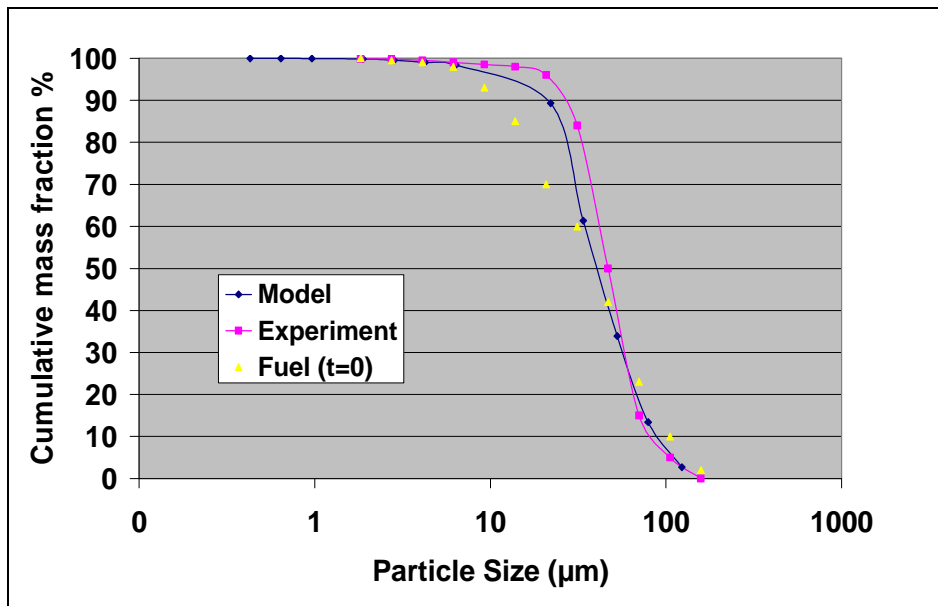


Figure 6. 4: Modeled vs. experimental particle size evolution - Polish coal

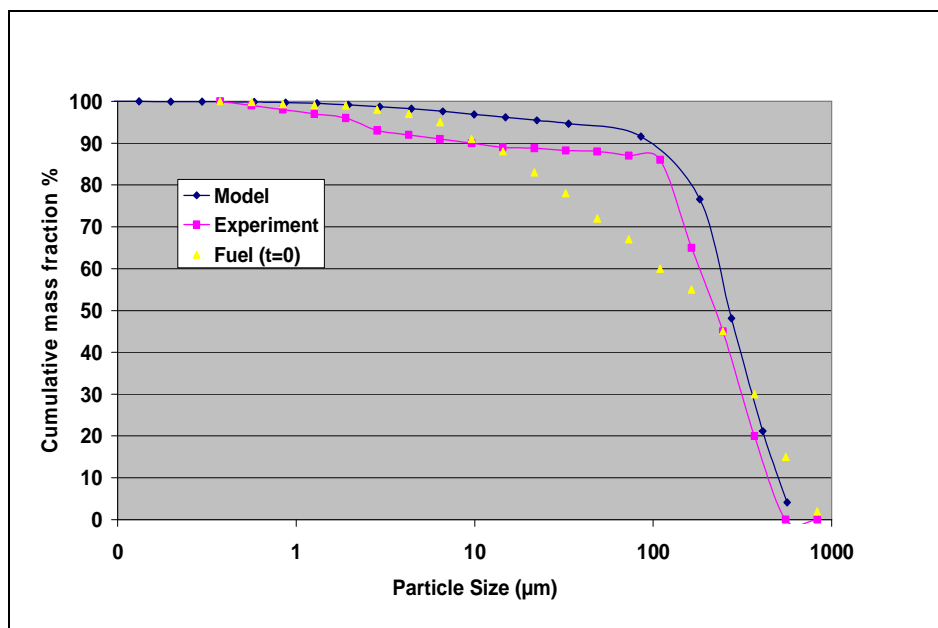


Figure 6. 5: Modeled vs. experimental particle size evolution - Olive residue

6.4.3 Mineralogical transformations in the different particle sizes after combustion

In the model calculations, the release of the mineral elements calculated using empirical indices have been subtracted from each size bin. The residual amount of the inorganics has then been normalized for each size bin and compared with the results of the ICP-AES

analyses performed for different particle size bins, as obtained from the LCS experiments. The results of the said comparison are graphically presented in Figures 6.6 and 6.7.

The model results show considerable deviation from the experiments in the elemental composition of different ash particle sizes formed after combustion. The deviation is less for Polish coal compared to Olive residue. This is due to the fact that the Polish coal is less volatile which means that after the devolatilization (mineral elemental redistribution) in each ash size bin the concentrations of all elements will not vary significantly. In contrast, the elemental mineral release is quite high in the case of the Olive residue. It is observed that a higher fragmentation is expected together with a higher devolatilization of minerals. Moreover, the condensation of released volatile minerals will occur mostly on smaller-sized particles which will alter the mineral composition in the different ash sizes after combustion even further. This is one of the reasons for the observed large deviation in the ash elemental mineral composition for the lower size particles for the Olive residue.

In sum, the deviations in the prediction of ash formation with the present model in comparison of the Polish coal and Olive residue experiments are mainly due to the following reasons:

1. The indices for the elemental mineral release are developed only for S, Na, Ca, Mg, Cl and K. For other elements, it is assumed that the release will be negligible for the present calculations while experimental results for the Polish coal do show considerable release of P (likely by chemical reactions of organically bonded P) and Ti (likely due to fragmentation of small excluded mineral particles).
2. The empirical indices are developed for overall elemental release with eight different coal and biomass fuels ranging in particle sizes (around $>500\ \mu\text{m}$ to $<1\ \mu\text{m}$). As, the empirical indices have been developed with a broad range of inorganics volatility, it is not working well for the Polish coal. Moreover, the present model assumes that the devolatilization for higher and lower size particles will be same which is not the case in reality. Nonetheless, in the case of coal large differences in release are particularly found for potassium and chlorine, both of which are present only at trace levels compared with the main ash forming elements Si and Al. Therefore in absolute terms the model still predicts the composition of the ash fairly reliably.

3. The particle-to-particle chemical interactions and condensation mechanisms are not included in the present model.
4. The present model crudely assumes that particle will fragment into only two size classes after complete devolatilization and will have the same elemental mineral composition in the newly formed particles while in reality attritive, breakage and percolation kind of fragmentation are observed throughout char oxidation and particles will be fragmenting into families of small parent particles rather than just two corresponding size particles. Moreover, the particles will fragment randomly and the elemental mineral distribution will not be same in the newly formed ash particles after fragmentation and char burnout.
5. The effects of particle temperature and heating rates have not been included in the model.

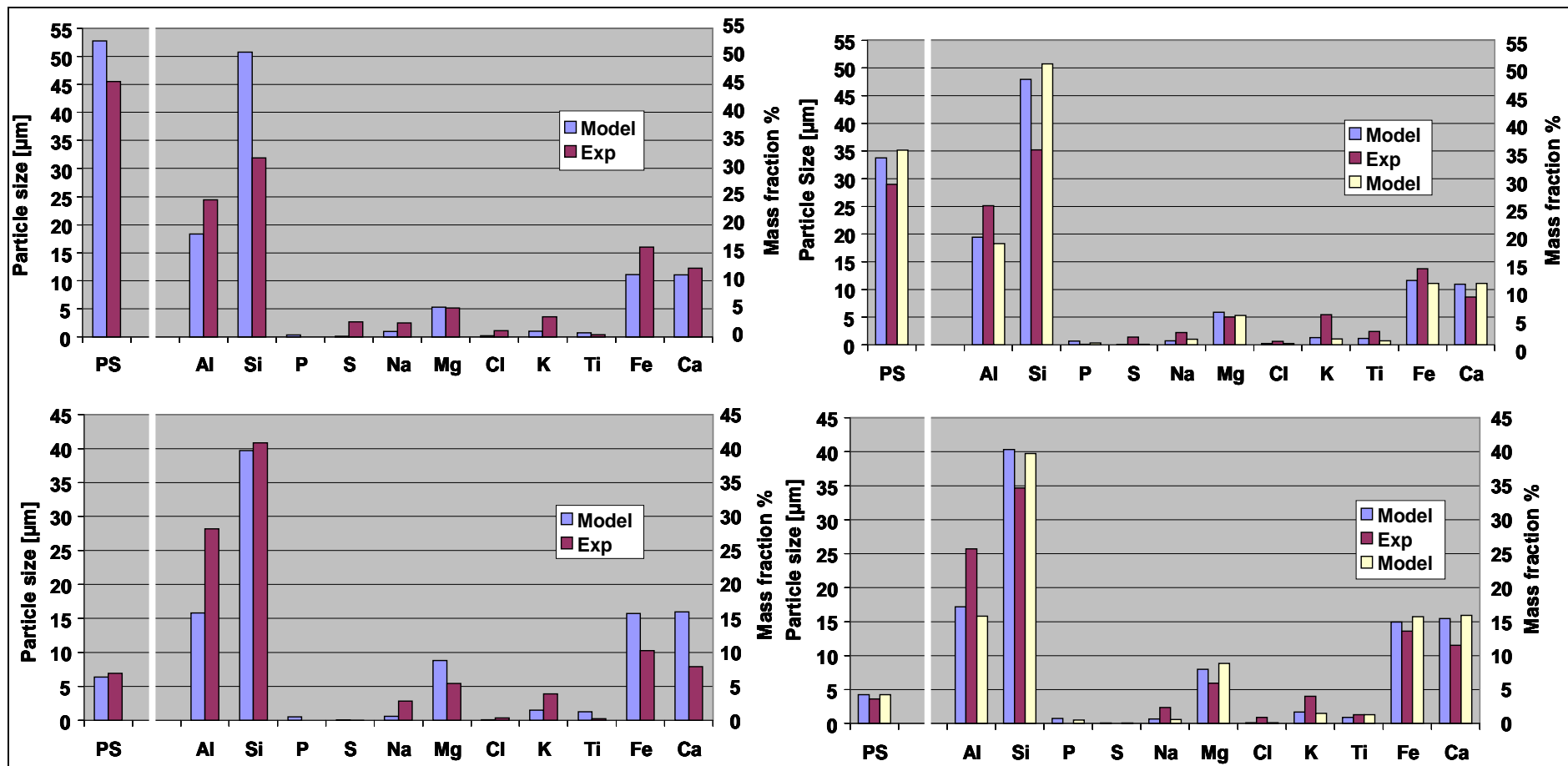


Figure 6. 6: Mineral elemental distribution in different ash particles formed after combustion for Polish coal

Note: The two model lines (blue and yellow color) in the above graphs shows that two particles of nearly same sizes have been produced during the ash formation process from the corresponding size bins which has different mineral elemental composition. PS= Particle size

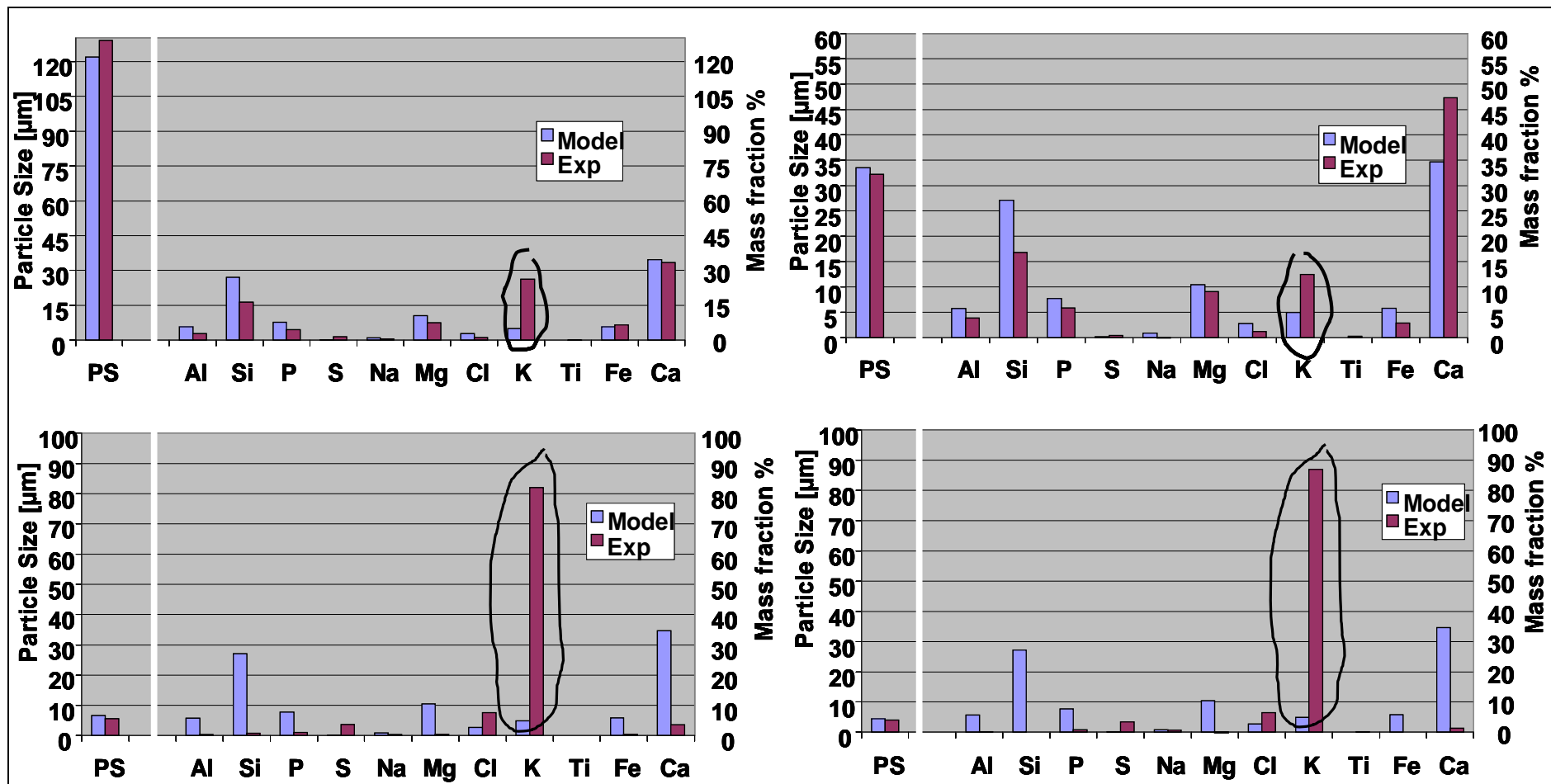


Figure 6. 7: Mineral elemental distribution in different ash particles formed after combustion for Olive residue
 Note: PS= Particle size

6.5 Conclusions

The ash formation process is complex and comprises several mechanisms occurring in parallel on a milliseconds timescale. The presented model predicts ash formation in terms of the particle size evolution alongside with their respective mineralogical compositions after combustion. The discussed model is developed and applicable only for typical pulverised fuel firing conditions, characterised by high temperatures in the range of 1450-1650°C and high heating rates of 10^5 K/s. The output of the present model can be used as an input in CFD and other numerical models, for predicting the extent and criticality of several ash-related problems such as slagging, fouling and possibly also for corrosion and erosion of boiler surfaces. The developed model also allows for pinpointing the needs for further laboratory, pilot or plant scale trials. The development and application of such a model, which predicts PSD and elemental mineral composition after combustion, is highly desirable. However, its development and application is very limited today due to the complex nature of the modeled processes and it needs much improvement in the future.

6.6 Future Recommendations

1. The indices for the mineral element release are developed only for S, Na, Ca, Mg, Cl and K. For other elements, it is assumed that the release will be either nil or negligible and therefore can be neglected in the present calculations. Therefore, it is highly recommended that indices should be developed for other elements in the future.
2. As suggested in Chapter 4, the indices for the release will work better for different group of fuels according to their elemental mineral association into the char matrix. So, it is recommended in future to develop dedicated indices for different groups of fuels as well as for blends.
3. In the present ash formation model, the indices are developed for eight different coal and biomass fuels having particle sizes in the range of around >500 μm to <1 μm . These indices are applied to each size bin by assuming that ash release is independent of particle size, shape and density. This is indeed a very crude assumption and leads to deviation in the ash mineral

elemental composition with varying particle size after combustion. To minimize this error, particle size resolved indices are suggested in future.

4. The particle to particle chemical interactions are not included in the present model which needs to be included in future for better accuracy.
5. The physical condensation of released mineral element will be preferably taking place onto the smaller sized particles, due to their large surface-to-volume ratio. Chemical condensation/capture of volatile alkalis will be more efficient in the case of clay-rich particles. However none of the condensation mechanisms are considered in the present model and should be incorporated in a future model for improved accuracy.
7. It is also assumed that fragmentation will occur only after complete devolatilization which is unlikely in the actual process. So, in future these two physical transformations need to be considered in parallel.
8. According to the simplified PPM model developed in Chapter 5, each size will be fragmented into two corresponding size classes only which is also a rather crude assumption. The incorporation of a multiple size classes fragmentation is crucial and could possibly be done by dedicated MATLAB or CFD models. This will generate the family of corresponding size bins after combustion and give a more realistic picture.
9. It is assumed in the present model that fragmented particles from each size bin will have the same mineralogical composition after devolatilization, which is highly unlikely for inhomogeneous fuels, such as many biomasses. To resolve this, random fragmentation events have to be introduced in the model.
10. The newly formed particle after the certain char burnout and fragmentation which in size matches with the original fuel particle will not behave the same in the combustion environment as the particle will attain different temperature, heating rate and mineral composition. Therefore, the effect of particle temperature and heating rate should be included in the model.

Reference

1. A. F. Sarofim, J.J. Helbe, The impact of Ash Deposition on Coal Fired Plants: Proceedings of the Engineering Foundation Conference, England, Year (1993).
2. A. Tortosa-Masia, F. Anherth, H. Spliethoff, K. R. G Hein, Slagging and Fouling in biomass co-combustion, Thermal Science 9 (3) (2005) 85 – 98.
3. T. Heinzl, J. Maier, J. Baum, H. Spliethoff, K. R. G. Hein, Slagging and Fouling in dry and molten ash PF combustion, University of Stuttgart, JOULE III – OPTEB, Contract JOR3-CT95-0057, Germany, (1998).
4. Cortes, O. Bella, A. Valero, Ash fouling monitoring and sootblowing optimization in a pulverised coal fired utility boiler, thermal annual international Pittsburgh coal conference, Pittsburgh, (1993).
5. F. C. Lockwood, P. G. Costen, M. M. Siddiqi, P. J. Harrison, Mineral ash Transformations, Technical report SW7 2BX JOF3-CT95-0024, The Imperial College of Science, Technology and Medicine, Mechanical Engineering Department, London. <ftp://ftp.euro-cleancoal.net/pub/pdf/JOF3-CT95-0024-pdf-files/JOF3-CT95-0024-02%20Lockwood-ICSTM.pdf>.
6. T. Valero and C. Cortés, Ash fouling in coal-fired utility boilers. Monitoring and optimization of on-load cleaning, Progress in Energy and Combustion Science 22 (2) (1996) 189-200.
7. J. Barrosoa, J. Ballester, A. Pinaa, Study of coal ash deposition in an entrained flow reactor: Assessment of traditional and alternative slagging indices, Fuel processing technology 88 (2007) 865-876.
8. D. M Farrell, B. J. Robbins, Online Corrosion and Thermal Mapping of Industrial Plants by Non-intrusive Means, Rowan Technologies Ltd, UK, NACE International, Corrosion, (2000).
9. H. Ban, Z. Li, A Novel Sensor and Measurement System for Fireside Corrosion Monitoring in Coal-Fired Boilers, University of Alabama, Birmingham, (2002).

10. D. B. Meadowcroft, A. B. Tomkings, Recent developments in methods to aid boiler tube life prediction, ERA Technology Ltd, Denver, NACE International, Corrosion, (1996).
11. P.H. McMurry, A review of atmospheric aerosol measurements, Atmospheric Environment 34 (12) (2000) 1959-1999.
12. R. E. Mitchell, Char fragmentation and its effect on unburned carbon during pulverized coal combustion, Contract no.: DE-FG22-92PC92528, For U.S Department of Energy (1997).
13. J. P. Mathews, P. G. Hatcher, A. W. Scaroni, Particle size dependence of coal volatile matter: is there a nonmaceral- related effect?, Fuel 76 (1997) 359–362.
14. A.R. Kerstein, S. Niksa, Fragmentation during carbon conversion: predictions and measurements, In Proceedings of Twentieth Symposium (International) on Combustion, The Combustion Institute (1984) 941-949.

Chapter 7

Practical implications, Conclusions and Future recommendations

The aim of this research work is to deepen the understanding on ash transformation mechanisms and parameters responsible for ash formation during PF combustion/co-firing. The research was initiated with the detailed literature review (Chapter 2) on ash formation during PF combustion. Specific objectives were gained from the thorough literature review. Based on the literature review, an extensive experimental parametric test matrix was formulated with two coals and six different biomass fuels. Char conversion, devolatilization, fragmentation, ash particle size distribution, reduction and mineral elemental distribution have been investigated (Chapter 3). A qualitative prediction tool is proposed to predict the extent of the char conversion, devolatilization and fragmentation. The release of several elements is also quantified and novel linear correlations with $R^2 > 0.95$ have been developed for predicting the release of alkalis, sulfur, chlorine and alkaline earth metals such as calcium and magnesium as a function of elemental mineral matter composition and their association in the char matrix (Chapter 4). The particle size evolution after PF combustion has been predicted by simplifying the particle population balance model developed by Dunn-Rankin and Mitchell. The simplified model has been validated with experimental results obtained using five different coal and biomass fuels along with one co-firing experiment (Chapter 5). The overall ash formation model was also developed and validated using experimental data obtained with Polish coal and Olive residue (Chapter 6).

The following sections will address the potential practical implications, conclusions and future recommendations emerging out of the research work carried out on ash formation mechanisms during co-firing of biomass and coal.

7.1 Practical implications

- ❖ The detailed literature review carried out in the research project concludes that the ash transformations are complex and depend on several operating parameters and fuel characteristics. Numerous experimental results are reviewed to understand the parameters responsible for such ash transformations. A number of analytical methods/tools along with modeling efforts to date in this area is also reviewed. Numerous conclusions were drawn and future recommendations suggested based on the literature review are discussed in Chapter 2. The present review provides a brief overview on the progress made in understanding ash transformations so far and will also provide useful information for novice researchers in this research field for follow-up activities.
- ❖ An extensive experimental program was carried out as described in Chapter 3 and some new interesting facts (on the char oxidation, devolatilization and fragmentation which decide the ash formation in the radiation zone) are gathered and numerous past observations are reconfirmed. It is concluded that the particle size evolution and mineral transformations during PF combustion are a result of various simultaneously occurring processes. The integration of them is therefore essential to understand the overall ash formation process.
- ❖ Several of the critical observations also made during the experimental runs are as follows.
 - Higher volatiles in the fuel result in a higher devolatilization and thus a higher overall conversion in the initial phases of the combustion process.
 - The higher overall conversion can result in a higher fragmentation.
 - The higher carbonaceous matter and lower ash content increases the char particle temperature to a great extent during combustion which leads to high fragmentation due to the increased thermal gradient.
 - Silica and alumina are both responsible for lowering the devolatilization of alkalis. Sulfur on the other hand volatilizes quickly and fully.

- The observations in this chapter can be very useful in further investigations and modeling of ash formation process in the radiation zone.
- ❖ Moreover, the qualitative predictions suggested based on the fuels mineral elemental matter composition, as well as the volatile matter contents appear to approach the experimental results very closely and can be used as an efficient predictive tool for new fuels.
- ❖ Ash release of several elements is also quantified separately. Linear expressions (empirical indices) have been attempted for the release of several mineral elements as a function of elemental mineral matter composition and its association into the char matrix. The correlations developed for the release of several mineral elements in this chapter are too simple but innovative and not developed nor attempted (or reported) in any of the scientific journal or thesis with such a massive experimental study to the best of authors' knowledge. The release of sodium, potassium, chlorine and sulfur can be calculated with simple linear correlations presented in this chapter having $>0.95 R^2$ value. These simple linear equations (with $>0.95 R^2$ value) can be considered as a valuable tool for predicting ash release as a function of elemental mineral matter composition and their association in the fuel matrix for the typical constant PF firing conditions.
- ❖ Based on the experimental observations and literature review, the particle population balance model has been selected and simplified further to predict the particle size evolution during PF combustion. The present model works well with a maximum of 15-20 % absolute standard deviation. The model is still at initial stage of development, though it can be used to identify particle size distribution evolution in the radiation zone during any PF combustion for laboratory, pilot and plant scale measures with any type of fuel.
- ❖ The empirical indices for the ash release and particle population model are working well separately. In an extended effort, these two models are integrated with a simple approach together to predict overall ash formation in terms of ash release and ash particle size mass fractions and their elemental mineral composition. The approach developed adequately predicts ash formation. However, the model needs to be greatly improved in many areas.

Moreover, the developed model will be incorporated in the commercial software - CAT (Co-firing advisory tool) at ECN.

7.2 Conclusions

- ❖ From an extensive experimental parametric test matrix planned with two coals and six different biomass fuels, many conclusions have been drawn which helped in improving understanding about the ash formation process during PF combustion. It is concluded from the experiments that the ash transformations and char combustion will be in the kinetic-diffusion controlled regime, even with extended residence time with typical pulverized fuel firing conditions. Char chemical conversion and devolatilization are found to be dependent on ash content and volatile matter at typical pulverized fuel firing conditions. Devolatilization of the fuels also depends on the elemental mineral matter and its association with the carbon matrix. Fragmentation is found to be dependent on fuel chemical conversion and devolatilization. Mineral matter and its association in the char matrix can significantly alter the ash release. Ash release of several mineral elements can be linearly correlated based on the mineral chemistry of the fuel at typical PF firing conditions. The linear correlations can be worked out better for the fuels having similar physical and chemical properties.
- ❖ From the modeling efforts made in this research project, it is concluded that the empirical indices developed for the different elemental mineral release under PF combustion firing conditions, work well for predicting the overall elemental release. However, such correlations may work better for more same group of fuels. Moreover, the simplified particle population model also predicts particle evolution in terms of particle size and their respective mass fractions with reasonable agreement. However, the model needs to be improved further for better accuracy. In an extended effort, the integration of the above two models was done to predict the ash formation in terms of ash release and ash formation in terms of particle size, their respective mass fractions and mineral elemental composition. The simplified approach seems good but the model fails to predict the mineral elemental redistribution in the

different ash particle size after the combustion and needs to be improved further.

7.3 Future recommendations

- ❖ The present experimental work studied the effect of mineral elemental matter and its association in the char matrix with first line physical and chemical transformations such as devolatilization, char burnout and fragmentation. In future, the study of several other potential physical parameters such as particle shape, size, density, mineralogy (included/excluded) should also be investigated to determine the impact of them on the extent of first line physical and chemical transformations.
- ❖ In the present experimental study, combustion tests of different coal and biomass fuels were planned. In future, more focus should be placed on co-firing tests.
- ❖ The empirical indices (linear expressions) have been developed for predicting the release of several mineral elements with eight different coal and biomass fuels. It is also proved that such indices work well for the same group of fuels. Therefore, in future a larger number of fuels of the same group having similar physical and chemical properties should be studied to develop the robust empirical predictive tool (linear expressions) for the release of several mineral elements during PF combustion.
- ❖ The simplified particle population model developed in the present PhD project, predicts the ash particle size evolution after combustion. However, for better accuracy in future, fragmentation and burning rate constants for each size bins should be derived more accurately by performing specific narrow size range tests. Particle size reduction and chemical conversion methods in the models needs to be studied more accurately by specific size reduction experiments. Instead of two fragmentation events per size bin, more fragmented ash sizes should be attempted. The shape factor should also be incorporated into the current simplified PPM model, especially for biomass. The present model can be integrated for CFD applications. Moreover, specific co-firing experiments are required for model validation.

- ❖ The ash formation modeling has the highest scope of improvement as the sub models used in this model from Chapters 4 and 5 need further improvements. The empirical indices for the elemental mineral release should be attempted for mineral elements which are released in minor amounts. These indices should also be corrected with a greater number of the same group fuels and with different particle size ranges. The particle to particle chemical interactions should be understood properly and incorporated in the present model for better accuracy. The condensation mechanisms of the released mineral elements should also be included in future. To simultaneously simulate the devolatilization, char oxidation and fragmentation events, the model should be further integrated into MATLAB or CFD. Random fragmentation events and effects of particle temperature and heating rate should also be included in the present model.
- ❖ Model validation should also be done for specific biomass combustion and co-firing experiments in the future.
- ❖ The model developed in this PhD work will be incorporated in the co-firing advisory tool (CAT) at ECN. Further, the developed model should be used in the ash deposition post processor developed at ECN as an input to predict ash deposition. Applications of CAT to new processes such as Ultra Super Critical vapor characteristics, colorless combustion (OXY- or MILD) should also be evaluated in future.

Appendix A

Proximate and ultimate analyses of fuels along with elemental mineral matter composition

Table A. 1: Proximate and ultimate analyses

Details	Unit	Bark (BM1)	Wood chips (BM2)	Waste wood (BM3)	Saw dust (BM4)	Olive Residue (BM5)	Straw (BM6)	Polish Coal (C1)	UK Coal (C2)
Volatiles	(% w/w d.a.f)	70.31	83.90	79.90	82.30	71.20	74.40	26.40	32.00
Ash	(% w/w d.b)	4.90	0.5	1.6	1.73	8.86	8.21	18.92	7.30
C		49.90	48.71	48.24	49.69	48.39	44.71	64.79	74.10
H		5.84	6.15	6.14	6.04	5.81	5.83	4.02	4.66
N		0.46	0.08	0.86	0.17	1.45	0.59	1.15	1.60
S	(mg/kg d.b)	369	62.0	503	212	1469	1410	6014	13151
LHV	(MJ/kg)	19.1	18.1	18.5	20.2	20.5	18.0	26.1	30.2

Elemental distribution of minerals									
Ca	(% w/w d.a.b)	59.0	44.76	40.34	13.11	15.16	7.60	7.92	3.86
Si		13.83	12.13	12.43	62.51	11.26	41.11	42.74	25.55
Mg		3.50	6.84	5.11	2.55	4.55	0.87	4.47	1.22
K		10.63	15.37	13.08	7.83	51.62	32.44	3.83	2.22
Na		0.61	1.10	6.33	1.07	0.49	0.12	1.43	2.88
Mn		2.08	6.17	1.03	0.97	0.06	0.03	0.21	0.10
S		1.86	2.38	7.23	1.71	2.71	3.06	5.68	23.22
Cl		0.57	1.73	7.02	1.33	6.14	12.96	2.72	12.98
P		1.63	2.25	1.01	0.85	3.22	1.27	0.33	0.33
Fe		2.26	3.44	2.90	2.05	2.40	0.28	9.92	12.09
Al		4.05	3.83	3.52	6.02	2.38	0.26	20.75	15.55

Appendix B

Particle size distributions of the raw coals and biomass fuels

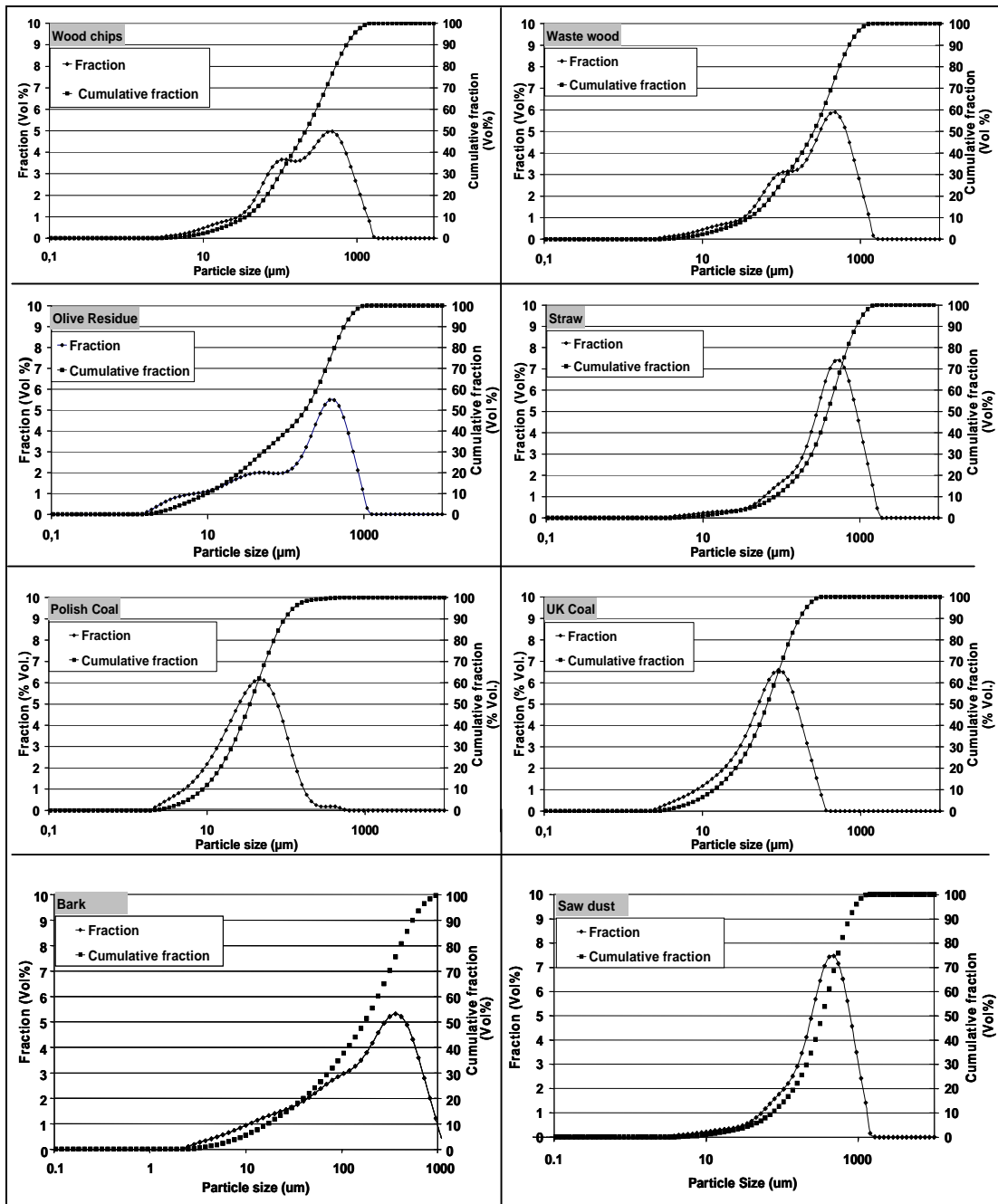


Figure B. 1: Particle size distribution of raw coals and biomass fuels

Appendix C

Tabulation of experimental data

C.1 Mass fraction of different particle sizes at different residence time

Table C. 1: Mass fraction of different particle sizes at different residence time

Residence time (ms)	Ash particle size	Mass fraction (wt%)					
		Wood chips	Waste wood	Olive residue	Straw	Poilish coal	UK coal
20	Coarse	92.71%	74.51%	97.85%	97.54%	96.77%	90.39%
	Fine	0.37%	0.14%	0.12%	0.59%	0.17%	0.25%
	Aerosol	0.17%	0.04%	0.09%	0.03%	0.07%	0.30%
	Vap	6.74%	25.30%	1.94%	1.84%	2.99%	9.07%
90	Coarse	75.92%	75.70%	72.68%	83.19%	94.67%	75.01%
	Fine	2.69%	0.89%	0.30%	0.60%	0.24%	0.05%
	Aerosol	1.05%	0.88%	0.51%	0.65%	0.09%	0.14%
	Vap	20.34%	22.53%	26.51%	15.55%	5.01%	24.80%
210	Coarse	53.43%	74.68%	62.61%	73.84%	92.05%	65.06%
	Fine	5.76%	1.59%	0.56%	2.79%	0.54%	0.72%
	Aerosol	3.52%	1.08%	0.87%	1.66%	0.24%	0.15%
	Vap	37.83%	22.80%	36.14%	21.97%	7.17%	34.07%
1300	Coarse	37.44%	45.51%	37.37%	57.78%	87.53%	61.22%
	Fine	9.05%	2.70%	1.22%	1.15%	3.22%	2.69%
	Aerosol	3.52%	0.76%	6.07%	1.08%	0.56%	0.49%
	Vap	49.99%	51.03%	55.33%	39.99%	8.69%	35.60%

C.2 Elemental mineral composition and mass fraction for different ash particle sizes at different residence time

Table C. 2: Elemental mineral composition and mass fraction for different ash particle sizes at different residence time for Wood chips

Residence time (ms)	Ash particle size	Si	Al	Fe	Ca	Mg	Na	K	Ti	P	S	Cl	Mn	Zn	Pb
		Mineral composition (Wt%)													
20	Coarse	8.75	2.76	5.69	43.83	3.50	0.98	10.61	1.08	2.68	1.34	3.64	3.74	0.43	10.97
	Fine	9.51	4.42	8.81	58.18	6.14	1.14	2.02	0.60	3.56	0.38	0.22	4.42	0.21	0.41
	Aerosol	5.84	2.59	2.63	65.97	8.37	1.59	1.42	0.61	4.07	0.37	1.27	4.87	0.23	0.17
	Vap	0.00	0.00	0.00	13.06	3.69	0.00	53.43	0.59	0.00	12.07	9.74	7.14	0.30	0.00
90	Coarse	10.93	2.20	4.40	41.98	3.74	0.58	8.15	1.94	3.05	0.00	2.20	2.78	1.33	16.73
	Fine	11.79	4.33	9.12	49.86	5.28	0.67	7.15	0.40	2.61	0.06	0.82	3.43	3.49	0.99
	Aerosol	5.65	2.61	3.73	25.87	2.83	0.76	37.21	3.81	1.70	1.52	4.09	5.41	0.87	3.94
	Vap	0.00	0.00	0.00	36.48	5.59	0.23	40.72	0.00	0.54	7.43	0.00	8.29	0.70	0.03
210	Coarse	7.38	2.26	8.34	58.08	6.77	1.00	3.80	0.99	2.68	0.68	0.30	6.44	0.68	0.59
	Fine	14.64	5.74	11.70	50.80	7.08	1.06	0.62	0.47	3.31	0.28	0.10	3.43	0.43	0.34
	Aerosol	11.65	5.39	5.24	56.88	6.06	0.81	3.27	0.63	5.68	0.33	0.31	1.40	1.17	1.18
	Vap	0.00	0.00	0.00	40.88	7.34	1.17	28.96	0.00	0.00	4.59	6.81	9.50	0.73	0.03
1300	Coarse	11.09	5.18	27.76	42.02	3.63	0.45	1.32	0.32	3.78	0.21	0.49	3.08	0.00	0.65
	Fine	13.52	4.95	31.23	38.41	3.68	0.34	0.59	0.53	2.35	0.01	0.15	2.85	1.05	0.33
	Aerosol	12.13	5.83	16.34	52.26	4.49	0.85	0.88	0.51	4.83	0.13	0.19	1.01	0.24	0.32
	Vap	0.00	0.00	0.00	45.02	6.35	1.56	29.17	0.00	0.00	4.17	5.20	7.86	0.64	0.03
		Mineral mass fraction (distribution) in different sizes (Wt%)													
20	Coarse	99.44	99.19	99.30	97.11	91.91	99.24	73.14	95.88	99.19	60.40	83.64	87.27	94.98	99.98
	Fine	0.43	0.64	0.62	0.52	0.65	0.46	0.06	0.21	0.53	0.07	0.02	0.41	0.19	0.01
	Aerosol	0.12	0.17	0.08	0.27	0.41	0.30	0.02	0.10	0.28	0.03	0.05	0.21	0.09	0.00
	Vap	0.00	0.00	0.00	2.11	7.04	0.00	26.79	3.81	0.00	39.50	16.28	12.10	4.74	0.00
90	Coarse	95.66	92.07	92.14	77.92	68.45	85.87	41.10	96.67	92.09	0.02	96.26	53.52	80.40	99.41
	Fine	3.66	6.43	6.78	3.28	3.43	3.50	1.28	0.71	2.80	0.10	1.27	2.34	7.52	0.21
	Aerosol	0.68	1.50	1.08	0.66	0.71	1.54	2.59	2.62	0.71	1.04	2.47	1.43	0.72	0.32
	Vap	0.00	0.00	0.00	18.14	27.40	9.08	55.04	0.00	4.40	98.83	0.00	42.71	11.36	0.05
210	Coarse	75.86	69.85	83.84	60.34	51.56	50.07	15.45	91.47	78.57	17.17	5.88	47.27	51.36	80.97
	Fine	16.24	19.16	12.68	5.69	5.82	5.75	0.27	4.69	10.47	0.75	0.21	2.72	3.53	4.98
	Aerosol	7.90	11.00	3.48	3.90	3.05	2.68	0.88	3.84	10.96	0.55	0.40	0.68	5.84	10.71
	Vap	0.00	0.00	0.00	30.07	39.57	41.51	83.40	0.00	0.00	81.53	93.52	49.33	39.27	3.34
1300	Coarse	71.58	74.83	75.36	36.13	27.08	16.66	3.27	64.44	78.71	3.63	6.61	21.43	0.01	80.73
	Fine	21.08	17.26	20.48	7.98	6.63	3.08	0.35	25.94	11.84	0.03	0.49	4.80	22.47	9.79
	Aerosol	7.35	7.90	4.16	4.22	3.14	2.95	0.20	9.63	9.45	0.21	0.24	0.66	1.96	3.72
	Vap	0.00	0.00	0.00	51.68	63.15	77.31	96.18	0.00	0.00	96.14	92.67	73.10	75.57	5.76

Table C. 3: Elemental mineral composition and mass fraction for different ash particle sizes at different residence time for Waste wood

Residence time (ms)	Ash particle size	Si	Al	Fe	Ca	Mg	Na	K	Ti	P	S	Cl	Mn	Zn	Pb
		Mineral composition (Wt%)													
20	Coarse	6.06	3.70	1.06	30.74	2.28	2.23	10.16	1.19	2.98	9.01	6.39	9.76	13.49	0.97
	Fine	8.92	4.47	6.60	56.96	5.15	1.15	2.04	2.48	1.33	4.84	1.97	1.54	0.48	2.07
	Aerosol	7.34	3.70	5.44	60.50	4.87	1.31	2.04	3.07	2.19	4.80	1.44	1.09	0.93	1.27
	Vap	0.00	0.00	0.00	47.18	4.70	2.44	15.99	3.40	0.59	4.53	14.48	1.02	3.03	2.63
90	Coarse	2.50	4.19	5.56	34.31	5.61	6.56	15.55	2.71	1.66	5.73	3.00	0.00	10.39	2.23
	Fine	8.95	4.62	7.29	62.70	4.70	1.36	1.82	3.14	1.29	0.38	1.40	1.21	0.66	0.48
	Aerosol	2.96	0.95	3.60	27.41	2.86	10.47	19.66	0.13	1.28	1.70	14.52	3.29	4.90	6.29
	Vap	0.00	0.00	0.00	29.52	3.89	8.25	16.44	1.42	0.00	10.33	24.05	0.76	3.97	1.38
210	Coarse	5.16	1.47	2.56	66.51	3.59	1.91	9.82	1.82	0.80	3.10	2.87	0.34	0.00	0.07
	Fine	10.74	5.08	8.38	58.51	6.48	1.74	1.83	2.57	1.34	0.34	1.74	0.44	0.12	0.68
	Aerosol	6.77	3.71	6.04	46.56	4.17	6.81	11.23	2.11	1.61	1.99	5.41	0.31	0.79	2.50
	Vap	0.00	0.00	0.00	8.18	2.16	13.92	23.49	0.26	0.00	15.71	25.85	0.57	5.88	3.98
1300	Coarse	11.81	4.02	15.32	53.81	5.62	0.67	0.49	2.50	0.94	0.23	2.70	1.65	0.00	0.25
	Fine	10.39	4.81	13.92	52.45	5.50	0.95	0.55	2.10	1.34	0.07	5.69	0.92	0.57	0.74
	Aerosol	9.02	4.25	11.04	50.73	3.60	1.28	2.33	3.32	1.96	0.18	7.48	0.45	2.70	1.66
	Vap	0.00	0.00	0.00	29.37	3.85	9.33	20.48	1.98	0.66	11.54	14.27	0.74	4.97	2.81
		Mineral mass fraction (distribution) in different sizes (Wt%)													
20	Coarse	99.65	99.71	98.52	65.53	58.63	72.80	65.14	50.54	93.58	85.30	56.48	96.55	92.89	51.96
	Fine	0.28	0.23	1.19	0.24	0.26	0.07	0.03	0.21	0.08	0.09	0.03	0.03	0.01	0.21
	Aerosol	0.07	0.06	0.29	0.07	0.07	0.02	0.01	0.08	0.04	0.03	0.01	0.01	0.00	0.04
	Vap	0.00	0.00	0.00	34.16	41.04	27.10	34.82	49.18	6.30	14.58	43.48	3.42	7.10	47.79
90	Coarse	94.70	98.46	97.75	77.71	81.82	71.67	75.14	85.42	98.22	64.90	29.03	0.27	89.30	82.04
	Fine	4.00	1.28	1.51	1.67	0.81	0.18	0.10	1.17	0.90	0.05	0.16	5.09	0.07	0.21
	Aerosol	1.30	0.26	0.74	0.72	0.48	1.33	1.10	0.05	0.88	0.22	1.63	13.68	0.49	2.69
	Vap	0.00	0.00	0.00	19.90	16.89	26.83	23.66	13.36	0.00	34.83	69.18	80.96	10.15	15.07
210	Coarse	94.06	90.08	90.60	93.78	80.74	30.34	57.13	91.67	93.92	39.07	26.37	64.40	0.00	5.13
	Fine	4.16	6.63	6.31	1.75	3.10	0.59	0.23	2.75	3.36	0.09	0.34	1.77	0.15	1.09
	Aerosol	1.78	3.29	3.09	0.95	1.35	1.56	0.94	1.53	2.72	0.36	0.72	0.84	0.63	2.70
	Vap	0.00	0.00	0.00	3.52	14.81	67.51	41.70	4.05	0.00	60.48	72.57	32.98	99.22	91.08
1300	Coarse	93.89	91.86	93.80	59.32	54.46	6.01	2.06	50.92	52.64	1.72	14.09	64.84	0.00	7.28
	Fine	4.91	6.52	5.07	3.44	3.17	0.50	0.14	2.54	4.45	0.03	1.76	2.16	0.60	1.26
	Aerosol	1.20	1.62	1.13	0.93	0.58	0.19	0.17	1.13	1.83	0.02	0.65	0.30	0.80	0.80
	Vap	0.00	0.00	0.00	36.31	41.79	93.29	97.63	45.41	41.07	98.23	83.50	32.70	98.60	90.65

Table C. 4: Elemental mineral composition and mass fraction for different ash particle sizes at different residence time for Olive residue

Residence time (ms)	Ash particle size	Si	Al	Fe	Ca	Mg	Na	K	Ti	P	S	Cl	Mn	Zn	Pb
		Mineral composition (Wt%)													
20	Coarse	9.13	2.60	2.83	26.17	6.08	0.44	40.62	0.38	4.70	1.97	3.79	0.61	0.00	0.68
	Fine	9.89	2.62	3.35	29.95	7.80	0.25	30.60	0.30	5.46	2.23	7.14	0.21	0.00	0.20
	Aerosol	7.03	1.75	1.87	21.38	5.79	0.59	45.36	0.19	3.52	3.93	7.34	0.00	0.00	1.26
	Vap	0.00	0.00	0.00	0.01	0.01	0.10	0.01	1.65	2.31	42.05	53.82	0.01	0.01	0.01
90	Coarse	10.25	3.01	3.06	28.54	7.09	0.31	37.65	0.00	4.54	1.45	2.57	0.49	0.00	1.03
	Fine	15.36	4.51	3.98	41.18	11.16	0.22	14.33	0.16	6.18	1.01	1.62	0.29	0.00	0.00
	Aerosol	0.18	0.11	0.25	0.99	0.26	0.54	77.68	0.08	0.91	6.11	12.61	0.29	0.00	0.00
	Vap	0.00	0.00	0.00	0.00	0.48	0.30	78.79	0.07	2.79	7.02	10.54	0.00	0.00	0.00
210	Coarse	9.91	2.78	3.89	28.99	6.28	0.45	38.55	0.27	4.67	1.15	2.88	0.18	0.00	0.00
	Fine	11.46	3.23	5.03	32.29	7.67	0.50	29.57	0.09	6.19	1.36	2.32	0.10	0.00	0.19
	Aerosol	0.78	0.32	1.43	2.33	4.20	1.27	72.82	0.06	0.74	9.07	6.30	0.31	0.00	0.00
	Vap	0.00	0.00	0.00	0.49	0.00	0.11	82.75	0.00	1.85	6.30	8.50	0.00	0.00	0.00
1300	Coarse	16.50	3.46	4.84	38.63	8.45	0.38	20.21	0.11	4.95	1.07	1.25	0.15	0.00	0.00
	Fine	2.95	0.83	0.63	9.34	1.97	0.47	71.61	0.12	1.94	3.09	6.01	0.14	0.00	0.89
	Aerosol	0.11	0.07	0.83	0.68	0.25	1.05	84.22	0.14	1.53	3.29	6.54	0.11	0.00	1.18
	Vap	0.00	0.00	0.00	0.00	0.00	0.66	84.89	0.00	1.47	4.87	8.05	0.00	0.05	0.00
		Mineral mass fraction (distribution) in different sizes (Wt%)													
20	Coarse	99.80	99.82	99.80	99.79	99.76	99.34	99.81	91.91	98.83	70.11	77.77	99.93	0.00	99.77
	Fine	0.13	0.12	0.14	0.14	0.15	0.07	0.09	0.09	0.14	0.09	0.17	0.04	0.00	0.03
	Aerosol	0.07	0.06	0.06	0.07	0.09	0.12	0.10	0.04	0.07	0.13	0.14	0.00	0.00	0.17
	Vap	0.00	0.00	0.00	0.00	0.00	0.47	0.00	7.96	0.96	29.67	21.92	0.03	100.00	0.03
90	Coarse	99.37	99.36	99.41	99.38	96.92	73.45	56.20	0.40	81.20	35.69	39.50	99.29	0.00	99.91
	Fine	0.62	0.62	0.54	0.60	0.63	0.22	0.09	2.37	0.46	0.10	0.10	0.24	0.00	0.00
	Aerosol	0.01	0.03	0.06	0.02	0.02	0.90	0.81	2.01	0.11	1.06	1.36	0.41	0.00	0.00
	Vap	0.00	0.00	0.00	0.00	2.42	25.44	42.90	95.21	18.22	63.15	59.04	0.06	100.00	0.09
210	Coarse	98.87	98.81	98.36	97.97	98.79	84.40	44.01	99.29	80.57	23.38	36.44	96.96	0.00	1.94
	Fine	1.02	1.03	1.14	0.97	1.08	0.83	0.30	0.29	0.80	0.25	0.26	0.49	0.00	82.30
	Aerosol	0.11	0.16	0.50	0.11	0.13	3.27	1.15	0.31	0.18	2.56	1.11	2.37	0.00	0.00
	Vap	0.00	0.00	0.00	0.95	0.01	11.50	54.53	0.12	18.45	73.82	62.19	0.18	100.00	15.76
1300	Coarse	99.31	98.90	96.89	98.94	98.77	24.40	12.48	80.13	66.59	11.99	8.67	86.66	0.00	0.00
	Fine	0.58	0.77	0.41	0.78	0.75	1.00	1.44	3.02	0.85	1.13	1.36	2.63	0.00	12.75
	Aerosol	0.11	0.33	2.69	0.28	0.48	11.03	8.45	16.45	3.35	6.00	7.36	10.39	0.00	84.36
	Vap	0.00	0.00	0.00	0.00	0.01	63.57	77.63	0.40	29.21	80.88	82.61	0.32	100.00	2.89

Table C. 5: Elemental mineral composition and mass fraction for different ash particle sizes at different residence time for Straw

Residence time (ms)	Ash particle size	Si	Al	Fe	Ca	Mg	Na	K	Ti	P	S	Cl	Mn	Zn	Pb
		Mineral composition (Wt%)													
20	Coarse	50.41	0.15	0.00	6.50	0.37	0.00	29.33	0.14	1.00	1.64	10.41	0.07	0.00	0.00
	Fine	45.15	1.00	1.95	31.78	2.44	0.05	7.89	0.10	3.45	0.65	5.46	0.09	0.00	0.00
	Aerosol	27.21	0.99	1.83	29.68	3.00	0.00	16.34	0.00	3.75	0.87	16.33	0.00	0.00	0.00
	Vap	0.00	0.00	0.00	4.30	0.89	0.01	0.01	0.38	11.49	34.30	48.51	0.03	0.08	0.01
90	Coarse	44.41	0.08	0.27	10.53	0.69	0.14	30.95	0.11	2.16	2.65	7.94	0.08	0.00	0.00
	Fine	58.78	0.96	1.66	26.77	2.32	0.38	4.29	0.06	1.86	0.43	2.04	0.44	0.00	0.00
	Aerosol	15.47	0.55	0.58	12.50	0.66	0.04	40.07	0.17	1.40	0.77	27.66	0.14	0.00	0.00
	Vap	0.00	0.00	0.00	1.20	0.03	0.00	28.42	0.01	1.98	6.42	61.90	0.00	0.04	0.00
210	Coarse	39.71	0.08	0.00	10.14	0.78	0.47	37.00	0.10	2.02	3.18	6.33	0.00	0.00	0.19
	Fine	39.16	0.94	1.29	16.41	1.33	0.05	23.93	0.12	1.35	1.55	13.82	0.03	0.00	0.00
	Aerosol	6.04	0.59	0.29	5.38	0.36	0.00	51.07	0.11	1.18	3.93	30.67	0.18	0.00	0.20
	Vap	0.00	0.00	0.00	0.00	0.00	0.00	53.12	0.00	1.92	7.74	37.15	0.00	0.05	0.00
1300	Coarse	46.95	0.16	0.24	8.48	0.97	0.34	30.21	0.00	1.14	2.17	6.74	0.46	0.72	1.43
	Fine	48.35	1.38	1.59	28.76	1.92	0.19	12.33	0.15	2.15	0.53	2.46	0.20	0.00	0.00
	Aerosol	3.79	0.51	0.32	3.14	0.22	0.15	53.12	0.04	2.87	5.52	29.48	0.06	0.00	0.79
	Vap	0.00	0.00	0.00	0.92	0.08	0.09	60.85	0.00	2.20	6.90	28.92	-0.01	0.04	0.00
		Mineral mass fraction (distribution) in different sizes (Wt%)													
20	Coarse	99.45	95.90	0.85	95.86	91.85	22.29	99.82	94.70	80.75	71.62	91.61	98.35	0.00	0.00
	Fine	0.54	3.93	95.14	2.83	3.71	45.40	0.16	0.41	1.68	0.17	0.29	0.79	0.00	0.00
	Aerosol	0.01	0.18	4.01	0.12	0.20	0.01	0.02	0.00	0.08	0.01	0.04	0.00	0.00	0.00
	Vap	0.00	0.00	0.00	1.20	4.24	32.31	0.00	4.89	17.49	28.20	8.06	0.87	100.00	100.00
90	Coarse	98.78	87.39	94.17	95.32	96.16	97.66	84.54	96.21	84.58	68.67	40.22	94.55	0.00	0.00
	Fine	0.95	7.79	4.22	1.76	2.35	1.93	0.09	0.41	0.53	0.08	0.08	3.84	0.00	0.00
	Aerosol	0.27	4.81	1.60	0.89	0.72	0.24	0.86	1.20	0.43	0.16	1.10	1.32	0.00	0.00
	Vap	0.00	0.00	0.00	2.03	0.77	0.17	14.51	2.17	14.46	31.09	58.60	0.29	100.00	100.00
210	Coarse	96.09	63.33	0.19	93.18	92.97	99.55	67.44	93.32	75.67	56.50	34.05	1.87	0.00	97.39
	Fine	3.58	26.73	88.13	5.70	6.04	0.38	1.65	4.23	1.92	1.04	2.81	21.78	0.00	0.00
	Aerosol	0.33	9.94	11.68	1.11	0.96	0.01	2.10	2.16	1.00	1.57	3.71	71.61	0.00	2.40
	Vap	0.00	0.00	0.00	0.00	0.03	0.06	28.82	0.29	21.42	40.89	59.43	4.75	100.00	0.21
1300	Coarse	97.85	81.69	86.48	86.99	90.52	83.80	41.07	2.74	41.26	30.72	24.63	99.87	96.38	98.95
	Fine	2.00	13.60	11.35	5.86	3.58	0.95	0.33	71.79	1.55	0.15	0.18	0.89	0.00	0.00
	Aerosol	0.15	4.70	2.16	0.60	0.39	0.70	1.35	16.99	1.95	1.46	2.01	0.23	0.00	1.03
	Vap	0.00	0.00	0.00	6.55	5.51	14.55	57.25	8.49	55.25	67.67	73.17	-0.99	3.62	0.02

Table C. 6: Elemental mineral composition and mass fraction for different ash particle sizes at different residence time for Polish coal

Residence time (ms)	Ash particle size	Si	Al	Fe	Ca	Mg	Na	K	Ti	P	S	Cl	Mn	Zn	Pb
		Mineral composition (Wt%)													
20	Coarse	31.79	21.09	10.57	6.22	4.35	2.15	4.03	1.64	0.92	4.45	1.83	0.00	8.80	2.17
	Fine	16.70	15.25	7.43	6.93	3.69	7.30	12.94	3.00	3.36	10.68	2.12	0.85	1.33	8.44
	Aerosol	3.42	1.85	6.74	2.40	4.46	13.89	16.62	0.63	3.40	20.85	8.50	0.00	14.88	2.37
	Vap	0.00	0.00	0.00	8.82	0.96	0.07	0.63	18.36	0.62	69.33	0.07	0.56	0.34	0.26
90	Coarse	37.79	24.00	8.59	6.66	4.63	2.39	4.38	3.35	0.72	2.39	2.01	0.90	1.60	0.59
	Fine	33.92	24.40	11.84	6.17	5.33	1.34	2.95	1.48	0.76	1.01	6.19	0.67	1.58	2.33
	Aerosol	15.67	10.38	9.25	4.49	4.68	1.52	6.66	2.35	1.69	7.41	17.12	0.83	9.30	8.65
	Vap	0.00	0.00	0.00	0.40	0.40	4.12	1.83	8.05	1.25	77.17	6.01	0.13	0.37	0.26
210	Coarse	37.04	26.64	8.33	8.74	4.79	2.12	5.38	1.50	0.19	1.33	1.51	0.59	0.93	0.91
	Fine	38.15	27.12	10.73	8.11	5.71	2.46	3.44	1.33	0.23	0.43	1.35	0.07	0.13	0.75
	Aerosol	32.63	25.29	15.39	8.86	6.16	3.04	2.84	2.03	0.14	0.83	1.75	0.50	0.22	0.32
	Vap	0.00	0.00	0.00	0.28	0.28	2.85	2.50	3.88	1.18	62.97	25.45	0.12	0.30	0.18
1300	Coarse	32.14	23.70	14.21	9.98	4.86	2.26	4.35	1.37	0.05	1.94	0.79	0.52	3.25	0.56
	Fine	35.98	25.75	12.52	9.06	5.83	2.52	3.37	1.21	0.08	0.26	0.75	0.12	2.07	0.48
	Aerosol	27.51	19.58	18.96	10.79	4.97	2.79	4.14	1.41	0.94	2.37	1.11	0.86	2.15	2.43
	Vap	0.00	0.00	0.00	0.23	0.23	3.60	2.58	3.25	1.35	61.45	26.82	0.03	0.28	0.17
		Mineral mass fraction (distribution) in different sizes (Wt%)													
20	Coarse	99.90	99.86	99.83	95.60	99.10	98.85	98.67	74.09	97.07	67.17	99.36	0.60	99.74	98.87
	Fine	0.09	0.13	0.13	0.19	0.15	0.61	0.57	0.24	0.64	0.29	0.21	8.15	0.03	0.69
	Aerosol	0.01	0.01	0.04	0.03	0.07	0.45	0.29	0.02	0.25	0.22	0.32	0.00	0.12	0.08
	Vap	0.00	0.00	0.00	4.19	0.67	0.10	0.47	25.65	2.04	32.32	0.11	91.25	0.12	0.36
90	Coarse	99.78	99.75	99.66	99.45	99.26	91.53	97.67	88.63	91.36	36.94	85.80	99.06	98.54	96.80
	Fine	0.22	0.25	0.34	0.23	0.29	0.13	0.16	0.10	0.24	0.04	0.66	0.18	0.24	0.96
	Aerosol	0.00	0.00	0.00	0.00	0.00	0.00	0.00	0.00	0.00	0.00	0.00	0.00	0.00	0.00
	Vap	0.00	0.00	0.00	0.32	0.45	8.34	2.17	11.27	8.40	63.02	13.55	0.76	1.22	2.24
210	Coarse	99.17	99.16	98.78	98.95	98.53	89.67	96.04	82.65	67.12	21.27	43.10	98.12	97.41	97.90
	Fine	0.60	0.59	0.75	0.54	0.69	0.61	0.36	0.43	0.47	0.04	0.23	0.07	0.08	0.47
	Aerosol	0.23	0.24	0.47	0.26	0.33	0.33	0.13	0.29	0.13	0.03	0.13	0.22	0.06	0.09
	Vap	0.00	0.00	0.00	0.25	0.45	9.39	3.47	16.62	32.28	78.65	56.54	1.59	2.45	1.53
1300	Coarse	95.54	95.67	96.07	95.92	94.76	82.81	91.45	78.46	26.98	24.03	22.72	97.63	96.50	91.75
	Fine	3.93	3.82	3.11	3.20	4.18	3.40	2.61	2.54	1.43	0.12	0.78	0.86	2.26	2.90
	Aerosol	0.52	0.51	0.82	0.66	0.62	0.66	0.56	0.52	3.07	0.19	0.20	1.03	0.41	2.53
	Vap	0.00	0.00	0.00	0.22	0.45	13.13	5.38	18.48	68.52	75.66	76.30	0.49	0.83	2.82

Table C. 7: Elemental mineral composition and mass fraction for different ash particle sizes at different residence time for UK coal

Residence time (ms)	Ash particle size	Si	Al	Fe	Ca	Mg	Na	K	Ti	P	S	Cl	Mn	Zn	Pb
		Mineral composition (Wt%)													
20	Coarse	25.02	17.25	9.35	5.60	2.76	3.37	4.05	0.74	0.42	18.44	12.45	0.53	0.00	0.00
	Fine	22.78	17.31	9.46	3.62	1.48	8.70	4.54	0.00	1.93	18.53	11.40	0.24	0.00	0.00
	Aerosol	2.50	4.33	2.70	2.93	1.67	16.37	4.96	0.67	0.53	34.68	24.64	0.05	0.93	3.05
	Vap	0.00	0.00	0.00	1.23	0.20	3.41	0.71	1.65	0.23	92.31	0.02	0.02	0.09	0.13
90	Coarse	30.75	21.03	8.44	5.85	1.22	3.41	2.10	1.56	0.42	14.06	6.64	0.66	0.00	3.86
	Fine	30.55	21.31	13.64	2.87	1.20	7.59	2.91	1.65	0.47	5.42	12.39	0.00	0.00	0.00
	Aerosol	5.74	5.09	4.73	1.80	0.39	24.78	6.22	1.27	0.74	14.76	32.86	0.52	0.00	1.08
	Vap	0.00	0.00	0.00	1.48	0.22	4.31	1.15	0.52	0.15	59.57	32.40	0.05	0.08	0.07
210	Coarse	36.02	24.78	12.05	8.30	1.54	2.08	3.34	2.09	0.63	4.74	2.90	0.30	0.84	0.38
	Fine	41.51	28.41	12.49	4.53	1.79	3.63	2.85	2.05	0.19	0.94	1.44	0.18	0.00	0.00
	Aerosol	19.30	14.95	15.98	6.56	1.29	11.25	7.71	1.51	0.66	6.62	12.03	0.63	0.37	1.13
	Vap	0.00	0.00	0.00	0.16	0.10	5.34	0.95	0.38	0.09	65.46	27.36	0.03	0.07	0.07
1300	Coarse	35.70	27.59	16.00	8.50	0.68	1.30	3.63	1.30	0.75	1.16	3.38	0.00	0.00	0.00
	Fine	41.06	27.90	10.33	6.01	2.05	4.47	4.20	1.63	0.52	0.46	1.20	0.17	0.00	0.00
	Aerosol	26.82	21.52	15.22	10.49	2.42	5.95	5.62	3.28	1.48	1.99	4.59	0.16	0.00	0.46
	Vap	0.00	0.00	0.00	0.65	0.20	4.62	1.06	0.24	0.29	66.91	25.83	0.05	0.07	0.06
		Mineral mass fraction (distribution) in different sizes (Wt%)													
20	Coarse	99.72	99.65	99.63	97.51	96.53	88.90	97.60	81.58	93.27	66.18	99.09	99.44	0.00	0.00
	Fine	0.25	0.27	0.27	0.17	0.48	0.63	0.30	0.00	1.17	0.18	0.25	0.12	0.00	0.00
	Aerosol	0.03	0.08	0.09	0.17	0.65	1.43	0.39	0.24	0.38	0.41	0.65	0.03	25.09	43.85
	Vap	0.00	0.00	0.00	2.15	2.34	9.05	1.70	18.18	5.18	33.23	0.02	0.40	74.91	56.15
90	Coarse	99.90	99.89	99.79	92.20	94.34	69.75	84.15	89.89	88.96	41.62	38.11	97.63	0.00	99.35
	Fine	0.06	0.07	0.11	0.03	0.06	0.10	0.08	0.06	0.06	0.01	0.05	0.00	0.00	0.00
	Aerosol	0.04	0.05	0.11	0.05	0.06	0.97	0.48	0.14	0.30	0.08	0.36	0.15	0.00	0.05
	Vap	0.00	0.00	0.00	7.72	5.54	29.18	15.29	9.91	10.68	58.29	61.48	2.22	100.00	0.59
210	Coarse	98.62	98.61	98.57	98.27	95.48	42.14	85.91	90.37	92.33	12.15	16.80	93.41	95.75	90.79
	Fine	1.27	1.26	1.14	0.60	1.24	0.82	0.82	0.99	0.32	0.03	0.09	0.61	0.00	0.00
	Aerosol	0.12	0.13	0.29	0.17	0.18	0.51	0.44	0.15	0.22	0.04	0.16	0.44	0.09	0.61
	Vap	0.00	0.00	0.00	0.96	3.10	56.53	12.83	8.49	7.13	87.79	82.95	5.53	4.15	8.61
1300	Coarse	94.64	95.17	96.52	92.10	74.84	30.77	81.05	84.46	78.93	2.90	18.27	0.24	0.00	0.00
	Fine	4.78	4.23	2.74	2.86	9.94	4.64	4.12	4.64	2.41	0.05	0.29	19.35	0.00	0.00
	Aerosol	0.57	0.60	0.74	0.92	2.16	1.14	1.01	1.72	1.25	0.04	0.20	3.29	0.00	9.09
	Vap	0.00	0.00	0.00	4.13	13.06	63.45	13.81	9.18	17.41	97.01	81.24	77.13	100.00	90.91

C.3 Elemental release at different residence times

Table C. 8: Elemental release at different residence times

Fuel	Residence time (ms)	Mass fraction (Wt%)	Mineral composition (Wt%)													
			Si	Al	Fe	Ca	Mg	Na	K	Ti	P	S	Cl	Mn	Zn	Pb
Wood chips	20	6.74	0.00	0.00	0.00	13.06	3.69	0.00	53.43	0.59	0.00	12.07	9.74	7.14	0.30	0.00
	90	20.34	0.00	0.00	0.00	36.48	5.59	0.23	40.72	0.00	0.54	7.43	0.00	8.29	0.70	0.03
	210	37.83	0.00	0.00	0.00	40.88	7.34	1.17	28.96	0.00	0.00	4.59	6.81	9.50	0.73	0.03
	1300	49.99	0.00	0.00	0.00	45.02	6.35	1.56	29.17	0.00	0.00	4.17	5.20	7.86	0.64	0.03
Waste wood	20	25.30	0.00	0.00	0.00	47.18	4.70	2.44	15.99	3.40	0.59	4.53	14.48	1.02	3.03	2.63
	90	22.53	0.00	0.00	0.00	29.52	3.89	8.25	16.44	1.42	0.00	10.33	24.05	0.76	3.97	1.38
	210	22.80	0.00	0.00	0.00	8.18	2.16	13.92	23.49	0.26	0.00	15.71	25.85	0.57	5.88	3.98
	1300	51.03	0.00	0.00	0.00	29.37	3.85	9.33	20.48	1.98	0.66	11.54	14.27	0.74	4.97	2.81
Olive residue	20	1.94	0.00	0.00	0.00	0.01	0.01	0.10	0.01	1.65	2.31	42.05	53.82	0.01	0.01	0.01
	90	26.51	0.00	0.00	0.00	0.00	0.48	0.30	78.79	0.07	2.79	7.02	10.54	0.00	0.00	0.00
	210	36.14	0.00	0.00	0.00	0.49	0.00	0.11	82.75	0.00	1.85	6.30	8.50	0.00	0.00	0.00
	1300	55.33	0.00	0.00	0.00	0.00	0.00	0.66	84.89	0.00	1.47	4.87	8.05	0.00	0.05	0.00
Straw	20	1.84	0.00	0.00	0.00	4.30	0.89	0.01	0.01	0.38	11.49	34.30	48.51	0.03	0.08	0.01
	90	15.55	0.00	0.00	0.00	1.20	0.03	0.00	28.42	0.01	1.98	6.42	61.90	0.00	0.04	0.00
	210	21.97	0.00	0.00	0.00	0.00	0.00	0.00	53.12	0.00	1.92	7.74	37.15	0.00	0.05	0.00
	1300	39.99	0.00	0.00	0.00	0.92	0.08	0.09	60.85	0.00	2.20	6.90	28.92	-0.01	0.04	0.00
Polish coal	20	2.99	0.00	0.00	0.00	8.82	0.96	0.07	0.63	18.36	0.62	69.33	0.07	0.56	0.34	0.26
	90	5.01	0.00	0.00	0.00	0.40	0.40	4.12	1.83	8.05	1.25	77.17	6.01	0.13	0.37	0.26
	210	7.17	0.00	0.00	0.00	0.28	0.28	2.85	2.50	3.88	1.18	62.97	25.45	0.12	0.30	0.18
	1300	8.69	0.00	0.00	0.00	0.23	0.23	3.60	2.58	3.25	1.35	61.45	26.82	0.03	0.28	0.17
UK coal	20	9.07	0.00	0.00	0.00	1.23	0.20	3.41	0.71	1.65	0.23	92.31	0.02	0.02	0.09	0.13
	90	24.80	0.00	0.00	0.00	1.48	0.22	4.31	1.15	0.52	0.15	59.57	32.40	0.05	0.08	0.07
	210	34.07	0.00	0.00	0.00	0.16	0.10	5.34	0.95	0.38	0.09	65.46	27.36	0.03	0.07	0.07
	1300	35.60	0.00	0.00	0.00	0.65	0.20	4.62	1.06	0.24	0.29	66.91	25.83	0.05	0.07	0.06
Bark	1300	30.00	0.00	0.00	0.00	52.00	3.00	1.00	33.00	0.00	2.00	4.00	2.00	2.00	0.00	0.00
Saw dust	1300	6.00	0.00	0.00	0.00	8.00	0.50	3.00	61.00	0.00	0.50	20.00	4.00	3.00	0.00	0.00

Appendix D

Tabulations of modeling results for various cases

D.1 Fragmentation rate constants derived from the experiments

Table D. 1: Fragmentation rate constants

Fuel	Residence time (ms)			
	20	90	210	1300
Polish coal	0.107	0.690	1.343	1.193
UK coal	2.399	2.990	4.849	3.125
Wood chips	2.104	0.807	2.336	2.119
Olive residue	1.923	3.462	2.939	1.198
Straw	1.095	1.393	2.950	2.091

Note: Fragmentation rate constants are derived crudely from the experiments by summing up the particle number density for all size bins for a particular residence time. In future, different narrow size ranged experiments should be performed to get more accurate constant because the fragmentation rate constant will be different for different size particles due to higher probability of larger size particles to fragmenting more than lower sizes.

D.2 Burning rate constant

The burning rate constant is dependant on the char conversion. The total char conversion for a given time step is derived from the LCS experiments, as described further. The char conversion for each size bin is assumed with the help of 1-DICOG program in such a way that total char conversion derived from experiments matches with the sum of the assumed char conversion for all size bins. So, the burning rate constant will be different for each size bin according to the assumed char conversion. Therefore, tabulation of the burning rate constant is not done. However, the methodology to derive burning rate constant is quite simple and already explained well in Chapter 5.

D.3 Ash particle size evolution at different residence times during combustion (model and LCS-experimental results)

Ash particle size evolution at different residence time during PF combustion for model and experimental results are tabulated together as follows. The graphs of the comparison and standard average deviation are already discussed in Chapter 5.

Table D. 2: Particle size evolution at 20 ms (model and LCS-experimental results)

<u>Wood chips</u>				<u>Olive residue</u>				<u>Straw</u>				<u>Polish coal</u>				<u>UK coal</u>			
MODEL		EXPERIMENT		MODEL		EXPERIMENT		MODEL		EXPERIMENT		MODEL		EXPERIMENT		MODEL		EXPERIMENT	
PSD (μm)	CM (Wt%)	PSD (μm)	CM (Wt%)	PSD (μm)	CM (Wt%)	PSD (μm)	CM (Wt%)	PSD (μm)	CM (Wt%)	PSD (μm)	CM (Wt%)	PSD (μm)	CM (Wt%)	PSD (μm)	CM (Wt%)	PSD (μm)	CM (Wt%)	PSD (μm)	CM (Wt%)
1654.4	0.1	1660.0	0.0	824.4	2.7	830.0	0.0	1648.9	0.6	1660.0	0.0	157.6	2.6	158.0	0.0	362.0	0.0	363.0	0.0
1087.9	9.5	1106.7	2.0	544.0	19.9	553.3	15.0	1087.9	10.7	1106.7	15.0	105.0	13.1	105.3	30.0	240.4	6.1	242.0	15.0
717.6	27.9	737.8	60.0	362.6	39.7	368.9	55.0	725.3	33.5	737.8	82.0	69.9	31.1	70.2	60.0	160.2	20.9	161.3	40.0
474.9	51.3	491.9	90.0	241.8	59.5	245.9	87.0	474.9	58.9	491.9	90.0	46.5	54.8	46.8	82.0	106.8	42.9	107.6	70.0
298.0	69.3	327.9	95.0	158.3	72.0	164.0	98.2	304.4	81.5	327.9	94.0	31.0	78.1	31.2	97.0	69.3	65.4	71.7	96.5
167.6	77.4	218.6	97.0	103.5	77.9	109.3	98.4	179.2	89.2	218.6	95.0	20.7	91.1	20.8	97.5	46.1	89.1	47.8	97.5
98.0	86.3	145.7	98.0	66.2	85.2	72.9	98.6	111.8	95.6	145.7	98.0	10.2	99.0	13.9	98.0	27.6	93.2	31.9	98.0
61.5	91.8	97.2	99.0	42.1	89.7	48.6	98.8	68.5	98.6	97.2	99.0	3.4	99.5	9.2	99.0	15.7	98.2	21.2	99.0
38.1	94.7	64.8	99.1	26.5	94.3	32.4	98.9	40.9	99.6	64.8	99.1	2.3	99.9	6.2	99.1	9.0	98.8	14.2	99.1
25.4	97.5	43.2	99.2	15.3	96.7	21.6	99.0	16.0	99.8	43.2	99.2	1.5	99.9	4.1	99.2	6.0	99.7	9.4	99.2
16.9	98.7	28.8	99.3	9.1	98.4	14.4	99.2	10.6	99.8	28.8	99.3	1.0	100.0	2.7	99.3	2.3	99.8	6.3	99.3
11.3	99.9	19.2	99.4	6.1	99.5	9.6	99.3	7.1	99.9	19.2	99.4	0.7	100.0	1.8	99.6	1.5	99.9	4.2	99.6
2.8	99.9	12.8	99.5	2.4	99.8	6.4	99.4	4.7	100.0	12.8	99.5					1.0	99.9	2.8	99.8
1.8	99.9	8.5	99.6	1.6	99.9	4.3	99.5	1.8	100.0	8.5	99.6					0.7	99.9	1.9	99.9
1.2	100.0	5.7	99.7	1.1	100.0	2.8	99.6	1.2	100.0	5.7	99.7					0.5	100.0	1.2	100.0
0.8	100.0	3.8	99.8	0.4	100.0	1.9	99.7	0.8	100.0	3.8	99.8					0.3	100.0	0.8	100.0
0.5	100.0	2.5	99.9	0.3	100.0	1.3	99.8	0.5	100.0	2.5	99.9								
0.4	100.0	1.7	99.9	0.2	100.0	0.8	99.9	0.4	100.0	1.7	99.9								
0.2	100.0	1.1	100.0	0.1	100.0	0.6	100.0	0.2	100.0	1.1	100.0								
0.2	100.0	0.7	100.0	0.1	100.0	0.4	100.0	0.2	100.0	0.7	100.0								

Table D. 3: Particle size evolution at 90 ms (model and LCS-experimental results)

<u>Wood chips</u>				<u>Olive residue</u>				<u>Straw</u>				<u>Polish coal</u>				<u>UK coal</u>			
MODEL		EXPERIMENT		MODEL		EXPERIMENT		MODEL		EXPERIMENT		MODEL		EXPERIMENT		MODEL		EXPERIMENT	
PSD (μm)	CM (Wt%)	PSD (μm)	CM (Wt%)	PSD (μm)	CM (Wt%)	PSD (μm)	CM (Wt%)	PSD (μm)	CM (Wt%)	PSD (μm)	CM (Wt%)	PSD (μm)	CM (Wt%)	PSD (μm)	CM (Wt%)	PSD (μm)	CM (Wt%)	PSD (μm)	CM (Wt%)
1509.5	0.2	1660.0	0.0	770.9	5.6	830.0	0.0	1440.0	1.0	1660.0	0.0	152.6	3.0	158.0	0.0	356.8	0.1	363.0	0.0
960.4	16.1	1106.7	0.0	503.1	39.7	553.3	8.0	908.7	16.9	1106.7	5.0	99.8	14.4	105.3	10.0	237.9	8.2	242.0	15.0
522.1	33.6	737.8	10.0	320.0	74.1	368.9	42.0	567.2	46.1	737.8	20.0	66.5	33.0	70.2	32.0	157.0	27.1	161.3	33.0
333.5	52.8	491.9	60.0	170.3	89.2	245.9	86.0	348.1	73.2	491.9	85.0	44.4	60.1	46.8	80.0	103.8	55.0	107.6	75.0
222.2	71.0	327.9	88.0	90.3	95.4	164.0	97.5	210.1	92.2	327.9	92.0	29.0	84.3	31.2	95.0	62.2	77.2	71.7	96.0
139.6	82.6	218.6	89.0	60.2	98.3	109.3	98.0	118.3	98.7	218.6	94.0	18.9	97.1	20.8	97.0	36.8	93.5	47.8	97.0
86.4	97.5	145.7	90.0	16.3	98.8	72.9	98.2	32.0	99.4	145.7	96.0	6.5	99.6	13.9	98.5	20.6	95.9	31.9	98.5
21.3	98.7	97.2	92.0	10.9	99.0	48.6	98.4	21.3	99.6	97.2	98.0	2.0	99.9	9.2	99.0	11.6	98.4	21.2	99.0
14.1	99.1	64.8	92.5	7.2	99.2	32.4	98.6	14.2	99.8	64.8	98.1	1.3	100.0	6.2	99.5	7.7	99.1	14.2	99.5
9.4	99.4	43.2	94.5	4.8	99.4	21.6	98.8	9.5	99.8	43.2	98.5	0.9	100.0	4.1	99.6	4.5	99.6	9.4	99.6
6.3	99.6	28.8	95.0	3.2	99.6	14.4	99.0	6.3	99.9	28.8	98.9	0.6	100.0	2.7	99.7	2.4	99.7	6.3	99.7
4.2	99.7	19.2	95.5	2.1	99.7	9.6	99.2	4.2	99.9	19.2	99.0	0.4	100.0	1.8	99.8	1.6	99.8	4.2	99.8
2.8	99.8	12.8	96.0	1.4	99.8	6.4	99.4	2.8	100.0	12.8	99.1					1.0	99.9	2.8	99.9
1.9	99.9	8.5	97.0	1.0	99.9	4.3	99.6	1.9	100.0	8.5	99.3					0.7	99.9	1.9	99.9
1.2	100.0	5.7	97.5	0.6	99.9	2.8	99.8	1.2	100.0	5.7	99.4					0.5	100.0	1.2	100.0
0.8	99.9	3.8	98.5	0.4	100.0	1.9	99.9	0.8	100.0	3.8	99.5					0.3	100.0	0.8	100.0
0.5	100.0	2.5	98.7	0.3	100.0	1.3	99.9	0.5	100.0	2.5	99.6								
0.4	100.0	1.7	99.2	0.2	100.0	0.8	100.0	0.4	100.0	1.7	99.8								
0.5	100.0	1.1	99.8	0.1	100.0	0.6	100.0	0.2	100.0	1.1	99.9								
0.2	100.0	0.7	100.0	0.1	100.0	0.4	100.0	0.2	100.0	0.7	100.0								

Table D. 4: Particle size evolution at 210 ms (model and LCS-experimental results)

<u>Wood chips</u>				<u>Olive residue</u>				<u>Straw</u>				<u>Polish coal</u>				<u>UK coal</u>			
MODEL		EXPERIMENT		MODEL		EXPERIMENT		MODEL		EXPERIMENT		MODEL		EXPERIMENT		MODEL		EXPERIMENT	
PSD (μm)	CM (Wt%)	PSD (μm)	CM (Wt%)	PSD (μm)	CM (Wt%)	PSD (μm)	CM (Wt%)	PSD (μm)	CM (Wt%)	PSD (μm)	CM (Wt%)	PSD (μm)	CM (Wt%)	PSD (μm)	CM (Wt%)	PSD (μm)	CM (Wt%)	PSD (μm)	CM (Wt%)
988.0	0.4	1660.0	0.0	616.6	6.5	830.0	0.0	1281.0	1.7	1660.0	0.0	149.8	5.0	158.0	0.0	323.1	0.1	363.0	0.0
437.3	9.4	1106.7	0.0	401.0	35.2	553.3	0.0	787.3	25.9	1106.7	0.0	97.9	23.8	105.3	10.0	210.3	21.4	242.0	10.0
291.3	29.1	737.8	0.0	251.9	67.5	368.9	15.0	524.9	68.2	737.8	5.0	63.9	52.8	70.2	45.0	107.8	57.2	161.3	30.0
194.4	55.9	491.9	5.0	142.0	88.7	245.9	90.0	197.5	91.6	491.9	18.0	38.5	84.0	46.8	90.0	77.6	84.3	107.6	65.0
95.5	68.9	327.9	10.0	65.8	95.4	164.0	97.4	77.1	96.3	327.9	82.0	20.5	97.3	31.2	98.0	30.4	95.6	71.7	90.0
63.7	77.0	218.6	30.0	25.7	96.5	109.3	97.8	51.4	97.5	218.6	88.0	4.7	99.1	20.8	98.5	11.9	98.1	47.8	94.0
33.7	83.6	145.7	45.0	17.1	97.0	72.9	97.9	34.3	98.4	145.7	93.0	3.1	99.5	13.9	98.7	7.9	98.6	31.9	96.0
22.5	88.6	97.2	75.0	11.4	97.5	48.6	98.0	22.8	99.0	97.2	95.0	2.1	99.8	9.2	99.1	5.3	99.3	21.2	99.1
15.0	91.8	64.8	89.0	7.6	98.0	32.4	98.1	15.2	99.4	64.8	96.0	1.4	99.9	6.2	99.6	3.5	99.5	14.2	99.6
10.0	94.8	43.2	90.0	5.1	98.5	21.6	98.2	10.1	99.6	43.2	97.0	0.9	100.0	4.1	99.7	2.3	99.7	9.4	99.7
6.7	96.4	28.8	90.5	3.4	98.9	14.4	98.3	6.8	99.7	28.8	97.5	0.6	100.0	2.7	99.8	1.6	99.7	6.3	99.8
4.4	97.7	19.2	91.0	2.3	99.2	9.6	98.4	4.5	99.8	19.2	98.0	0.4	100.0	1.8	100.0	0.9	99.8	4.2	99.9
3.0	98.2	12.8	92.0	1.5	99.5	6.4	98.5	3.0	99.9	12.8	98.5					0.6	99.9	2.8	100.0
2.0	98.7	8.5	92.5	1.0	99.7	4.3	98.6	2.0	99.9	8.5	99.7					0.4	99.9	1.9	100.0
1.3	99.2	5.7	94.0	0.7	99.8	2.8	98.7	1.3	99.9	5.7	99.7					0.3	100.0	1.2	100.0
0.9	99.7	3.8	95.0	0.4	99.9	1.9	99.2	0.8	100.0	3.8	99.8					0.2	100.0	0.8	100.0
0.6	99.7	2.5	96.0	0.3	99.9	1.3	99.5	0.6	100.0	2.5	99.9								
0.4	99.8	1.7	98.0	0.2	99.9	0.8	99.8	0.4	100.0	1.7	99.9								
0.2	99.9	1.1	99.8	0.1	100.0	0.6	99.9	0.2	100.0	1.1	100.0								
0.2	100.0	0.7	100.0	0.1	100.0	0.4	100.0	0.2	100.0	0.7	100.0								

Table D. 5: Particle size evolution at 1300 ms (model and LCS-experimental results)

<u>Wood chips</u>				<u>Olive residue</u>				<u>Straw</u>				<u>Polish coal</u>				<u>UK coal</u>			
MODEL		EXPERIMENT		MODEL		EXPERIMENT		MODEL		EXPERIMENT		MODEL		EXPERIMENT		MODEL		EXPERIMENT	
PSD (μm)	CM (Wt%)	PSD (μm)	CM (Wt%)	PSD (μm)	CM (Wt%)	PSD (μm)	CM (Wt%)	PSD (μm)	CM (Wt%)	PSD (μm)	CM (Wt%)	PSD (μm)	CM (Wt%)	PSD (μm)	CM (Wt%)	PSD (μm)	CM (Wt%)	PSD (μm)	CM (Wt%)
810.0	0.1	1660.0	0.0	563.4	4.1	830.0	0.0	1196.6	1.1	1660.0	0.0	123.1	2.7	158.0	0.0	300.9	0.2	363.0	0.0
540.0	5.7	1106.7	0.0	411.0	21.2	553.3	0.0	797.7	22.3	1106.7	0.0	79.1	13.4	105.3	5.0	181.8	16.4	242.0	0.0
360.0	20.5	737.8	0.0	274.0	48.1	368.9	20.0	684.6	56.6	737.8	10.0	52.8	33.9	70.2	15.0	116.3	58.8	161.3	15.0
240.0	42.0	491.9	0.0	182.7	76.6	245.9	45.0	402.1	84.0	491.9	20.0	33.7	61.4	46.8	50.0	92.0	88.3	107.6	55.0
127.2	57.6	327.9	0.0	85.5	91.6	164.0	65.0	126.3	94.6	327.9	92.0	22.0	89.3	31.2	84.0	36.1	93.5	71.7	85.0
84.8	66.8	218.6	20.0	33.5	94.7	109.3	86.0	84.2	96.4	218.6	93.0	6.4	98.4	20.8	96.0	24.1	96.1	47.8	95.0
56.5	78.4	145.7	45.0	22.3	95.4	72.9	87.0	56.1	97.6	145.7	94.5	4.2	99.0	13.9	98.0	16.0	97.4	31.9	96.0
37.7	89.7	97.2	76.0	14.9	96.2	48.6	88.0	37.4	98.6	97.2	95.0	2.8	99.5	9.2	98.5	10.7	98.5	21.2	96.5
25.1	97.5	64.8	89.0	9.9	96.9	32.4	88.2	24.9	99.1	64.8	95.5	1.9	99.8	6.2	99.0	7.1	99.0	14.2	97.0
3.6	99.9	43.2	90.0	6.6	97.6	21.6	88.8	16.6	99.4	43.2	96.0	1.0	99.9	4.1	99.5	4.8	99.4	9.4	98.0
2.4	99.9	28.8	91.0	4.4	98.2	14.4	89.0	11.1	99.6	28.8	96.5	0.6	100.0	2.7	99.8	3.2	99.6	6.3	99.0
1.6	99.9	19.2	92.0	2.9	98.7	9.6	90.0	7.4	99.8	19.2	97.0	0.4	100.0	1.8	99.9	1.0	99.7	4.2	99.2
1.1	100.0	12.8	93.0	2.0	99.1	6.4	91.0	4.9	99.9	12.8	97.5					0.7	99.8	2.8	99.4
0.7	100.0	8.5	94.0	1.3	99.5	4.3	92.0	3.3	99.9	8.5	98.0					0.4	99.8	1.9	99.6
0.5	100.0	5.7	95.0	0.9	99.7	2.8	93.0	2.2	99.9	5.7	98.5					0.3	100.0	1.2	99.8
0.3	100.0	3.8	95.5	0.6	99.8	1.9	96.0	0.9	100.0	3.8	99.0					0.2	100.0	0.8	100.0
0.1	100.0	2.5	96.0	0.3	99.9	1.3	97.0	0.6	100.0	2.5	99.2								
0.1	100.0	1.7	97.0	0.2	99.9	0.8	98.0	0.4	100.0	1.7	99.6								
0.1	100.0	1.1	98.0	0.1	100.0	0.6	99.0	0.3	100.0	1.1	99.9								
0.0	100.0	0.7	100.0	0.1	100.0	0.4	100.0	0.2	100.0	0.7	100.0								

Appendix E

CCSEM analysis of Polish coal

Table E. 1: CCSEM analysis of Polish coal

Average composition of mineral categories (mass fraction of elements in %)														
Category	Al	Si	P	S	Na	Mg	Cl	K	Ti	Cr	Fe	Ca	total	
Quartz	1,0	94,8	0,3	0,2	0,4	0,3	0,9	0,4	0,2	0,3	0,7	0,5	100,0	
Iron Oxide	0,9	1,3	0,0	0,0	1,5	2,4	0,8	0,8	0,2	0,3	89,9	1,9	100,0	
Alumina	74,3	8,0	1,9	2,9	0,4	0,0	5,3	1,7	3,5	0,0	1,8	0,2	100,0	
Calcite	0,6	0,8	0,2	0,2	0,5	0,5	0,6	0,2	0,2	0,2	1,2	94,8	100,0	
Dolomite	0,5	0,8	0,2	0,4	0,3	28,1	0,4	0,3	0,3	0,5	13,0	55,3	100,0	
Ankerite	0,4	0,8	0,2	0,2	0,4	20,5	0,4	0,3	0,3	0,5	26,5	49,6	100,0	
Kaolinite	37,7	49,0	0,5	0,9	0,8	1,2	0,8	4,0	1,5	0,4	2,7	0,5	100,0	
Montmorillonite	29,8	54,9	0,4	0,7	0,9	1,6	0,7	5,0	1,3	0,3	4,1	0,5	100,0	
Illite	30,4	51,7	0,3	0,4	1,0	1,5	0,6	8,6	1,2	0,3	3,6	0,4	100,0	
Fe-Al Silicate	21,8	36,1	0,3	0,4	1,0	6,6	0,6	2,8	0,7	0,4	28,8	0,6	100,0	
Ca-Al Silicate	33,2	27,9	3,8	0,6	0,2	1,7	7,2	3,9	1,8	4,7	0,3	14,6	100,0	
Na-Al Silicate	24,3	58,1	0,4	0,1	12,5	0,2	0,5	2,2	0,2	0,5	0,4	0,7	100,0	
Aluminosilicate	21,4	61,6	0,3	1,0	0,8	1,6	0,4	4,5	1,9	0,4	5,9	0,4	100,0	
Mixed Silicate	19,4	56,9	0,5	0,0	11,4	0,1	0,6	10,5	0,2	0,0	0,3	0,1	100,0	
Fe Silicate	3,4	46,5	0,5	0,1	0,1	3,9	0,5	0,0	0,3	0,2	44,1	0,4	100,0	
Pyrite	0,4	0,6	0,1	51,5	0,2	0,2	0,3	0,2	0,1	0,2	45,5	0,8	100,0	
Clay-Pyrite	19,2	27,2	0,0	27,0	0,0	0,0	0,1	3,7	0,0	0,0	22,9	0,0	100,0	
Fe-Cr Oxide	1,1	0,9	0,4	0,2	0,7	7,6	0,2	0,4	0,2	0,3	83,1	4,9	100,0	
Gypsum	0,3	0,2	0,0	44,9	1,2	0,8	0,4	0,0	0,5	0,7	0,0	51,0	100,0	
Apatite	1,1	0,8	27,7	0,1	0,3	0,4	0,2	0,3	0,1	0,5	0,9	67,7	100,0	
Ca-Al-P	43,8	3,0	28,6	2,8	1,9	0,1	3,7	0,6	0,0	0,0	2,9	12,5	100,0	
Gypsum-Al Silicate	15,5	50,2	0,3	4,0	2,7	3,3	0,8	1,8	0,9	0,1	5,4	15,1	100,0	
Si-rich	12,7	79,5	0,4	0,4	0,3	0,7	0,4	2,7	0,5	0,2	1,4	0,7	100,0	
Ca-rich	2,4	5,1	0,9	0,2	0,0	10,5	1,5	0,6	0,7	0,8	7,9	69,4	100,0	
Ca-Si-rich	4,0	21,1	0,9	3,6	6,7	1,5	0,7	0,0	1,2	1,8	1,2	57,2	100,0	
Unknown	5,2	21,0	0,4	1,9	2,5	14,1	3,1	3,5	1,4	0,7	16,8	29,4	100,0	
Average composition of mineral particle size ranges (mass fraction of elements in %)														
Size range [µm]	Al	Si	P	S	Na	Mg	Cl	K	Ti	Cr	Fe	Ca	total	
1-2	0,0	0,0	0,0	0,0	0,0	0,0	0,0	0,0	0,0	0,0	0,0	0,0	0,0	
2-4	21,6	42,0	1,1	2,3	1,1	3,7	6,5	4,2	1,5	1,0	9,5	5,7	100,0	
4-8	21,1	42,4	1,0	2,0	0,8	5,1	3,0	4,4	1,1	0,4	9,1	9,7	100,0	
8-16	15,5	36,5	0,6	4,8	0,9	7,6	0,6	4,1	0,8	0,5	13,5	14,7	100,0	
16-32	14,5	36,5	0,5	3,5	0,8	8,5	0,5	4,0	1,2	0,4	14,4	15,4	100,0	
32-64	17,8	43,8	0,6	3,9	0,9	5,7	1,1	3,7	1,1	0,5	10,6	10,5	100,0	
64-125	16,3	45,2	0,3	6,2	1,3	5,0	1,1	3,3	0,7	0,4	9,9	10,4	100,0	
125-250	0,0	0,0	0,0	0,0	0,0	0,0	0,0	0,0	0,0	0,0	0,0	0,0	0,0	
average	16,7	42,8	0,5	4,6	1,0	6,0	1,0	3,6	0,9	0,4	11,1	11,4	100,0	

Appendix F

Full manuscripts of the published articles
